First row late d-block metal pincer complexes: exploring their coordination chemistry and catalysis

---

Thesis submitted for the degree of Doctor of Philosophy at University of Leicester

Jinting Xu MSc

Department of Chemistry

University of Leicester

27/03/2020

First row late d-block metal pincer complexes: exploring their coordination chemistry and catalysis

Jinting Xu

Abstract

In this thesis, the synthesis and characterisation of a series of sterically and electronically distinct *N,N*$_{py}$*,O* and *N,N*$_{Py}$*,N* pincer complexes based on the late 3d metals, Zn, Co, Ni and Fe, are described; some reaction chemistry including catalysis is also disclosed. **Chapter 1** presents an overview of the development and application of first row transition metal pincer complexes and their role in modern homogeneous catalysis. In **Chapter 2**, the synthesis of a series of novel unsymmetrical *N,N*$_{py}$*,O* and *N,N*$_{py}$*,N* (pro)ligands and their reactions with zinc(II) chloride and zinc(II) tetrafluoroborate are documented. The resulting complexes are all diamagnetic and adopt both mono- and bimetallic structures based on neutral species or cation-anion pairs; in one case a bis(pincer ligand) complex has been isolated. The amenability of selected BF_4-containing zinc complexes to undergo BF_4-coordination or B-F bond cleavage/hydrolysis has been demonstrated. **Chapters 3** and **4** report the preparation of cobalt(II) and nickel(II) chloride/tetrafluoroborate complexes of the same (pro)ligands. A wide variety of structural types are exhibited including those based on square planar or square pyramidal geometries with steric and electronic effects proving influential. Where appropriate the paramagnetic behaviour of selected Co(II) and Ni(II) complexes has been the subject of a ^{1}H NMR spectroscopic investigation. As with the zinc work, evidence for B-F bond hydrolysis has been noted with the *N,N,N*-family of pincer complexes. As an underlying theme across these three synthetic chapters, chloride exchange reactions by using CsF, AgF AgOAc and $AgBF_4$ have been explored. **Chapter 5** discusses the synthesis of one *N,N,O*-iron(II) chloride along with two iron(II) tetrafluoroborate complexes bearing symmetrical and unsymmetrical *N,N,N*-ligands. Investigations reveal that the *N,N,N*-complexes are suitable for use as ethylene polymerisation precatalysts when treated with either MAO or MMAO as co-catalyst. Indeed, the catalytic activity of the symmetrical *N,N,N*-iron(II) tetrafluoroborate catalyst has proved exceptionally high affording highly linear high molecular weight polyethylene. All experimental details for Chapters 2 – 5, including the single crystal X-ray diffraction parameters, are provided in **Chapter 6**.

Acknowledgements

Firstly, I would like to thank my supervisor Dr. Gregory Solan. Thank you so much give me this opportunity be your student. I would not able to finish these four years without your help and encouragement. You always being so kind and so patient with me all the time even when I made mistakes or lost direction and motivation, and your inspiring advises and feedback guided me though a lot of difficult problems. My parents and I cannot express to you how grateful we are. Second, I would also like to thank Professor Eric hope, thank you for your help and your encouragement and comfort when I was confused and depressed. I must also thanks Kuldip Singh, Vanessa, Sharad Mistry, Mick Lee and Gerry Griffith for their continuous support with X-ray crystallography, mass spectrometry and NMR spectroscopy, respectively. Meanwhile, I also would like to thanks Professor Sun, Wang Zheng and whole research group which gave me a lot of help when I went to Institute of Chemistry of Chinese Academy of Sciences for examine my catalysts for ethylene polymeristion. And I am also very grateful to have this valuable opportunity to study with them.

Thirdly, I would like to thank my family, my father, mother and grandfather. I want to thank their continuous support, financially and emotionally. As the only child of them I also feel very guilty because I could not accompany when you are missing me. Even sometimes you have to bear my anxious and complaints. So I would like to say sorry to let you worry me a lot and I love you forever. You are the best parents and family in the world, and I am so happy be your child. I also want to apologize to my grandma who left me in my fist PhD year. As your favorite child, I am so sorry I am not with you in your last moment. I want to say I love you forever and missing you so much, really hoping you can be proud and happy of me.

I also want to thank all the very dear friends I made in the last four years hear—Martyna, Rusul, Mona, Rena, Simran, Will, Meshari, Ahmed, Amina, Anna, and all the colleges who are working or worked in the 0.21 office. Thank you for your help and support in my whole PhD life. Because of you, the most difficult lab hours become joyful and easier. I also want to thank my friends in China, UK and other countries. Thank you for bearing my complaining, crying and angry about my failed experiments, depression and overall stress writing up. Thank you for your listening, support and making me happy.

Contents

Abbreviations

°	degrees
Å	angstrom (0.1nM)
Ar	aryl fragment
ASAP	atmospheric solid analysis probe
BnOH	benzyl alcohol
BM	unit of magnetic moment
Bn	benzyl group
br s	broad singlet
Bu	'normal' butyl
br	broad peak
ca.	circa (about/around)
cat	catalyst
$CHCl_3$	chloroform
cod	1,5-cyclooctadiene
Cp	cyclopentadienyl
COSY	correlation spectroscopy
°C	degree centigrade
δ	delta (NMR chemical shift)
DCM	dichloromethane
DMSO	dimethylsulfoxide
Et_2O	diethyl ether
dipp	2,6-diisopropylphenyl
d	doublet
dd	doublet of doublets
dt	doublet of triplets
DSSC	dye-sensitised solar cell
DSC	differential scanning calorimetry
eq.	equivalents
ESI	electrospray ionisation
eqn.	equation
EtOH	ethanol
η	eta

fac-	facial arrangement
FAB	fast atom bombardment
Fig.	figure
g	gram
GCMS	gas Chromatography-Mass Spectrometry
GPC	gel permeation chromatography
g(PE)	grams polyethylene
h	hour
Hz	hertz
HSAB	hard and soft acid and base theory
HMBC	heteronuclear multiple bond correlation
HSQC	heteronuclear single quantum coherence
HOAc	acetic acid
HDPE	high density polyethylene
OH	hydroxy
i.e.	id est (that is)
IR	infra-red
^{i}Pr	isopropyl
J	joules
M	molar concentration
M	metal
m/z	mass/charge ratio
m	multiplet
M.p.	metlting point
MS	mass spectrometry
MeOH	methanol
MeCN	aceteonitrile
Me	methyl
MHz	mega hertz
MAO	methylaluminoxane
MMAO	modified methylaluminoxane
mg	milligrams
mL	millilitres

mol	moles
μ	mu
μ_{eff}	magnetic moment
min	minute
M_w	molecular weight
M_n	number average molecular weigh
NMR	nuclear magnetic resonance
NOESY	nuclear overhauser effect spectroscopy
NHC	N-heterocyclic carbene
NEt_3	trimethylamine
OAc	acetate
OTf	triflate
ppm	parts per million
Pr	propyl fragment
Py	pyridine fragment
Ph	phenyl
PPh_3	triphenylphosphine
PMe_3	trimethylphosphine
PLA	polylactic acid
PCL	polycarprolactone
q	quart
R	alkyl fragment
r.t.	room temperature
ROP	ring opening polymerisation
s	singlet
sept.	septet
TOFMS	time-of-flight mass spectrometry
THF	tetrahydrofuran
TFA	trifuoroacetic acid
T_m	melting temperature of polyethylene
TEMPO	(2,2,6,6-ttetramethyl-piperidin-1-yl)oxyl
TMA	trimethylaluminium
t	triplet

td	triplet of doublets
*t*Bu	*tert*-butyl fragment
UHMWPE	ultra-high-molecular-weight polythylene
v/v	volume/volume
π	pi
δ	chemical shift

Chapter 1
Introduction

1.1 Introduction

This thesis is concerned with the application of pyridine-based pincer ligands as supports for first row late d-block metals (e.g., Zn, Co, Ni, Fe), the reactivity of their complexes and their use in homogeneous catalysis. To set the scene for the experimental work, this introductory chapter is principally concerned with reviewing the two main types of pincer complex: i) carbon-based and ii) pyridine-based. The special properties of pincer ligands and their complexes are discussed as is their role in modern day catalysis.

1.2 From simple ligands to pincer ligands

In coordination chemistry, a ligand is an ion or molecule (functional group) which can bind to a metal centre to produce a coordination complex. Ligands can act as Lewis bases (electron pair donors), while the central atom acts as a Lewis acid (electron pair acceptor). Ligands have at least one donor atom with an electron pair in order to form covalent bonds with the central atom. Hard and Soft acid and base theory (HSAB) is useful in coordination chemistry, as it recognises that hard bases can stabilise high oxidation states and soft bases stabilise low oxidation states. Ligands can be anions, cations, or neutral molecules and can be further distinguished as monodentate, bidentate, tridentate etc.

1.2.1 Tridentate pincer ligands

A tridentate ligand is a chelating agent that binds tightly to the metal centre through three donor atoms. Pincer ligands represent a particular type of tridentate ligand that prefer to bind to a metal centre in a meridional fashion. These types of ligands have received considerable attention in the development of metal coordination complexes because of their distinctive combination of properties.[1] The connectors between the three donor groups are often rigid enforcing a strict *mer* geometry while flexible linkers allow *fac* binding and even fluxionality between the two forms.[1] Meanwhile, there is

now plenty of evidence that pincer ligand scaffolds render more robust complexes when compared with monodentate analogues, allowing more extreme reactions conditions (high temperature and pressure) to be applied. The upshot is that their catalysts can operate in the presence of wide range of external reagents and conditions such as CO, CO_2, isocyanides, H_2, halogens, oxidising and reducing agents, water, acids or even sodium metal without leading to catalyst decomposition.[1]

Pincer ligands can be further classified in terms of their symmetry (symmetrical or unsymmetrical) and charge (neutral or ionic). The symmetrical neutral and monoanionic pincers are the most common and were the first ones to be reported (*e.g., P,C,P*, *P,N,P*, *N,N,N* etc).[2] On the other hand, examples of unsymmetrical pincer complexes are relatively scarce but have in recent years attracted more attention.

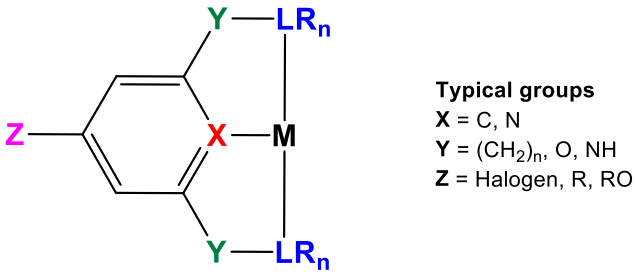

Figure 1.2.1: Steric and electronic control of a pincer ligand complex.[1]

The electronic and steric properties of the pincer complex can be fine-tuned without significant modification to the coordination properties. **Fig. 1.2.1** shows a pincer complex containing a central 2,6-substituted aromatic ring; the steric hindrance on the metal centre can be directly impacted by the steric bulk of the **R** groups while the chelate ring size can be determined by the size of the linker arms **Y**. Meanwhile, variation of the nature of **Z** (a substituent on the central aromatic ring) allows a means to modify the electronic properties of the pincer. The central donor atom **X** also allows important electronic effects, particularly though the *trans*-influence.[3,4] In addition, employing chiral $\mathbf{LR_n}$ donor groups allows a method of introducing chirality to the resulting complexes.[5]

In this section below we focus on carbon- and pyridine-based pincer ligands and sub-divide this sections on the basis of their symmetry; the reactivity and applications in coordination chemistry is then surveyed.

1.2.1.1 Carbon-based pincer ligands and their complexes

The synthesis and application of pincer metallacycles have been well-studied in the organometallic chemistry.[6,7] A carbon-based pincer ligand usually binds to a metal centre via a central anionic carbon and two neutral exterior donor groups. This central C-donor can have useful effects on the properties of the complex, for example labilisation of the *trans*-site on account of its high *trans*-effect. By way of contrast, the monodentate C_6H_5 ligand is not favourable for applications due to its ready dissociation by protonation or reductive elimination.[1] Therefore, carbon-based tridentate complexes have been extensively studied in various applications, for example in Heck reactions[8], asymmetric allylic alkylations,[9] asymmetric aldol condensations,[10] aliphatic dehydrogenations[11] and in C-H bond activation/functionalisation. In addition, this class of compound can also show interesting photochemical and photophysical properties in bio-organometallic chemistry.[6]

***a*:** Symmetrical carbon-based pincer ligands

The most common carbon-based pincer ligands are the symmetrical *E,C,E*-type (E = P, S, N). Amongst these, *P,C,P* pincer transition metal complexes have been most widely studied.[4] There are many different synthetic methods available for the synthesis of *P,C,P* pincer ligands depending on the linker **Y** moieties positioned between the central aromatic ring and the phosphines. If **Y** is a methylene group, *P,C,P* ligands can be typically prepared from 1,3-bis(bromomethyl)benzene upon treatment with lithium phosphides *in situ*.[12,13]

Since the 1960s, one of the earliest examples involving the use of pincer complexes was discovered by Heck and co-workers, and this reaction has been widely used in organic synthesis.[14] In this reaction, the coupling of an α-olefin with a bromo- or iodo-aryl derivative in the presence of excess PPh_3 was carried out (**Scheme 1.2.1**).[14] Milstein and co-workers were the first research group to employ Pd(II)-*P,C,P* pincer complexes **1** and **2** in the Heck coupling reaction.[15] At the same time, an analogous *P,C,P* pincer-type ligand **3** based on a phosphine unit as the P donor was synthesised by Jensen *et al*.[16] Subsequently, Shibasaki *et al.* synthesised a more reactive complex **4** which showed turnover numbers of greater than 980,000. Milstein found that **1** and **2** were able to deliver full conversion in the coupling of iodobenzene with methylacrylate, using NMP (N-methyl-2-pyrrolidone) as solvent and sodium carbonate as base resulting

in catalytic turnover numbers of 5,000,000 for iodobenzene and 132,900 for bromobenzene. On the other hand, palladium complex **3** showed high efficiency in the coupling of chlorobenzenes; indeed it has been reported previously by Milstein to be as reactive as the *P,C,P* phosphine derivative.[15]

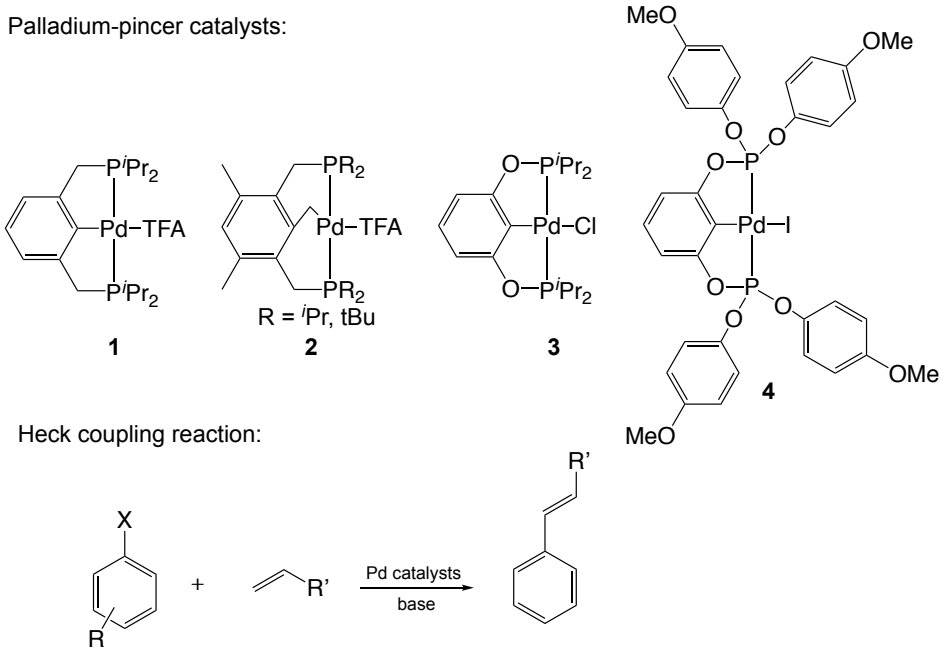

Scheme 1.2.1: *P,C,P*-type Pd(II) catalysts and their use in Heck reactions.[15]

Pincer nickel complexes also occupy a special place in the historical development of cyclometalation reactions. In 1976, Moulton and Shaw prepared the nickelacycle **5** which was formed by C-H activation of a pincer-type *P,C,P* tridentate ligand and NiX_2 (**Scheme 1.2.2**).[17] Various phosphine substituents have been investigated,[18] including phosphinites, while the central carbon can be sp^2-hybridised (*e.g.* phenyl, anthracyl[19]) or sp^3-hybridised as in **6** (**Scheme 1.2.2**).[20] Furthermore, these complexes can be used as excellent catalysts for a wide variety of key organic reactions, have unique reactivity for the cleavage of unreactive C-C and carbon-heteroatom bonds, can be incorporated into polymer networks, can reversibly bind small molecules and can be used as building blocks in supramolecular chemistry.[20] In addition, these nickel(II) complexes proved thermally stable and indeed could be sublimed without decomposition even at 240 ^oC in air.[17]

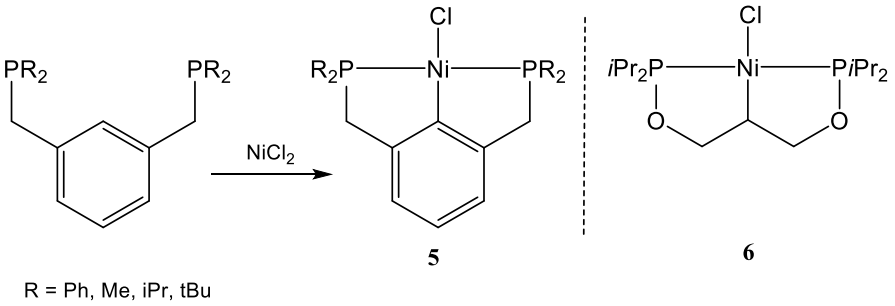

Scheme 1.2.2: Synthesis of *P,C,P*-nickel(II) complexes **5** and **6**.[17]

Another synthetic route to *P,C,P* pincer ligands involves the use of amines as the linker arms **Y**, which was first reported by Haupt and co-workers[21] and has been explored by many researchers (**Scheme 1.2.3:** ligands **7a-j**).[22] Both achiral and chiral substituents have been introduced to the phosphines by using chlorophosphines derived from the reaction of diols and amino alcohols and phosphorus trichloride.[23]

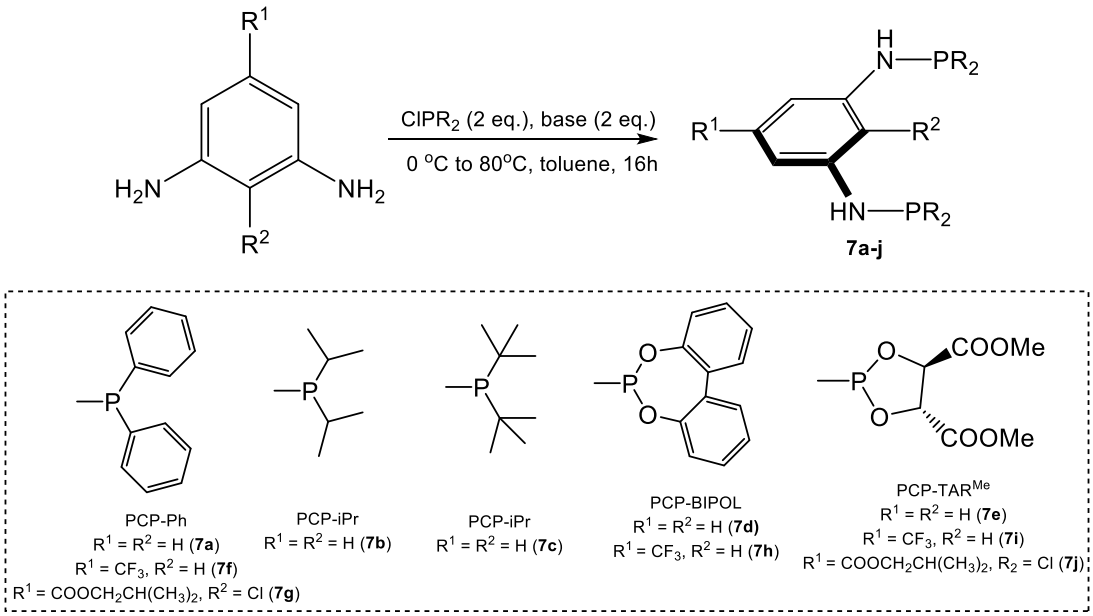

Scheme 1.2.3: The synthesis of symmetrical *P,C,P* pincer ligands, **7a**–**7j**.[21-23]

Specifically, **7a-j** when reacted with $NiCl_2 \cdot 6H_2O$, $Pd(cod)Cl_2$ and $Pt(cod)Br_2$ produced the symmetrical neutral square planar nickel, palladium and platinum *P,C,P* complexes, respectively (**Scheme 1.2.4: A**).[22] The nickel *P,C,P* complexes could only be produced with the aminophosphine ligands **7a-c**. In the preparation of the platinum *P,C,P* complexes, base (NEt_3) was added externally to facilitate the C-H bond activation process.[24] The palladium *P,C,P* complexes **10a-d** were obtained by the reaction of ligands **7a,7d** and **7e,f** with $Pd(TFA)_2$. The temperatures of these reactions (**10a-d**)

were lower than their chloride analogues **9a-g**, due to the basic nature of the TFA anion. The *P,C,P*-Pd complexes **12a,b** were also formed by oxidative addition of the C_{Ar}-Cl bond in the ligands **7g** and **7j** with $Pd_2(dba)_3$ (**Scheme 1.2.4: B**).[22] The palladium *P,C,P* complexes **9a-f** and **10a-d** were explored as catalysts in the Suzuki coupling of aryl and alkyl bromides with phenylboronic acid.[22] The results showed that the chloro complexes **9a-f** were better catalysts than the TFA complexes **10a-d** with lower catalyst loading necessary. For example, the reaction of 4-bromoacetophenone and phenylboronic acid employed only 0.00001 mol% of catalyst **9a** and allowed 97% isolated yield (TON = 9.7 $\times 10^6$). Indeed, the turnover frequency (TOF) was high as 600 000 h^{-1} (170 s^{-1}), which is among the highest ever reported for palladium pincer complexes in Suzuki reactions.[24]

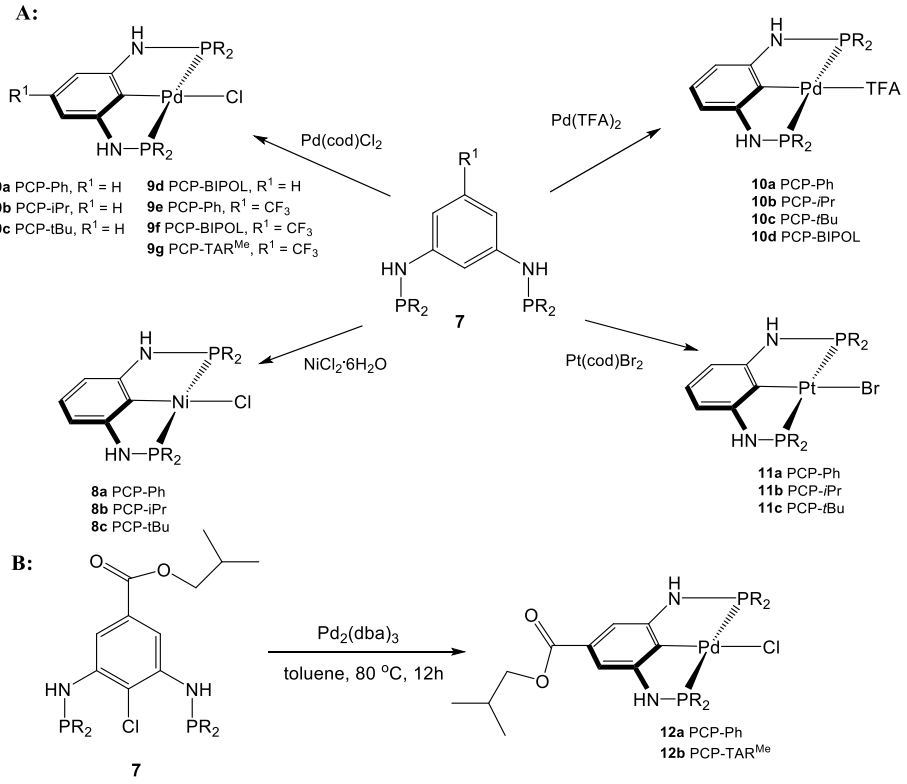

Scheme 1.2.4: A) Synthesis of various Pd, Pt and Ni complexes **8 - 11** from symmetrical *P,C,P* pincer ligands **7**; B) Synthesis of the *P,C,P*-Pd complexes **12a,b** by the oxidative addition of the *P,C,P* ligand.[22,24]

Elsewhere, symmetrical *N,C,N* pincer ligands have also been widely studied. In 2010, Liu *et al.* published the synthesis, characterisation and molecular structures of a variety of *N,C,N* pincer aluminium complexes (**13**), bis-ligated zinc complexes (**14**) and the mono-ligated *N,C,N* pincer zinc complex **15** (**Scheme 1.2.5**).[25] All these aluminium

and zinc complexes were efficient initiators for the ring-opening polymerisation (ROP) of *L*-lactide in the presence of benzyl alcohol. However, the productivity of the zinc complexes were generally higher than that of the aluminium complexes under similar conditions. Furthermore, the mechanism for the ROP of *L*-lactide initiated by **15**/BnOH was also explored by using ^{1}H NMR spectroscopy. The results indicated that the alkyl zinc complex had been converted to benzyloxy-zinc species before the polymerisation began and that the real initiator was in fact the benzyloxy zinc species shown in **Scheme 1.2.5.**

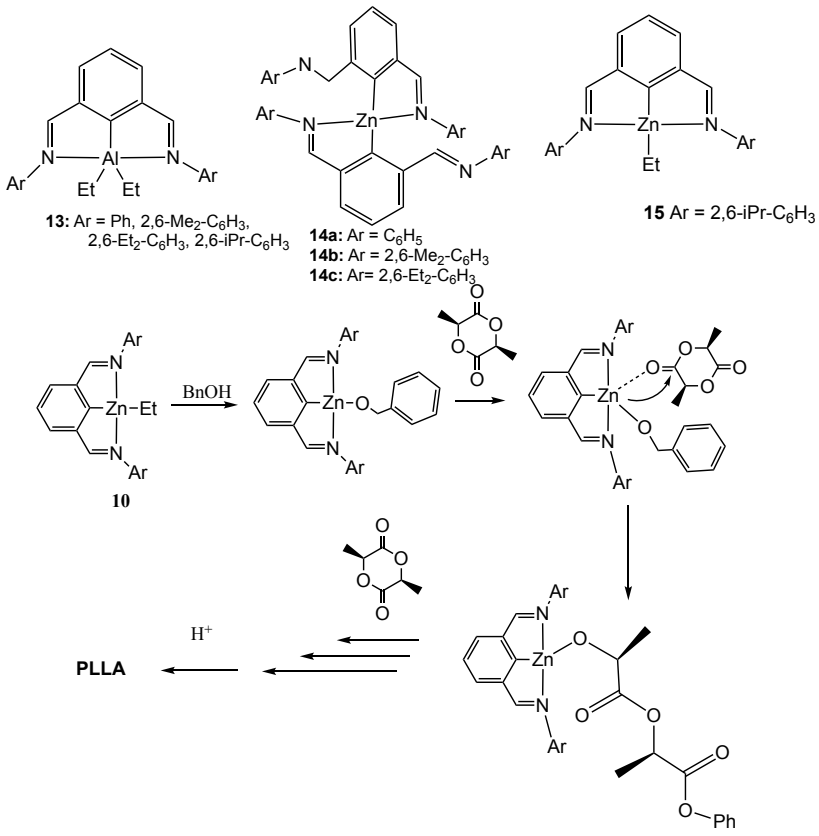

Scheme 1.2.5: *N,C,N* pincer aluminium complexes **13**, bis-ligated zinc complexes **14** and mono-ligated zinc complex **15**[25]. Proposed mechanism for the ROP of *L*-lactide initiated by **15**/BnOH.[25]

First row late transition metal complexes bearing *S,C,S* ligands are less well-known when compared to other types of pincer ligands. The first example of a *S,C,S* symmetrical nickel pincer was synthesised in 2008 (**Fig. 1.2.2**, complex **16**).[26] Subsequently, the nickel *S,C,S* pincer complexes **17** and **18** were published which contain benzylaminothicarbonyl units that are incorporated into a cyclophane macrocycle (**Fig. 1.2.2**).[27,28] It is worth noting that in **19**, the nitrogen atom of the

pyridine fragment is not coordinated to the nickel centre (**Fig. 1.2.2**). Furthermore, these nickel complexes have been widely applied in catalytic alcohol dehydrogenation.[29]

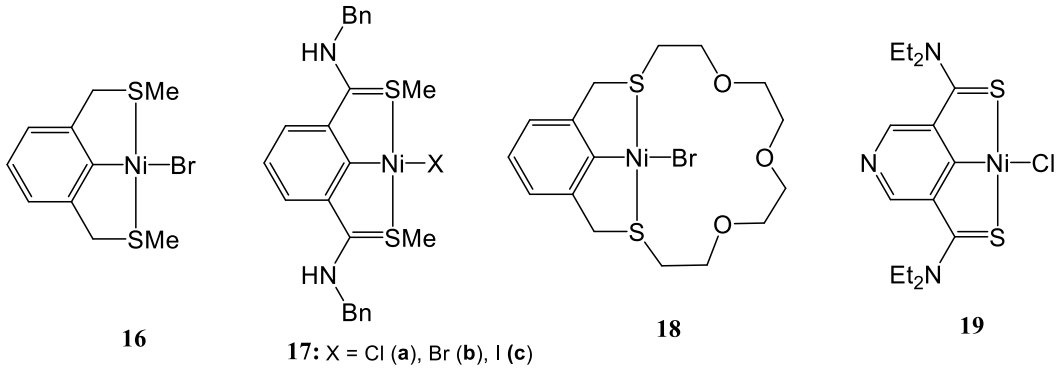

16 **17:** X = Cl (**a**), Br (**b**), I (**c**) **18** **19**

Figure 1.2.2: The first symmetrical *S,C,S*-nickel pincer complex **16** along with **17**, **18** and **19**[26-29]

***b**:* Unsymmetrical carbon-based tridentate pincer ligands

Recently, there has been some interest in the development of pincer metal complexes bearing two different donor groups with the hope that these unsymmetrical systems may provide unique reactivities. Indeed, a variety of donating atoms, such as phosphorus, nitrogen, carbon, oxygen and sulfur have been introduced into the unsymmetrical framework. **Fig. 1.2.3** shows a selection of unsymmetrical carbon-based tridentate pincer ligands including *P,C,N* (**20a-d**),[30-33] *P,C,S* (**20e**),[34] *P,C,P* (**20f**),[35] *P,C,C* (**20g**),[36] *N,C,S* (**20h**),[37,38] *N,C,N* (**20i**) and [39] *N,C,C* (**20j**)[40].

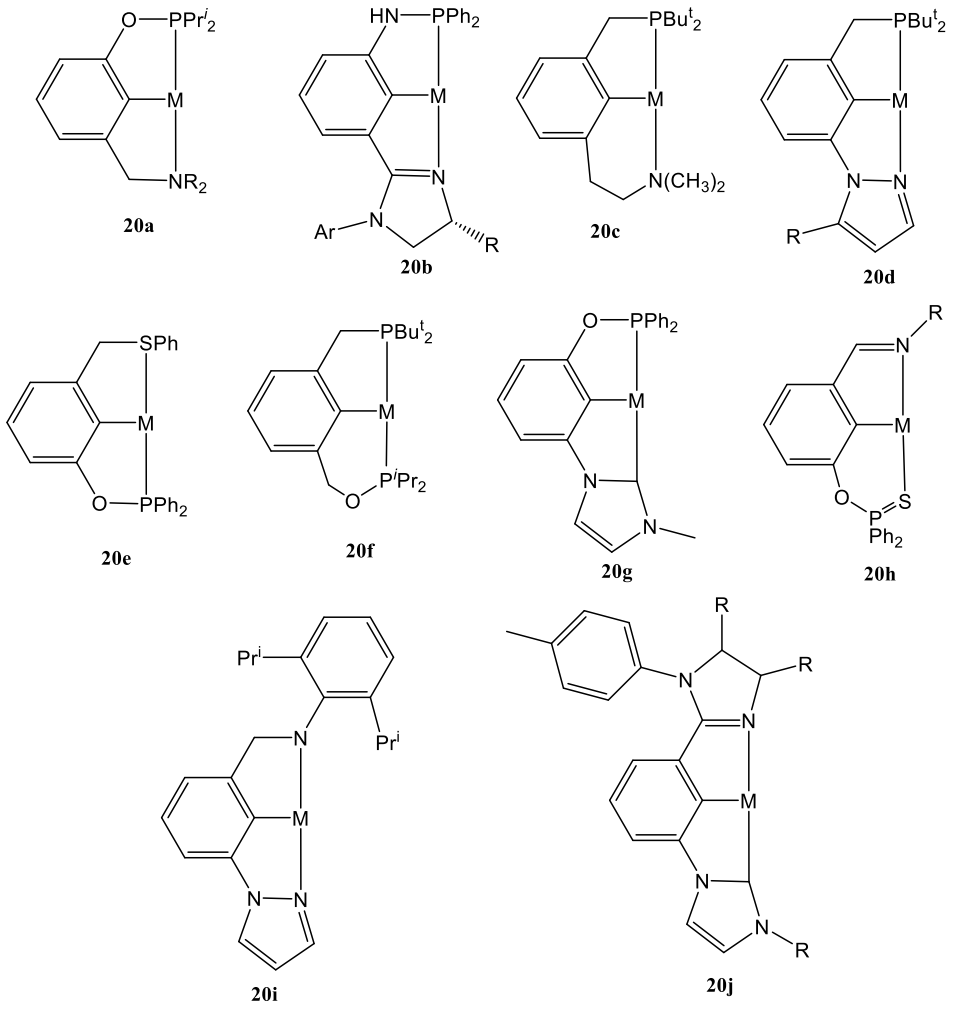

Figure 1.2.3: Various unsymmetrical carbon-based pincer complexes, **20a-j**[30-40]

In particular, the *P,C,N*-type pincer ligands possess special σ-donor and π-acceptor properties due to the combination of the bonding properties imparted by amines and phosphines (or phosphinites). Another advantage of these *P,C,N* ligands is their metal complexes can be produced by direct metalation using trimethylamine as a proton scavenger base.[29] The first *P,C,N* nickel complex **21** (**Fig. 1.2.4**) was reported in 2009, and was found to undergo oxidation with bromine to form the nickel(III) complex **22** (**Fig. 1.2.4**). Moreover, complexes **21a,b** and **22a,b** showed good activity in the cross-coupling of carbon tetrachloride with various olefins.[41] Furthermore, the *N,C,P*-nickel complex **23** bearing a secondary amine unit was synthesised by Spasyuk and co-workers in 2010 and shown to dimerise to **24** which proved an active catalyst for acrylonitrile functionalisation in alcoholic media (**Fig.1.2.4**).[42,43] Various other substituted analogues of complex **21a** are also known, such as **21d**[44] and chiral **25**

containing an imidazole fragment.[45-47] In the asymmetric Suzuki-Miyaura cross-coupling reaction, **25** has shown good activity as a catalyst.[40]

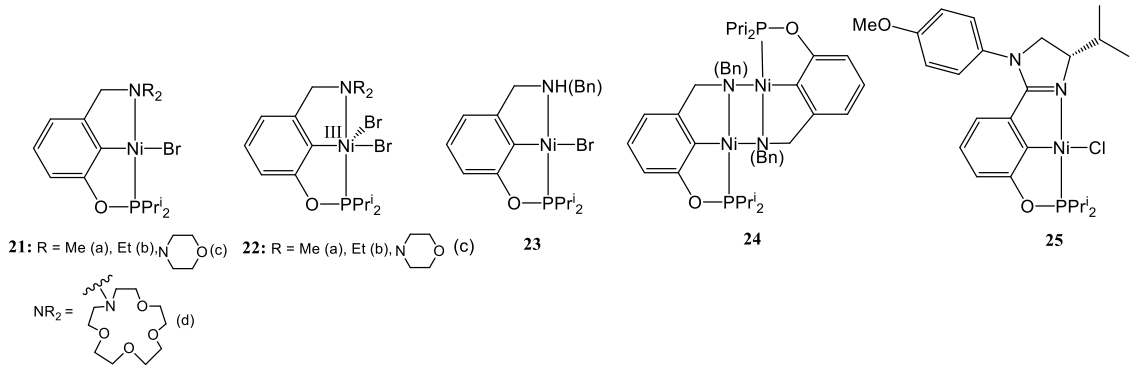

Figure 1.2.4: Various unsymmetrical *N,C,P* pincer nickel complexes, **21**-**25**.[40]

A series of (pyrazolyl)phosphinite, (amino)phosphinite and (imino)phosphinite palladium(II) pincer complexes **26**, **27** and **28** were synthesised in good yields (**Scheme 1.2.6**).[48,49] Complex **28** can be easily synthesised in two steps from inexpensive and commercially available *m*-hydroxybenzahdehyde.[49] In addition, the *N,C,N* unsymmetrical palladium(II) complexes **29** (**Scheme 1.2.6**) were also prepared by cyclopalladation of the corresponding ligands using $Pd(OAc)_2$.[49] The pincer palladium complexes, **26, 27** and **28** proved efficient catalysts for the coupling of phenylboronic acid with aryl bromides with 0.1 - 0.3% catalyst loadings; the highest yields were achieved by using **26b** (95%) and **28a** (> 99%) (**Scheme 1.2.6: A**).[48-50] Moreover, the *P,C,N* complexes **26** and the *N,C,N* complexes **29** also showed high activities in the coupling of aryl chlorides affording the expected products in excellent yields (70-99%) with a 1 mol% catalyst loading (**Scheme 1.2.6: B**).[48-50]

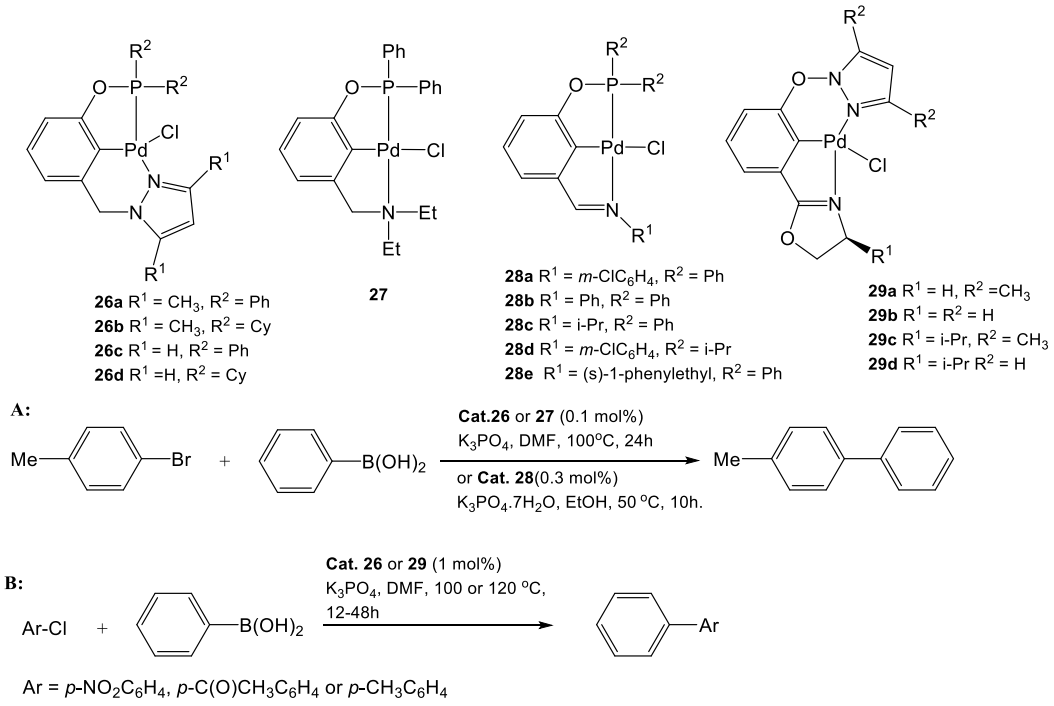

Scheme 1.2.6: Unsymmetrical pincer palladium(II) complexes used in the Suzuki-Miyaura reaction: A) palladium-catalysed coupling reaction of phenylboronic acid with aryl bromides, B) palladium-catalysed coupling of phenylboronic acid with aryl chlorides.[51]

1.2.1.2 Pyridine-based tridentate pincer ligands and their late transition metal complexes

A pyridine-based pincer ligand is a tridentate ligand that contains a central pyridine as the nitrogen donor atom along with two exterior donors. This type of pincer ligand can, like its carbon-based analogues, be classified as symmetrical and unsymmetrical depending on the nature of the exterior donors. Symmetrical pincer ligands and their steric and electronic properties have been widely studied in last 30 years.[52] Indeed these types of ligand usually behave as neutral ligands that do not require any C-H activation upon ligation and allow a variety of different oxidation states of the metal to be stabilised.

a: Symmetrical nitrogen based tridentate pincer ligands

The bis(imino)pyridine family of ligands has been well studied by a large number of research groups as their transition metal complexes (M = Fe, Ni, Co, Ti, Pd, Pt, *etc*.) can serve as excellent catalysts for many reactions, such as the hydrogenation of carbon dioxide, Suzuki-Miyaura coupling and some polymerisation reactions. **Fig. 1.2.5** shows

a selection of the reported symmetrical pyridine-based tridentate pincer ligands, such as *P,N,P* (**30a,b**), *N,N,N* (**30c,d,e**), *C,N,C* (**30f**) and *O,N,O* (**30g,h**).[52, 53, 54]

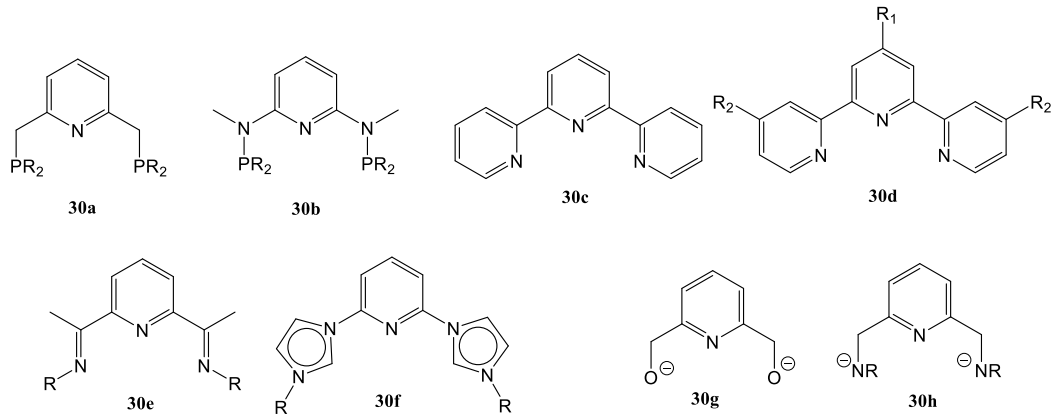

Figure 1.2.5: Symmetrical pyridine-based pincer ligands, **30a-h**.[52 53,54]

The ligands bearing phosphine or phosphite donor groups are the most widely utilised in applications. Similar to that described for carbon-based pincer ligands, the *P,N,P* pincer ligands can also be synthesised by similar routes depending on the **Y** arm linkers. If the **Y** is a methylene group, the *P,C,P* ligands can be produced from the reaction of 2,6-bis(bromomethyl)pyridine and lithium phosphides.[12,13] In 2011, Yang *et al.* reported the synthesis and characterisation of the *P,N,P*-ligated (*P,N,P* = 2,6-bis(di-iso-propylphosphinomethyl)pyridine) transition metal pincer complexes (*P,N,P*)IrH_3 (**31a**),[55] *trans*-(*P,N,P*)$Fe(H_2)CO$ (**31b**) and (*P,N,P*)-CoH_2 (**31c**) (**Scheme 1.2.7**). In addition, they studied the mechanism for the hydrogenation of carbon dioxide catalysed by these *P,N,P*-type complexes by using the density functional theory (DFT).[56] For the formation of formic acid from H_2 and CO_2, the iridium complex **31a** was a high efficiency catalyst, while the iron and cobalt catalysts were designed due to their low-cost. From the DFT results, the iron and cobalt complexes were proposed as promising low cost and high efficiency base metal catalyst candidates for CO_2 reduction (**Scheme 1.2.8**). Furthermore, the predicted reaction mechanism emphasised the essential role of the OH^- base in the catalytic cycle (**Scheme 1.2.8**), which may in general be critical for hydrogen activation and low energy proton transfers.[56]

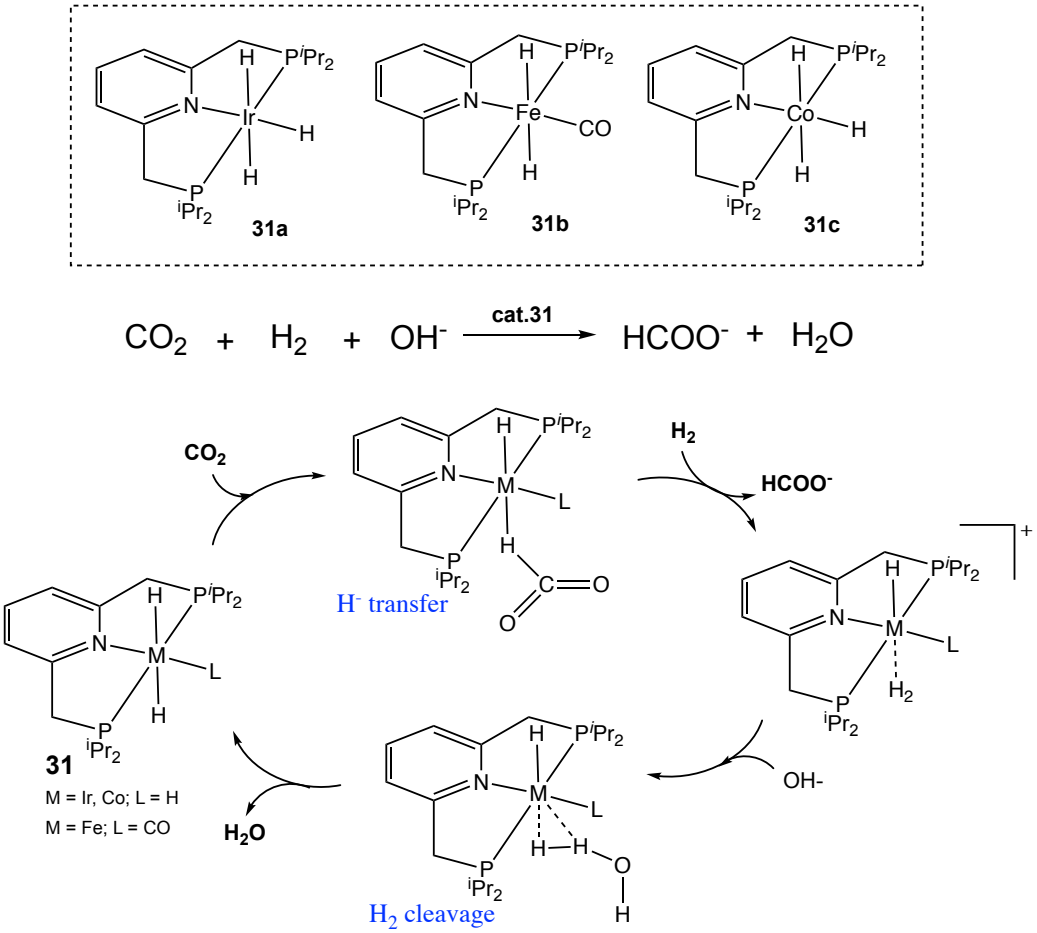

Scheme 1.2.7: The hydrogenation of carbon dioxide catalysed by *P,N,P*-containing **31a** (Ir), Fe **31b** (Fe) and **31c** (Co)[55,56]

An alternative synthetic route involves the use of amines as the linking **Y** group between the central aromatic ring and the phosphines. For example, a wide variety of *P,N,P* pincer ligands were synthesised by using 2,6-diaminopyridine (**Scheme 1.2.8:** ligands **32a-j**).

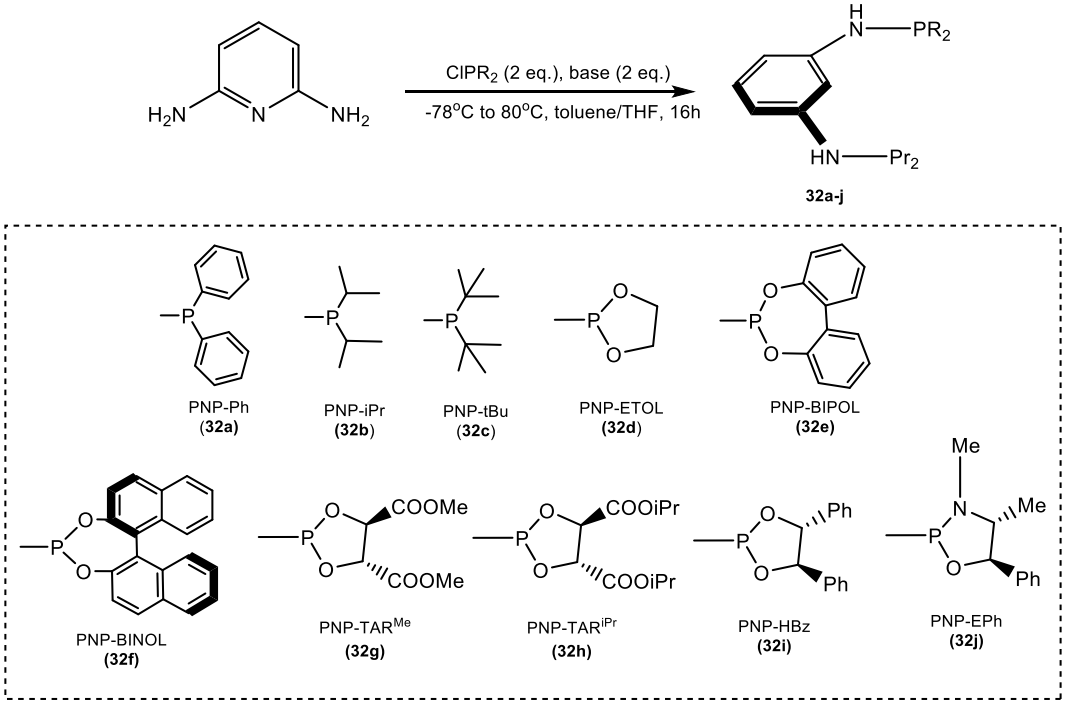

Scheme 1.2.8: Synthesis of unsymmetrical *N,C,N* pincer ligands, **32a-j**.[21-24]

These *P,N,P* ligands **32a-j** were also shown to act as effective supports for a number of transition metal ions. The octahedral diamagnetic Fe(II) complexes **33a,b** and **33d-g**, where the *P,N,P* ligand coordinates to the metal centre in a typical meridional fashion, were prepared by the reaction of the aminophosphine and phosphoramidite *P,N,P* ligands **32a,b** and **32d-g** with the hexaqua complex $[Fe(H_2O)_6][BF_4]_2$ (**Scheme 1.2.9**).[57] Complexes **33a** and **33b** can further be reacted with carbon monoxide to give the monocarbonyl complexes **34a,b**; no evidence was found for dicarbonyl complexes (**Scheme 1.2.9**).[58] The research group also reported that the synthesis of *P,N,P*-Fe(II) dichloride complexes was only possible when the ligands contained bulky substituents on the phosphines (*e.g.*, ^{i}Pr and ^{t}Bu), which was consistent with that reported by Milstein and co-workers with similar methylene-bridged *P,N,P* pincer ligands.[59] The penta-coordinate paramagnetic complexes **35a,b** were produced from the reaction of the *P,N,P* ligands **32b** and **32c** with $FeCl_2$ (**Scheme:1.2.9**).[58] All these Fe(II) complexes were applied as catalysts for the coupling of aromatic aldehydes and ethyl diazoacetate.[58] The most effective catalyst was found to be **34b**, the tris(acetonitrile) complexes **33a-c** were less efficient, possibly due to the carbonyl group in **34b** rendering the iron centre more Lewis acidic.

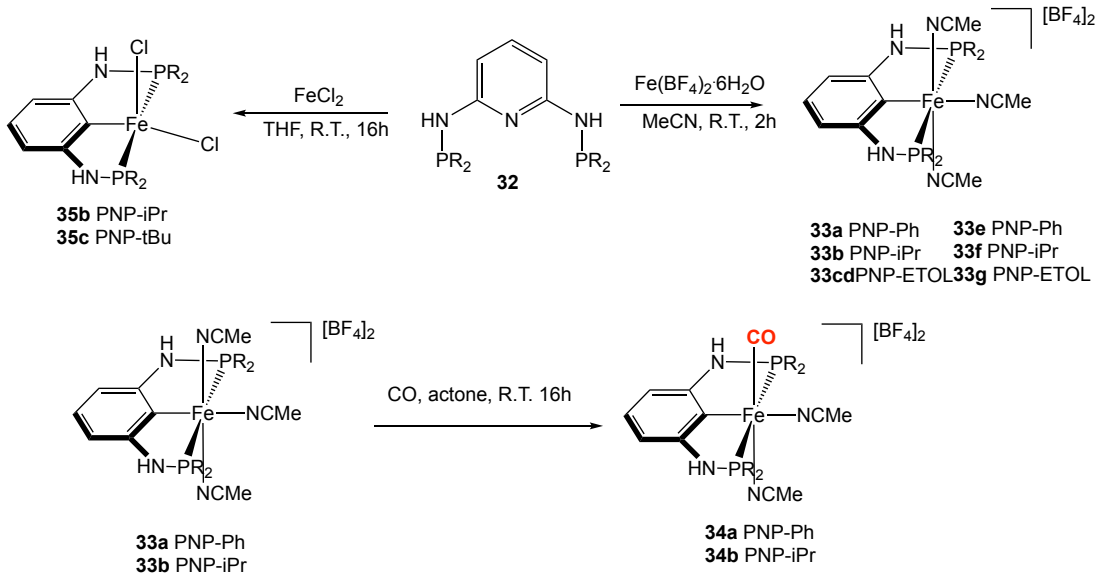

Scheme 1.2.9: Synthesis of iron complexes **33-35** from symmetrical *P,C,P* pincer ligands **32**[57-59]

For ethylene polymerisation, the 2,6-bis(arylimino)pyridine-iron(II) and -cobalt(II) halide complexes have been reported as exceptionally active catalysts, on activation with methylaluminoxane (MAO), producing high density polyethylene (HDPE) (**Fig. 1.2.6**).[60] The ligands were designed to impart steric bulk to the metal centre with higher molecular weight polyethylene achievable when two bulky substituents were located at the 2,6-positions of the N-aryl groups (*e.g.*, ^{i}Pr). On the other hand, with the less bulky 2-Me derivatives, lower molecular weight oligomer was formed. More details concerning ethylene polymerisation by using N,N_{py},N-type transition metal catalysts will be discussed in **Chapter 5**.

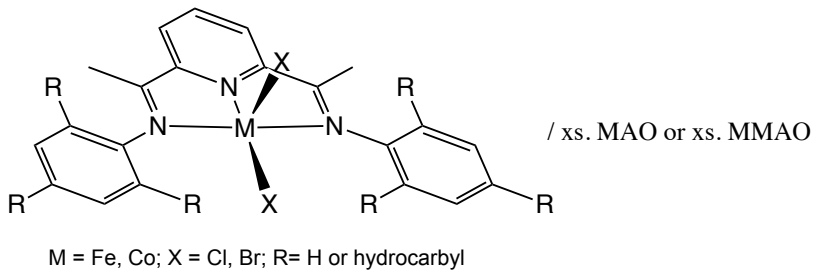

Figure 1.2.6: *N,N,N*-iron and cobalt catalysts for ethylene polymerisation and oligomerisation first developed.[60]

In addition to ethylene polymerisation, symmetrical *N,N,N* pincer complexes also show good activity for some cross-coupling reactions. In 2006, Morales-Morales *et al.* reported the synthesis and characterisation of a series of *N,N,N*-nickel(II) pincer

complexes [$NiCl_2\{C_5H_3N$-2,6-$(CHNAr_f)_2\}$] appended with different fluorinated aryl substituents. These nickel complexes were examined as catalysts in the alkyl- and arylthiolation reaction of halobenzenes.[61] The nickel complexes were produced by the reaction of one equivalent of tridentate ligand with one equivalent of $NiCl_2{\cdot}6H_2O$ in good yield. The magnetic moments for all the complexes, recorded at room temperature (297 K), were in the range of 2.8-3.4 BM as expected for high-spin five-coordinate nickle(II) complexes.[62] The highest yield (90%) was afforded by the 2,3,4-$Ar_{fluoride}$ substituted nickel complex **36** (**Scheme 1.2.10**). In this paper, different disulfides, chloro- or bromobenzene and different bromobenzenes have also been investigated using catalyst **36**.

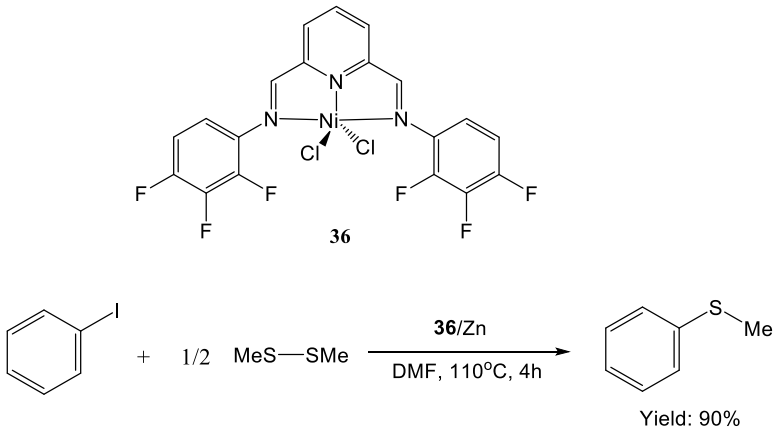

Scheme 1.2.10: Methylthiolation of iodobenzene by using symmetrical pincer *N,N,N*-nickel(II) complex **36** as catalyst.[61,62]

b: Unsymmetrical pyridine-based pincer ligands

As was mentioned above, interest in the synthesis of unsymmetrical pyridine-based pincer ligands has rapidly increased. The unsymmetrical approach can be achieved by adding substituents to the backbone of the C_{2v} pincer ligand, changing the donor or combining both of these techniques. As a result, a large number of potential ligands as well as additional parameters for tuning the stereoelectronic properties of the ligands system have been accomplished. Additionally, due to the significant differences in the donor properties, a free coordination site for the reactivity at the metal centre while maintaining stability with the two remaining ligand moieties can be generated by more labile donors.[63] **Fig. 1.2.7** shows a selection of reported unsymmetrical pyridine-based

tridentate pincer ligands such as *P,N,N* (**37a,b**), *N,N,N* (**37c,d**), *N,N,O* (**37e**), *C,N,O* (**37f**), *C,N,N* (**37g,h**) and *P,N,S* (**37i**).

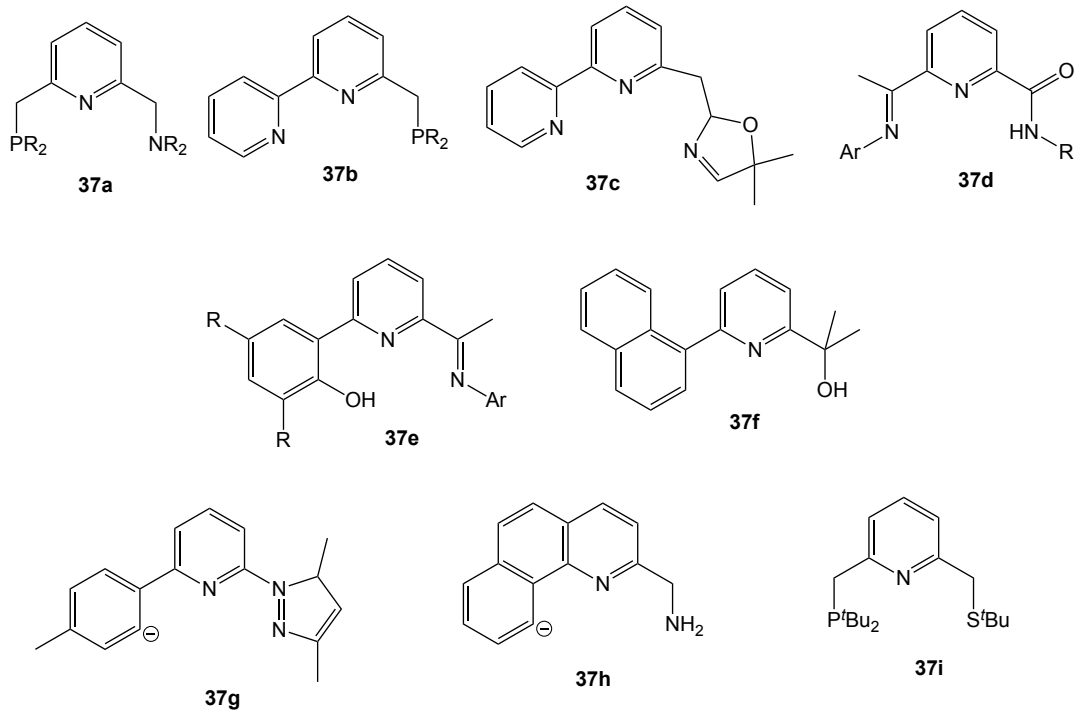

Figure 1.2.7: Unsymmetrical pyridine-based pincer ligands, **37a-i.** [53, 63]

For decades, many research groups have focused on the chemistry of cobalt-pincer complexes, due to the many advantages of pincer ligands themselves as well as the cheap, abundant and biocompatible alternative properties of cobalt.[64] Chirik's group initially explored the use of symmetrical pyridine-based pincer cobalt complexes for the hydrogenation of tri- and tetra-substituted non-activated alkenes such as *trans*-methyl stilbene, 1-methyl-1-cyclohexene and 2,3-dimethyl-2-butene under very mild conditions.[65] Based on this, the unsymmetrical cobalt complexes **38a,b** (**Scheme 1.2.11**), bearing one imine moiety substituted with a large aryl group and the other containing a chiral amine group were examined as catalysts for the asymmetric hydrogenation of selected olefins. The researchers noted that cyclometalation of the chiral element (alkylimine arm) is competitive with the formation of the cobalt hydride; the best performance was achieved by **38a**.[66a] On the other hand, the less hindered alkenes and electron-rich styrenes led to the highest selectivity and conversion. Meanwhile, a similar investigation of the unsymmetrical *N,N,N*-Co pincer catalysts **39a-c** for the enantioselective hydrogenation of alkenes was studied by Lu *et al.* (**Scheme 1.2.11**).[66b] Complex **39b** showed efficient activity for the reduction of

1,1-diarylethenes following activation with $NaBHEt_3$ and showed a unique O-chloride effect with high enantioselectivities (**Scheme 1.2.11**).

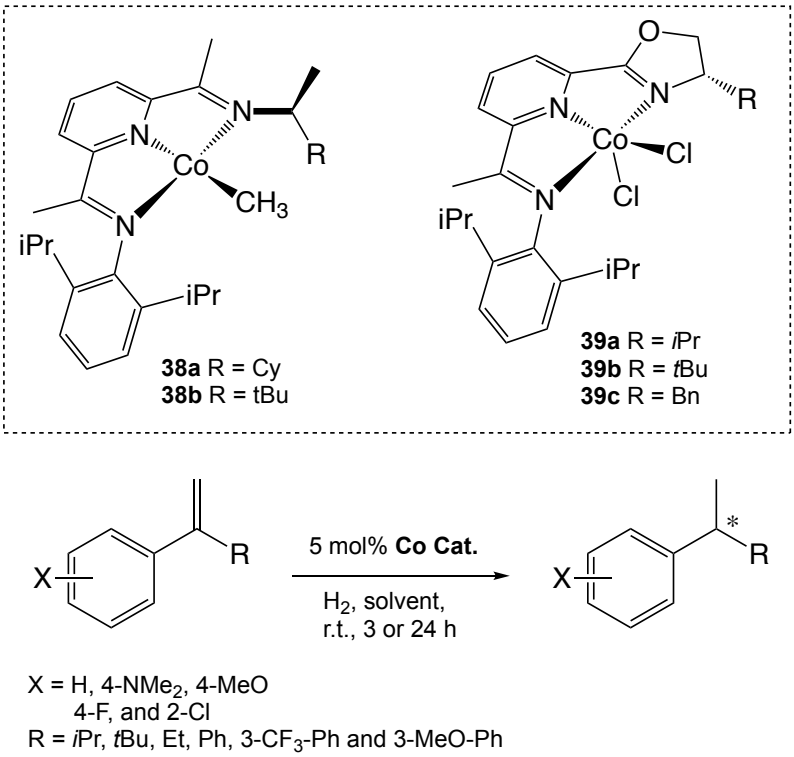

Scheme 1.2.11: Hydrogenation of selected olefins using unsymmetrical *N,N,N*-cobalt catalysts.[65,66a,b]

Most recently, pincer complexes based on first row transition metal complexes have attracted much attention due to their role in CO_2 reduction. This can be in part attributed to the strong chelate effect, preorganized geometry, high tunability and potential for ligand-based redox activity.[67a-i] In 2019, Jurss' group reported the synthesis and characterisation of the redox-active pincer first row transition metal complexes **41** (M = Fe, Co, Ni, Cu, Zn) and applied them for the electrocatalytic CO_2 reduction.[50] The unsymmetrical *P,N,N* pincer ligand **40** were produced by the Stille cross coupling reaction between 2-(tributylstannyl)pyridine and 2,8-dibromoquinoline, followed by a Pd-catalysed cross-coupling with $HPPh_2$ (**Scheme 1.2.12: A**). It was noted that due to the steric bulk of the phenyl substituents on the ligand, the metal centre preferred to coordinate with two ligands to form the pseudo-octahedral bis-chelate complexes **41** (**Scheme 1.2.12: B**).[68] Only the cobalt complex showed activity for CO_2 reduction. However, side reactions result in greatly limited activity. [68]

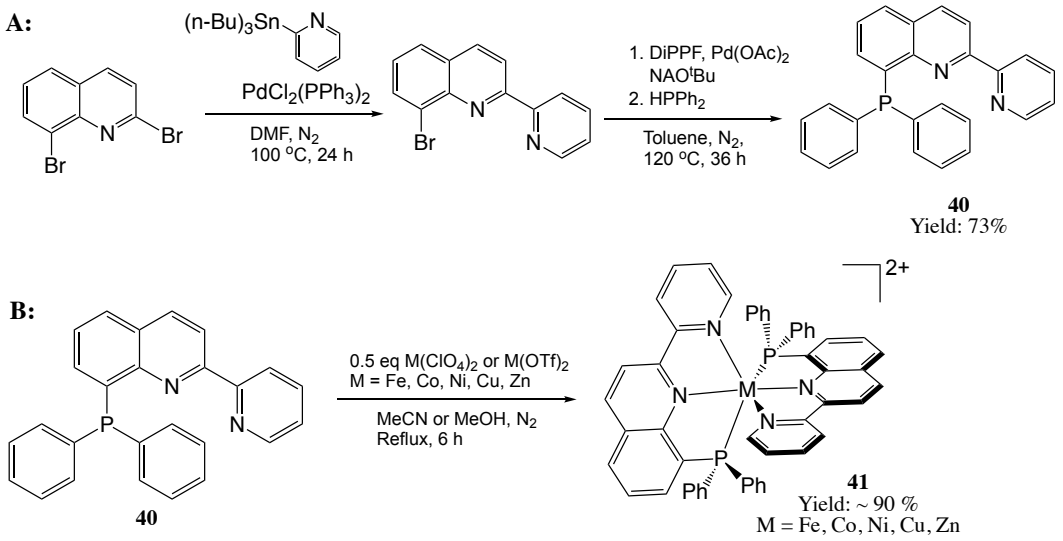

Scheme 1.2.12: Synthesis of the *P,N,N* pincer ligand **40**; b) General synthetic route to the metal complexes **41**.[68]

HSAB theory suggests that the harder oxygen donor of *N,N,O* pincer ligand will have a higher affinity for a metal(II) centre than the softer nitrogen. An unsymmetrical manganese complex **42** containing *N,N,O* pincer ligand were studied by Michaelos *et al.* (**Fig. 1.2.8**).[69] The *N,N,O* pincer ligand combines two softer N donors with the hard alkoxy group to produce a manganese(II) precatalyst for the long-lived O_2 evolution from aqueous oxone. Furthermore, this group also applied the dimeric manganese complex **43** incorporating two μ-O bridges in O_2 evolution catalysis.[69] Indeed, **43** proved one of the most active for this transformation.[70] It was considered, that deprotonation of the OH group in **42** was needed to give the strong donor alkoxide required to stabilise the oxidised form of the catalyst.[69]

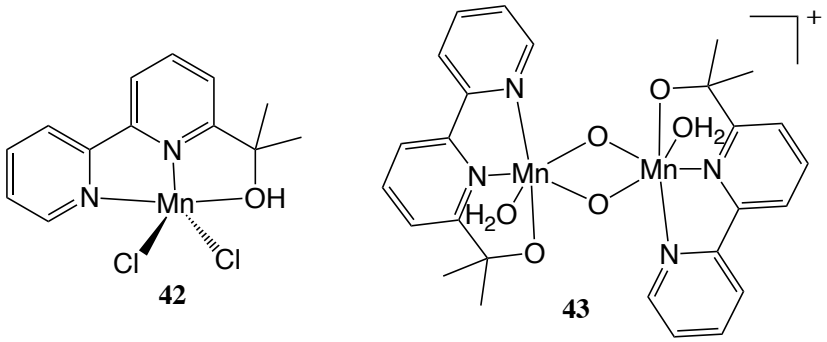

Figure 1.2.8: Pyridine-based *N,N,O*-manganese(II) complexes **42** and **43**.[69]

Group IV transition metal halide complexes containing *N,N,O* pincer ligands have been widely used as precatalysts in ethylene polymerisation. Typically a co-catalyst (*e.g.*,

methylaluminoxane (MAO)) is used to promote the *in situ* formation of the active catalyst via a combined process of alkylation and abstraction.[71] For example, Wright *et al.* reported the use of *O,N,N*-titanium(IV) fluoride precatalysts (**44a, 44b**) in ethylene polymerisation. These six-coordinate *N,N,O*-titanium(IV) fluoride complexes were prepared using a one-step HF elimination protocol from *cis*-[$(THF)_2TiF_4$] and the corresponding pincer ligand precursor. Furthermore, the chloride analogues **45a** and **45b** were also synthesised for comparison (**Scheme 1.2.13**). [72]

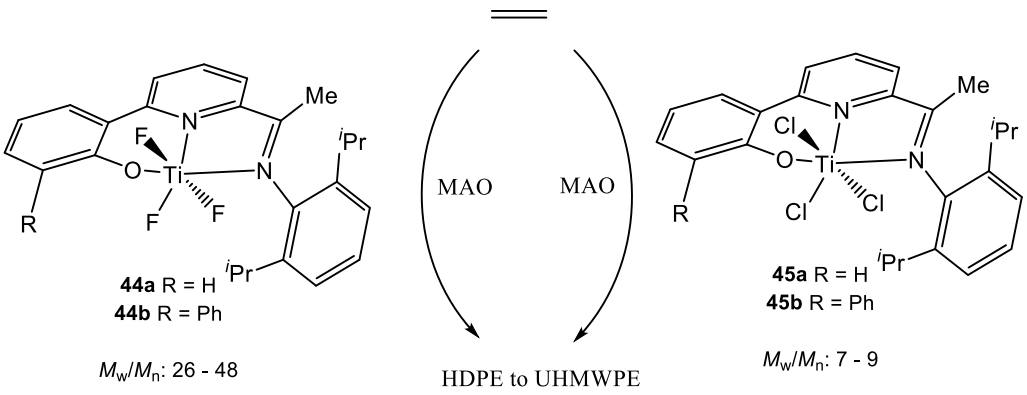

Scheme 1.2.13: Active *N,N,O*-titanium(IV) fluoride precatalysts for ethylene polymerisation.[72]

The results of ethylene polymerisation evaluation showed that both *N,N,O*-Ti(IV) complexes showed good activity in olefin polymerisation. Although the best activity was achieved by Ti(IV) chloride precatalyst (**45**) (340 g mol^{-1} h^{-1} bar^{-1}), the Ti(IV) fluoride complexes **44** produced ultra-high-molecular-weight polyethylene (UHMWPE). It was concluded that the fluoride complexes have a significant effect not only on the molecular weight but also on the molecular weight distribution.[72]

1.3 Overall conclusions to Chapter 1

The pincer ligand motif has gained the status of being a privileged platform in organometallic and coordination chemistry due to its many successful applications. In this introductory chapter, the synthesis and applications of mainly late first row d-block complexes containing different types of carbon- and nitrogen-based symmetrical and unsymmetrical tridentate pincer ligands have been reviewed. The *N,*N_{py}*,N* ligands are the most convenient type that can catalyse many coupling and polymerisation reactions. However, the introduction of inequivalent exterior donor atoms to the pincer ligand architecture has been shown to modify reactivity and, in some cases, enhance their ability to act as efficient catalysts. Therefore, the work in this thesis will build on this

potential by exploring the use of some less explored unsymmetrical pyridine-based pincer ligands as supports for late first row d-block metals.

1.4 Research Aims

This thesis is concerned with the application of unsymmetrical pyridine-based *N,N$_{py}$,N* and *N,N$_{py}$,O* ligands in the coordination chemistry of late d-block metals (e.g., Zn^{II}, Co^{II}, Ni^{II}, Fe^{II}); the reactivity and catalysis of selected complexes will also be examined.

More specifically the research aims of this work are:

1) To synthesise novel complexes containing unsymmetrical *N,N$_{py}$,N* and *N,N$_{py}$,O* (pro)ligands using a variety of first row d-block metal(II) chloride salts (**Chapters 2 (Zn), 3 (Co), 4 (Ni), 5 (Fe)**).

2) To use the same types of ligand to promote the formation of first row d-block metal(II) tetrafluoroborate pincer complexes with a view to investigating their B-F activation chemistry (**Chapters 2 (Zn), 3 (Co), 4 (Ni)**).

3) To explore the capacity of the chloride complexes prepared in part 1) to serve as precursors to metal fluoride complexes using fluorinating reagents such as CsF and AgF (**Chapters 2 (Zn), 3 (Co), 4 (Ni)**).

4) To explore the use of iron(II) tetrafluoroborate complexes in precatalysts in ethylene polymerisation (**Chapter 5**).

All products including (pro)ligands and complexes were characterised by using various spectroscopic techniques including multinuclear NMR, FT-IR spectroscopy, mass spectrometry, single crystal X-ray crystallography and elemental analysis. All *N,N$_{py}$,N* and *N,N$_{py}$,O* (pro)ligands to be explored in this thesis are depicted in **Fig. 1.2.9.**

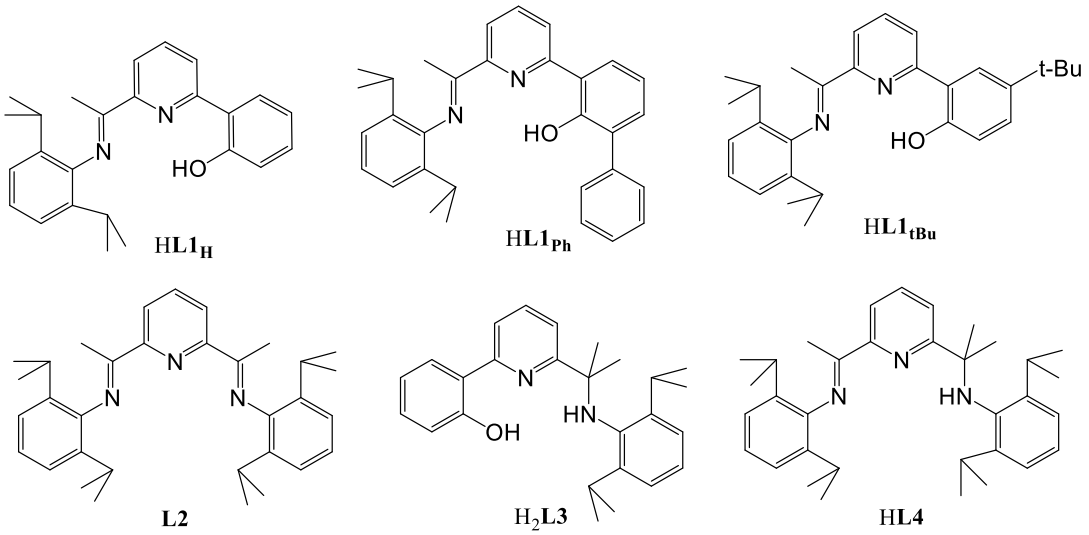

Figure 1.2.9: (Pro)ligand frames to be employed in this thesis.

References

1. E. Peris and H. Crabtree, *Chem. Soc. Rev.,* 2018, **47**, 1959-1968.
2. a) C. Gunanthan and D. Milstein, *Chem. Rev.,* 2014, **114**, 12024-12087. b) D. Benito-Garagorri and K. Kirchner, *Acc. Chem. Res.,* 2008, **41**, 201-213. c) N. Selander and K. J. Szabo, *Chem. Rev.,* 2011, **11**, 2048-2076. d) G. Bauer and X. Hu, *Inorg. Chem. Front.,* 2016, **3**, 741-765. e) M. E. O'Reilly and A. S. Veige, *Chem. Soc. Rev.,* 2014, **43**, 6325-6369.
3. J. Choi, A. H. R. MacArthur, M. Brookhart and A. S. Goldman, *Chem. Rev.,* 2011, **111**, 1761-1779.
4. G. van Koten and D. Milstein, *Organometallic Pincer Chemistry, Springer-Verlag, Beilin-Heidelberg*, 2013.
5. Q.-H. Deng, R. L. Melen and L. H. Gade, *Acc. Chem. Res.,* 1024, **47**, 3162-3173.
6. M. Albrecht, *Chem. Rev.,* 2010, **110**, 576-623.
7. a) J. I. van der Vlugt and J. N. H. Reek, *Angew. Chem., Int. Ed.,* 2009, **48**, 8832-8846. b) M. Albrecht and G. van Koten, *Angew. Chem., Int. Ed.,* 2001, **40**, 3750-3781. c) M. E. van der Boom and D. Milstein*, Chem. Rev.,* 2003, **103**, 1759-1792. d) H. Valdes, L. Gonzalez-Sebastian and D. Morales-Morales, *J. Organomet. Chem.,* 2017, **845**, 229-257. e) P. Pugh and A. A. Danopoulus, *Coord. Chem. Rev.,* 2007, **251**, 610-641. f) A. Kumar, T. M. Bhatti and A. S. Goldman, *Chem. Rev.,* 2017, **117**, 12357-12384.
8. M. Ohff, A. Ohff, M. E. van der Boom and D. Milstein, *J. Am. Chem.,* 1997, **119**, 11687-11690.
9. J. M. Longmire and X. Zhang, *Tetrahedron Lett.,* 1997, **38**, 1725-1730.
10. J. M. Longmire, X. Zhang and M Shang*, Organometallics,* 1998, **17**, 4374-4379.
11. C. Jensen, *Chem. Commun.,* 1999, 2443-2447.
12. S. M. Nelson and W. V. Dahlhoff, *J. Chem. Soc. A.,* 1971, **13**, 2184-2190.
13. a) C. J. Moulton and B. L. Shaw, *J. Chem. Soc., Dalton Trans.,* 1976, 1020-1024. b) H. Rimml and L. Venanzi, *J. Organomet. Chem.,* 1083, **259,** C6-C7.
14. a) R. F. Heck, *J. Am. Chem. Soc.,* 1968, **90**, 5518-5526. b) R. Heck., *Org. React.*, 1982, **27**, 345-348. c) R. F. Heck, *Comprehensive Organic Synthesis: selectivity, Strategy and efficiency in Modern Organic Chemistry;* B.M. Trost; Fleming, I., *Eds.;* 1991; **Vol. 4**. P 833, Chapter 4.3. d) W. Cabri, *Acc. Chem. Res.,* 1995, **28**, 2. e) I. P. Beletskaya and A. V. Cheprakov, *Chem. Rev.*, 2000, **200**, 3009-3012.

15. D. Morales-Morales, *Rev. Soc. Quím. Méx.,* 2004, **48**, 338-339.
16. a) D. Morales-Morales, R. Redon, C. Yung and C. M. Jensenm *Chem. Commun.,* 2000, 1619-1623. b) D. Morales-Morales, C. Grause, K. Kasaoka, R. Redón, R. E. Cramer and C. M. Jensen, *Inorg. Chem. Acta,* 2000, **300-302**, 958.
17. C. J. Moulton and B. L. Shaw, *J. Chem. Soc., Dalton Trans.,* 1976, 1020-1024.
18. a) H. Rimml and L. M. Venanzi, *J. Organomet. Chem.*, 1983, **259**, C6-C7. b) C. S. Creaser and W. C. Kaska, *Inorg. Chim. Acta,* 1978, **30**, L325-L326. c) A. R. Kennedy, R. J. Cross and K. W. Muir, *Inorg. Chim. Acta,* 1995, **231**, 195-200.
19. M. W. Haenel, D. Jakubik, C. Krüger and P. Betz, *Chem. Ber.,* 1991, **124**, 333-339.
20. V. Pandarus and D. Zargarian, *Chem. Commun.*, 2007, 978-980.
21. W. Schirmer, U. Flörke and H.-J. Haupt, *Z. Anorg. Allg. Chem.,* 1987, **545**, 83-97.
22. D. Benito-Garagorri, V. Bocokic, K. Mereiter and K. Kirchner, *Organometallics*, 2006, **25**, 3817-3823.
23. D. Benito-Garagorri and K. Kirchner, *Acc. Chem. Res.*, 2008, **41**, 201-213.
24. S. Fischer and O. F. Wendt, *Acta Crystallogr.*, 2004, **E60**, m69-m70.
25. Z.-Z Liu, W. Gao, J.-S. Zhang, D.-M. Cui, Q.-L. Wu and Y. Wu, *Organomallics,* 2010, **29**, 5783-5790.
26. C. A. Kruithof, H. P. Dijkstra, M. Lutz, A. L. Spek, R. J. M. K. Gebbink and G. van Koten, *Organometallics,* 2008, **27**, 4928-4927.
27. T.-A. Koizumi, T. Teratani, K. Okamoto, T. Yamamoto, Y. Shimoi and T. Kanbara, *Inorg. Chim. Acta,* 2010, **363**, 2474-2480.
28. S. M. Peterson, M. L. Helm and A. M. Appel, *Dalton Trans.,* 2015, **44**, 747-752.
29. Z. N. Gafurov, A. A. Kagilev, A. O Kantyukov, A. A. Balabaev, O. G. Sinyashin and D. G. Yakhvarov, *Russ. Chem. Bull., Int. Ed.,* 2018, **67**, 385-394.
30. E. Poverenov, M. Gandeleman, L. J. W. Shimon, H. Rozenberg, Y. Ben-David and D. Milstein, *Chem.–Eur. J.*, 2004, **10**, 4673-4684.
31. D, M, Spasyuk, D. Zargarian and A. van der Est, *Organometallics*, 2009, **28**, 6531-6540.
32. M.-J. Yang, Y.-J. Liu, J.-F Gong and M.-P. Song, *Organometallics*, 2011, **30**, 3793-3803.
33. W. D. Bailey, L. Luconi, A. Rossin, D. Yakhvarov, S. E. Flowers, W. Kaminsky, R. A. Kemp, G. Giambastiani and K. I. Goldberg, *Organometallics*, 2015, **34**, 3998-4010.

34. M. Gagliardo, N. Selander, N. C. Mehendale, G. van Koten, R. J. M. Klein Gebbink and K. J. Szabó, *Chem.–Eur. J.*, 2008, **14**, 4800-4809.
35. M. R. Eberhard, S. Matsukawa, Y. Yamamoto and C. M. Jensen, *J. Organomet. Chem*., 2003, **687**, 185-189.
36. B. Vabre, Y. Canac. C. Duhayon, R. Chaivin and D. Zargarian, *Chem. Commun*., 2012, **48**, 10446-10448.
37. S. S. Racharlawer, A. Kumar, N. Mirzadeh, S. K. Bhargava, J. Wagler and P. R. Likhar*, J. Organomet. Chem.*, 2014, **772-773**, 182-187.
38. V. A. Kozloc, D. V. Aleksanyan, Y. V. Neltubina, K. A. Lyssenko, A. A. Vasil'ev, P. V. Petrovskii and I. L. Odinets, *Organometallics,* 2010, **29**, 2054-2062.
39. L. Luconi, J, Klosin, A. J. Smith, S. Germain, E. Schulz, J. Hannedouche and G. Giambastiani, *Dalton Trans.,* 2013, **42**, 16056-16065.
40. J. Yan, Y.-B. Wang, Z.-H. Zhu, Y. Li, X. Zhu, X.-Q. Hao and M.-P, Song, *Organometallics,* 2018, **37**, 2325-2334.
41. D. M. Spasyuk, D. Zargarian and A. van der Est, *Organometallics*, 2009, **28**, 6531-6540.
42. D. M. Spasyuk and D. Zargarian, *Inorg. Chem.,* 2010, **49**, 6203-6213.
43. D. M. Spasyuk, S. I. Gorelsky, A. van der Est and D. Zargarian, *Inorg. Chem.*, 2011, **50**, 2661-2674.
44. J. B. Smith and A. J. M. Miller, *Organometallics,* 2015, **34**, 4669-4677.
45. B.-S. Zhang, W. Wang, D.-D. Shao, X.-Q. Hao, J.–F. Gong and M.-P. Song, *Organometallics,* 2010, **29**, 2579-2587.
46. M.-J. Yang, Y.-J. Liu, J.-F. Gong and M.-P. Song, *Organometallics*, 2011, **30**, 3793-3803.
47. J.-L. Niu, L.-T. Chen, X.-Q. Hao, Q.-X. Zhao, J.-F. Gong and M.-P. Song, *Organometallics,* 2010, **29**, 2148-2150.
48. J.-F. Gong, Y.-H. Zhang, M.-P, Song and C. Xu, *Organometallics*, 2007, **26**, 6487-6492.
49. B.-S. Zhang, C. Wang, J.-F. Gong and M.-P. Song, *J. Organomet. Chem.*, 2009, **694**, 2555-2561.
50. X.-Q. Hao, Y.-N. Wang, J.-R. Liu, K.-L. Wang, J.-F. Gong and M.-P. Song, *J. Organomet. Chem*., 2010, **695**, 82-89.
51. J.-L. Niu, X.-Q. Hao, J.-F. Gong and M.-P. Song, *Dalton Trans.,* 2011, **40**, 5135-5150.

52. M. Asay and D. Morales-Morales, *Dalton Trans.,* 2015, **44**, 17432-17438.
53. E. Peris and H. Crabtree, *Chem. Soc. Rev.*, 2018, **47**, 1959-1968.
54. K. Talukdar, A. Issa and J. W. Jurss, *Frontiers in Chemistry,* 2019, **7**, 1-11.
55. R. Tanaka, M. Yamashita and K. Nozaki, *J. Am. Chem. Soc.,* 2009, **131**, 14168-14169.
56. X.-Z. Yang, *ACS Catal.,* 2011, **1**, 849-854.
57. D. Benito-Garagorri, E. Becker, J. Wiedermann, W. Lackner, M. Pollak, K. Mereiter, J. Kisala and K. Kirchner, *Organometallics*, 2006, **25**, 1900-1913.
58. D. Benito-Garagorri, J. Wiedermann, M. Pollak, K. Mereiter and K. Kirchner, *Organometallics,* 2007, **26**, 217-222.
59. J. Zhang, M. Gandelman, D. Herrman, G. Leitus, L. J. W. Shimon, Y. Ben-David and D. Milstein, *Inorg. Chim. Acta.,* 2006, **359**, 1955-1960.
60. a) G. J. P. Britovsek, V. C. Gibson, B. S. Kimberley, P. J. Maddox, S. J. McTavish, G. A. Solan, A. J. P. White and D. J. Williams, *Chem. Commun.*, 1998, 849-850. b) B. L. Small and M. Brookhart, *J. Am. Chem. Soc.*, 1998, **120**, 7143-7144. c) B. L. Small, M. Brookhart and A. M. A. Bennett, *J. Am. Chem. Soc.,* 1998, **120**, 4049-4050. d) A. M. A. Bennett, *J. Am. Chem. Soc.*, 1998, **120**, 4049-4050. e) G. J. P. Britovsek, M. Bruce, V. C. Gibson, B. S. Kimberley, P. J. Maddox, S. Mastroianni, S. J. McTavish, C. Redshaw, G. A. Solan, S. Strömberg, A. J. P. White and D. J. Willams, *J. Am. Chem. Soc.*, 1999, **121**, 8728-8740.
61. O. Baldovino-Pantaleón, S. Hernández-Ortega and D. Morales-Morales, *Adv. Synth. Catal*., 2006, **348**, 236-242.
62. E. C. Alyea and P. H. Merrell, *Inorg. Chim. Acta,* 1978, **28**, 91-97.
63. D. Morales-Morales, *Rev. Soc. Quím. Méx.,* 2004, **48**, 338-339.
64. For selected reviews including homogeneous cobalt catalysis see: a) Y.-Y. Li, S. L. Yu, W.-Y. Shi and J.-X. Gao, *Acc. Chem. Res.,* 2015, **48**, 2587-2598. b) J.-L. Renaud and S. Gaillard, *Synthesis,* 2016, **48**, 3659-3683. c) F. Kallmeier, R. Kempe, *Angew. Chem. Int. Ed.,* 2018, **57**, 46-60; *Angew. Chem.* 2018, **130**, 48-63. d) G. A. Filonenko, R. V. Putten, E. J. M. Hensen and E. A. Pidko, *Chem. Soc. Rev.*, 2018, **47**, 1459-1483.
65. R. P. Yu, J. M. Darmon, C. Milsmann, G. W. Margulieux, S. C. E. Stieber, S. DeBeer and P. J. Chirik, *J. Am. Chem. Soc.,* 2013, **135**, 13168-13184.

66. a) S. Monfette, Z R. Turner, S. P. Semproni and P. J. Chirik, *J. Am. Chem. Soc.*, 2012, **134**, 4561-4564; b) J. Chen, C. Chen, C. Ji and Z. Lu, *Org. Lett.,* 2016, **18**, 1594-1597.

67. a) D. Benito-Garagorri, K. Kirchner, A. M. Trzeciak, E. Mieczyńisla and J. J. Ziólkowski, *Pol. J. of Chem.,* 2008, **82**, 1687-1687. b) C. Arana, S. Yan, M. Keshavarz-K, K. T. Potts and H. D. Abruna, *Inorg. Chem.,* 1992, **31**, 3680-3682. c) G. Chiericato Jr., C. R. Arana, C. Casado, I. Cuadrado and H. D. Abruña, *Inorg. Chim. Acta*, 2000, **300-302**, 32-42. d) N. Elgrishi, M. B. Chambers, V. Artero and M. Fontecave, *Phys. Chem. Chem. Phys.*, 2014, **16**, 13635-13644. e) M.-L. Sheng, N. Jiang, S. Gustafson, B. You, D. H. Ess and Y.-J. Sun, *Dalton Trans.,* 2015, **44**, 16247-16250. f) G. K. Rao, W. Pell, I. Korobkov and D. Richeson, *Chem. Commun.*, 2016, 8010-8013. g) J. D. Cope, N. P. Liyanage, P. K. Kelley, J. A. Denny, E. J. Valente, C. E. Webster, J. H. Delcamp and T. K. Hollis, *Chem. Commun.*, 2017, **52**, 9442-9445. h) J. A. Therrien, M. O. Wolf and B. O. Patrick, *Dalton Trans*., 2018, **47**, 1827-1840. i) T. H. T. Myren, A. M. Lilio, C. G. Huntzinger, J. W. Horstman, T. A. Stinson, T. B. Donadt, C. Moore, B. Lana, H. H. Funke and O. R. Luca, *Organometallics*, 2019, **38**, 1248-1253.

68. K. Talukdar, A. Issa and J. W. Jurss, *Frontiers in Chemistry*, 2019, **7**, 1-11.

69. T. K. Michaelos, D. Y. Shopov, S. B. Sinha, L. S. Sharinghausen, K. J. Fisher, H. M. C. Lant, R. H. Crabtree and G. W. Brudvig, *Acc. Chem. Res.,* 2017, **50**, 952-959.

70. a) M. D. Kärkäa, O. Verho, E. V. Johnston and B. Åkermark, *Chem. Rev.,* 2014, **114**, 11863-12001. b) J. D. Blakemore, R. H. Crabtree and G. W. Brudvig, *Chem. Rev.,* 2015, **115**, 12974-13005.

71. a) M. Bochmann, *Organometallics,* 2010, **28**, 4711-4719. b) E. Y. X. Chen and T. J. Marks, *Chem. Rec.,* 2000, **100**, 1391-1396.

72. L. A. Wright, E. G. Hope, G. A. Solan, W. B. Cross and K. Singh, *Organometallics,* 2016, **35**, 1183-1190.

Chapter 2

Zinc(II) chloride and tetrafluoroborate complexes supported by *N,N,O*- and *N,N,N*-pincer ligands

2.1 Introduction

In this chapter, the overall aim is develop and explore the coordination chemistry of zinc(II) chloride and tetrafluoroborate complexes bearing N,N_{py},O and N,N_{py},N pincer ligands. As a secondary aim, the mode of degradation of a tetrafluoroborate counterion/ligand, when part of a zinc pincer complex, will be studied with a view to exploring this approach as a potential route to zinc-fluoride complexes. Additional attempts to make zinc fluorides by chloride-fluoride exchange strategies are also presented. To set the scene for the synthetic work, some background of zinc chemistry to be provided, zinc-based pincer complexes and the use of BF_4^- ions as a fluoride source in zinc chemistry.

2.1.1 Zinc(II) pincer complexes and their applications

Pincer ligands and their use in stabilising metal complexes has already been introduced and discussed in Chapter 1. In this chapter the focus is mainly on symmetrical and unsymmetrical tridentate pincer ligands and their use in zinc chemistry. Indeed, many examples of zinc pincer complexes have been reported including those based on *P,N,P, P,N,N* and *C,N,N etc*.[1] However, this introduction is concerned with solely *N,N,N*- and *N,N,O*-types that form the basis of the synthetic work described in this work.

In general, zinc and its complexes have been attracting attention in biology, medicine, materials and catalysis. For example, the discovery of zinc finger proteins and their key function in gene expression has been the subject of much interest. Moreover, with an expanding understanding of its role in the central nervous system and neurodegenerative disorders as well as a critical cofactor for many cellular functions, interest in zinc chemistry is set to continue.[2]

In 2005, the first two examples of zinc(II) pincer complexes bearing sterically bulky bis(imino)pyridine ligands (**Fig. 2.1.1:** complexes **1**, **2**) were reported by Fan and co-workers.[4] Both complexes showed blue luminescence at room temperature in solution and in the solid state; this observation was attributed to the π*-π transition centred on the ligands with the Zn(II) centre playing a key role in enhancing the fluorescent emission of the ligands. In addition, complex **2** was reported again in 2010, when supported onto a nanocrystalline TiO_2 film to form a co-sensitised photoelectrode for dye-sensitised solar cell (DSSC) applications.[5] Such a cell yields a remarkably high photocurrent density, one circuit voltage and an energy conversion efficiency under standard irradiation conditions, which are higher than those for DSSCs using single organic sensitisers.[5]

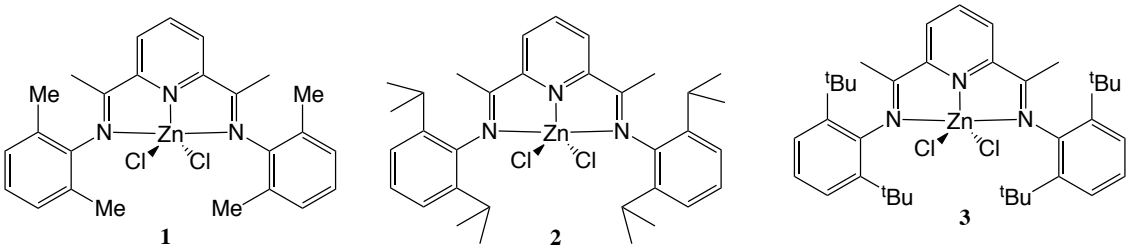

Figure 2.1.1: Structures of Zn(II) pincer complexes bearing bis(imino)pyridine ligands[5,6]

Elsewhere, complexes **2** and **3** (the latter bearing a 2,5-di-*tert*-butylphenyl *N*-aryl group) were synthesised and investigated as precatalysts for ethylene and norbornene polymerisation by Chen *et al*. (**Fig. 2.1.1**).[6] A range of different conditions such as the amount of MAO (methylaluminoxane) co-catalyst and temperature of the polymerisation were studied. However, the results showed that **2** and **3** were inactive for the polymerisation of ethylene or norbornene over all the conditions explored.[6]

The Solan group published the synthesis of neutral monozinc complex **4** and dizinc **5** (**Fig. 2.1.2**).[7] For **5**, the $ZnCl_2$ units fill inequivalent binding sites (tridentate and bidentate) within the ligand. Bimetallic **5** could also be obtained from the reaction of **4** and a further equivalent of $ZnCl_2$ in acetonitrile at room temperature. In solution, fluxional behaviour was observed for both. In 2018, Patil *et al.* studied the photophysical properties of the two novel mononuclear zinc(II) complexes, **6** and **7**, in both solution and solid phase (**Fig. 2.1.2**). In solution, the absolute quantum yield of fluorescence for the complexes was in the order **6**(0.01) < **7**(0.030), while in the solid-state it changed to **7**(0.034) < **6**(0.69). It was viewed that the intense and extensive

non-covalent interactions present in the crystal structure resulted in the quenching of fluorescence intensity of **7** in the solid-state.[7]

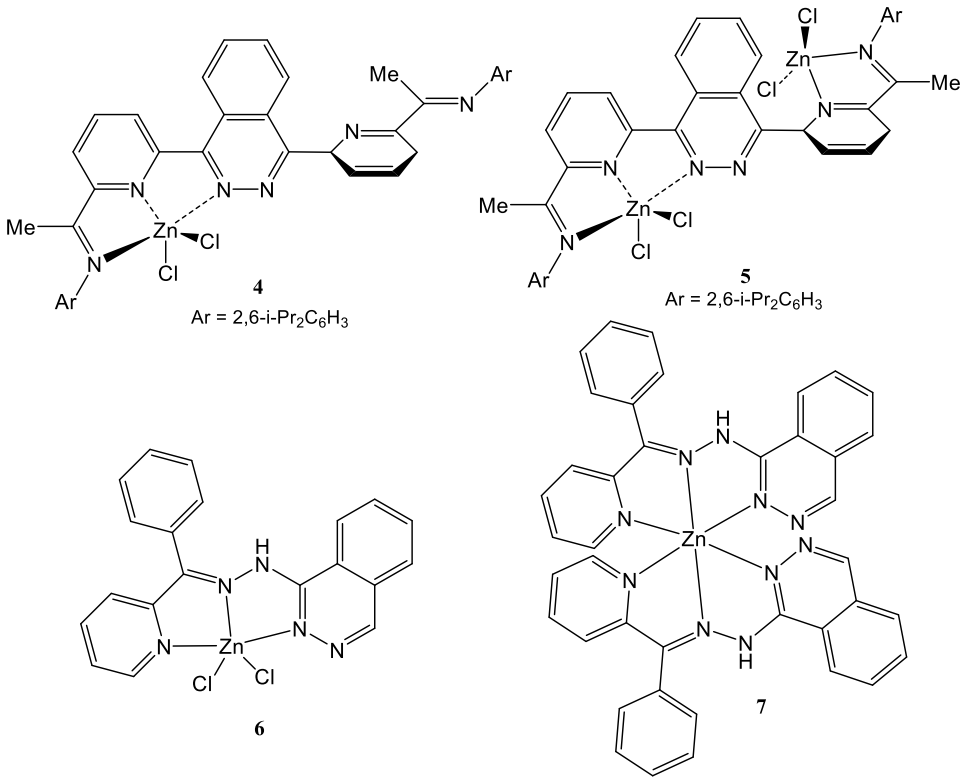

Figure 2.1.2: *N,N,N*-containing zinc(II) complexes, **4**, **5**, **6** and **7.**[6,7]

Elsewhere, on account of the nontoxic and harmless properties of zinc along with its cost-effectiveness, its complexes have been explored as catalysts for the ring opening polymerisation (ROP) of lactide and other cyclic esters.[3] The first Schiff base zinc complex used as an initiator for polymerisation of *L*-lactide was published by Chisholm *et al.*[43] Due their simple synthesis, tridentate nitrogen containing Schiff base ligands derived from β-diketones have been widely been explored as supports for a wide variety of metal including zinc.[44] In 2019, the binuclear Zn(II) complexes **8a-f** supported by pyridyl-based tridentate amino-phenolate ligands were reported and their catalytic properties for the ROP of *rac*-lactide were examined (**Scheme 2.1.1: A** & **B**).[45] All of these complexes showed efficient activity in toluene or tetrahydrofuran in the presence or absence of isopropanol, affording atactic or moderate isotactic bias PLAs. The researchers also noticed the importance of the type of substituent and position on the pincer framework and their effect on the activity and stereoselectivity.

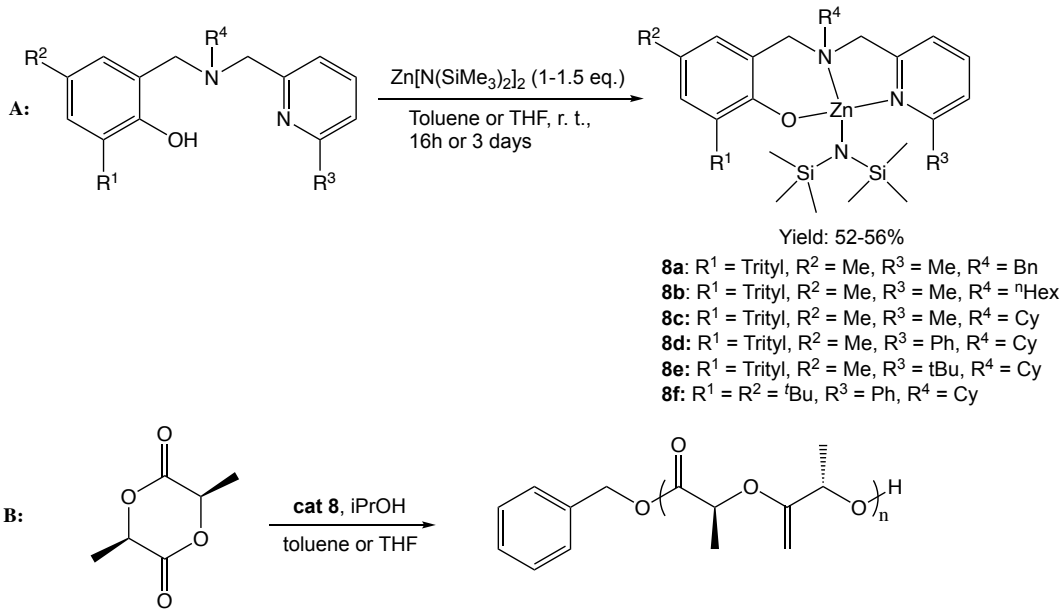

Scheme 2.1.1: A) Synthetic route to zinc complexes **8a-8f**. **B**) ROP of *rac*-lactide by using **8** as catalysts.[45]

2.1.2 Zinc(II) tetrafluoroborate complexes and their applications

Owing to the poor solubility, toxicity, general sensitivity and hydroscopic character of typical fluorinating agents (*e.g.,* F_2, HF, KF, XeF_2, CoF_3, etc.)[8], the controlled decomposition of a tetrafluoroborate anion (BF_4^-), through hydrolysis or fluoride abstraction, has emerged as a potential means of delivering a fluoride to a coordination compound.[9] Moreover, the use of metal tetrafluoroborate salts as a one-pot means to generate fluoride avoids the need to remove by-products that can be generated when using fluorinating agents.[10]

In 2007, the synthesis and characterisation of the dinuclear difluoride-bridged zinc(II) complex **9** bearing Schiff base oligopyrrolic octazamacrocycle ligand was reported by Sessler and co-workers (**Scheme 2.1.2**).[10] In their report, the macrocyclic ligand was reacted with zinc(II) tetrafluoroborate resulting in fluoride anion abstraction to generate **12**. Single crystal X-ray studies provided support for the notion that hydrogen-bonding interactions, involving the pyrrole N-H groups of the macrocycle and the coordinated fluoride ions, play an important role in stabilising these complexes.[10]

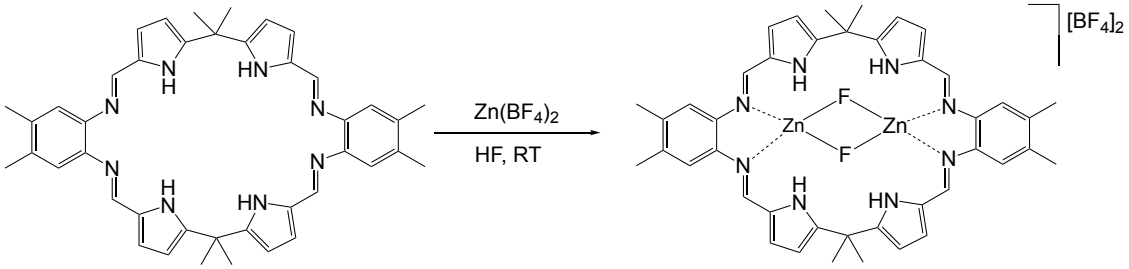

9

Scheme 2.1.2: Synthesis of dinuclear difluoride-bridged Zn(II) complex **9.**[10]

In terms of the zinc-fluoride distances in **9** (1.938–2.187 Å), these were found to fall within the range observed for other fluoride-bridged zinc complexes [11]. Moreover, these distances were notably longer than those for zinc cations coordinated to terminal fluorides (*ca.* 1.85 Å).[12] However no signal attributable to the fluoride ligands was observed in the ^{19}F NMR spectrum of **9**. The authors indicated that this is a rather common phenomenon and its origin not fully understood.[13] Elsewhere, it has been attributed by others to interactions with the residual water in the deuterated solvents employed for the analyses.[14] Furthermore, this paper also mentioned that the Lewis acid promoted decomposition of the tetrafluoroborate anion can occur *via* two different mechanisms involving fluoride abstraction or hydrolysis. Notably, the ^{19}F NMR spectrum of the crude reaction mixture showed a resonance for a molecule of BF_3 (δ -148.6) as a reaction by-product. These findings, as well as the lack of signals attributable to tetrafluoroborate hydrolysis products, ruled out a hydrolysis-based mechanism. Accordingly, they attributed the formation of the fluoride bridges seen in **9** to a fluoride abstraction mechanism.[10]

Elsewhere, a range of zinc(II) fluoride-bridged complexes bearing alkylidene-linked ditopic bis(pyrazoly)methane ligands were reported by Hahn *et al.* in 2007, which showed similar results to that discussed above.[12] The ^{19}F NMR spectra of the pure complexes showed the expected BF_4^- signal at δ -150.0 as well as much weaker signals corresponding to the solvated BF_3. No fluoride resonances were observed but the observation of BF_3 implies the presence of F^-. They concluded it is likely that low concentrations combined with longer relaxation times (T_1) prevent the detection of the fluoride anion, presumably coordinated to zinc.[12]

In 2003, the unsymmetrical, aliphatic tripodal ligand $N(CH_2CH_2NH_2)_2(CH_2CH_2OH)$ was prepared and its coordination chemistry with $Zn(BF_4)_2$ studied by Hahn *et al*.[12]

Following work-up, the trigonal-bipyramidal complex **10** (**Scheme 2.1.3**) incorporating a monodentate fluoride ligand was isolated. The monodentate ligand was successfully refined as a fluoride in the X-ray determination. This was confirmed by ^{19}F NMR spectroscopy, which revealed two signals at δ -162.0 and δ -143.1 for the monodentate fluoride and BF_4^- anion, respectively. The authors assumed that after initial BF_4^- coordination to the zinc atom, the addition of diethyl ether and DMSO facilitated the liberation of $F_3B{\cdot}$solvent and the formation of complex **10**.[12]

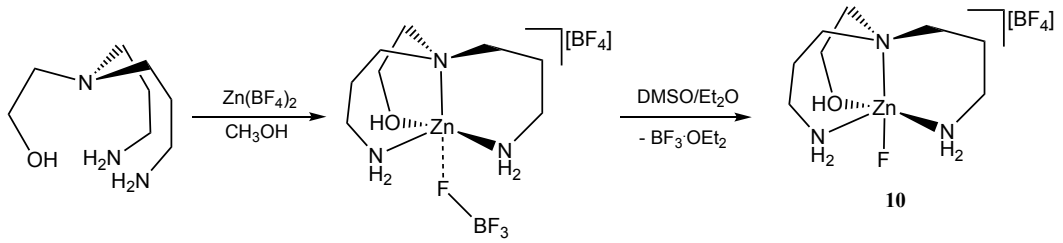

Scheme 2.1.3: Proposed mechanism for the formation of fluoride complex **10.**[12]

On the other hand, there are many examples of zinc(II) tetrafluoroborate complexes in which the BF_4^- ions acts solely as a counteranion. For example, in 1998 Fenton and co-workers published a mononuclear zinc(II) complex $[LZn(C_6H_5CO_2)][BF_4]{\cdot}CH_3OH$ (L = tris(4-nitrophenyl)-phosphate) (**Fig. 2.1.3**: complex **11**), which was prepared from the reaction of tetradentate L and $Zn(BF_4)_2{\cdot}H_2O$ in methanol.[41] In 2012, Spiropulos *et al.* reported the synthesis and characterisation of the zinc O-alkyl thiocarbonate and dithiocarbonate complexes **12** and **13** (**Fig. 2.1.3**) as well as the cationic zinc hydrosulfide complex **14** (**Fig. 2.1.3**).[42] Complexes **12** and **13** were prepared from the reaction of tris(2-pyridylmethyl)amine and $Zn(BF_4)_2{\cdot}H_2O$, KOH and carbonyl sulphide in dry methanol (**15**) or ethanol (**13**), respectively. The zinc hydrosulfide complex **14** was formed by two methods, i) from the hydrolysis of **12** and **13** in a mixture of acetonitrile and water and ii) from reaction of same ligand with $Zn(BF)_2{\cdot}6H_2O$, KOH and H_2S in methanol.

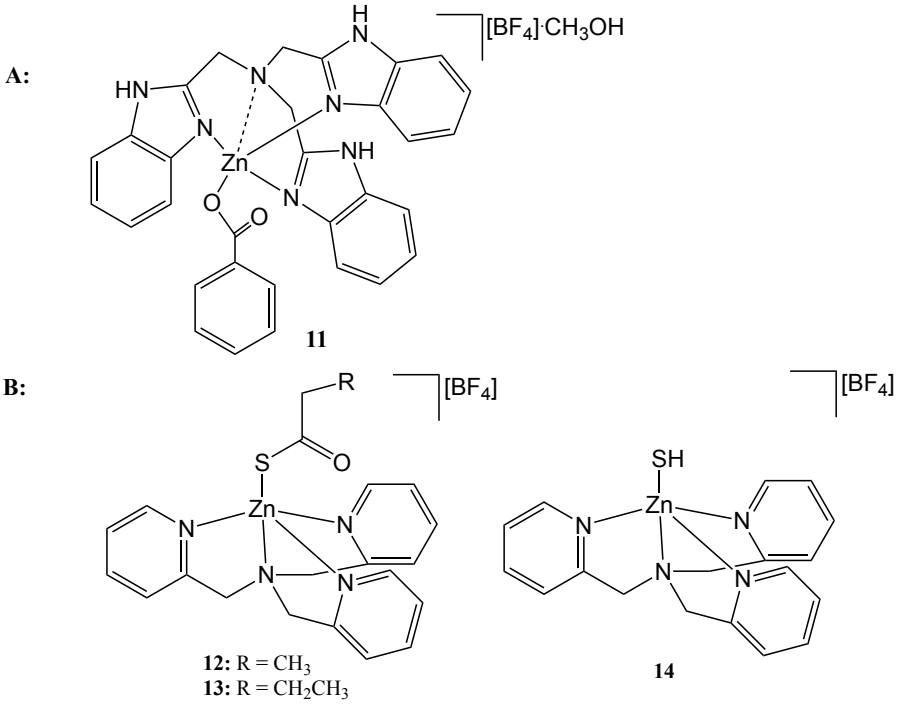

Figure 2.1.3: A) (Benzoate-O){tris[(2-benzimidazolyl-N3)-methyl]amine-N}-zinc(II) tetrafluoroborate complex **11**. **B**) Dithiocarbonate and thiocarbonate zinc complexes **12** and **13** along with zinc hydrosulfide complex **14.**[41,42]

2.2 Aims and objectives of Chapter 2

This chapter initially describes the synthesis and characterisation of four types of *N,N*$_{py}$*,O(H)* and two types of *N,N*$_{py}$*,N* pyridine-based pincer (pro)ligands that will be used in this Chapter and throughout the thesis (**Figure 2.2.1**). The four *N,N*$_{py}$*,O(H)* (pro)ligands targeted (H**L1**$_{\mathbf{H}}$, H**L1**$_{\mathbf{Ph}}$, H**L1**$_{\mathbf{tBu}}$, H$_2$**L3**) differ in their steric and electronic properties exerted by the phenol group (H, 6-Ph and 4-*tert*-butyl) and the exterior nitrogen donor (*N*$_{imine}$ *vs.* *N*$_{amine}$). In addition, the well-known symmetrical bis(2,6-diisopropylphenylimino)pyridine ligand, **L2**, is targeted along with its methylated derivative H**L4** to again allow an understanding of the effect of imine vs. amine nitrogen donors (**Figure 2.2.1**). In all cases, a *N*-2,6-diisopropyphenyl group was incorporated into the corresponding ligand structure. This was selected for three reasons: (a) recrystallisation of the metal complexes would be expected to be more straightforward; (b) the septet signal of the diisopropyl group in the ^{1}H NMR spectrum offers a straightforward, easy-to-spot resonance for tracking the progress of reactions; (c) the steric properties would likely impede aggregation in the resulting complexes.

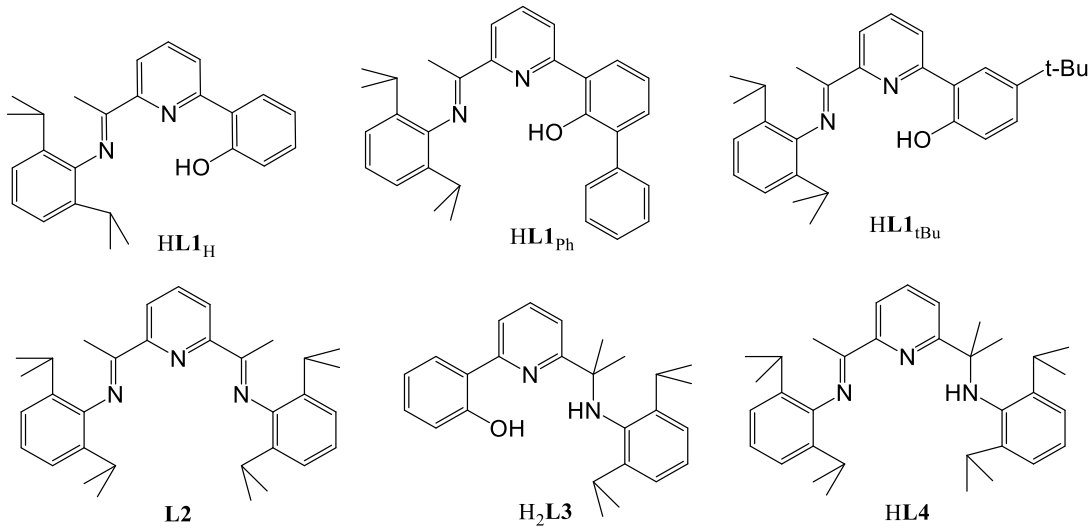

Figure 2.2.1: Types of (pro)ligand to be investigated in **Chapter 2.**

In the second part of this chapter, the synthesis of two classes of zinc(II) complex will be described namely those involving chloride and tetrafluoroborate. These complexes will be prepared from the reactions of the *N,N*$_{py}$*,O* or *N,N*$_{py}$*,N* (pro)ligands, H**L1**$_{R}$, **L2**, H_2**L3** and H**L4**, with either zinc(II) chloride or zinc(II) tetrafluoroborate. For each complex, characterisation will be undertaken by ^{1}H NMR and IR spectroscopy, mass spectrometry and elemental analysis. In addition, ^{19}F and ^{11}B NMR spectroscopy will be employed to explore the structures of tetrafluoroborate complexes in solution. Furthermore, single crystal X-ray diffraction will be used, where possible, to elucidate the structural type.

With particular regard to the tetrafluoroborate chemistry, the propensity of the BF_4 ion to serve as a counterion, ligand or undergo B-F bond cleavage/hydrolysis will also be examined. In addition, the capacity of selected zinc(II) chloride complexes to undergo reactions with CsF and AgF will also be probed.

2.3 Results and Discussion

2.3.1 Pincer ligand synthesis

2.3.1.1 Synthesis of phenol-pyridylimines, H**L1**$_{H}$, H**L1**$_{Ph}$ and H**L1**$_{tBu}$

The preparation of the phenol-pyridylimines, H**L1**$_{H}$, H**L1**$_{Ph}$ and H**L1**$_{tBu}$, was readily achieved in three steps from 2-bromo-6-acetyl pyridine.[15] Installation of the phenol

group was realised by the palladium-mediated Suzuki cross coupling reaction of 2-bromo-6-acetyl pyridine with either 2-hydroxyphenylboronic acid, 2-hydroxy-biphenyl-3-ylboronic acid or 2-hydroxy-4-tertiarybutylphenylboronic acid, respectively. These boronic acids were typically prepared by treating their corresponding bromide precursors with two equivalents of *n*-butyllithium at low temperature followed by the addition of an excess of triisopropylborate (**Scheme 2.3.1**). The resulting boron ester intermediates were then hydrolysed to give the target materials, **boronic acid-a**, **boronic acid-b** and **boronic acid-c**, in good yield.

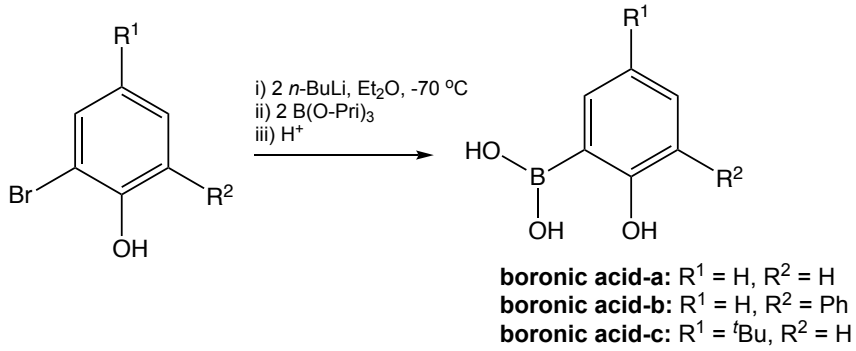

Scheme 2.3.1: Synthesis of the 2-hydroxylphenylboronic acids.

The three boronic acids were characterised by ^{1}H NMR spectroscopy to confirm their formation. It was noted that the ^{1}H NMR spectrum of **boronic acid-b** showed many broad and overlapping signals making the spectrum difficult to analyse; this broadening is likely attributable to potential aggregation processes as a result of the hydroscopic nature of the product.[16] Nevertheless, it was considered of sufficient purity to proceed into the next step.

Interaction of 2-bromo-6-acetylpyridine with the corresponding boronic acid in the presence of a catalytic quantity of $Pd(PPh_3)_4$ (**Scheme 2.3.2**) afforded, following crystallisation from methanol, the desired ketone product, **ketone-a, ketone-b** and **ketone-c**, in good yields. All data for the three ketones were found to be consistent with that given in the literature.[17-19]

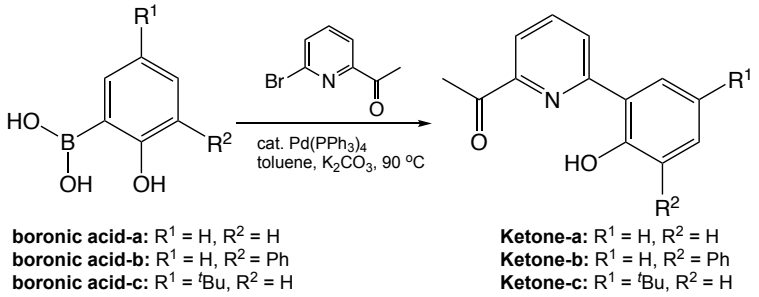

Scheme 2.3.2: Synthesis of **ketones a-c** from **boronic acids a-c.**

The phenol-pyridylimines, H**L1**$_{H}$, H**L1**$_{Ph}$ and H**L1**$_{tBu}$, could then be prepared in good yield from the condensation reaction of **ketone-a**, **ketone-b** and **ketone-c** with 2,6-diisopropylaniline in a 1:2 molar ratio using methanol as solvent and in the presence of formic acid as acid catalyst (**Scheme 2.3.3**).[19,20]

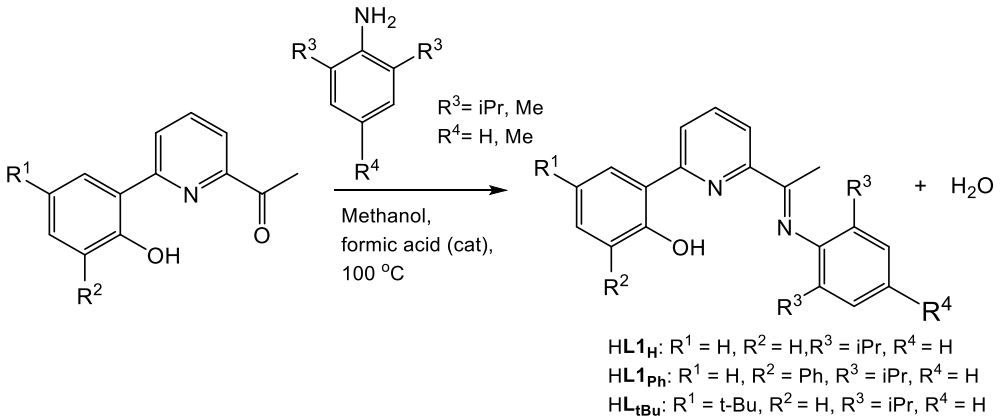

Scheme 2.3.3: Synthetic route to (pro)ligands H**L1**$_{H}$, H**L1**$_{Ph}$ and H**L1**$_{tBu}$

Compounds H**L1**$_{H}$, H**L1**$_{Ph}$ and H**L1**$_{tBu}$ were isolated as yellow solids by precipitation from cold methanol in yields of up to 90%. There was no sign of any impurities in either the ^{1}H or ^{13}C{^{1}H} NMR spectra of the products. The proton NMR spectra showed 2H septets in the range δ 2.06 - 2.71 and 1H singlets between δ 13.38-14.16 corresponding to the protons on the diisopropylphenyl and OH groups, respectively. All of the methyl protons (N=CCH_3) were clearly seen as singlets between δ 2.23 to 2.29. The ^{1}H NMR spectrum for H**L1**$_{tBu}$ showed a 9H singlet at δ 1.09 which corresponded to the *tert*-butyl group. The IR data of all three (pro)ligands typically revealed peaks at around 1578 cm^{-1}, 1640 cm^{-1} and 1222 cm^{-1} which were indicative of C=N$_{pyridine}$, C=N$_{imine}$ and OH absorptions, respectively. ESMS and HRMS spectrometric analysis displayed peaks characteristic of their protonated molecular ions. The crystal structure of H**L1**$_{Ph}$ has been reported elsewhere, [18] while that for H**L1**$_{tBu}$ is disclosed below.

Single crystals of H**L1**$_{tBu}$, suitable for a single crystal X-ray diffraction study, were grown by slow evaporation of a saturated dichloromethane solution. A view of the structure is shown in **Fig. 2.3.1**, while selected bond and angles are illustrated in **Table 2.3.1**. The structure revealed a *cis* arrangement between pyridine nitrogen and the phenol group, which was held in place as a result of a hydrogen bonding interaction between the pyridine nitrogen (N1) and the phenolic hydrogen (H1) atom; this accounted for the downfield shift of the phenolic proton in the ^{1}H NMR spectrum (δ 13.38 – 14.16). The C(12)-N(2) bond length of 1.279(4) Å was indicative of a C=N bond while the N(2)-C(12)-C(11) bond angle [117.3(3)°] was typical of a sp^{2} hybridised imine unit. In addition, a tetrahedral environment at C(20) was observed for the *tert*-butyl group.

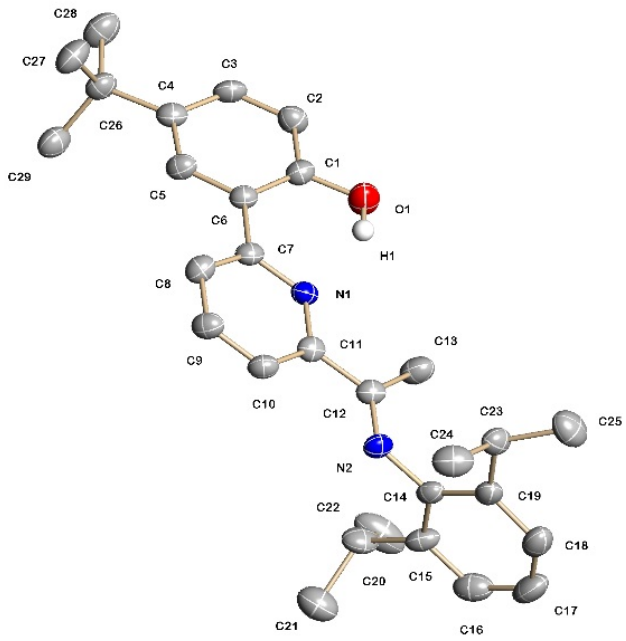

Figure 2.3.1: Molecular structure of H**L1**$_{tBu}$

Table 2.3.1: Selected bond lengths and angles for H**L1**$_{tBu}$

Bond Lengths (Å)	
O(1)-C(1)	1.368(4)
N(2)-C(12)	1.279(4)
C(6)-C(7)	1.473(4)
C(11)-C(12)	1.489(5)
O(1)-H(1)···N(1)	1.890
Bond Angles (°)	
N(2)-C(12)-C(11)	117.3(3)

C(12)-N(2)-C(14)	121.3(3)
C(11)-C(12)-C(13)	118.2(3)

The *gem*-dimethyl-containing compound H_2**L3** was additionally synthesised in good yield by sequential reductive methylation and hydrolysis of H**L1**$_H$ (**Scheme 2.3.4**).

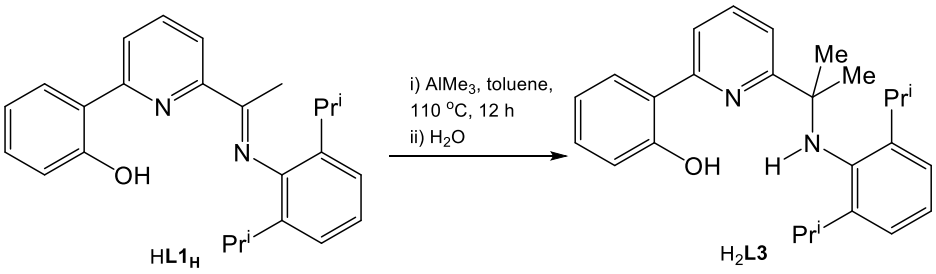

Scheme 2.3.4: Reductive methylation of H**L1**$_H$ to give *gem*-dimethyl amine H_2**L3**

Analysis of H_2**L3** by ^{1}H NMR spectroscopy revealed a characteristic 6H singlet peak at δ 1.48 corresponding to the equivalent *gem*-dimethyl protons. In addition, a broad peak was found at δ 3.34 which was ascribed to the NH proton. All data for H_2**L3** were found to be consistent with that reported in the literature.[21]

2.3.1.2 Preparation of **L2** and H**L4**

The ligand **L2** was synthesised according to a literature procedure involving an acid catalysed condensation reaction of 2,6-diacetylpyridine with two equivalents of 2,6-diisopropyl aniline.[22] The spectroscopic and analytical properties were as previously reported. As with H**L1**$_H$, one of the imine groups in **L2** could be readily reduced and methylated to give *gem*-dimethyl amine H**L4** in good yield (**Scheme 2.3.5**). Compound H**L4** has been characterised by ^{1}H, ^{13}C NMR, IR spectroscopy and mass spectrometry.

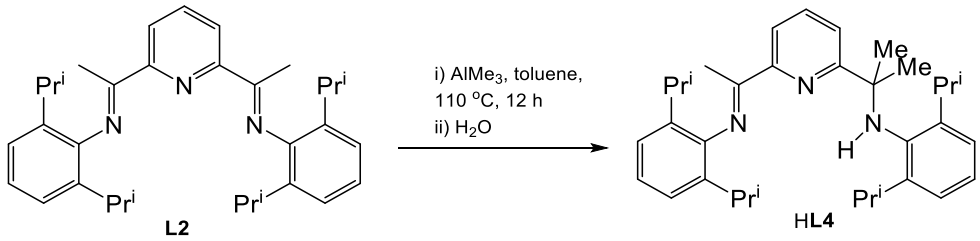

Scheme 2.3.5: Reductive methylation of H**L2** to give *gem*-dimethyl amine H**L4**

Analysis of H**L4** by ^{1}H NMR spectroscopy revealed a 6H singlet peak at δ 1.51 for the equivalent *gem*-dimethyl proton environments along with a broad resonance for the NH proton at δ 4.47. In addition, two pairs of 12H doublets (δ 1.17 and 1.07) and 2H (δ 3.31 and 2.77) septet peaks were seen highlighting the inequivalency of the isopropyl proton environments. The presence of an amine functional group in H**L4** was confirmed by the presence of a N-H absorption at 3362 cm^{-1} in its IR spectrum. H**L4** also displayed a protonated molecular ion peak on analysis by mass spectrometry. All data were found to be consistent with those given in the literature.[23]

2.3.2 Zinc(II) chloride complex synthesis

2.3.2.1 Reactivity of H**L1**$_{R}$ towards zinc(II) chloride

The three *N,N,O(H)* pincer (pro)ligands, H**L1**$_{H}$, H**L1**$_{Ph}$ and H**L1**$_{tBu}$, were first reacted with anhydrous $ZnCl_2$ in dry THF at room temperature for 16 hours. Two types of zinc(II) chloride products, namely mononuclear (H**L1**$_{R}$)$ZnCl_2$ (R = H **2.1a**, R = Ph **2.1b**) and binuclear complexes (**L1**$_{tBu}$)$_2Zn_2Cl_2$ (**2.2c**), could be isolated (**Scheme 2.3.6**).

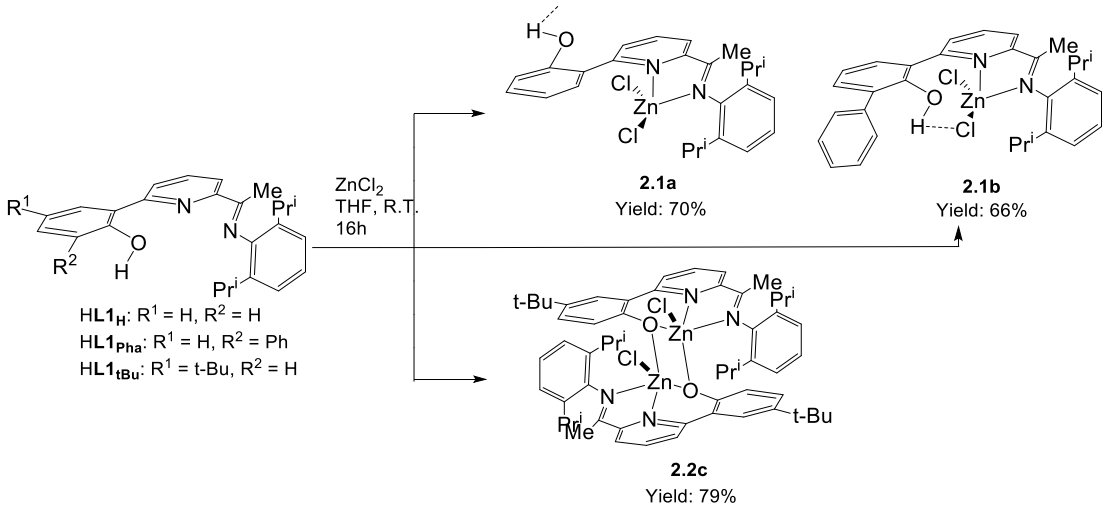

Scheme 2.3.6: Synthesis of zinc(II) chloride complexes **2.1a**, **2.1b** and **2.2c**

The spectroscopic data recorded for **2.1a**, **2.1b** and **2.2c** suggested that coordination of the ligands to zinc had been successful. For example, in **2.1a** two 6H doublets (δ 1.09 and δ 1.21) for CH*Me*$_2$ protons were seen which differs from one 12H doublet (δ 1.07) present in H**L1**$_{H}$. Furthermore, the *para*-H of the central pyridine shifted downfield due to its coordination to zinc. The signal of OH group shifted to highfield at δ 5.67 from

corresponding ligand δ 14.16, due to the hydrogen connection with chloride. Both **2.1b** and **2.2c** showed similar results in ^{1}H NMR spectrum. Infrared spectroscopy also confirmed the coordination of the zinc. For example, the stretching frequency of the bonded imine had shifted from 1640 (H**L1**$_{H}$), 1625 (H**L1**$_{Ph}$) and 1648 cm^{-1} (H**L1**$_{tBu}$) to 1618 (**2.1a**), 1621 (**2.1b**) and 1595 cm^{-1} (**2.2c**), which is consistent with imine coordination. The electrospray mass spectra (ESI-MS) rendered peaks at *m/z* 471, 547 and 1021 which could be assigned to the fragmentation peaks, [M-Cl]$^{+}$ (**2.1a**), [M-Cl]$^{+}$ (**2.1b**) and [M-Cl]$^{+}$ (**2.2c**), respectively. In addition, the X-ray structures of all three complexes (**2.1a, 2.1b** and **2.2c**) unambiguously confirmed their structural composition.

Crystallisation of **2.1a**, **2.1b** and **2.2c** from hot acetonitrile gave yellow crystals that proved suitable for single crystal X-ray diffraction studies. Views of their structures are shown in **Fig. 2.3.2** (**2.1a** and **2.1b**) and **Fig. 2.3.4** (**2.2c**); selected bond lengths and angles are collected in **Tables 2.3.2** and **2.3.3**.

The structures of **2.1a** and **2.1b** both revealed mononuclear zinc(II) chloride species supported by an intact *N,N$_{py}$,O(H)* ligand that coordinated as a *N,N*-bidentate ligand; the four-coordinate geometry can be best described as distorted tetrahedral. For both complexes, the phenol proton was retained and underwent either inter- (**2.1a**) or intramolecular (**2.1b**) hydrogen bonding interaction between the O-H proton and a chloride (OH···Cl 3.041 Å (**2.1a**), 2.450 Å (**2.1b**)) (**Fig. 2.3.3**). A single five-membered chelate ring size is present in each structure which incorporates a N(2)-Zn(1)-N(1) bond angle of 79.4(2)° (**2.1a**) and 80.07(12)° (**2.1b**). The imine unit retained its sp^{2} hybridisation as was evidenced by the N(2)-C(6)-C(7) bond angle of around 123.5(7)°, while the imine bonds have typical double-bond character with C-N bond lengths of 1.283(8) Å (**2.1a**) and 1.279(4) Å (**2.1b**).

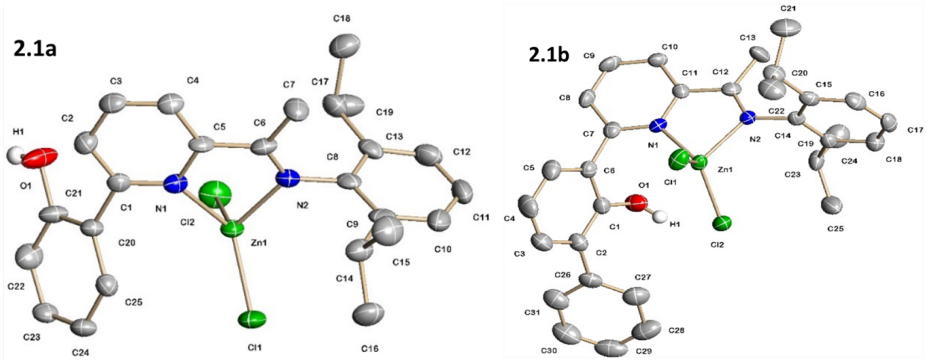

Figure 2.3.2: Molecular structures of **2.1a** and **2.1b.**

Table 2.3.2: Selected bond lengths and angles for **2.1a** and **2.1b.**

*Bond Lengths (Å) for **2.1a***		*Bond Lengths (Å) for **2.1b***	
Zn(1)-N(1)	2.075(6)	Zn(1)-N(1)	2.051(3)
Zn(1)-N(2)	2.073(6)	Zn(1)-N(2)	2.075(3)
Zn(1)-Cl(1)	2.185(2)	Zn(1)-Cl(1)	2.201(11)
C(6)-N(2)	1.283(8)	C(12)-N(2)	1.279(4)
O(1)-H(1)···Cl(2)	3.041	O(1)-H(1)···Cl(2)	2.45
*Bond Angles (°) for **2.1a***		*Bond Angles (°) for **2.1b***	
N(2)-Zn(1)-N(1)	79.4(2)	N(2)-Zn(1)-N(1)	80.07(12)
N(2)-Zn(1)-Cl(1)	112.36(17)	N(2)-Zn(1)-Cl(1)	112.12(8)
N(2)-C(6)-C(7)	123.5(7)	N(2)-C(12)-C(13)	124.5(4)

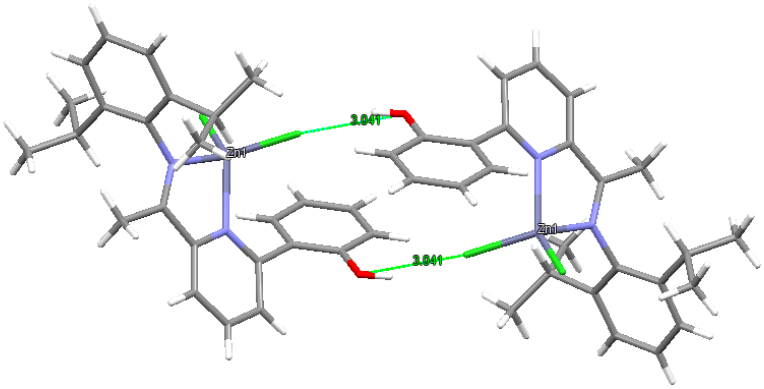

Figure 2.3.3: Bimetallic assembly through intermolecular OH···Cl hydrogen bonding in **2.1a**; image generated using Mercury software.

A view of **2.2c** is shown in **Fig. 2.3.4**, while selected bond lengths and angles are given in **Table 2.3.3**. The structure consists of a neutral dizinc species in which the two zinc centres are each *N,N,O*-chelated and linked by two μ-$O_{phenoxy}$ groups that derive from the pincer ligand. A chloride ligand completes the five coordinate geometry at each metal centre that can be best described as square pyramidal. Each tridentate ligand in **2.2c** contains an anionic phenoxy donor [O(1)] and two neutral nitrogen donors [N(1) and N(2)] which differs from the *N,N*-coordination seen in **2.1a** and **2.1b**. There are relatively few reports of μ-OR[34,35] and μ-OH[36] dizinc complexes bearing N-containing ligands; moreover those containing *N,N,O* ligands have not to the knowledge been reported. The central Zn-$N_{pyridine}$ bond length [2.1181(17) Å] is shorter than the exterior Zn-N_{imine} distance [2.1329(17) Å]. The Zn(1)-O(1) bond is the shortest bond from the chelating ligand to the zinc centre [2.049(15) Å]; similar values have

previously been published for μ-OR dizinc complexes [range: 2.039(5) to 2.114(4) Å].[34,35] The Zn···Zn separation of 3.181 Å is also comparable to that observed in previously reported $Zn^{II}(\mu\text{-}OR)_2Zn^{II}$ type structures [range: 3.166 to 3.309 Å].[34,35,36] Two types of chelate ring sizes are present with the larger six-membered ring containing an O(1)-Zn(1)-N(1) bond angle of 82.44(6)° while the five-membered ring a N(1)-Zn(1)-N(2) angle of 76.53(7)°. The N(2)-C(6)-C(7) bond angle [125.03(19)°] confirmed the presence of a sp^2 hybridised imine unit.

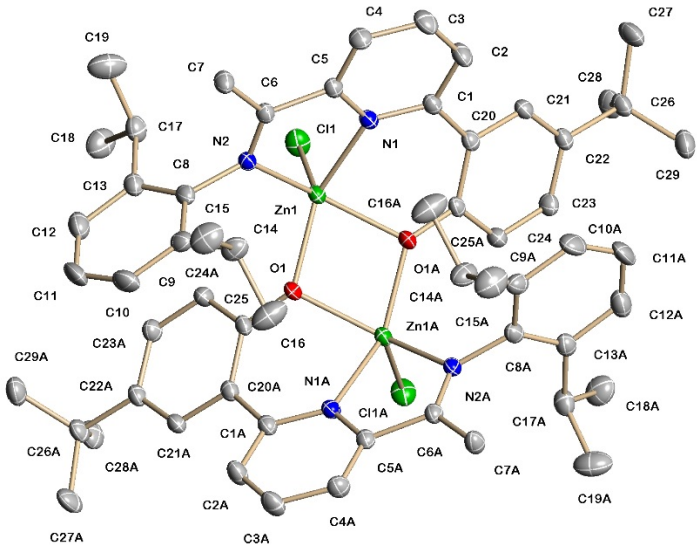

Figure 2.3.4: Molecular structure of **2.2c**

Table 2.3.3: Selected bond lengths and angles for **2.2c**

Bond Lengths (Å)	
Zn(1)-O(1)	2.0191(15)
Zn(1)-O(1A)	2.0499(15)
Zn(1A)-O(1)	2.0499(15)
Zn(1A)-O(1A)	2.0191(15)
Zn(1)-N(1)	2.1181(17)
Zn(1)-N(2)	2.1329(17)
Zn(1)-Cl(1)	2.2373(7)
Zn(1)···Zn(1A)	3.181
Bond Angles (°)	
N(1)-Zn(1)-N(2)	76.53(7)
O(1A)-Zn(1)-N(1)	82.44(6)
O(1)-Zn(1)-O(1A)	77.13(6)

N(1)-Zn(1)-Cl(1)	99.89(5)
N(2)-C(6)-C(7)	125.03(19)

The atoms labelled with an 'A' have been generated by symmetry

2.3.2.2 Reactivity of **L2** and H**L4** towards zinc(II) chloride

The reactions of the *N,N,N*-compounds **L2** and H**L4** with zinc(II) chloride were also investigated affording (**L2**)$ZnCl_2$ and (H**L4**)$ZnCl_2$ (**2.3**) in good yields (**Scheme 2.3.7**). The spectral data obtained for (**L2**)$ZnCl_2$ are all consistent with that reported in the literature.[24] Despite no crystallographic data being obtained for **2.3**, its structure could be readily assigned by mass spectrometry, elemental analysis and IR/NMR spectroscopy.

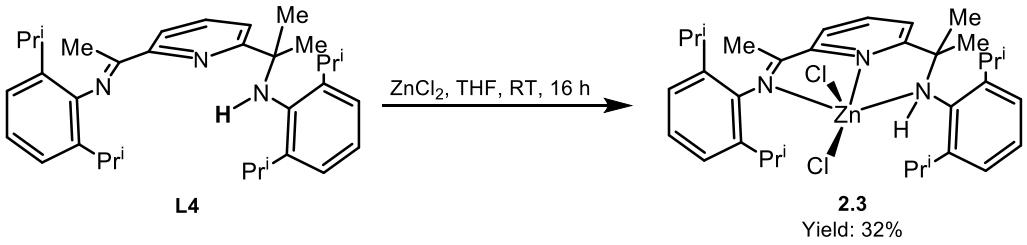

Scheme 2.3.7: Synthesis of *N,N,N*-zinc(II) chloride complex **2.3.**

In the infrared spectrum of **2.3**, the N-H_{amine} peak shifted from 3360 cm^{-1} in the free ligand to 3298 cm^{-1} which provided strong evidence for amine coordination. In addition, a strong fragmentation peak at 561 $[M\text{-}2Cl]^{2+}$ was observed in the FAB mass spectrum, while the elemental analysis gave results in good accordance with the calculated elemental composition.

Given the resistance to ligand deprotonation observed using H**L1**$_H$ and H**L1**$_{Ph}$ on reaction of $ZnCl_2$, we also explored using $ZnEt_2$ as the zinc reactant. Hence, reaction of H**L1**$_{Ph}$ and H**L1**$_{Phmes}$ (the synthetic details for latter have been reported elsewhere[46]) with diethylzinc were explored under inert conditions (**Scheme 2.3.8**). Bright orange crystals for both complexes were formed following csryatllisation from acetonitrile after standing in an inert atmosphere for few days. However the crystals of (**L1**$_{Ph}$)$_2$Zn proved too small for the X-ray beam no matter how many times the recrystallisations were attempted. Fortunately, a data set was collected for (**L1**$_{Phmes}$)$_2$Zn (**2.4**) (**Scheme 2.3.8**). Varying the molar ratio of H**L1**$_{Phmes}$ to diethylzinc from 1:1 to 2:1 also gave bis(ligand) complex **2.4** but in higher yield.

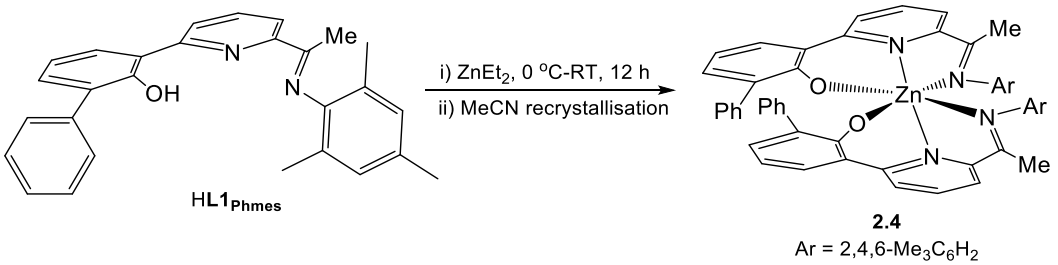

Scheme 2.3.8: Synthesis of bis(ligand) complex **2.4**.

Attempts to characterise **2.4** by ^{1}H NMR spectroscopy (in $CDCl_3$ and C_6D_6) were unsuccessful as hydrolysis occurred to re-form free H**L1**$_{Phmes}$; mass spectrometry also only showed evidence of free ligand. In the solid state IR spectrum of **2.4**, the ν(C=N$_{imine}$) and ν(C=N$_{pyridine}$) bands were both shifted to 1610 cm^{-1} and 1545 cm^{-1} from 1648 cm^{-1} and 1591 cm^{-1} (H**L1**$_{Phmes}$), respectively.

A representation of the X-ray structure of **2.4** is shown in **Figure 2.3.5**, while selected bond lengths and angles are compiled in **Table 2.3.4**.The structure comprised a zinc(II) centre that is bis-ligated by two *N,N$_{py}$,O* tridentate ligands to form a distorted octahedral geometry; the phenol proton of the proligand was deprotonated and the oxygen atom coordinated to zinc. The Zn(1)-O(1) bond length [1.9611(6) Å] is typical of that involving an anionic phenoxy donor [range: 1.973-2.168 Å][37,38] and is the shortest of the three metal-ligand distances. The central Zn-N$_{pyridine}$ bond length [2.146(19) Å] is slightly shorter than the Zn-N$_{imine}$ one [2.242(19) Å]. Within each five- and six-membered chelate rings the internal angles involving zinc were, N(1)-Zn(1)-N(2) 76.57(7)° and O(1)-Zn(1)-N(1) 88.36(7)°, respectively.

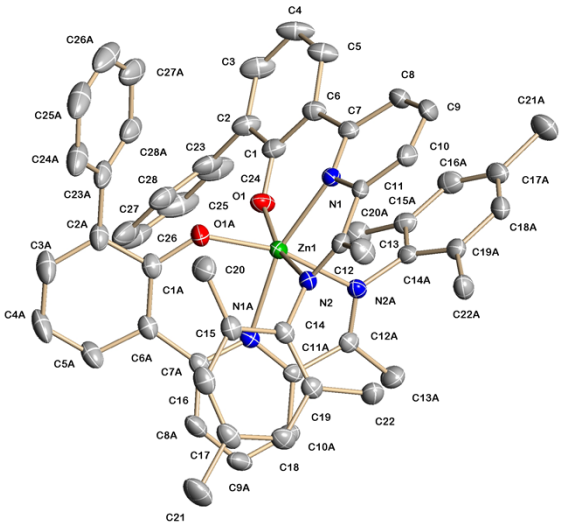

Figure 2.3.5: Molecular structure of **2.4**

Table 2.3.4: Selected bond lengths and angles of **2.4**

Bond Lengths (Å)	
Zn(1)-O(1)	1.9611(6)
Zn(1)-O(1)A	1.9611(6)
Zn(1)-N(1)	2.1464(19)
Zn(1)-N(2)	2.2422(19)
C(1)-O(1)	1.291(3)
Bond Angles (°)	
N(1)-Zn(1)-N(2)	76.57(7)
O(1)-Zn(1)-N(1)	88.36(7)
O(1)-Zn(1)-N(2)	164.79(7)
O(1)-Zn(1)-O(1A)	93.79(10)
N(2)-C(6)-C(7)	125.03(19)

2.3.3 Complexation with Zn(II) tetrafluoroborate

2.3.3.1 Reactivity of H**L1**$_R$ towards salts of the type $[Zn(OH_2)_6][BF_4]_2$, $[Zn(py)_4(NCMe)_2][BF_4]_2$ or $[Zn(NCMe)_6][BF_4]_2$

As noted in the introduction, there have been a number of reports that a tetrafluoroborate counterion in salts of the type $[L_nZn^{II}][BF_4]_n$ can act as a source of a F^- ligand for late d-block ions. [25] Herein, we explore the use of pincer complexes of zinc as a potential platform to mediate such B-F activation.

In the first instance the reactions of H**L1**$_H$ with $[Zn(OH_2)_6][BF_4]_2$ in acetonitrile at 80 ^oC in the presence or absence of pyridine were investigated. In the presence of pyridine $[(\mathbf{L1}_H)_2Zn_2(MeCN)(Py)][BF_4]_2$ (**2.5a**) was isolated while in the absence of pyridine $[(\mathbf{L1}_H)_2Zn_2(MeCN)_2(\mu\text{-}BF_4)][BF_4]$ (**2.5a'**) was formed (**Scheme 2.3.9**). We assumed that either $[Zn(py)_4(NCMe)_2][BF_4]_2$ or $[Zn(NCMe)_6][BF_4]_2$ were formed as intermediates in the corresponding reactions.[39] Similarly, reactions of H**L1**$_{Ph}$ and H**L1**$_{tBu}$ with $[Zn(py)_4(NCMe)_2][BF_4]_2$ (made *in-situ via* reaction of $[Zn(OH_2)_6][BF_4]_2$ with acetonitrile and pyridine) in acetonitrile at 80 ^oC were conducted affording $[\{\mathbf{L1}_R(BF_3)\}Zn(MeCN)(L)][BF_4]$ (R = Ph, L = Py **2.6b**, R = ^{t}Bu, L = MeCN **2.6c**). All four complexes were characterised by ^{1}H NMR, ^{19}F NMR, ^{11}B NMR, IR spectroscopy, ESI-MS, elemental analysis and X-ray diffraction.

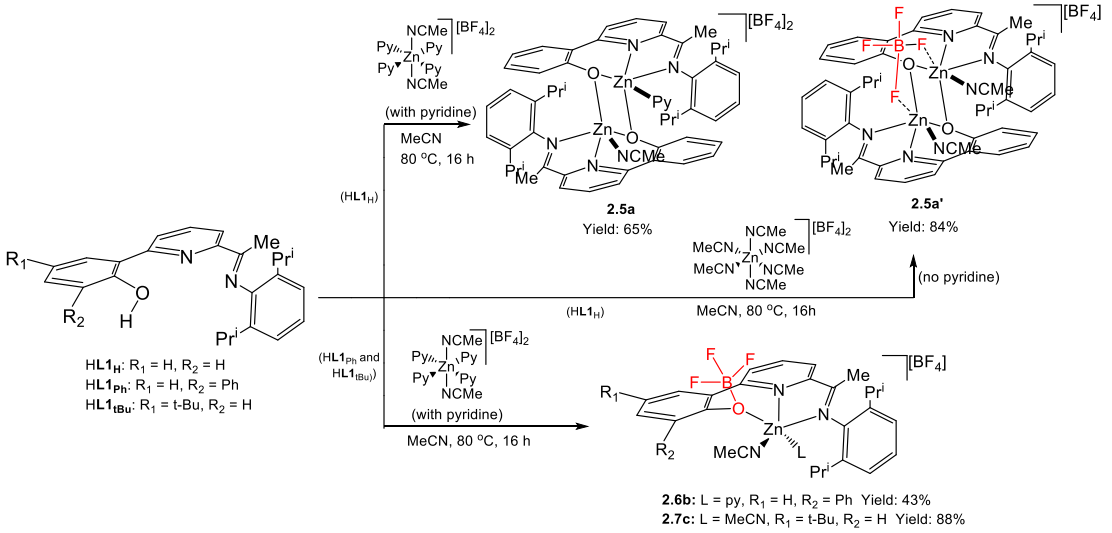

Scheme 2.3.9: Synthetic route to **2.5a**, **2.5a'**, **2.6b** and **2.7c**.

For 2.5a, two 2H septets (δ 2.73 and δ 2.59) for C*H*Me$_2$ and two 12H doublets (δ 0.89 and δ 0.48) for CH*Me*$_2$ were found in ^{1}H NMR spectra, which just show two signals in corresponding ligand H**L1$_H$** at δ 2.62 and δ 1.07, respectively. Moreover the triplet *para*-H of the central pyridine also shifted to downfield δ 7.89 to δ 8.44. Similar results can also been seen for **2.5a'**. The ^{19}F NMR spectra of **2.5a** and **2.5a'** both showed a singlet at *ca.* δ -151.83 corresponding to the BF_4^- counterion (*nb.* this signal comprised two resonances for $^{11}BF_4^-$ and $^{10}BF_4^-$ in a 4:1 ratio). In the case of **2.5a'**, there was an additional singlet resonance at δ -147.26 which has been assigned to the partially coordinated BF_4^- ligand. Meanwhile, in the ^{11}B NMR spectrum, both **2.5a** and **2.5a'** showed singlet resonances for the BF_4^- signals at δ -1.19, while **2.5a'** also showed a broad signal at δ -0.54 for μ-BF_4 ligand. In their IR spectra, the ν(C=N)$_{imine}$ absorption bands were both shifted by 45 cm^{-1} to lower wavenumber when compared alongside the same band in the free ligand. Analysis of **2.5a** and **2.5a'** by FAB mass spectrometry showed strong fragmentation peaks at 870.7612 [M-2BF_4-Py-MeCN]$^+$ and 870.7667 [M-2BF_4-2MeCN]$^+$, respectively, while their elemental analysis gave results consistent with the calculated elemental compositions. In addition, yellow cube-like crystals of **2.5a** ad **2.5a'** were grown from a layered MeCN-Et_2O (1:10) solution, which proved suitable for single crystal X-ray diffraction.

Perspective views of **2.5a** and **2.5a'** are shown in **Fig. 2.3.6**; selected bond lengths and angles are compiled in **Table 2.3.5**. The structures consist of a dizinc dicationic unit that is charge balanced by two tetrafluoroborate ions (in the case of **2.5a'**, one of the

BF_4 units has ligand-like character). As with **2.2c**, each zinc centre is chelated by an anionic *N,N,O*-ligand with the O unit additionally involved in bridging the two metal centres. In **2.5a**, the coordination spheres are completed by an acetonitrile at Zn(1) and a pyridine at Zn(2). By contrast, in **2.5a'** molecules of acetonitrile complete the coordination sphere of each zinc centre. Overall, the geometries can be best described as distorted square pyramidal geometry with pyridine or acetonitrile filling the apical position. In each structure the monodentate ligands on neighbouring metal centres (MeCN/Py (**2.5a**), MeCN/MeCN (**2.5a'**)) are positioned *cis* to one another. The shortest bond from the tridentate ligand to the zinc centre involves the phenoxy oxygen [Zn-O: 2.013(4), 2.025(4) Å (**2.5a**), 1.973(3) Å (**2.5a'**)], which are comparable with that previously observed in **2.2c** [2.0191(15) Å]. As a notable difference to **2.5a**, one BF_4^- ion in **2.5a'** can be seen to undergo Zn-F contacts *via* two fluorides on the side of the complex opposite from the acetonitrile ligands [Zn(1)···F(1) 2.716 Å, Zn(1A)···F(2) 2.716 Å]. The Zn···Zn distance in **2.5a** [3.156(14)] is similar to that seen in the dizinc chloride complex **2.2c** [3.181 Å], but **2.5a'** shows a shorter distance [3.087(14)] (**2.5a'**) which may be attributed to the bridging-like interaction of one BF_4 (μ-BF_4).

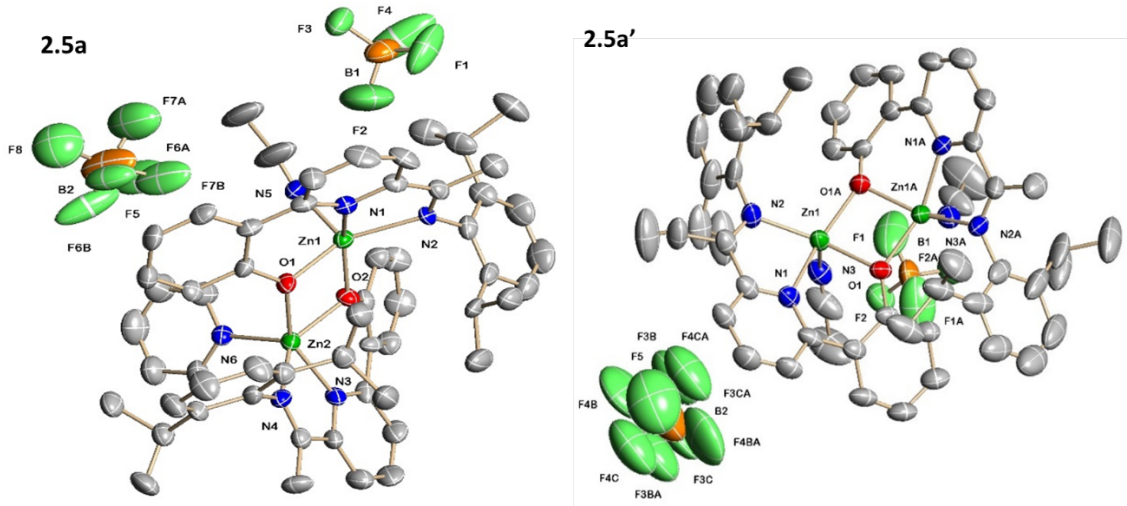

Figure 2.3.6: Molecular structures of **2.5a** and **2.5a'**

Table 2.3.5: Selected bond lengths and angles for **2.5a** and **2.5a'**.

*Bond Lengths (Å) for **2.5a***		*Bond Lengths (Å) for **2.5a'***	
Zn(1)-O(1)	2.025(4)	Zn(1)-O(1)	1.973(3)
Zn(1)-O(2)	2.031(4)	Zn(1)-O(1A)	2.066(4)
Zn(2)-O(1)	2.049(4)	Zn(1A)-O(1)	1.973(3)
Zn(2)-O(2)	2.013(4)	Zn(1A)-O(1A)	2.066(4)

Zn(1)-N(1)	2.102(5)	Zn(1)-N(1)	2.069(4)
Zn(1)-N(2)	2.104(4)	Zn(1)-N(2)	2.128(5)
$Zn(1)\text{-}N(5)_{MeCN}$	2.055(5)	$Zn(1)\text{-}N(3)_{MeCN}$	2.074(6)
$Zn(1)\text{-}N(6)_{pyridine}$	2.047(5)	Zn(1)···Zn(1A)	3.087(14)
Zn(1)···Zn(2)	3.156(14)	Zn(1)···F(1)	2.716
		Zn(1A)···F(2)	2.716
Bond Angles (°) for ***2.5a***		*Bond Angles (°) for* ***2.5a'***	
O(1)-Zn(1)-N(1)	85.59(6)	O(1)-Zn(1)-N(1)	85.73(16)
N(1)-Zn(1)-N(2)	78.84(18)	N(1)-Zn(1)-N(2)	78.69(18)
O(1)-Zn(1)-N(5)	104.74(19)	O(1)-Zn(1)-N(3)	95.04(18)
Zn(1)-O(1)-Zn(2)	101.57(17)	Zn(1)-O(1)-Zn(2)	99.66(15)
O(1)-Zn(1)-O(2)	77.98(15)	O(1)-Zn(1)-O(2)	80.33(15)
N(6)-Zn(2)-O(1)	104.85 (18)	N(6)-Zn(1A)-O(1)	102.18 (18)

For **2.5'** the atoms labelled with an 'A' have been generated by symmetry

In the ^{1}H NMR spectrum of **2.6b**, fourteen aromatic proton resonances could be identified which compared with nine in **2.7c**. For **2.6b**, 3H singlet and a 2H septet at δ 2.50 and δ 3.07 were assignable to methyl-imine (N=C*Me*) and isopropyl protons (C*H*Me_2), respectively. The signals for the CH*Me*$_2$ protons were also split into two 6H doublets at δ 1.09 and δ 0.91. For **2.7c**, two 1H septets signals appeared at δ 2.81 and δ 2.68, and the CHMe2 protons were split into four 3H doublets at δ 1.15 to δ 0.84. In their ^{19}F NMR spectra, signals for the BF_4^- counterion was seen at δ -151.81 while the -OBF_3 unit appeared as a broad singlet at δ -145.39 (**2.6b**) and δ -146.84 (**2.7c**) respectively. The ^{11}B NMR spectrum of **2.6b** and **2.7c** also showed two signals at δ -19.89 (s, br, -OBF_3) and δ -1.19 (s, BF_4^-). The presence of a strong $\nu(C{=}N)_{imine}$ absorption band at around 1593 cm^{-1} for each complex supported metal coordination. Complexes **2.6b** and **2.7c** also displayed molecular ion and strong fragmentation peaks in their FAB mass spectra with *m/z* values of 511.1735 [M-BF_4-BF_3-MeCN-Py] (**2.6b**) and 532.1024 [M-BF_4-MeCN-BF_3] (**2.7c**). The elemental analysis of both complexes was in good agreement with the calculated elemental composition. Further confirmation of the structural composition was provided by single crystal X-ray diffraction.

Views of **2.6b** and **2.7c** are shown on **Fig. 2.3.7**, while selected bond lengths and angles in **Tables 2.3.6**. The structures of **2.6b** and **2.7c** are similar and will be discussed together. Both are based on a zinc-containing cationic unit and a tetrafluoroborate

counterion. Within the cationic unit the zinc centre is surrounded by an anionic *N,N,O*-chelating ligand and two monodentate ligands [1 x MeCN and 1 x pyridine (**2.6b**), 2 x MeCN (**2.7c**)] to complete a distorted square pyramidal geometry. In addition, the phenoxy donor of the *N,N,O*-ligand is linked to a BF_3 group (B(1)-O(1) 1.500(6) **2.6b**, 1.499(8) Å **2.7c**), which presumably derives from B-F bond cleavage of one BF_4^- group. The B-O bond lengths for both complexes are consistent with previously reported examples [range: 1.43-1.50 Å].[40] On the other hand, similar to previous examples within this deprotonated *N,N,O*-ligand family, the O(1)-Zn(1) bond represents the shortest distance to zinc [2.033(3)-2.082(3) Å]. Two types of chelate rings also present, a six-membered ring containing O(1)-Zn(1)-N(1) angles of 82.67(11)° (**2.6b**) and 83.72(14)° (**2.7c**) and a five–membered ring with N(1)-Zn(1)-N(2) angles of 78.14(13)° (**2.6b**) and 78.47(16)° (**2.7c**).

It is unclear as to the difference in reactivity of H**L1**$_H$ and H**L1**$_{Ph}$/H**L1**$_{tBu}$ towards $[Zn(py)_4(NCMe)_2][BF_4]_2$, but it likely the steric and electronic differences in the *N,N,O*-ligand frames are influential on the product type (dimeric **2.5a** vs. monomeric **2.6c**/**2.7c**, see **Scheme 2.3.10**). It is noteworthy, in both the ^{19}F NMR and ^{11}B NMR spectra of **2.5a'** there were additional minor resonances (see above) that could be attributed to a -OBF_3 unit belonging to a monomeric species resembling **2.6c**/**2.7c**.

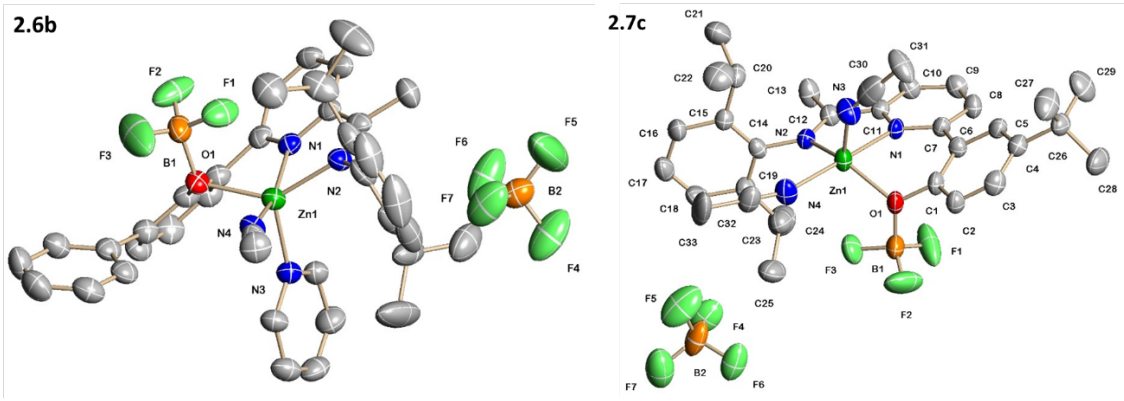

Figure 2.3.7: Molecular structures of **2.6b** and **2.7c.**

Table 2.3.6: Selected bond lengths and angles for **2.6b** and **2.7c.**

Bond Lengths (Å) for ***2.6b***		*Bond Lengths (Å) for* ***2.7c***	
Zn(1)-O(1)	2.082(3)	Zn(1)-O(1)	2.033(3)
Zn(1)-N(1)	2.103(3)	Zn(1)-N(1)	2.099(4)

Zn(1)-N(2)	2.090(3)	Zn(1)-N(2)	2.094(4)
Zn(1)-N(3)	2.066(3)	Zn(1)-N(3)	2.007(5)
Zn(1)-N(4)	2.081(4)	Zn(1)-N(4)	2.069(5)
B(1)-O(1)	1.500(6)	B(1)-O(1)	1.499(8)
B(1)-F(1)	1.393(6)	B(1)-F(1)	1.370(7)
Bond Angles (°) for ***2.6b***		*Bond Lengths (Å) for* ***2.7c***	
N(1)-Zn(1)-N(2)	78.14(13)	N(1)-Zn(1)-N(2)	78.47(16)
O(1)-Zn(1)-N(1)	82.67(11)	O(1)-Zn(1)-N(1)	83.72(14)
N(3)-Zn(1)-N(1)	100.99(12)	N(3)-Zn(1)-N(1)	92.31(18)
N(4)-Zn(1)-N(1)	160.50(13)	N(4)-Zn(1)-N(1)	171.19(17)
O(1)-B(1)-F(1)	110.5(4)	O(1)-B(1)-F(1)	109.1(5)
C(1)-O(1)-B(1)	120.6(3)	C(1)-O(1)-B(1)	121.9(4)

2.3.3.2 Reactivity of **L2** and H**L4** towards $[Zn(Py)_4(NCMe)_2][BF_4]_2$

The symmetrical bis(imino)pyridine ligand **L2** and its unsymmetrical derivative H**L4** were also reacted with $[Zn(Py)_4(NCMe)_2][BF_4]_2$ (made *in-situ* as before) (**Scheme 2.3.10**). However, due to poor solubility of **L2** and H**L4** in acetonitrile, the reactions were conducted at 80 °C in a mixed solvent system composed of dry dichloromethane and acetonitrile. On work-up, [(**L2**)Zn(MeCN)(Py)(BF_4)][BF_4] (**2.8**) and [(H**L4**)Zn(MeCN){BF_3(OH)}][BF_4] (**2.9**) have been isolated in good yields. Both products have been fully characterised by ^{1}H and ^{19}F NMR spectroscopy, IR spectroscopy, FAB mass spectrometry, X-ray diffraction and elemental analysis.

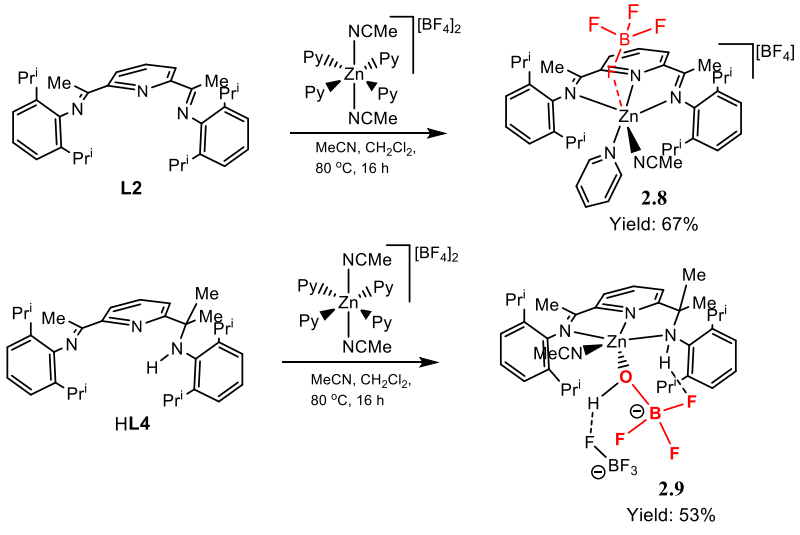

Scheme 2.3.10: Synthesis of **2.8** and **2.9.**

In the ^{1}H NMR spectra of **2.8** and **2.9** either fourteen or nine aromatic protons resonances could be observed, respectively. In **2.8** the CH*Me*$_2$ protons are seen as 2×12H doublets (δ 0.95 and δ 1.53) and a shifted signal is seen for the C*H*Me$_2$ septet (δ 2.52) integrating to four hydrogens. Furthermore, the presence of an additional resonances corresponding to coordinated pyridine ligand were evident. In the ^{1}H NMR spectrum of **2.9** (**Fig 2.3.9**), a 24H multiplet at δ 1.23 and a broad 6H singlet at δ 2.31 could be assigned to the isopropyl CH*Me*$_2$ protons and the C*Me*$_2$-NH protons, respectively. The OH proton on the BF_3(OH) ligand could not be detected.

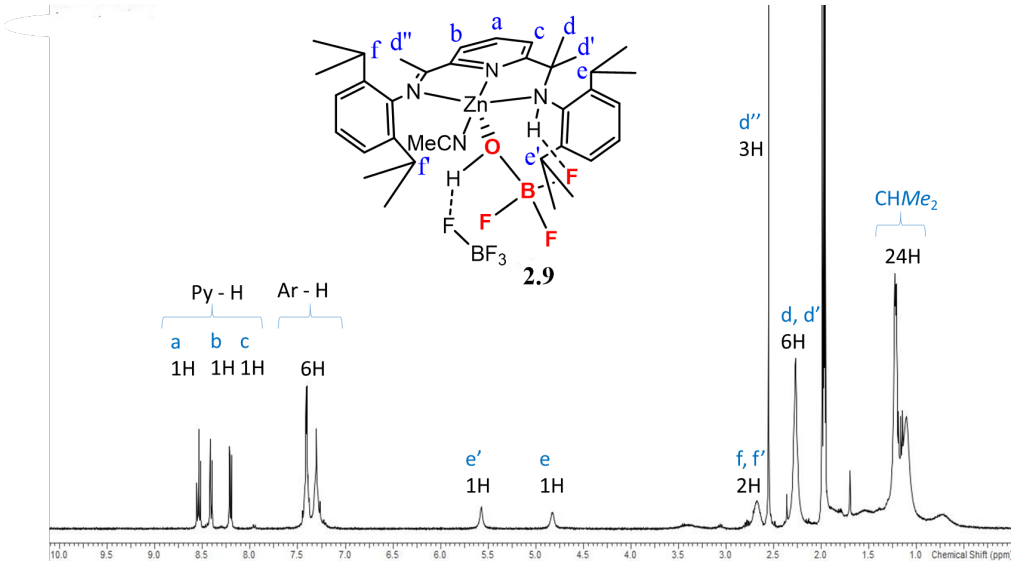

Figure 2.3.9: ^{1}H NMR spectrum of **2.9** (recorded in CD_3CN at room temperature)

In the ^{19}F NMR spectrum of **2.8**, two signals could be seen, one for the BF_4 counterion at δ -151.45 and the other a broad singlet at δ -147.71 which has been attributed to the η^1-BF_4. Similarly, in the ^{19}F NMR spectrum of **2.9** two main signals were observed centred at δ -144.55 and δ -151.85 (as noted before a weaker resonance at δ -151.77 can be assigned to a $^{10}BF_4$ ion) (**Fig. 2.3.10**). The signal at δ -144.55 has been attributed to the coordinated $OHBF_3$ group in **2.9**, which on closer inspection reveals a pseudo quartet (J_{BF} = 7.6 Hz) which can arise through coupling of the fluoride with a quadrupolar boron (I = 3/2). In contrast to the ^{19}F NMR spectrum, two signals were observed in ^{11}B NMR spectrum of **2.9** (**Fig. 2.3.11**), one a singlet at δ -1.19 for the BF_4^- anion and another peak at δ -0.34 for $OHBF_3$ moiety that splits into a quartet due to coupling of the boron with the three equivalent fluoride substituents (J_{BF} = 7.7 Hz).

In their negative ESI mass spectra, both **2.8** and **2.9** exhibit a peak corresponding to the counterion at *m/z* 87 $[BF_4]^-$. In the case of **2.9** an additional peak at *m/z* 65 is seen that can be assigned to $[BF_2O]$ fragmentation peak. The results of the elemental analysis for both **2.8** and **2.9** are in good agreement with the calculated elemental compositions.

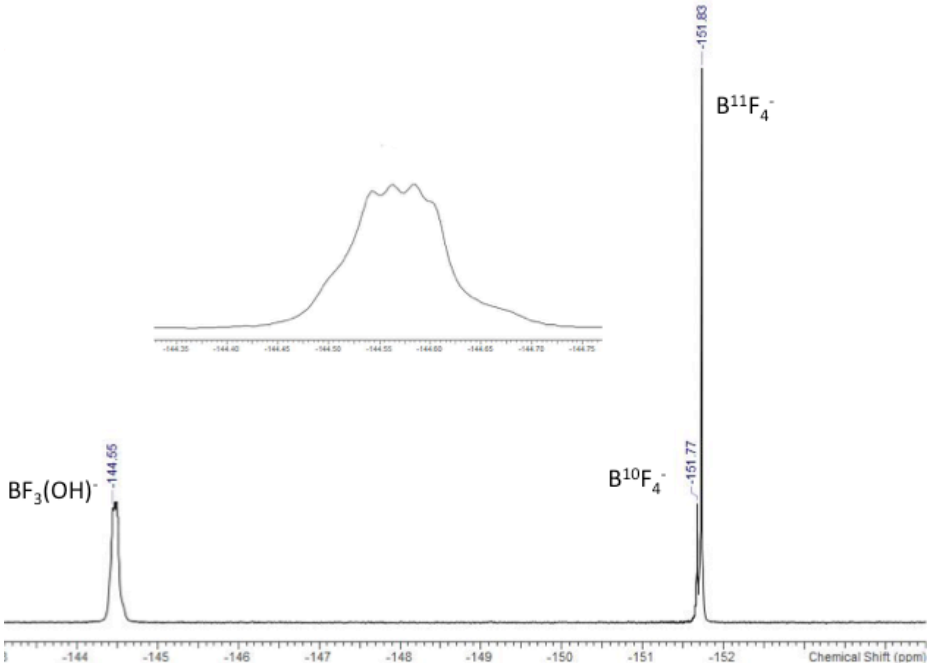

Figure 2.3.10: ^{19}F NMR spectrum of **2.9** (recorded in CD_3CN at room temperature) with an expansion of the signal at δ -144.55.

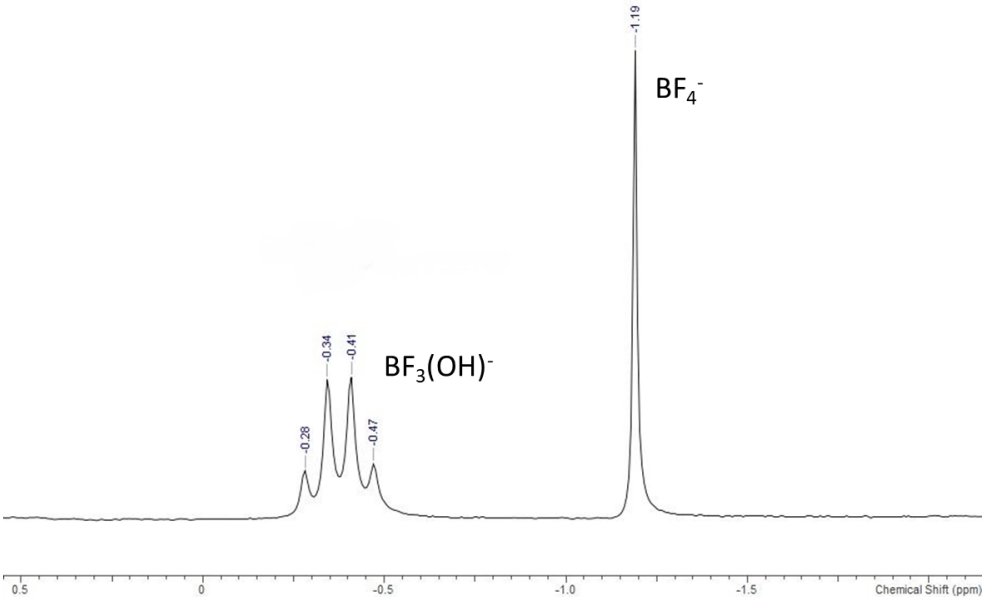

Figure 2.3.11: ^{11}B NMR spectrum of **2.9** (recorded in CD_3CN at room temperature)

As with previous zinc complexes, dissolution of **2.8** and **2.9** in acetonitrile and slow diffusion of diethyl ether gave yellow cube-like crystals that were suitable for the X-ray diffraction studies. Representations of each structure are given in **Fig. 2.3.12** and **2.3.13**; selected bond lengths and angles are reported in **Table 2.3.7** and **2.3.8**.

The structure of **2.8** consists of a cation-anion pair based on a zinc complex cation and a non-coordinating BF_4 anion. In the cationic unit the zinc centre displays a distorted octahedral geometry based on a *mer*-configured terdentate **L2**-ligand along with a monodentate acetonitrile, pyridine and a F-coordinated BF_4 [Zn(1)···F(3) 2.530 Å]; the acetonitrile and BF_4 ligands are disposed *trans*. For **2.9**, a cation-anion pair also exists but with the BF_4 counteranion associated to the zinc cationic unit through OH···FBF_3 hydrogen bonding. The cationic unit in **2.9** contains a *mer*-configured H**L4** tridentate ligand and molecule of acetonitrile and O-coordinated OHBF anionic ligand to form a geometry best described as square based pyramidal. The amine donor within H**L4** is also involved in a NH···F hydrogen bonding interaction with the coordinated $OHBF_3$ ligand [N(3)-H(3A)··· F(1) 2.40 Å]. The $OHBF_3$ unit was found to adopt a slightly distorted tetrahedral geometry with F-B-F and O-B-F bond angles in the range of 108.7(5) - 109.9(5)°. Within both structures the Zn-N bond lengths were consistent with previously reported *N,N,N*-bound zinc(II) complexes.[37,38]

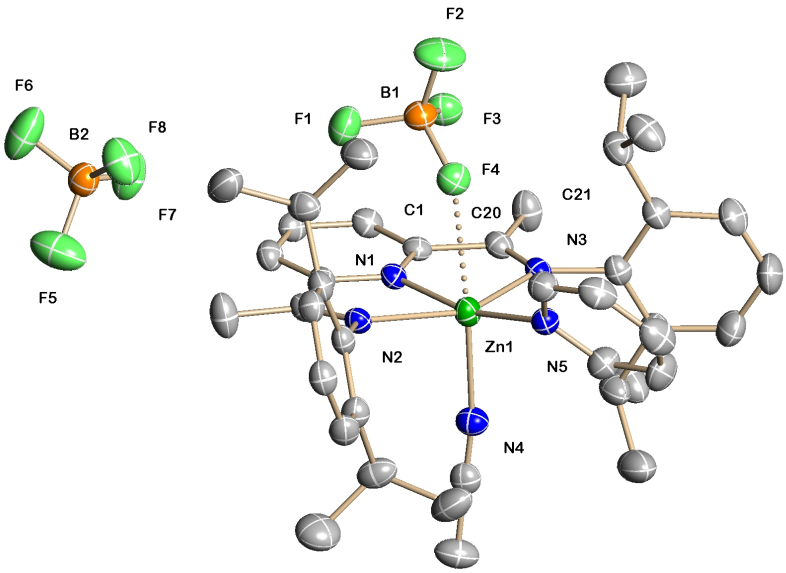

Figure 2.3.12: Molecular structure of **2.8**; the dotted line represents the association of the η^1-BF_4.

Table 2.3.7: Selected bond lengths and angles for **2.8**.

Bond Lengths (Å)	
Zn(1)-N(1)	1.990(2)
Zn(1)-N(2)	2.297(2)
Zn(1)-N(4)	2.069(5)
Zn(1)-N(5)	1.999(2)
Zn(1)···F(3)	2.530
Bond Angles (°)	
N(1)-Zn(1)-N(2)	76.14(9)
N(4)-Zn(1)-N(3)	91.22(9)
N(4)-Zn(1)-N(2)	98.32(9)
N(5)-Zn(1)-N(2)	104.79(9)

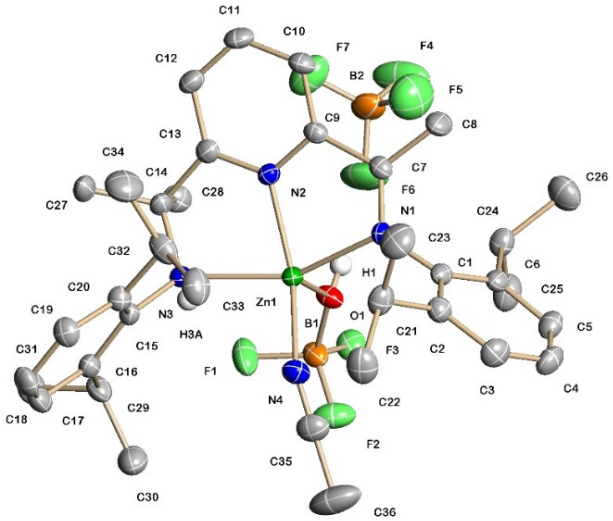

Figure 2.3.14: Molecular structure of **2.9.**

Table 2.3.8: Selected bond lengths and angles for **2.9.**

Bond Lengths (Å)	
Zn(1)-O(1)	1.968(2)
Zn(1)-N(1)	2.172(2)
Zn(1)-N(2)	2.037(2)
Zn(1)-N(3)	2.227(2)
Zn(1)-N(4)	2.069(5)
B(1)-O(1)	1.476(4)
B(1)-F(1)	1.397(4)
N(3)-H(3A)···F(1)	2.40

O(1)-H(1)···F(6)	1.94
Bond Angles (°)	
O(1)-Zn(1)-N(2)	109.69(9)
O(1)-Zn(1)-N(1)	101.77(9)
N(2)-Zn(1)-N(1)	77.25(9)
B(1)-O(1)-Zn(1)	130.68(19)
F(2)-B(1)-O(1)	108.7(3)

2.3.3.3 Hydrolysis/boron-fluoride bond cleavage of BF_4

As shown above the BF_4 ion had undergone partial hydrolysis in solution to form zinc product **2.9** containing an anionic $OHBF_3$ ligand. A number of transition metals have shown to form similar types of complexes such as those with rhodium[26], manganese[27], rhenium[28] and ruthenium[29]. However, for late first row d-block metals, this type of complex has been rarely reported. Wamser and Mesmer reported that hydrolysis of BF_4^- occurs in a stepwise manner to give BF_3OH, $BF_2(OH)_2^-$, $BF(OH_3)^-$ and ultimately $B(OH)_4^-$ accompanied by the formation of hydrofluoric acid. Due to the strong affinity of boron for fluoride complete hydrolysis of BF_4 occurs only at low concentration.[30] It should be noted that the presence of water is also necessary to initiate the hydrolysis. Interestingly, Wamser and Mesmer showed that a molecule of water can be produced *in situ* by the reaction of HF (generated during the reaction) with glass (**eqn.a**), resulting in the formation of SiF_4 which can detected by ^{19}F NMR spectroscopy and mass spectrometry.[31]

$$SiO_2 + 4HF \rightleftharpoons SiF_4 + 2H_2O \qquad \textbf{(eqn.a)}$$

In 2014, the hydrolysis behaviour of [DEME][BF_4] (DEME = *N,N*-diethyl-*N*-methyl-*N*-(2-methoxyethyl)) was probed by Saihara and co-workers in which they showed using NMR spectroscopy that the BF_4^- anion can hydrolyse into $[BF_3(OH)]^-$ and HF (**eqn.b)**. In particular, the ^{19}F NMR spectrum showed not only signals for BF_4^-, but also two peaks at δ -129.6 and δ -143.8 in a 1:3 ratio that corresponded to $[BF_3(OH)]^-$ and HF (**Figure 2.3.14: A**). In addition, in the ^{11}B NMR spectrum (**Fig. 2.3.14: B**), signals of δ -18.84 and δ -20.53 were observed corresponding to $BF_3(OH)^-$ and BF_4^- respectively.[32]

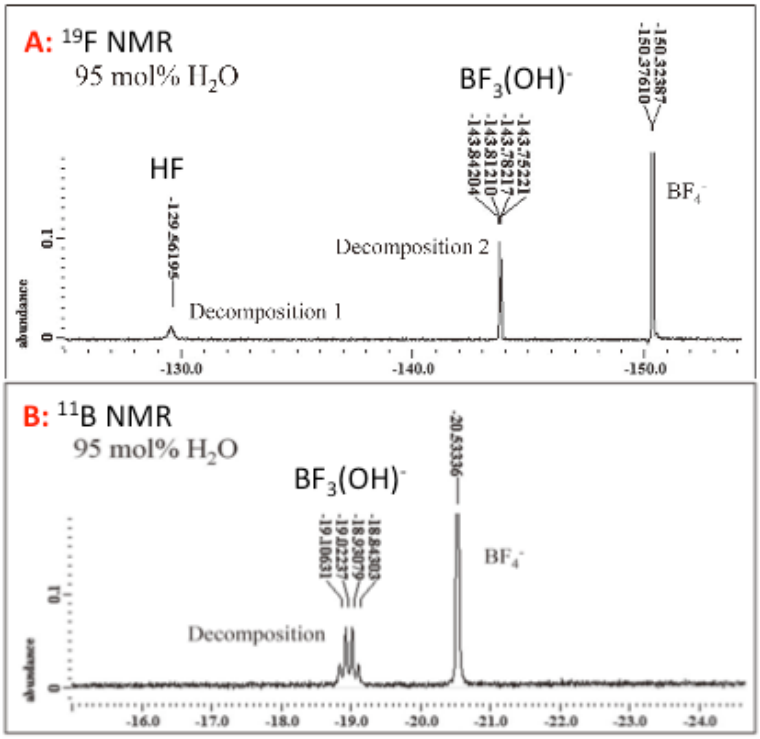

Figure 2.3.14: (a) ^{19}F NMR spectrum of [DEME][BF_4]·H_2O mixture after 7 days; (b) ^{11}B NMR spectrum of [DEME][BF_4]·H_2O mixture after 7 days[32]

In complexes **2.6b** and **2.7b**, cleavage of a B-F bond in a BF_4 anion to form BF_3 and F^- (not detected) was evident. Such B-F bond cleavage has been seen previously. Indeed as highlighted in the introduction to this chapter, several examples of fluoride-bridged metallacyclic iron, zinc and cadmium complexes were found to proceed by fluoride abstraction from BF_4^- (see for example **Scheme 2.1.1**).[32] In addition, fluoride abstraction from BF_4^- has been noted in reactions of arene-linked bis(pyrazolyl) methane ligands with BF_4^- salts of divalent iron, zinc and cadmium to generate fluoride-bridged metallacyclic complexes (see **Scheme 2.1.2**).[33] Although the authors did not provide any mechanistic information about how this hydrolysis occurred, they concluded that the hydrolysis cannot occur in the absence of water. This implies that the activation of a water molecule is a key mechanistic step. Therefore, it would seem reasonable that B-F bond cleavage described in this work (see **2.6b** and **2.7c**) also proceeds by initial reaction of BF_4^- with water to generate initially $BF_3(OH_2)$ and HF (**eqn.b**).

$$BF_4^- + H_2O \overset{H^+}{\rightleftharpoons} BF_3OH_2 + HF \qquad \textbf{(eqn.b)}$$

2.3.3.4 Attempted reactions of **2.1** and **2.2** with CsF and AgF

With the aim to exchange the chloride ligands in selected zinc complexes with fluorides, two types of fluorinating reagents were explored for their potential in realising this transformation. Caesium fluoride (CsF) was the first fluorination reagent assessed as there has been some discussions in the literature that this should be a suitable but underexplored reagent.[39] Hence, two of the zinc(II) chloride complexes, **2.1a** and **2.2c**, were examined as potential precursors and their reactions with CsF monitored by NMR spectroscopy. Each complex was dissolved in CD_2Cl_2 and 1.0 and 1.5 equivalents of CsF introduced (**Scheme 2.3.11**). However, no new zinc complexes were observed after stirring for 1, 2, 3, and 16 hours at room temperature. Indeed, in the ^{1}H NMR spectrum it appeared that the complexes were decomposing to their free ligands after one hour. It is unclear as to the origin of these observations but low solubility of CsF in organic solvent and the hygroscopic nature of this alkali metal fluoride may be influential. Alternatively, the chloride ligands in **2.1a** and **2.2c** may have undergone displacement by fluoride with concomitant oxidation and decomplexation.

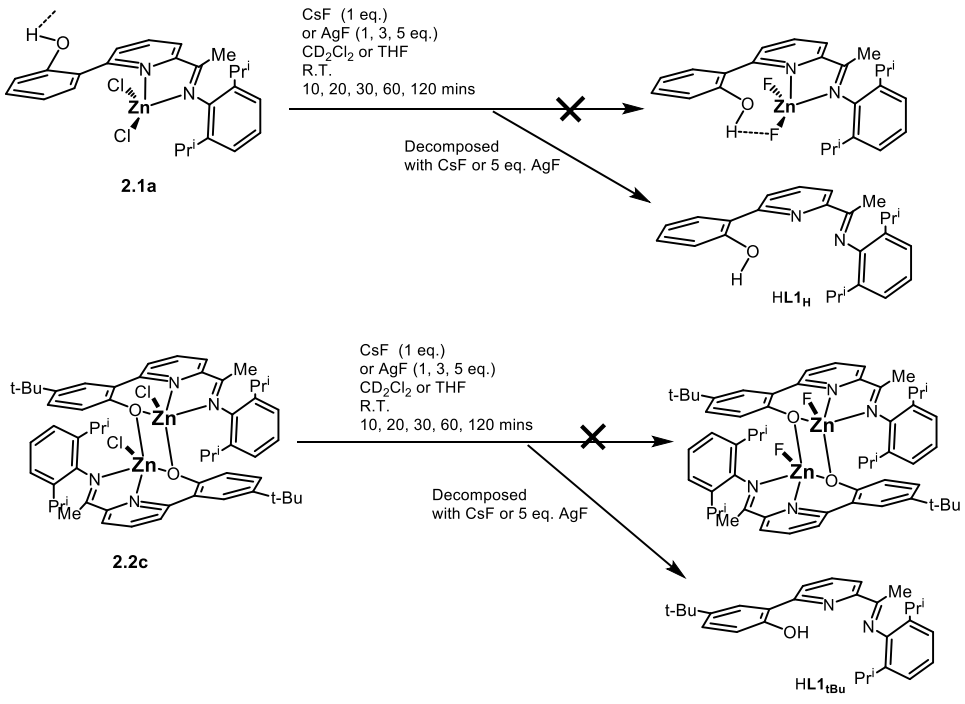

Scheme 2.3.11: Attempted synthesis of Zn(II) fluoride complexes.

Silver fluoride (AgF) was also examined as a reagent to promote a Cl-F exchange. Typically, the reactions were performed in anhydrous THF. However, there was once again no evidence for the formation of a zinc fluoride complex by ^{1}H NMR

spectroscopy, instead the formation of the free ligand was evident. In addition, in the ^{19}F NMR spectra just one signal corresponding to AgF was observed.

2.3.4 Conclusions to Chapter 2

A series of *N,N*$_{Py}$*,O(H)* (H**L1**$_{\mathbf{H}}$, H**L1**$_{\mathbf{Ph}}$, H**L1**$_{\mathbf{tBu}}$, H_2**L3**) and *N,N*$_{py}$*,N* pincer (pro)ligands (H**L4**) were successfully synthesised *via* a series of steps in good overall yield. Subsequently, a range of zinc(II) chloride complexes **2.1a**, **2.1b**, **2.2c** and **2.3**, were prepared and in several cases structurally characterised (**Fig. 2.3.15**). For **2.1a** and **2.1b**, mononuclear complexes were formed that adopt tetrahedral geometries with the phenol unit in H**L1**$_R$ retaining its proton and uncoordinated. Although, the crystallographic data for **2.3** could not be obtained, a mononuclear five-coordinate complex similar to (**L2**)$ZnCl_2$ would seem likely based on the spectroscopic and analytical data. Unlike **2.1a** and **2.1b**, complex **2.2c** showed a neutral binuclear structure in which the two zinc centres were linked by two μ-$O_{phenoxy}$ bridges. The structural difference observed in **2.2c** was attributed to the different electronic properties of the H**L1**$_{tBu}$ ligand. It was also noted that bis(ligand) complex formation could be achieved on reaction of H**L1**$_{Phmes}$ with diethylzinc (**Fig. 2.3.15**).

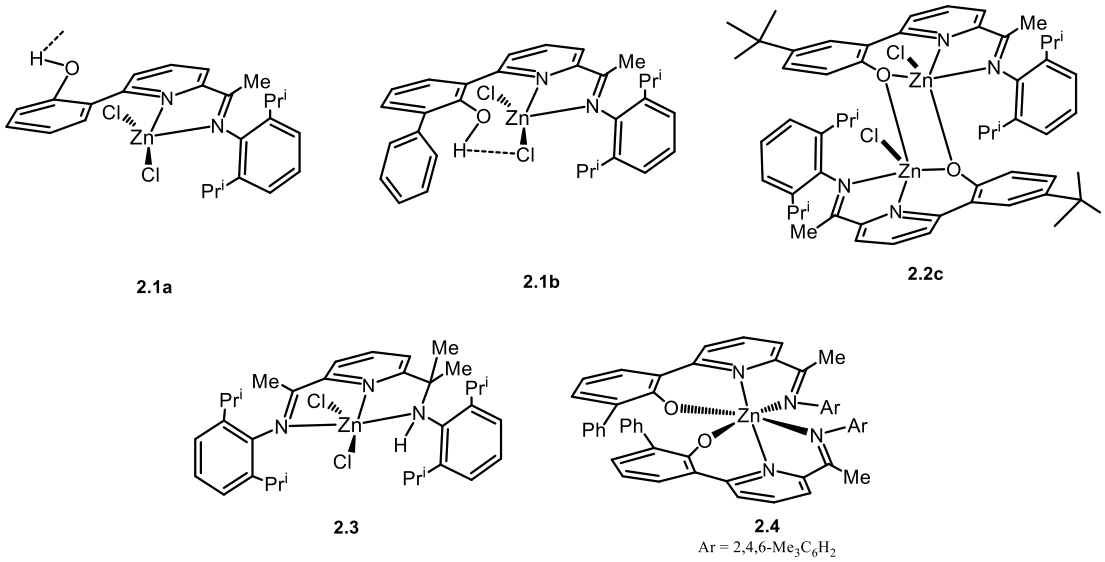

Figure 2.3.15: New zinc(II) chloride complexes **2.1**, **2.2**, **2.3** and **2.4** prepared in **Chapter 2.**

All the (pro)ligands were reacted with zinc(II) tetrafluoroborate hydrate in the presence or absence of pyridine; zinc intermediates of the type $[Zn(py)_4(NCMe)_2][BF_4]_2$ and $[Zn(NCMe)_6][BF_4]_2$ were proposed. Two types of products namely monozinc (**2.6b**,

2.6c, **2.7**, **2.8**, **2.9**) and dizinc cations (**2.5a**, **2.5a'**) were obtained in good yields (**Figure 2.3.16**). In the solid state, the zinc centres in all these new complexes displayed either distorted square pyramidal or octahedral geometries. Complex **2.8** revealed an Zn···F intermolecular contact involving one of the BF_4^- ions while complex **2.5a'** showed the presence of a bridging Zn···$FB(F)_2F$···Zn interaction. In **2.6b** and **2.7c**, B-F bond cleavage had clearly occurred as a molecule of BF_3 had formed a bond to an oxygen atom of the *N,N,O* ligand. On the other hand, an unusual BF_4 hydrolysis reaction occurred to give the $OHBF_3$-containing product **2.9**. The ^{19}F NMR, ^{11}B NMR spectra and mass spectra confirmed this assertion.

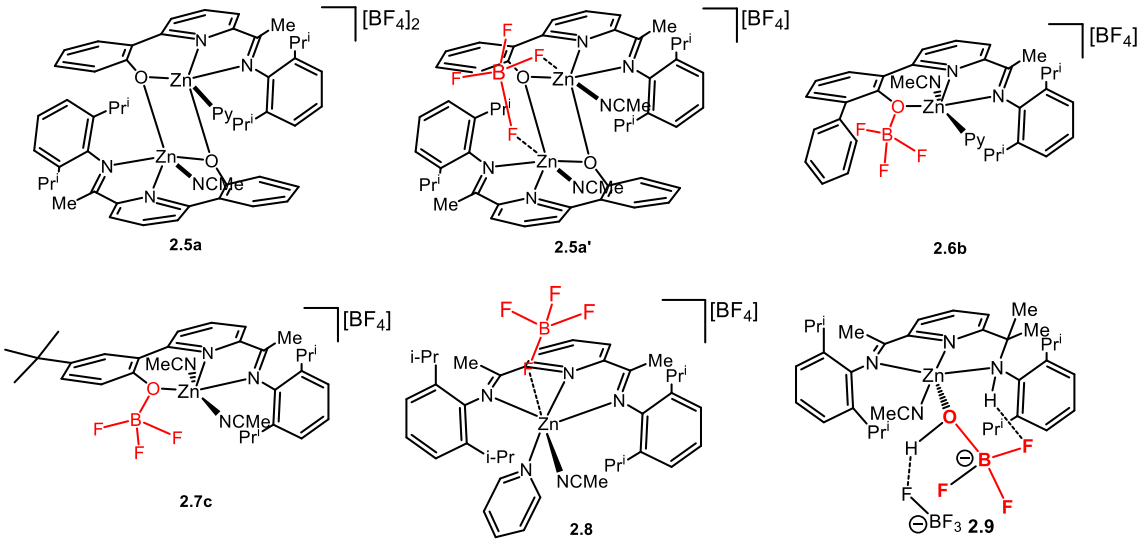

Figure 2.3.16: New zinc(II) tetrafluoroborate complexes, **2.5**, **2.6**, **2.7**, **2.8** and **2.9** prepared in **Chapter 2**.

Chloride-fluoride exchange was attempted by using two different fluorinating reagents namely CsF and AgF. In particular, the reaction of monozinc **2.1a** and dizinc **2.2c** were studied under a range of different conditions including by varying the equivalents of reagents and reaction time. However, there was no evidence by ^1H NMR and ^{19}F NMR spectroscopy for the formation of zinc-fluoride complexes. Indeed, decomposition to free ligand was an outcome in each case. The reasons behind the decomposition remain unclear but the hygroscopic properties and poor solubility of CsF and AgF and in organic solvents may be a contributing factor.

References

1. a) D. Morales-Morales, *Rev. Soc. Quím. Méx*., 2004, **48**, 338-346. b) M. Asay and D. Morales-Morales, *Dalton Trans*., 2015, **44**, 17432-17447.
2. J. M. Berg and Y. G. Shi, *Science*, 1996, **271**, 1085-1085.
3. Z.-Z. Liu, W. Gao, J.-S. Zhang, D.-M. Cui, Q.-L. Wu and Y. Mu, *Organometallics,* 2010, **29**, 5783-5790.
4. F. Ruiqingm Z. Dongsheng, D. Hong, M. Ying, S. Qing and X. Hong, *Synthetic Metals,* 2005, **149**, 135-141.
5. W. Xin, Y. Yulin, F. Ruiqing and J. Zhaohua, *New J. Chem.,* 2010, **34**, 2599-2604.
6. C. Jianxin, H. Yuanbiao, L. Zhongshui, Z. Zhichun, W. Chunxia, L. Tingyan and Z. Wenjie, *J. Mol. Cat. A: Chem.*, 2006, **259**, 133-141.
7. N. Savjani, K. Singh and G. A. Solan, *Inorg. Chim. Acta*, 2015, **436**, 184-194.
8. J. Verbiest, J. A. C. van Ooijen and J. Reedijk, *J. Inorg. Nucl. Chem.,* 1980, **42**, 971-975.
9. J. Reedijk, *Comm. Inorg. Chem*., 1982, **1**, 379-381.
10. E. Tomat, L. Cuesta, V. M. Lynch and J. L. Sesseler, *Inorg. Chem.,* 2007, **46**, 6624-6226.
11. D. L. Reger, R. P. Watson, M. D. Smith and P. J. Pellechia, *Inorg. Chem.,* 2006, **45**, 10088-10097.
12. F. E. Hahn, C. Jocher, T. Lügger and T. Pape, *Z. Anorg, Allg. Chem.,* 2003, **629**, 2341-2347.
13. N. H. Doherty and N. W. Hoffman, *Chem. Rev.,* 1991, **91**, 553-573.
14. V.V. Grushin, *Chem.-Eur. J.,* 2002, **8**, 1006-1014.
15. J. E. Parks, B. E. Wagner and R.H. Holm, *J. Organomet. Chem.,* 1973, **56**, 53-66.
16. J. Dupont, C. Consorti and J. Spencer, *Chem. Rev*., 2005, **105**, 2527-2571.

17. a) H. Makio, H. Terao, A. Iwashita and T. Fujita, *Chem. Rev*., 2011, **111**, 2363-2449. b) M. Mitani, J. Saito, I. S. Ishii and T. Fujita, *Chem. Rev*., 2004, **4**, 137-158.

18. C. J. Davies, A. Gregory, P. Griffith, T. Perkins, K. Singh and G. A. Solan, *Tetrahedron,* 2008, **64**, 9864-9864.

19. W. Alkarekshi, A. P. Armitage, O. Boyron, C. J. Davies, M. Govere, A. Gregory, K. Singh and G. A. Solan, *Organometallics*, 2013, **32**, 249-259.

20. V. C. Gibson, C. Redshaw and G. A. Solan, *Chem. Rev.*, 2007, **107**,1745-1776.

21. L. A. Wright, W. B. Cross, K. Singh, E. G. Hope and G. A. Solan, *Dalton Trans.,* 2015, **44**, 6040-6051.

22. G. J. P. Britovsek, M. Bruce, V. C. Gibson, B. S. Kimberley, P. J. Maddox, S. Mastroianni, S. J. McTavish, C. Redshaw, G. A. Solan, S. Strömberg, A. J. P. White and D. J. Williams, *J. Am. Chem. Soc*., 1999, **121**, 8740-8741.

23. a) M. Bruce, V.C. Gibson, C. Redshaw, G.A. Solan and D. J. Williams. *Chem. Commun.,* 1998, 2523-2524. b) G. J. P. Britovsek, V. C. Gibson, G. A. Solan and D. J. Williams, *Eur. J. Inorg. Chem*., 2001, 431-437.

24. X. Wang, Y. Yang, R. Fan and Z. Jiang, *New J. Chem.,* 2010, **34**, 2599-2604.

25. a) S. Dammers, T. P. Zimmermann, S. Walleck, A. Stammler, H. Bögge, E. Bill and T. Glaser, *Eur. J. Inorg. Chem*., 2017, **56**, 1779-1782. b) J. Olguín, M. Kalisz, R. Clérac and S. Brooker, *Inorg. Chem.*, 2012, **51**, 5058-5062. c) C. M. Grunert, S. Reimanm, H. Spiering, J. A. Kitchen, S. Brooker and P. Gütlich, *Angew. Chem. Int. Ed.,* 2008, **47**, 2997-3002. d) Y. I. Cho, M. L. Ward and M. J. Rose, *Dalton Trans.,* 2016, **45**, 13466-13471.

26. S. J. Thompson, P. M. Bailey, C. White and P. M. Maitlis, *Angew. Chem. Int. Ed.,* 1976, **15**, 490-491.

27. F. Wimmer and M. R. Snow, *Aust. J. Chem.,* 1978, **31**, 267-278.

28. E. Horn and M. R. Snow, *Aust. J. Chem.,* 1980, **33**, 2369-2376.

29. G. Smith, D. J. Cole-Hamiltion, A. C. Gregory and N. G. Gooden, *Polyhedron*, 1982, **1**, 97-103.

30. a) R.E Mesmer and A.C. Rutenberg*, Inorg. Chem.*, 1997, **12(3),** 699-679. (b) C. A. Wamser *J. Am. Chem. Soc.,* 1948, **70**, 1215-1219.

31. R. Fernandez-Galan, B. R. Manzano, A. Otero, M. Lanfranchi and M. A. Pellinghelli, *Inorg. Chem.,* 1994, **33**, 2309-2312.

32. K. Saihara, A. Shimizu, H. Abe and Y. Yoshimura., *J. Jpn. Ins. Energy,* 2014, **93**, 328-332.

33. D. L. Reger, R. P. Watson, M. D. Smith and P. J. Pellechia, *Crystal Growth & Design*, 2007, **7**, 1163-1170.

34. H. Adams, L. R. Cummings, D. E. Fenton and P. E. McHugh, *Inorg. Chem. Commun.,* 2013, **6**, 19-22.

35. H. Adams, N. A. Baily, P. Bertrand, C. O. Barbarin, D. E. Fenton and S.-H. Gou, *J. Chem. Soc., Dalton Trans.,* 1995, 275-279.

36. H. Adam, N. A. Bailey, D. E. Fenton and Q.-Y. He, *J. Chem. Soc., Dalton Trans.,* 1995, 697-699.

37. C.-H. Chang, H.-J. Chuang, T.-Y. Chen, C.-Y. Li, C.-H. Lin, T.-Y. Lee, B.-T. Ko and H.-Y. Huang*, J. Polym. Chem.,* 2016, **54**, 714-725.

38. Q. Hu, S. Jie, P. Braunstein and B.-G. Li*, J. Organomet. Chem*., 2019, **882**, 1-9.

39. W. A. Gobeze, V. A. Milway, N. F. Chilton, B. Moubaraki, K. S. Murry and S. Brooker*, Eur. J. Inorg. Chem*., 2013, 4485-4498.

40. D. G. Hall, J. Wiley and Sons, Inc. Boronic Acids: Preparation and Applications in Organic Synthesis and Medicine, 2005.

41. D. E. Fenton, H. Adams and Q.-Y. He, *Acta Crys.,* 1998, **C54**, 286-287.

42. N. G. Spiropulos, E. A. Standley, I. R. Shaw, B. L. Ingalls, B. Diebels, S. V. Krawczyk, B. F. Gherman, A. M. Arif and E. C. Brown, *Inorg. Chim. Acta,* 2012, **386**, 83-92.

43. M. Bero, J. Kasperczyk and G. Adamus, *Macromol. Chem.,* 1993, **194**, 907-912.

44. a) N. Novoa, J. P. Soto, R. Henríquez, C. Manzur, D. Carrillo and J.-R. Hamon, *J. Inorg. Organomet. Polym. Mater.*, 2013, **23**, 1247-1254; b) A. Trujillo, M.

Fuentealba, D. Carrillo, C. Manzur, I. Ledoux-Rax, J.-R. Hamon and J.-Y. Saillard, *Inorg. Chem.* 2010, **49**, 2750-2764; c) N. Novoa, F. Justaud, P. Hamon, T. Roisnel, O. Cador, B. Le Guennic, C. Manzur, D. Carrillo and J.-R. Hamon, *Polyhedron,* 2015, **86**, 81-88; d) N. Novoa, T. Roisnel, P. Hamon, S. Kahlal, C. Manzur, H. M. Ngo, I. Ledoux-Rak, J.-Y. Saillard, D. Carrillo and J.-R. Hamon, *Dalton Trans.*, 2015, **44**, 18019-18037.

45. C.-L. Fang and H.-Y. Ma, *Eur. Polym. J.,* 2019, **119**, 289-298.

46. Jinting Xu, First year PhD report, University of Leicester, 2016.

Chapter 3

Cobalt(II) chloride and tetrafluoroborate complexes supported by *N,N,O*- and *N,N,N*-pincer ligands

3.1 Introduction

In this chapter, the overall aim is develop and explore the coordination chemistry of a series of d^7 cobalt(II) chloride and tetrafluoroborate complexes bearing a range of *N,N,O* and *N,N,N*-pincer ligands. As an underlying theme, the mode of degradation of the tetrafluoroborate anion will be studied with a view to exploring this approach as a route to cobalt-fluoride complexes. Additional attempts to make cobalt-fluoride complexes using exchange strategies are also presented. To set the scene for the synthetic work, we aim to provide some background to related cobalt chemistry, cobalt-based pincer complexes and the use of BF_4^- ions as a source of fluoride in cobalt chemistry.

3.1.1 Cobalt(II) chloride pincer complexes and their applications

Since the mid to late 1990s, the use of cobalt pincer complexes as homogeneous catalysts in alkene polymerisation catalysis has been extensively explored and remains an active field of research to this day.[1-4] Elsewhere, related cobalt complexes have attracted attention in other types of catalysis due to the abundance, low cost and environmentally benign nature of this metal centre. Indeed, such cobalt catalysts have been now been shown to promote many important transformations including, i) the hydrogenation of olefin, carbonyl compounds, carboxylic acid derivatives and CO_2 [5-10], ii) the dehydrogenation of alcohols, amines and alkanes [11], iii) transfer hydrogenation reactions [12,30]] and iv) dehydrogenative cross-coupling [13]. In addition to their role as catalysts for olefin polymerisation, [3,14,15] cobalt pincer complexes have also proved potent catalysts for shorter chain oligomerisation reactions.[15,16,17]

A variety of first row transition metal catalytic systems have been reported for ester hydrogenation,[18-20] including those based on iron[21-24] and cobalt.[6,9] Indeed, cobalt catalysts can mediate the hydrogenation of many different substrates such as alkynes, alkenes, ketones, aldehydes and imines.[25-28] In 2015, Srimani and co-workers published the first hydrogenation of esters catalysed by the *N,P,N*-, *P,N,N(H)*- and *P,N,N*-cobalt pincer complexes **1**, **2** and **3** (**Scheme 3.1.1: A**).[6] On activation by $NaHBEt_3$, the best performance was achieved by **2,** giving 99% yield of the corresponding alcohol with a catalyst loading of 4 mol% and 50 mol% of base in 48 hours. Elsewhere, **2** was also examined using a wide variety of esters including primary, secondary and tertiary alphatic examples resulting in excellent conversions.[6] In 2017, a range of cobalt pincer catalysts were employed for the additive-free hydrogenation of carboxylic acid ester to alcohols by the Yuwen group.[5] In particular, pincer complex **4** showed higher activity with ethyl and benzyl ester substrates when compared to methyl esters (**Scheme 3.1.1: B).** In addition, the biomass-derived γ-valerolactone was successfully converted to 1,4-pentanediol in the presence of **1** with a turnover number of 3890.[5]

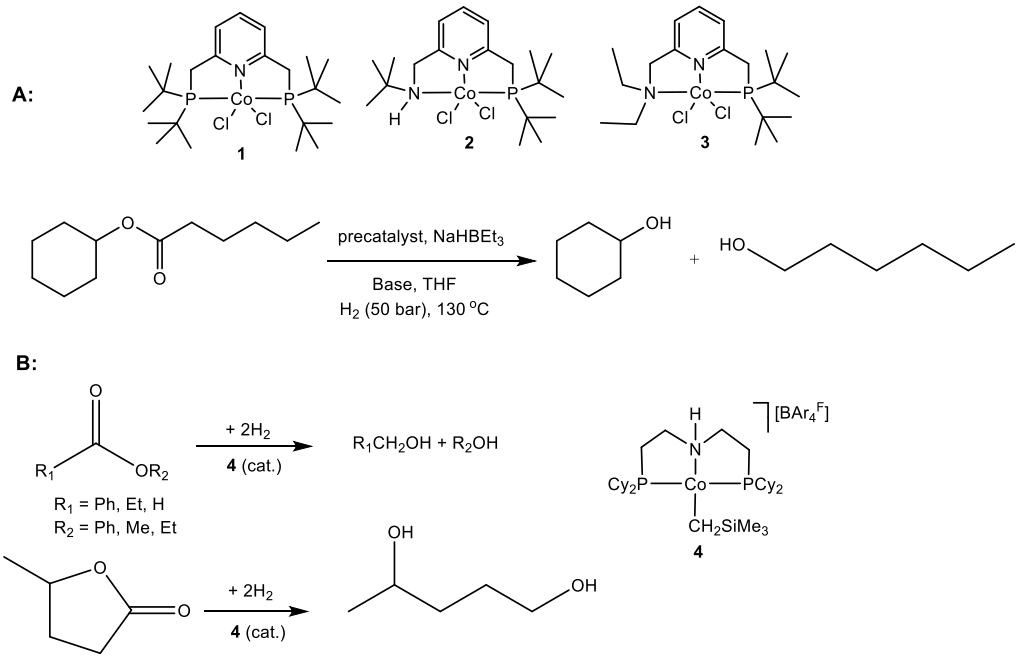

Scheme 3.1.1: **A**) cobalt-catalysed hydrogenation of esters.[6] **B**) Catalytic hydrogenation of esters using cobalt pincer catalyst **4** ($BAr^F_4 = B\{3,5\text{-}(CF_3)_2C_6H_3\}_4$).[5]

Elsewhere, **4** was also employed as a catalyst for the acceptorless dehydrogenation of alcohols and for the synthesis of imines from alcohols and amines (**Scheme 3.1.2**).[11] Zhang and co-workers reported that **4** was effective for a range of benzylic and aliphatic alcohols and amines and it notably displayed comparable activity to that previously reported for ruthenium catalysts.[29a,b] No additives were necessary in this transformation, highlighting the potential of cobalt as an alternative to precious-metal iridium, ruthenium and osmium catalysts.

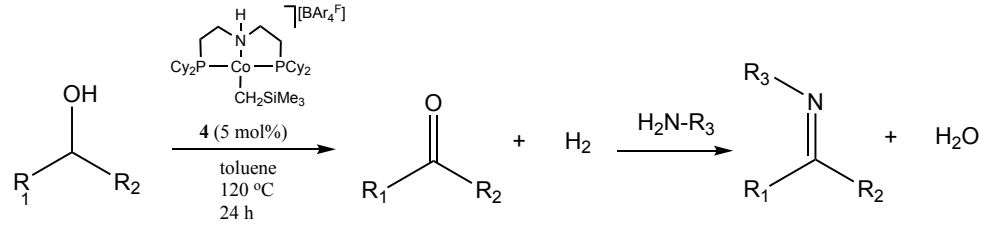

Scheme 3.1.2: Acceptorless dehydrogenation of selected alcohols using pincer catalyst **4** and sequential imine formation.[11]

More recently, cobalt pincer catalysts have been shown to be effective in cyclisation and multicomponent coupling reactions for the synthesis of functionalised pyrroles. For example, Daw and co-workers reported the use of cobalt pincer complexes to promote the acceptorless dehydrogenative coupling of 1,4-butanediols with various amines to generate 1,2,5-substituted pyrroles with water and hydrogen as the only by-products.[13] A range of reaction conditions were screened, such as the amount of base, type of base and reaction temperature. In terms of the catalyst, four types of *P,N,P*- and *P,N,N*-Co dihalide complexes **5**, **6**, **7** and **8** were investigated. The optimal performance was achieved by **5** in the presence of $NaHBEt_3$ (5 mol%), ^{t}BuOK (5 mol%) with the temperature set at 150 ^oC, allowing high conversions and high yields (**Scheme 3.1.3**).

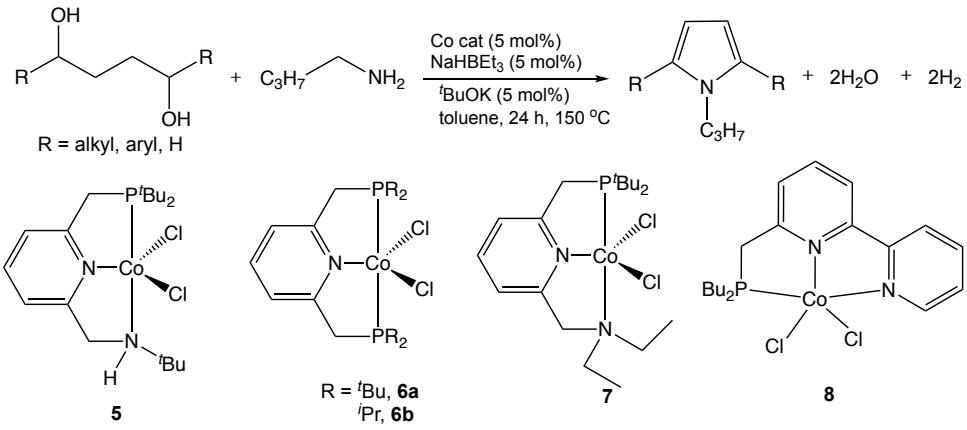

Scheme 3.1.3: Cobalt pincer complexes used in pyrrole synthesis.[13]

In 1998, bis(arylimino)pyridine-cobalt complexes were discovered independently by the Brookhart [31] and Gibson [32,33] groups as catalysts for ethylene oligo-/polymerisation. They reported that activation of **9** (M = Co; X = Cl, Br) (**Fig. 3.1.1**) with methylaluminoxane (MAO) [32,33] or modified methylaluminoxane (MMAO) [31] led to high catalytic activity (up to 17.0 × 10^6 g PE mol^{-1}(Co) h^{-1} for Ar = 2,4,6-trimethylphenyl). More significantly, these catalysts facilitated the formation of high density/highly linear polyethylene with high molecular weight (M_w ~ 10^5 g mol^{-1}).[33] In subsequent years, many groups have been concerned with modifying the bis(arylimino)pyridine pincer framework in order to enhance the catalytic activities and thermal stability of their complexes *e.g.* complex **10** (**Fig 3.1.1**).[34,35]

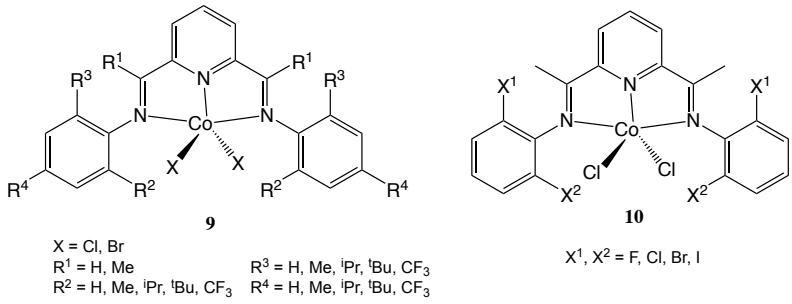

Figure 3.1.1: Bis(arylimino)pyridine-Co(II) precatalysts **9** and their halide-substituted derivatives **10.**[31-35]

3.1.2 Cobalt(II) tetrafluoroborate complexes and their applications

In the Chapter 2, the reactivity of a B-F bond when present within a tetrafluoroborate-containing complex was discussed. The BF_4^- anion is less nucleophilic and basic (and therefore more coordinating) than nitrates, halides or even triflates. In addition, it is slightly sensitive to hydrolysis and has the capacity to decompose *via* loss

of a fluoride anion.[36-39] Extremely reactive cations such as those derived from Ti, Zr, Hf and Si are able to abstract fluoride from BF_4^- with the resulting fluoride ion acts as a bridging ligand between boron and the cationic centre.[40] For instance, the gold complex [μ-(DTBM-SEGPHOS)(Au-BF_4)$_2$] was found to contain two Au-F-B bridges.[41,42] Therefore, in this chapter, part of the objective is develop cobalt pincer complexes that contain tetrafluoroborate anions with a view to exploring their amenability to undergo B-F bond cleavage.

The Olguín group in 2012 investigated a series of di- and tetra-nuclear Cu(II), Ni(II) and Co(II) complexes bearing bis-tetradentate triazole-based ligands.[37] The reactions of ligands L^{Tz1} and L^{Tz3} with $M^{II}(BF_4)_2{\cdot}6H_2O$ (M = Cu, Ni or Co) were conducted to determine whether complexes of the type $[M_2L(X)_n]^{m+}$ (where X is a solvent or anion) could be formed. In the case of cobalt, dinuclear cobalt(II) tetrafluoroborate complexes, namely **10** and **11**, were afforded with **10** exhibiting an unusual bridging tetrafluoroborate anion (**Figure 3.1.2**). These findings suggested that this class of compound could potentially recognise tetrahedral anions, such as phosphates or sulphates, which are important in biological systems.[37]

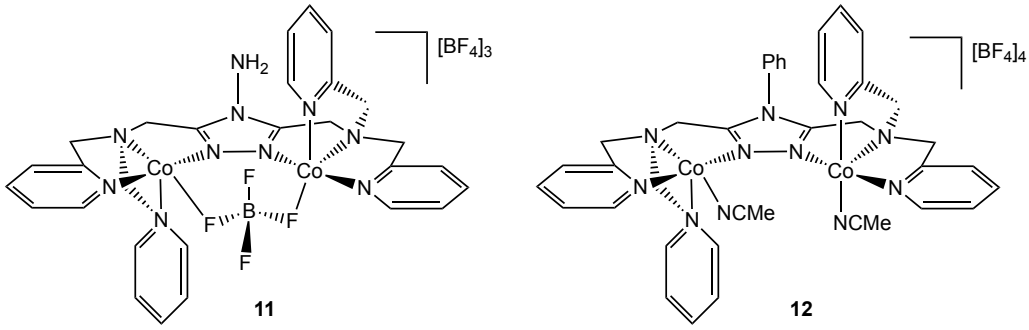

Figure 3.1.2: Dinuclear cobalt(II) tetrafluoroborate complexes $[Co^{II}_2(L^{Tz1})(\mu\text{-}BF_4)]\text{-}[BF_4]_3{\cdot}2CH_3CN$ (**11**) and $[Co^{II}_2(L^{Tz3})(CH_3CN)_2][BF_4]_4{\cdot}0.5H_2O$ (**12**).[37]

Related bis-tetradentate ligands (L_{Et}, L_{Mix}) with the triazole unit in L^{Tz1} and L^{Tz3} replaced with a pyrimidine have been used in related chemistry by Brooker *et al*.[38] Notably, the multinuclear cobalt complexes $[Co_4^{II}(L_{Et})_2(\mu\text{-}F)_4][BF_4]_4$ (**13a**) and $[Co_4^{II}\text{-}(L_{Mix})_2(\mu\text{-}F)_4][BF_4]_4$ (**13b**), containing metal centres linked by two μ-F bridges, were isolated.[38] In 2014, Inomata *et al.* published a crystal structure of dimeric $[Co_2(\mu\text{-}F)_2(C_{21}H_{24}N_4)_2][BF_4]_2$ (**14**) which contains one tripodal tris[(6-methylpyridine-2-yl)methyl]amine per metal centre and two bridging fluorides (**Fig. 3.1.3**).[43]

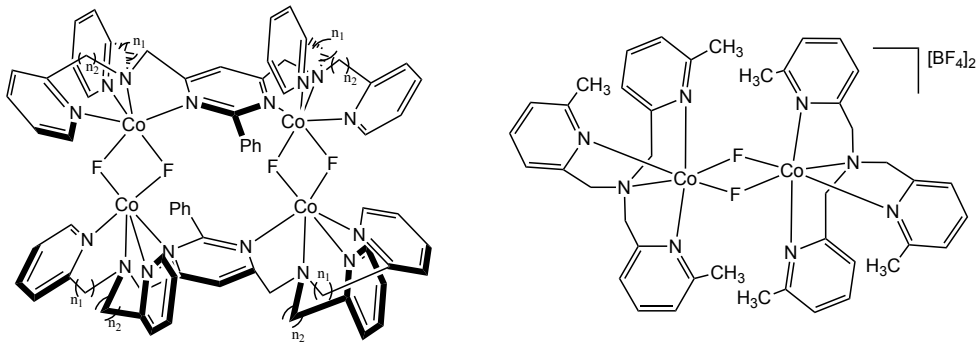

Figure 3.1.3: Fluoride-bridging in multinuclear cobalt complexes **13a,b** and **14**.[38, 43]

In 2014, Cho *et al.* demonstrated that reactions of the bis(bidentate) ligands, pnN_4, pnN_4-OMe and pnN_4-PhCl with $[Co(OH_2)_6][BF_4]_2$ resulted in fluoride abstraction from the tetrafluoroborate counterion to generate the mono-fluoride bridged dimer $[Co_2(\mu\text{-}F)(pnN_4\text{-}PhCl)_2(OH_2)(MeCN)][BF_4]_3$ (**15**) along with the bis-fluoride-bridged dimer $[Co_2^{II}(\mu\text{-}F)_2(pnN_4\text{-}PhCl)_2][BF_4]_2$ (**16**) (**Scheme 3.1.5**). In addition, the authors noticed that modification of both the linker length (backbone flexibility) and pyridine *ortho*-substituent disfavoured O_2 activation and instead favoured fluoride abstraction from the tetrafluoroborate anion.[39]

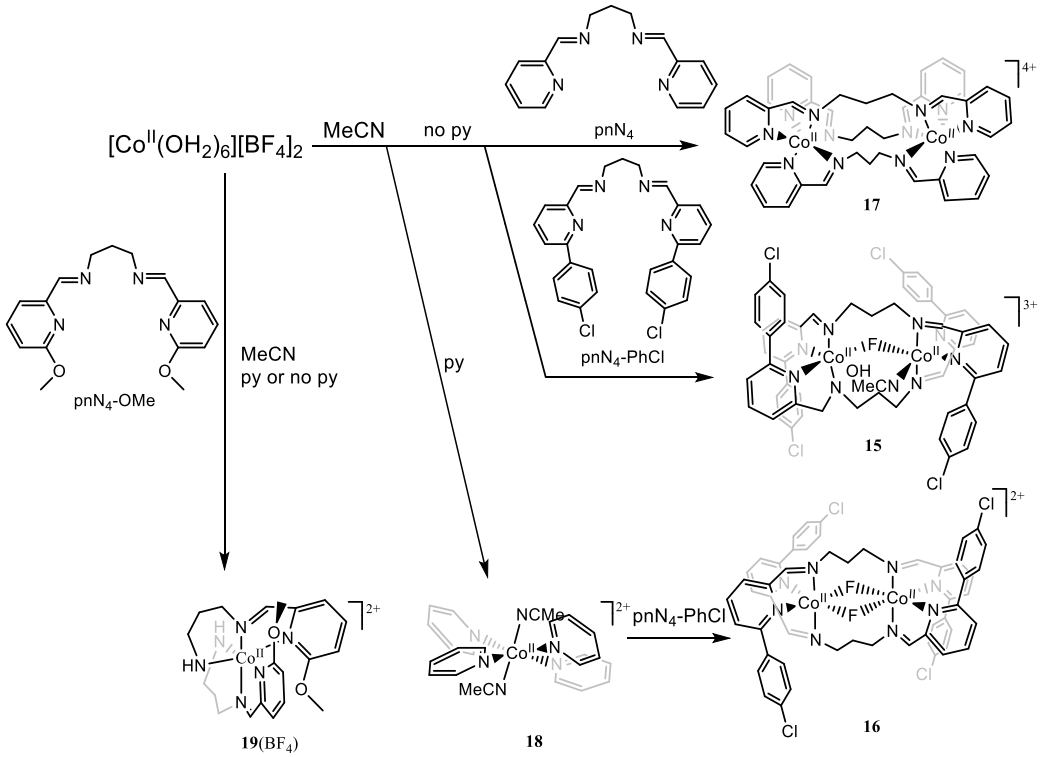

Scheme 3.1.5: Products from the reactions of $[Co(OH_2)_6][BF_4]_2$ with pnN_4, pnN_4-OMe and pnN_4-PhCl. [39]

The bulkiest ligand pnN_4-PhCl was investigated for the metalation reaction in the presence and absence of pyridine. With no pyridine present, the mono-fluoride bridged dimer $[Co_2(\mu\text{-}F)(pnN_4\text{-}PhCl)_2(OH_2)(MeCN)][BF_4]_3$ (**15**) was produced from the reaction of PnN_4-PhCl with an acetonitrile solution of $[Co^{II}(OH_2)_6][BF_4]_2$. Inspection of the structure of **15** revealed that one fluoride had been abstracted from the BF_4 anion (presumably also generating one equivalent of BF_3). However, with pyridine, a different di-fluoride bridged dimer $[Co_2(\mu\text{-}F)_2(pnN_4\text{-}PhCl)_2][BF_4]_2$ (**16**) was isolated. In order to identify whether pyridine could promote B-F cleavage, the independent complexation reaction of $[Co^{II}(OH_2)_6][BF_4]_2$ with excess pyridine was investigated. The coordination complex $[Co^{II}(Py)_4(MeCN)_2][BF_4]_2$ (**18**) was isolated which confirmed that the combination of only $[Co^{II}(OH_2)_6][BF_4]_2$ and pyridine is not enough to promote the fluoride abstraction. The direct reaction of **18** with pnN_4-PhCl (assisted by extra pyridine) also produced the di-fluoride bridged complex **16**. Thus, **18** was considered as the intermediate species to form **16** from $[Co^{II}(OH_2)_6][BF_4]_2$.[39] On the basis of this finding, the authors suggested that the electronic and steric properties of multidentate ligand is the key reason for the observed B-F abstraction.

Gobeze *et al.* and others noted that a protic solvent (such as methanol),[44] in the presence of strong base containing bulky substituents (such as quinuclidine and 3,5-dimethylpyrazole), was capable of promoting decomposition of tetrafluoroborate leading to metal-fluorides [45] or polymeric $MF_2(ligand)_2$ complexes.[46] The authors were uncertain as to the origin of these observations but suggested that it could be due to the bulky chlorophenyl group being able to stabilise the transient and coordinatively unsaturated cobalt species which could then react with the BF_4 anion to enhance fluoride abstraction. Alternatively, binding of the BF_4 anion or the BF_3 by-product to the –PhCl unit could act as a driving force for B-F bond cleavage.[39]

3.2 Aims and objectives of Chapter 3

This chapter is concerned with exploring the reactivity of cobalt(II) chloride and tetrafluoroborate salts towards the *N,N$_{py}$,O(H)* or *N,N$_{py}$,N* (pro)ligands H**L1$_R$** (R = H, Ph, t-Bu), **L2**, H_2**L3** and H**L4** **(Figure 3.2.1)**. The difference in donor properties of the pincer (pro)ligand as well as the steric and electronic factors will be explored in the resulting coordination chemistry. With regard to the tetrafluoroborate work, the

capacity of the BF_4 anion to act as ligand, undergo hydrolysis or act as a source of F^- will additionally be probed. Comparisons will be made where possible with the corresponding zinc(II) chemistry developed in **Chapter 2**.

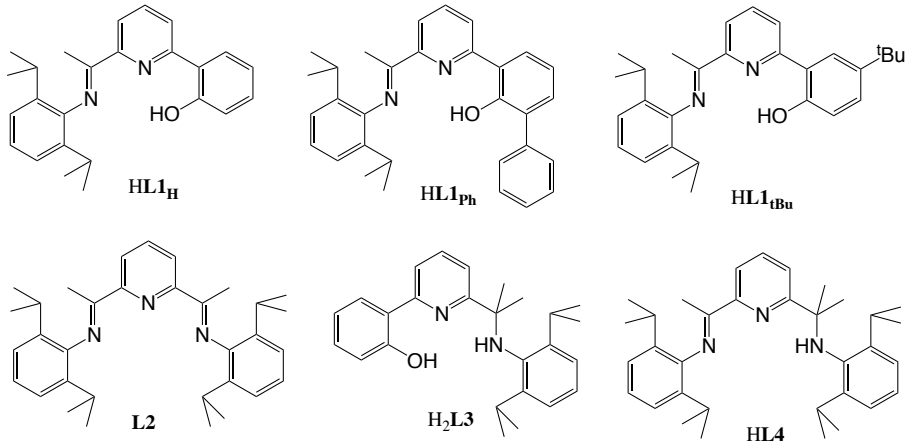

Figure 3.2.1: Types of (pro)ligand to be investigated in **Chapter 3**.

All products will be characterised by a combination of $^{1}H/^{19}F/^{11}B$ NMR and IR spectroscopy, mass spectrometry and elemental analysis. In addition, the inherent paramagnetism of the Co(II) complexes will assessed using the Evans NMR method. Furthermore, considerable efforts will be directed towards growing single crystals to allow structural identification by X-ray diffraction.

3.3 Results and discussion

3.3.1 Cobalt(II) chloride complex synthesis

3.3.1.1 Reactivity of H**L1$_R$** towards cobalt(II) chloride

In a manner similar to that described in Chapter 2, the three sterically and electronically distinct *N,N,O(H)* (pro)ligands, H**L1$_H$**, H**L1$_{Ph}$** and H**L1$_{tBu}$**, were first reacted with anhydrous $CoCl_2$ to examine their ability to undergo complexation either as intact ligands or as deprotonated derivatives. Typically, the reactions were carried out by stirring the reactants in dry THF at room temperature for 16 hours affording in the case of H**L1**$_H$ and H**L1**$_{Ph}$ mononuclear, (H**L1**$_R$)$CoCl_2$ (R = H **3.1a**, R = Ph **3.1b**) and for H**L1**$_{tBu}$, binuclear (**L1$_{tBu}$**)$_2Co_2Cl_2$ (**3.2c**), as green solids in high yield (**Scheme 3.3.1**). Conversely, reaction of H**L1$_H$** with $CoCl_2$ in *n*-BuOH at 90 ^oC resulted in deprotonation of the *N,N,O(H)* (pro)ligand to form the bimetallic analogue of **3.2c**, (**L1$_H$**)$_2Co_2Cl_2$

(**3.2a**). In addition, **3.2a** could been formed by treating **3.1a** with base (trimethylamine) or by the direct reaction of the sodium salt Na**L1$_H$** (made by reaction of H**L1$_H$** with NaH) with anhydrous $CoCl_2$ in THF. In addition, all complexes were characterised by ^{1}H NMR and IR spectroscopy, magnetic measurements, ESI and FAB mass spectrometry and elemental analysis.

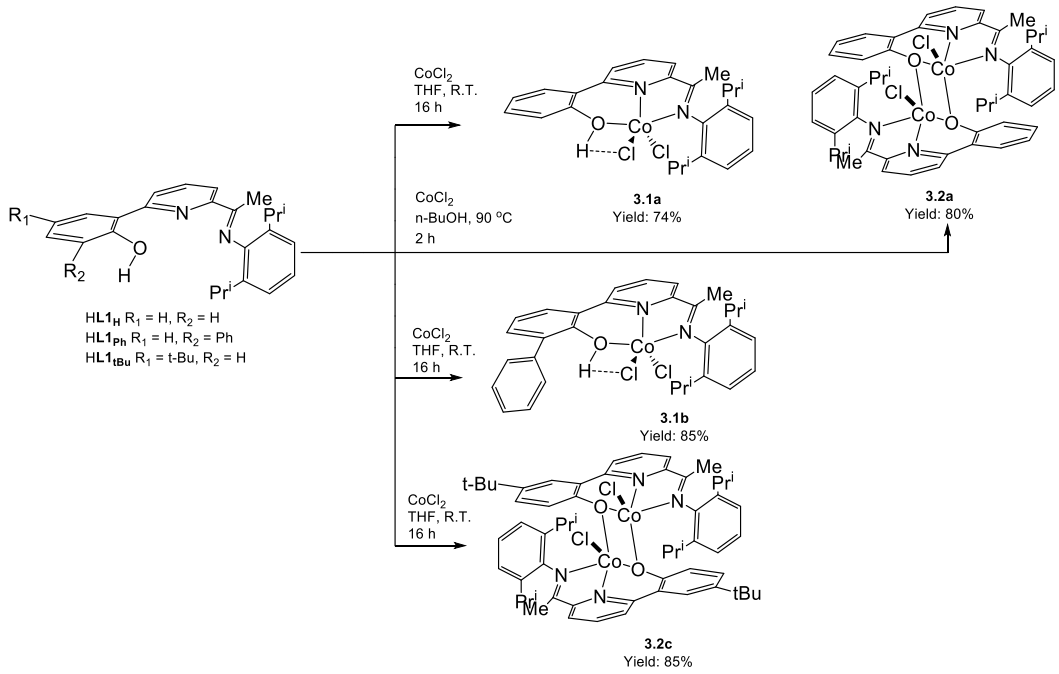

Scheme 3.3.1: Synthetic route to **3.1a**, **3.2a**, **3.1b** and **3.2c**.

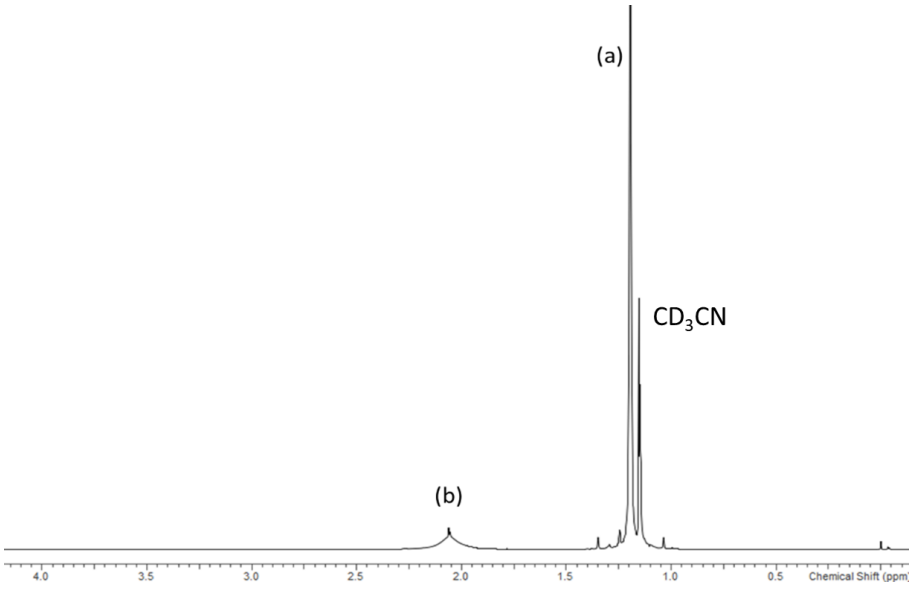

Figure 3.3.1: The Evans' NMR spectrum showing the cyclohexane reference peak for both the control (a) and paramagnetic **3.1a** (b).

All Co(II) complexes were paramagnetic on account of their d^7 configurations. For mononuclear **3.1a** and **3.1b** magnetic susceptibility measurements (Evans NMR method [47,48]) gave values (μ_{eff} ~ 4.60 BM) consistent with three unpaired electrons [S = 3/2]. For bimetallic **3.2a** and **3.2c** values of ~ 6.0 BM were obtained that were consistent with two non-interacting Co(II)-Co(II) (S = 3/2) metal centres (using $\mu^2 = \sum\mu_i^2$, where μ_i is the magnetic moment of the individual metal centres[39]). As a representative example of the Evans NMR method, **Fig. 3.3.1** shows the two peaks observed in the spectrum of **3.1a** corresponding to the reference compound (cyclohexane) and **3.1a**. The peak separation of the solvent resonance between that of pure solvent (outside of the capillary) and that shifted by the paramagnet (in the capillary) was determined to be 79.80 Hz. Using this data the effective magnetic moment of **3.1a** was calculated to be 4.60 BM using approaches described elsewhere[39].

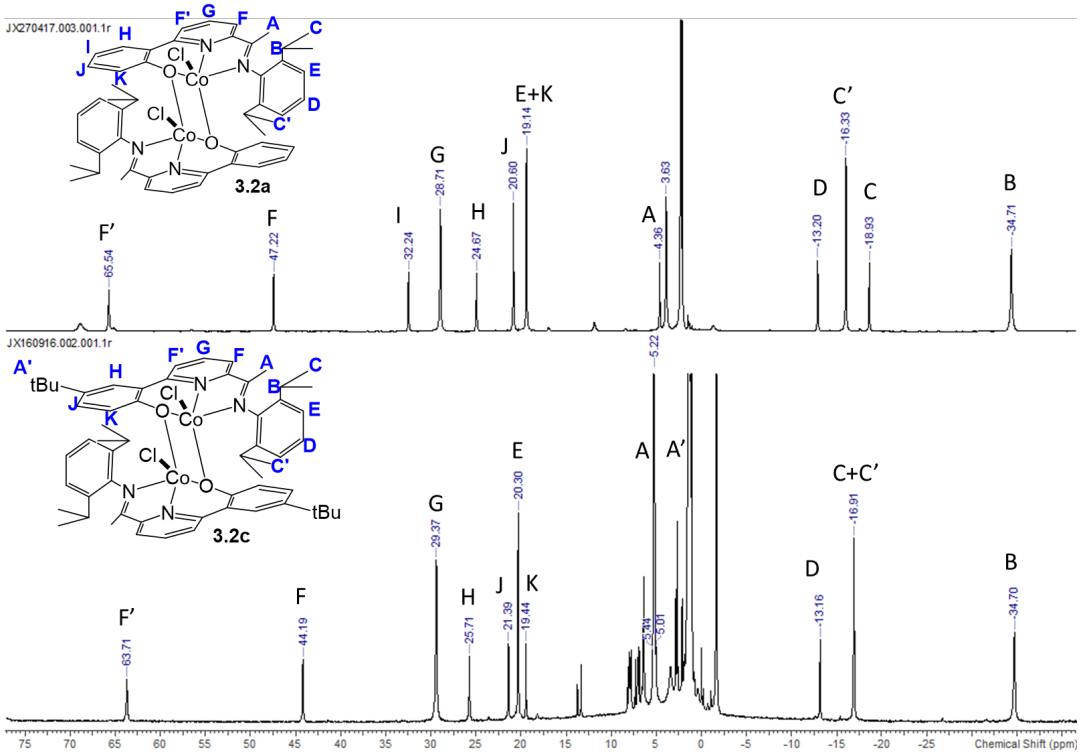

Figure 3.3.2: ^{1}H NMR spectra of isostructural **3.2a** and **3.2c** in CD_3CN at room temperature.

In the ^{1}H NMR spectra of all four complexes, broad paramagnetically shifted peaks were seen in the range δ -50 – 150. In the case of bimetallic **3.2a** and **3.2c** some degree of assignment was possible by direct comparison of their spectra, reference to chemical shifts reported in the literature along with relative integrations and proximity of the

particular proton to the metal centre.[33] **Fig. 3.3.2** shows the ^{1}H NMR spectra of both **3.2a** and **3.2c** along with the assignments (**A**-**G**) for the proton resonances. The *meta*-pyridyl (**F** and **F'**) and *para*-pyridyl (**G**) protons for both complexes **3.2a** and **3.2c** appeared downfield with similar signals at δ 64.63_{av}, δ 45.70_{av} and δ 32.24_{av}. The *meta*-aryl protons (**E**) and *para*-aryl protons appeared more upfield with similar shifts at δ 19.72_{av} and δ -13.18_{av}, respectively. By comparing both spectra, the key difference is the presence of aryl proton, **I**, in **3.2a** (δ 32.24) which is absent in **3.2c**; the other aryl protons (**J**, **H**, **K**) for both were found at similar chemical shifts between δ 24.57 – δ 19.14. The ketamine protons **A** of both could be seen at δ 4.36 (**3.2a**) and δ 5.24 (**3.2c**), however the *tert*-butyl protons **A'** of **3.2c** could not be unequivocally assigned. In addition, isopropyl methyl protons for **3.2a** showed two singlets at δ 16.33 and δ 18.93, while only one signal could be seen at δ 16.91 for **3.2c**.

The IR spectra of **3.1a**, **3.1b**, **3.2a** and **3.2c** displayed strong absorption bands around 1596 - 1620 cm^{-1} which were typically 30 cm^{-1} lower in wavenumber than in the free ligand; observations that are consistent with the coordination of the imine nitrogen atom.[49-53] The FAB mass spectra revealed peaks at *m/z* 430.1455, 895.2602, 506.2232 and 486.0012 corresponding to the fragmentation ions $[M\text{-}HCl_2]^+$ (**3.1a**), $[M\text{-}Cl]^+$ (**3.2a**), $[M\text{-}Cl]^+$ (**3.1b**) and $[M\text{-}HCl_2]^+$ (**3.2c**). In addition, the microanalytical data obtained for each complex were in support of the compositions proposed.

All four cobalt complexes were recrystallised from hot acetonitrile yielding, in the cases of **3.1a**, **3.2a** and **3.2c**, dark green cubes that proved suitable for X-ray determinations. Recrystallisation of **3.1b** was attempted several times but despite using different solvent systems and temperatures, the resulting crystals were not of suitable quality for single crystal X-ray diffraction.

A view of the molecular structure of **3.1a** is given in **Fig. 3.3.3**, while selected bond lengths and angles are presented in **Table 3.3.1**. The structure of **3.1a** consists of a single cobalt centre surrounded by an intact H**L1$_H$** ligand, acting as a tridentate ligand, and two chlorides to complete a five-coordinate geometry that can be best described as distorted square-pyramidal. The two nitrogen and one oxygen atoms along with Cl2 form the basal plane with Cl1 filling the apical position. The Co-N_{imino} and Co(1)-O(1) bond lengths, 2.070(3) Å and 2.083(2) Å, respectively, are shorter than the central Co-$N_{pyridine}$ one [2.127(3) Å]. The N(2)-Co(1)-N(1) [77.09 (2)º] and O(1)-Co(1)-N(1)

[78.60 (11)º] angles within the five- and six-membered chelate rings are consistent with previous observations for related stuctures.[49-53] Furthermore, the Co-$N_{pyridine}$ bond length [2.127(3) Å] is longer than that observed in these related systems [2.036 – 2.079 Å].[33, 49b, 51, 52] By contrast, the Co-N_{imine} bond [2.070 (3) Å] is shorter than those found in previous reports (range: 2.193 – 2.320 Å).[52] The N-aryl ring adopts a configuration that is almost perpendicular to the coordination plane with a dihedral angle of 83.4(4)º. Meanwhile the *N,N,O(H)* proton is involved in an intramolecular O(1)-H(1)···Cl(2) hydrogen bond (2.25 Å).

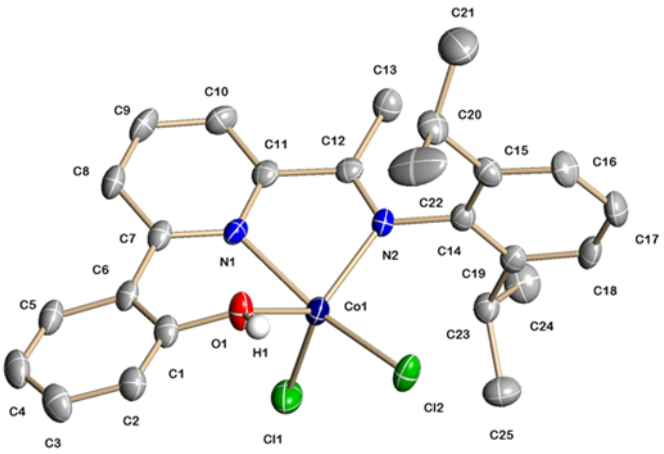

Figure 3.3.3: Molecular structure of **3.1a**.

Table 3.3.1: Selected bond lengths and angles for **3.1a.**

Bond Lengths (Å)	
Co(1)-N(1)	2.127(3)
Co(1)-N(2)	2.070(3)
Co(1)-O(1)	2.083(2)
Co(1)-Cl(1)	2.2705(13)
O(1)-H(1)···Cl(2)	2.25
Bond Angles (°)	
N(2)-Co(1)-N(1)	77.09(2)
O(1)-Co(1)-N(1)	78.60(11)
N(2)-Co(1)-Cl(1)	112.62(9)
N(2)-C(12)-C(13)	124.9(3)

The molecular structures of **3.2a** and **3.2c** are depicted in **Figure 3.3.4**, while the corresponding bond distances and angles are collected in **Table 3.3.2**. Both structures

are based on a dicobalt core in which the two cobalt(II) centres are linked by a μ-$O_{phenoxy}$ bridge that belongs to the chelating *N,N,O*-ligand. Each cobalt is almost square pyramidal geometry with two nitrogen atoms and two oxygen atoms forming the basal plane and Cl(1) filling the apical position. As with the dizinc analogue **2.2c**, each *N,N,O*-ligand in **3.2a** and **3.2c** has been deprotonated resulting in an anionic phenoxy donor [O(1)] and two neutral nitrogen donors [N(1) and N(2)]. The central Co-$N_{pyridine}$ bond length [2.099(2) Å (**3.2a**, **3.2c**)] is shorter than the exterior Co-N_{imino} distance [2.100(2) Å (**3.2a**), 2.115(2) Å (**3.2c**)], while the N(2)-Co(1)-N(1) [77.24(8)° **3.2a**, 77.10(9)° **3.2c**] and O(1)-Co(1)-N(1) [85.03(7)° **3.2a**, 147.60(7)° **3.2c**] angles present within each five- and six-membered chelate ring, respectively, are consistent with previous observations.[54] The N-aryl rings are almost perpendicular to the *N,N,O*-coordination plane with dihedral angles of 83.7(3)° and 93.5(2)° for **3.2a** and **3.2c**, respectively. Examples of dicobalt complexes containing a M(μ-OR)$_2$M core involving tridentate *N,N,O*-containing ligands are rare. However, there are a number of tetraimine ligated μ-OH, μ-$(O)_2$ complexes that have been published.[39,56,57] The Co(1)-O(1) bond distance is the shortest involving the tridentate ligand [2.0047(17) Å (**3.2a**), 2.031(2) Å (**3.2c**)] on account of its anionic nature; it is also notably longer than that observed in other tetraimine complexes [range: 1.839(3) to 1.877(4) Å].[54] Another interesting structural metric is the Co···Co separation. Both complexes **3.2a** and **3.2c** exhibit shorter internuclear distances [3.129 Å (**3.2a**), 3.163 Å (**3.2c**)] when compared with that seen in reported tetraimine complexes [range: 3.178 to 3.304 Å] and with related Co^{II}(μ-OR)$_2$$Co^{II}$ type structures [range: 3.224-3.338 Å].[37] Indeed, only the μ-OH, μ-$(O)_2$ and μ-NH_2-[$(NH_3)_3$Co]$_2$$(NO_3)_3$ reported by Werner *et al.* show a shorter distance [2.766 Å].[4]

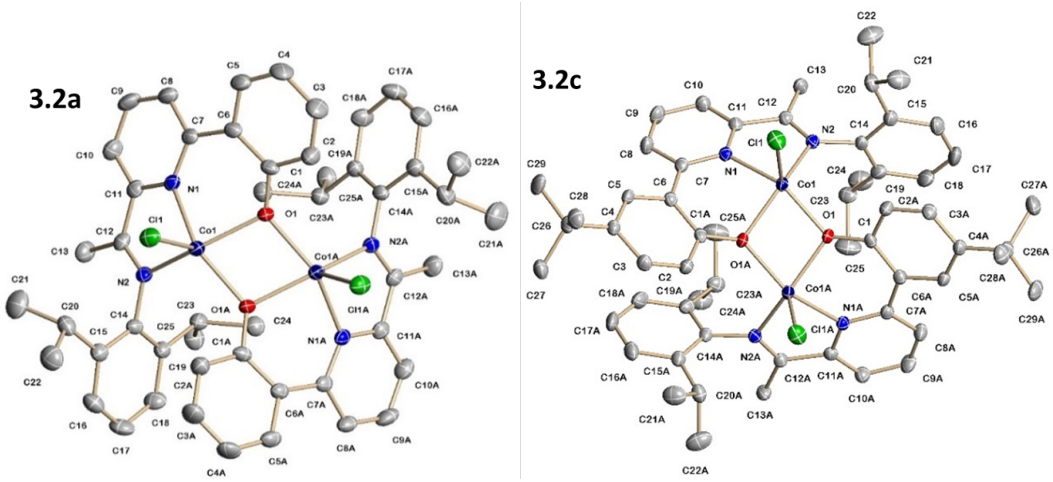

Figure 3.3.4: Molecular structures of **3.2a** and **3.2c.**

Table 3.3.2: Selected bond lengths and angles for **3.2a** and **3.2c.**

*Bond Lengths (Å) for **3.2a***		*Bond Lengths (Å) for **3.2c***	
Co(1)-O(1)	2.0047(17)	Co(1)-O(1)	2.031(2)
Co(1)-O(1A)	2.0355(19)	Co(1)-O(1A)	2.011(19)
Co(1A)-O(1)	2.0355(19)	Co(1A)-O(1)	2.011(19)
Co(1A)-O(1A)	2.0047(17)	Co(1A)-O(1A)	2.031(2)
Co(1)-N(1)	2.099(2)	Co(1)-N(1)	2.099(2)
Co(1)-N(2)	2.115(2)	Co(1)-N(2)	2.100(2)
Co(1)-Cl(1)	2.2985(9)	Co(1)-Cl(1)	2.2885(14)
Co(1)···Co(1A)	3.129	Co(1)···Co(1A)	3.163
*Bond Angles (°) for **3.2a***		*Bond Angles (°) for **3.2c***	
N(1)-Co(1)-N(2)	77.24(8)	N(1)-Co(1)-N(2)	77.10(9)
O(1)-Co(1)-N(1)	85.03(7)	O(1)-Co(1)-N(1)	147.60(7)
O(1)-Co(1)-O(1)A	77.53(7)	O(1)-Co(1)-O(1)A	76.88(9)
N(1)-Co(1)-Cl(1)	97.12(7)	N(1)-Co(1)-Cl(1)	94.93(7)
N(2)-C(12)-C(13)	125.1(3)	N(2)-C(12)-C(13)	125.1(2)

The atoms labelled with an 'A' have been generated by symmetry

3.3.1.2 Reactivity of H_2**L3**$_H$ towards cobalt(II) chloride

The *N(H),N,O(H)*-amine ligand H_2**L3**$_H$ was also reacted with anhydrous $CoCl_2$ in THF at room temperature (**Scheme 3.3.2**). Dark green crystals of $(H_2$**L3**$_H)_2CoCl_2$ (**3.3**) were formed by the slow evaporation of a hot concentrated acetonitrile solution of the

complex. The product was fully characterised by ^{1}H NMR, IR spectroscopy, X-ray diffraction, ESI-MS and elemental analysis.

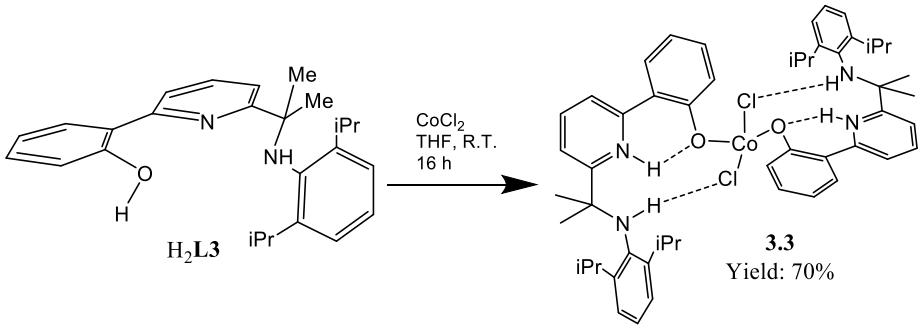

Scheme 3.3.2: Synthesis of cobalt(II) chloride complex **3.3.**

Complex **3.3** displayed a magnetic moment (μ_{eff}) of 4.89 BM which is consistent with three unpaired electrons. The ν(N-H) absorption band had shifted by 60 cm^{-1} to lower wavenumber when compared to that observed in free H_2**L3**. In addition, analysis of **3.3** by FAB mass spectrometry showed strong fragmentation peaks at *m/z* 446.4817 corresponding to the ions [M-H$\mathbf{L3_H}$-2Cl]$^{+}$. In addition, the microanalytical data for **3.3** were consistent with the calculated elemental compositions.

Crystallisation of **3.3** also from hot acetonitrile gave dark green cube crystals that proved suitable for single crystal X-ray diffraction studies. A view of **3.3** and selected bond lengths and angles are shown in **Fig 3.3.5** and **Table 3.3.3**, respectively. The structure of **3.3** revealed a Co(II) centre surrounded by two chlorides and two monodentate O-bound *N(H),N$_{py}$(H)O*-ligands to give a geometry at cobalt that can be best considered as tetrahedral. The H_2**L3** ligand remained protonated but with the OH hydrogen atom now linked to the central nitrogen with the result that it now acts as a *N(H),N$_{py}$(H)O*-type ligand. In addition, a hydrogen bond was formed between the proton of the exterior amine and a neighbouring chloride while another was formed between the pyridinium hydrogen and the coordinated oxygen atom. There were no intermolecular contacts of note.

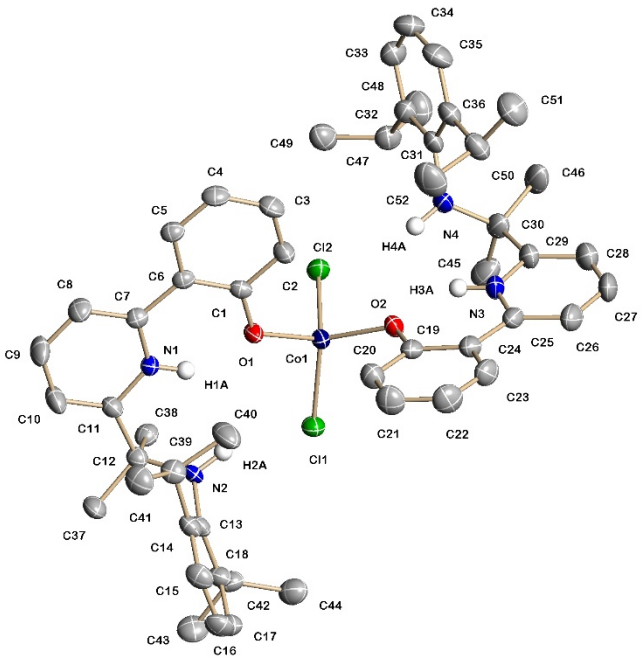

Figure 3.3.5: Molecular structure of **3.3.**

Table 3.3.3: Selected bond lengths and angles for complex **3.3**.

Bond Lengths (Å)	
Co(1)-O(1)	1.9553(16)
Co(1)-O(2)	1.9630(17)
Co(1)-Cl(1)	2.2773(9)
Co(1)-Cl(2)	2.2802(9)
N(1)-H(1A)···O(1)	1.81
N(3)-H(3A)···O(2)	1.83
N(2)-H(2A)···Cl(1)	2.70
N(4)-H(4A)···Cl(2)	2.63
Bond Angles (°)	
O(1)-Co(1)-O(2)	114.19(7)
O(1)-Co(1)-Cl(1)	105.16(5)
O(1)-Co(1)-Cl(2)	119.19(6)
O(1)-C(1)-C(2)	120.6(2)

3.3.1.3 Reactivity of **L2** and H**L4** towards cobalt(II) chloride

Complexation of the *N,N,N*-tridentate ligands, **L2** and H**L4**, with cobalt(II) chloride were also investigated using the same experimental procedure as that outlined in the last section affording (**L2**)$CoCl_2$ and (H**L4**)$CoCl_2$ (**3.4**) in good yields (**Scheme 3.3.3**). Bis(imino)pyridine complex (**L2**)$CoCl_2$ has been synthesised and characterised by several research groups,[33] so full characterisation, by ESI MS, FAB mass spectrometry, magnetic susceptibility, IR spectroscopy, ^{1}H NMR spectroscopy and X-ray diffraction, was performed on solely **3.4**. Nevertheless, some data for (**L2**)$CoCl_2$ was re-collected to allow a comparison with **3.4**.

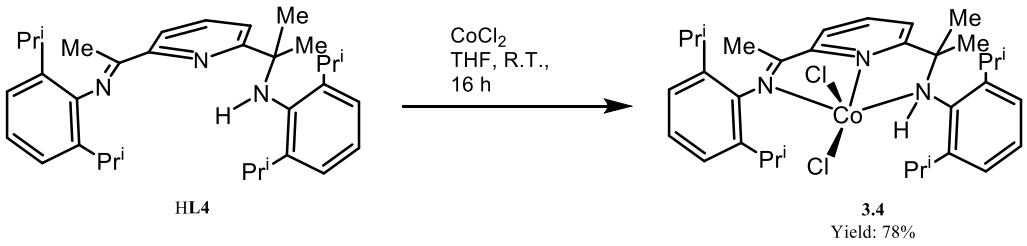

Scheme 3.3.3: Synthesis of *N,N,N*-cobalt(II) chloride complex **3.4**.

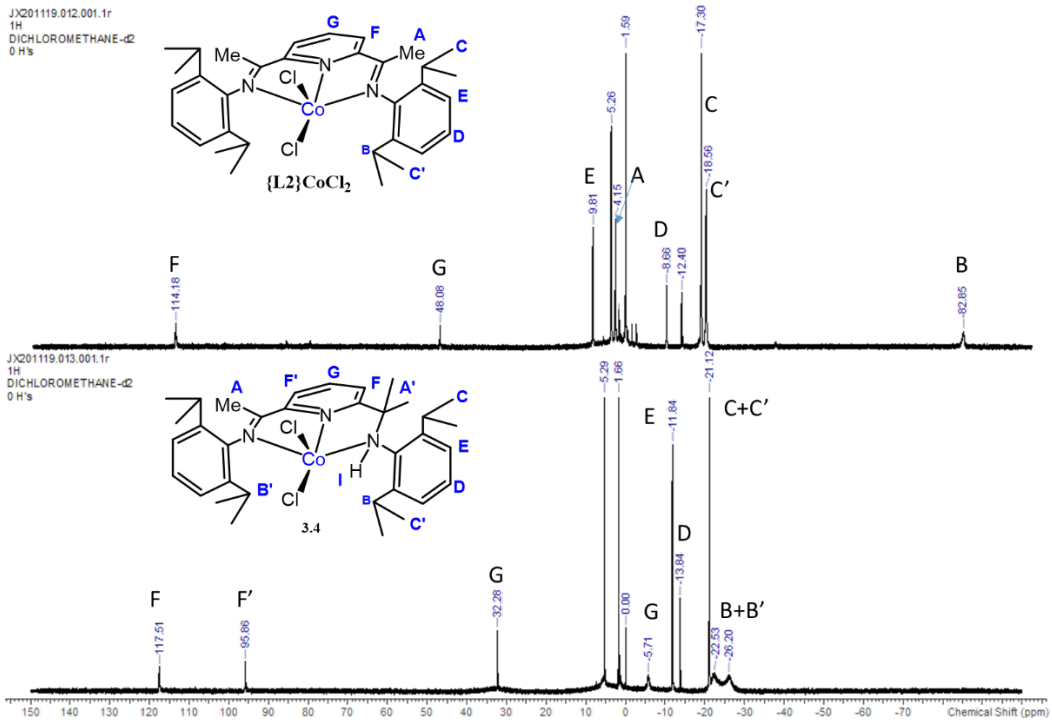

Figure 3.3.6: ^{1}H NMR spectrum of **3.4** in CD_2Cl_2 at room temperature along with the spectrum for (**L2**)$CoCl_2$. [33]

As with complex (**L2**)$CoCl_2$, **3.4** is paramagnetic and afforded a magnetic moment of ~4.6 BM, which is consistent with three unpaired electrons. **Fig. 3.3.6** shows the ^1H NMR spectra for (**L2**)$CoCl_2$ and **3.4** in which the proton signals (**A** - **I**) are highly shifted on account of the paramagnetism. For complex **3.4**, the two *meta*-pyridyl protons (**F'** and **F**) and *para*-pyridyl proton (**G**) can be seen downfield at δ 117.51, δ 95.86 and δ 32.28. The *meta*-aryl protons **E** and *para*-aryl protons **D** appear more upfield at δ -11.84 and δ -13.84. The ketimine and ketamine protons (**A** and **A'**) could be found at δ 5.29 and 1.66, which are possibly masked by signals belonging to the solvent CD_2Cl_2 and H_2O. Furthermore, the isopropyl methyl protons (**C**, **C'**) and (**B**, **B'**) appear at δ -21.12 and -28.20. By comparison with (**L2**)$CoCl_2$, the key differences are the presence of two signals for the *meta*-pyridyl protons (**F** and **F'**) while just one signal at δ 114.18 is seen for (**L2**)$CoCl_2$. Moreover, the *meta*-aryl and *para*-aryl protons are more upfield than seen in (**L2**)$CoCl_2$. In addition, the amine proton (N-H) of **3.4** shows a broad peak at δ -5.71.

The IR spectrum of **3.4** indicates that the N-coordinated imine and amine N-H absorptions at *ca.* 1590 cm^{-1} and 3300 cm^{-1}, respectively. In the FAB mass spectrum, **3.4** displayed two strong fragmentation peaks corresponding to *m/z*: $[M\text{-}Cl]^+$ 591.2819 and $[M\text{-}2Cl\text{-}H]^+$ 555.3147. The results of the elemental analysis were in good agreement with the calculated elemental composition.

Crystals of **3.4** suitable for an X-ray structural determination were also grown by the slow cooling of hot concentrated acetonitrile solution of the complex. The molecular structure of **3.4** is shown in **Fig. 3.3.7**; selected bond lengths and angles are presented in **Table 3.3.4**. The structure of **3.4** comprises a single cobalt(II) centre bound by a neutral *N(H),*N_{py}*,N*-chelating ligand and two chloride ligands to complete a distorted square pyramidal geometry. The Co-$N_{pyridyl}$ bond length is significantly shorter than the Co-N_{imino} and Co-N_{amino} bonds, with double and single bond character evident in the imino N(1)-C(7) and amino linkages N(3)-C(14), respectively. The planes of the 2,6-diisopropylphenyl rings are oriented essentially orthogonally to the plane of ligand backbone [ranging between 84.1° and 84.6°]. Two five-membered chelate rings are formed with internal N-Co-N angles of 74.89(6)° and 76.70(6)°. There is no dominant intermolecular interactions of note.

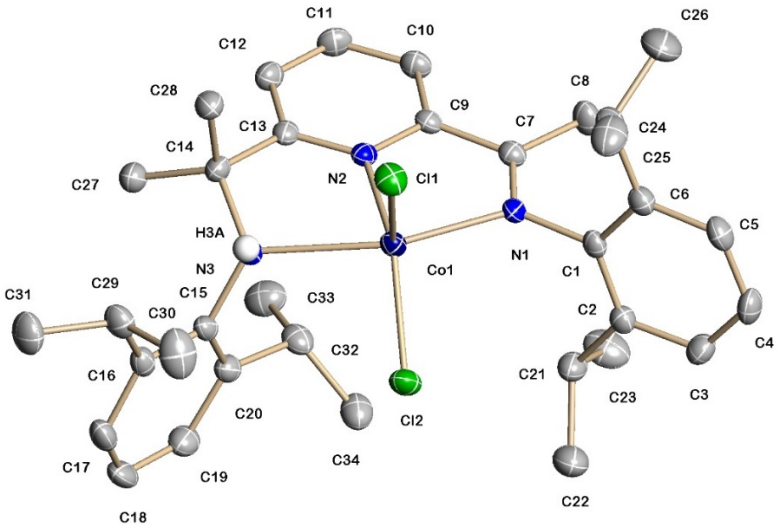

Figure 3.3.7: Molecular structure of **3.4**.

Table 3.3.4: Selected bond lengths and angles for **3.4.**

Bond Lengths (Å)	
Co(1)-N(1)	2.174(16)
Co(1)-N(2)	2.066(17)
Co(1)-N(3)	2.3319(16)
Co(1)-Cl(1)	2.3013(6)
Bond Angles (°)	
N(2)-Co(1)-N(1)	76.70(6)
N(2)-Co(1)-N(3)	74.89(6)
N(2)-Co(1)-Cl(1)	112.62(9)
N(2)-C(12)-C(13)	124.9(3)

3.3.2 Complexation with Co(II) tetrafluoroborate

3.3.2.1 Reactivity of H**L1**$_R$ towards $[Co(py)_4(NCMe)_2][BF_4]_2$

In the introductions to **Chapters 2** and **3**, we highlighted the ability of a tetrafluoroborate counterion, present in salts of the type $[LM^{II}][BF_4]_n$, to act as a source of a F^- ligand for late transition metals. Herein, a series of complexation reactions of H**L1**$_H$, H**L1**$_{Ph}$ and H**L1**$_{tBu}$ with $[Co(py)_4(NCMe)_2][BF_4]_2$ (where py = pyridine) have been the subject of the investigation. The tetrafluoroborate salt, $[Co(py)_4(NCMe)_2][BF_4]_2$, could be readily prepared in high yield by reacting $[Co(OH_2)_6][BF_4]_2$ with excess pyridine in dry acetonitrile and isolated by crystallisation. Indeed, $[Co(py)_4(NCMe)_2][BF_4]_2$ has been the subject of a single crystal X-ray

diffraction study (see appendix). However, all the reactions with H**L1**$_R$ were conducted using a sample of $[Co(py)_4(NCMe)_2][BF_4]_2$ that had been generated *in-situ*. Typically, these reactions were performed in acetonitrile at 80 ^oC for 16 hours. Two types of products were isolated namely, mono-cobalt $[(H\mathbf{L1}_{Ph})Co(NCMe)_3][BF_4]_2$ (**3.7b**) and the dicobalt complexes $[(\mathbf{L1_R})_2Co_2(MeCN)(L)][BF_4]_2$ (R = H, L = Py **3.5a**, R = t-Bu, L = MeCN **3.6c**) (**Scheme 3.3.4**). Upon work-up, bimetallic **3.5a** and **3.6c** were obtained in good yield, while the yield achieved for **3.7b** was lower. All three cationic complexes were characterised by ^1H NMR, ^{19}F NMR, IR spectroscopies, electrospray mass spectrometry (ESI-MS), magnetic measurements and elemental analysis.

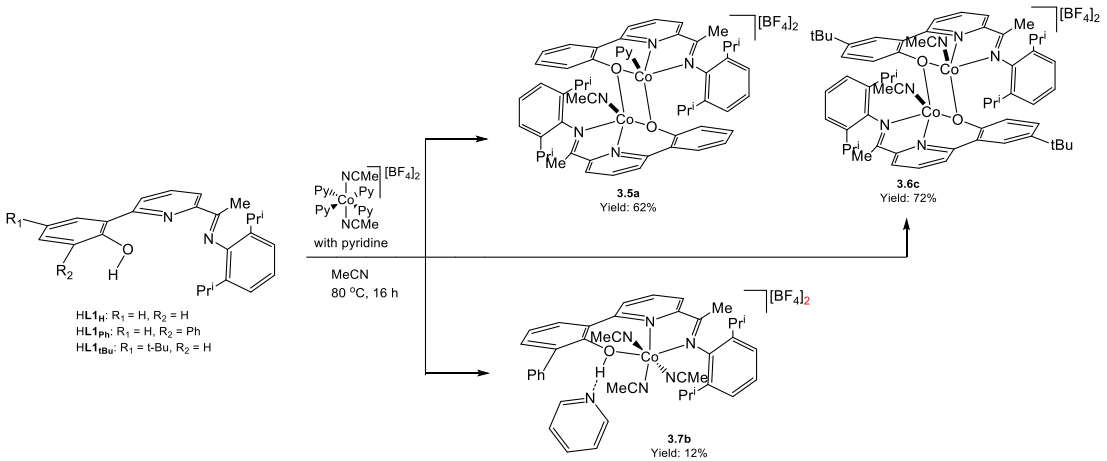

Scheme 3.3.4: Synthetic route to **3.5a**, **3.6c** and **3.7b**.

The effective magnetic moments for both dimeric structures (**3.5a** and **3.6c**) were determined as μ_{eff} = 6.24 BM (**3.5a**) and 6.43 BM (**3.6c**) at 300 K. Such values were consistent with two non-interacting Co(II)-Co(II) (S = 3/2) metal centres (using $\mu^2 = \sum\mu_i^2$, where μ_i is the magnetic moment of the individual metal centres[39]). The IR spectra of **3.5a** ad **3.6c** showed strong absorptions at 1609 cm^{-1} and 1588 cm^{-1} that can be assigned to $\upsilon(C{=}N)_{imine}$ bands. In addition, fragmentation peaks in their ESI MS and FAB mass spectra and the results of elemental analysis were consistent with their formulations.

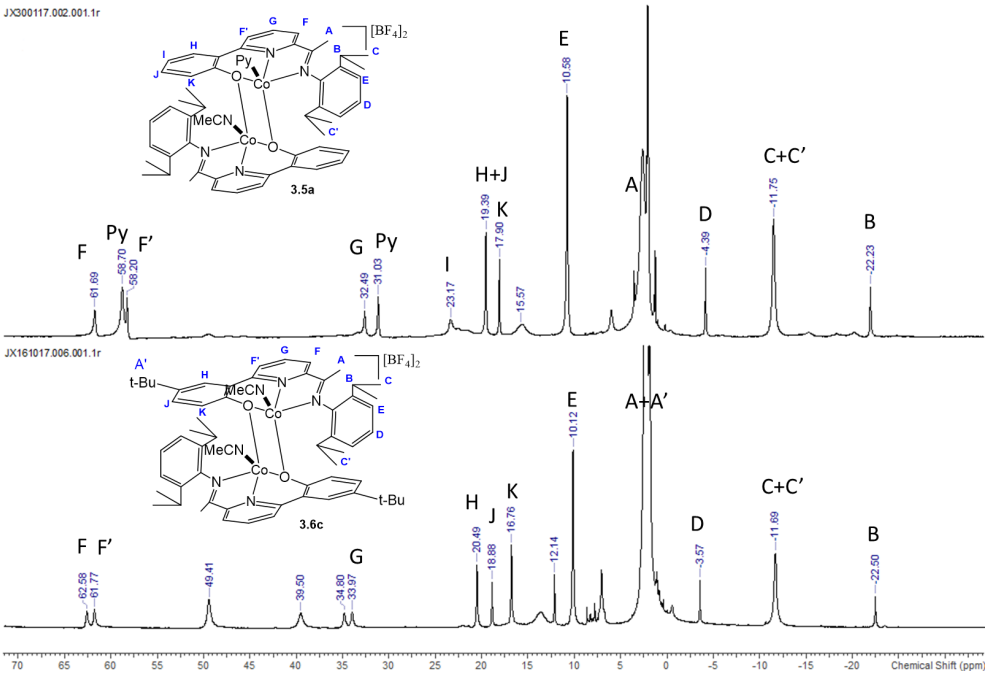

Figure 3.3.8: ^{1}H NMR spectrum of **3.5a** in CD_3CN at room temperature.

Broad paramagnetically shifted peaks were a feature of the ^{1}H NMR spectra of **3.5a** and **3.6c** making full assignment difficult. Nonetheless, by comparison of their ^{1}H NMR spectra with those obtained for **3.1** - **3.4** (see earlier), some degree of assignment for **3.5a** and **3.6c** was possible. **Fig 3.3.8** shows the ^{1}H NMR spectra of **3.5a** and **3.6c**. The *meta*-pyridyl and *para*-pyridyl protons appeared downfield δ 61.69 – δ 32.39. Due to one cobalt centre in **3.5a** possessing an N-bound pyridine ligand, there is an extra signal at δ 58.70 corresponding to the *para*-pyridyl proton. Unlike in **3.6c**, the spectrum of **3.5a** contains an aryl proton **I** in **3.5a**, otherwise other aryl protons (**J**-**K**) were observed at similar chemical shifts between δ 61.69 – 32.49. The *meta*-aryl protons (**E**) also appeared upfield at δ 10.32_{av}. Unfortunately, the ketimine protons and *tert*-butyl protons (**A** and **A'**) could not be assigned with any certainty. The *para*-aryl protons and isopropyl protons for both were seen at similar shifts: δ -3.98_{av} (**D**), δ -11.72_{av} (**C**,**C'**) and δ -22.365_{av} (**B**). Moreover, the ^{19}F NMR and ^{11}B NMR spectra for all complexes just showed one signal at δ *ca.* -150.0 and δ -1.19, which can be assigned to the BF_4^- counteranion, this is attributed to the paramagnetic property of Co(II) complexes.

Dark orange cube-like crystals of **3.5a** and **3.6c**, grown from a layered MeCN-Et_2O (1:10) solution, proved suitable for single crystal X-ray diffraction. Views of the molecular structures of **3.5a** and **3.6c** are shown in **Fig. 3.3.9**; selected bond distances

and angles are collected in **Table 3.3.5**. Both structures consist of dicationic unit that is charge balanced by two tetrafluoroborate counterions. Within the cationic unit, the two cobalt centres are chelated by their respective *N,N,O*-ligands with the anionic $O_{phenoxy}$ donor additionally acting as a bridging ligand. In **3.5a**, the coordination spheres of each cobalt centre are completed by either a pyridine [Co(1)-N(5) 2.047(9) Å] or acetonitrile [Co(2)-N(6) 2.043(10) Å]. By contrast in **3.6c**, two molecules of acetonitrile complete the coordination spheres. Nonetheless, the resulting 5-coordinate geometries of each cobalt centre can be best described as square pyramidal with two nitrogen atoms and two oxygen atoms forming the basal plane and an acetonitrile or pyridine ligand filling the apical position. For both complexes, the monodentate nitrogen donor ligands are configured *cis*. This unsymmetrical coordination of the nitrogen donors in **3.5a** is different from other binuclear complexes reported in this work (**3.2a**, **3.2c** and **3.6c**). The Co-O bond lengths of both **3.5a** and **3.6c** [range: 1.963(7)-2.069(6) Å] are similar to those observed in the dicobalt chloride complexes **3.2a** and **3.2c** [range: 2.005(17)-2.035(19) Å]. Two types of chelate rings are present, a larger 6-membered chelate ring containing O(1)-Co(1)-N(1) angles of 85.9(3)° (**3.5a**) and 87.6(3)° (**3.6c**), and a 5-membered chelate ring with N(1)-Co(1)-N(2) angles of 78.8(4)° (**3.5a**) and 79.2(3)° (**3.6c**). The distance between two cobalt centres [3.099 Å (**3.5a**) and 3.118Å (**3.6c**)] is slightly shorter then observed in dicobalt chloride complexes **3.2a** (3.129 Å) and **3.2c** (3.163 Å). There is no evidence of the BF_4 anions in either structure undergoing a contact with the complex cationic unit. As a general point, μ-$(OR)_2$-containing dicobalt tetrafluoroborate complexes bearing tridentate N-containing ligands like that in **3.5a** and **3.6c** have not, to the knowledge of the author, been reported.

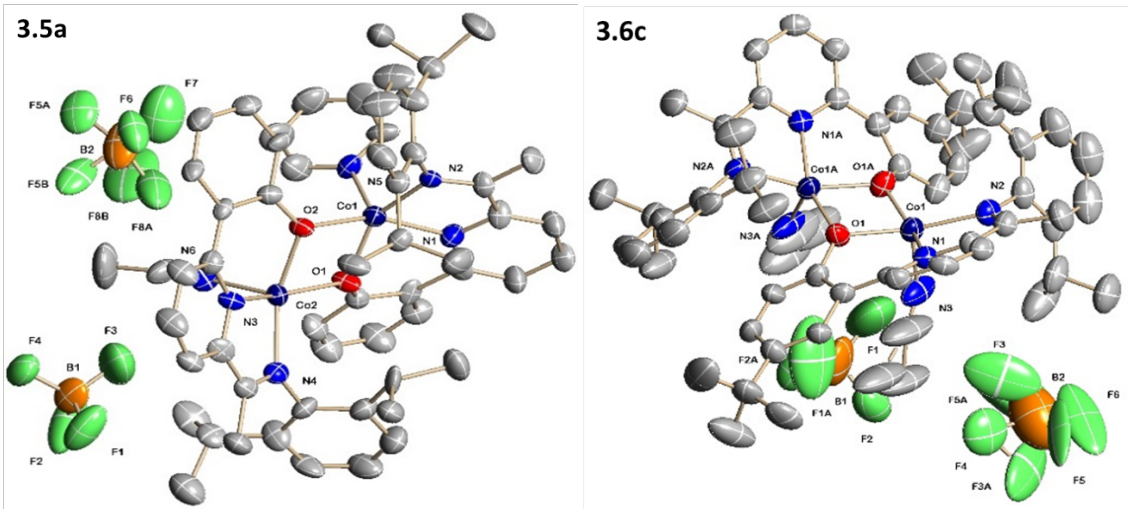

Figure 3.3.9: Molecular structures of **3.5a** and **3.6c.**

Table 3.3.5: Selected bond and lengths and angles for **3.5a** and **3.6c**

*Bond Lengths(Å) for **3.5a***		*Bond lengths (Å) for **3.6c***	
Co(1)-O(1)	1.963(7)	Co(1)-O(1)	2.009(5)
Co(1)-O(2)	2.069(6)	Co(1)-O(1)A	1.989(5)
Co(2)-O(1)	2.039(6)	Co(1)A-O(1)	1.989(5)
Co(2)-O(2)	1.984(7)	Co(1)A-O(1)A	2.009(5)
Co(1)-N(1)	2.100(9)	Co(1)-N(1)	2.089(7)
Co(1)-N(2)	2.053(7)	Co(1)-N(2)	2.099(7)
Co(1)-N(5)	2.047(9)	Co(1)-N(3)	2.050(9)
Co(2)-N(6)	2.043(10)	Co(1)-N(3)A	2.051(8)
Co(1)···Co(2)	3.118	Co(1)···Co(1A)	3.099
*Bond Angles(°) for **3.5a***		*Bond Angles(°) for **3.6c***	
O(1)-Co(1)-N(1)	86.0(3)	O(1)-Co(1)-N(1)	87.6(3)
N(2)-Co(1)-N(1)	78.8(4)	N(2)-Co(1)-N(1)	79.2(3)
N(5)-Co(1)-N(2)	108.2(4)	N(5)-Co(1)-N(2)	100.4 (3)
O(1)-Co(1)-O(2)	78.3(3)	O(1)-Co(1)-O1(A)	78.4(2)
Co(1)-O(1)-Co(2)	102.4(3)	Co(1)-O(1)-Co1(A)	101.6(2)

Atoms labelled with 'A' have been generated by symmetry

Recrystallisation of **3.7b** was the most challenging of the series and a wide variety of conditions were attempted (*e.g.* varying the solvent system, concentration of solution, temperature etc). However, on one occasion, a few crystals of **3.7b** were formed that proved suitable for the X-ray determination. A view of **3.7b** is shown in **Figure 3.3.10**,

while selected bonds and angles are gathered in **Table 3.3.8**. Unlike complexes **3.5a** and **3.6c**, the solid-state structure of **3.7b** revealed a mononuclear dication that was charge balanced by two BF_4^- counterions. Within the cationic unit the cobalt centre is bound by an intact *N,N,O(H)* ligand and three N-bound acetonitrile ligand ligands to complete a distorted octahedral geometry. In addition the *N,N,O(H)* proton is involved in an intermolecular hydrogen bond with a molecule of pyridine [O(1)-H(1)···N(6) 1.65 Å]. This type of structure was not be observed in the corresponding zinc(II) experiments and indeed with other *N,N,O* or *N,N,N*-ligand systems. It would seem likely that the steric properties of H**L1**$_{Ph}$ inhibit the formation of a dimeric structure analogous to **3.5a** and **3.6c**. As seen in previous examples within this family, the Co(1)-O(1) bond represents the shortest bond length involving the pincer ligand [1.949(8) Å]. Within the 6- and 5-membered metallacycles, the O(1)-Co(1)-N(1) bond angle is 87.0(4)° and the (1)-Zn(1)-N(2) bond angle is 76.53(7)°, respectively. The N(2)-C(12)-C(13) bond angle [125.7(13)°] confirmed that the imine unit retained its sp^2 hybridisation.

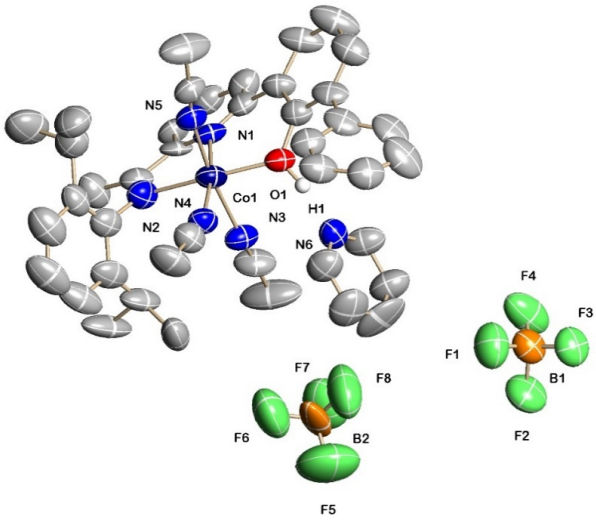

Figure 3.3.10: Molecular structure of **3.7b**.

Table 3.3.8: Selected bond lengths and angles for **3.7b**.

Bond Lengths (Å)	
Co(1)-O(1)	1.949(8)
Co(1)-N(1)	2.099(10)
Co(1)-N(2)	2.141(11)
C(12)-N(2)	1.250(15)
O(1)-H(1)···N(6)	1.65

Bond Angles (°)	
N(1)-Co(1)-O(1)	87.0(4)
N(1)-Co(1)-N(2)	77.6(4)
C(13)-C(12)-N(2)	125.7(13)

Given the inability of H**L1**$_{Ph}$ to form the bimetallic analogue of **3.5a** and **3.6c**, we decided to explore the capacity of its less sterically bulky *O,N,O(H)*-precursor, Ketone-Ph, to promote dimerisation. Hence, reaction of $[Co(py)_4(NCMe)_2][BF_4]_2$ with Ketone-Ph was explored under the same conditions that were used for the synthesis of **3.5a**, **3.6c** and **3.7b** (**Scheme 3.3.4**). Complex $[(O,N,O)_2Co_2(MeCN)_4][BF_4]_2$ (**3.8**) was isolated in reasonable yield and characterised by ^{1}H NMR, ^{19}F NMR and IR spectroscopies as well as by electrospray mass spectrometry (ESI-MS), elemental analysis and X-ray diffraction.

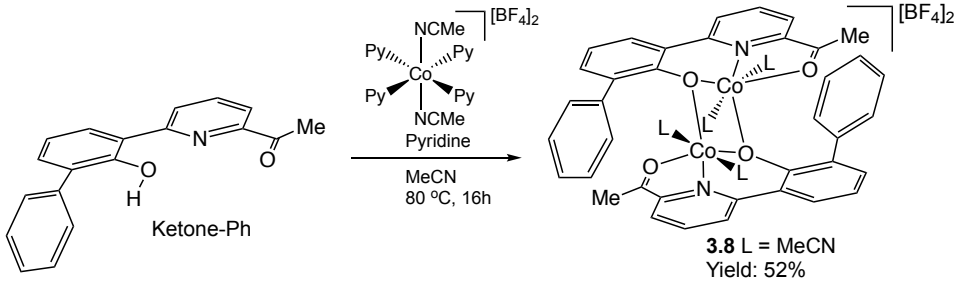

Scheme 3.3.5: Reaction of Ketone-Ph with $[Co(py)_4(NCMe)_2][BF_4]_2$ to give **3.8.**

Broad paramagnetically shifted peaks were a feature of the ^{1}H NMR spectra of **3.8** making full assignment difficult. The effective magnetic moment of **3.8** recorded at 300 K was determined as μ_{eff} = 6.12 BM. The ^{19}F NMR spectra showed a singlet at δ -150.97 assignable to the BF_4^- counterions. In the IR spectrum, the υ(C=O) absorption band was shifted by 48 cm^{-1} to lower wavenumber when compared to that observed in free Ketone-Ph. Furthermore, analysis of **3.8** by FAB mass spectrometry showed strong fragmentation peaks at 858.1821 corresponding the ions, $[M\text{-}2BF_4]^+$. In addition, the results of elemental analysis were consistent with the calculated element compositions for **3.8**.

Dark red crystals of **3.8**, suitable for the X-ray determination, were obtained from a hot concentrated acetonitrile solution layered with diethyl ether. The molecular structure is shown in **Fig. 3.3.11**, while selected bonds and angles are compiled in **Table 3.3.9**. The

structure reveals a complex dication and two tetrafluoroborate counterions. The dicationic unit adopts a dimeric similar to that seen in **3.6a** and **3.6c**, in which the *O,N,O(H)* proligand has been deprotonated and acts a chelating and bridging ligand. In addition two molecules of acetonitrile are bound to each cobalt(II) centre (Co(1)-N(3) 2.129(5) Å). Unlike the square pyramidal geometries exhibited in **3.6a** and **3.6c**, each cobalt centre in **3.8** is almost octahedral. The Co-$N_{pyridyl}$ and Co-O bond lengths of **3.8** are similar to the corresponding bond distances in dimers **3.2a**, **3.2c**, **3.6a** and **3.6c**. The Co(1)···Co(2) internuclear distance of 3.190 Å is comparable to that observed in the other the dicobalt complexes **3.6a** and **3.6c** [range: 3.099-3.118 Å], but shorter than in the dicobalt chloride complexes **3.2a** and **3.2c** [range: 3.129-3.163 Å]. The 6- and 5-membered chelate rings in **3.8** contain N(1)-Co(1)-O(1) and N(1)-Co(1)-O(2) angles of 85.81(17)^{o} and 76.35(17)^{o}, respectively. Lastly, the two planes of Ketone-Ph ligands are aligned in parallel fashion and perpendicular to the plane of Co(1)-O(1)-Co(2)-O(3) pocket (96.26(15)°). There is no evidence of any interactions between the dicationic unit and the tetrafluoroborate counterions.

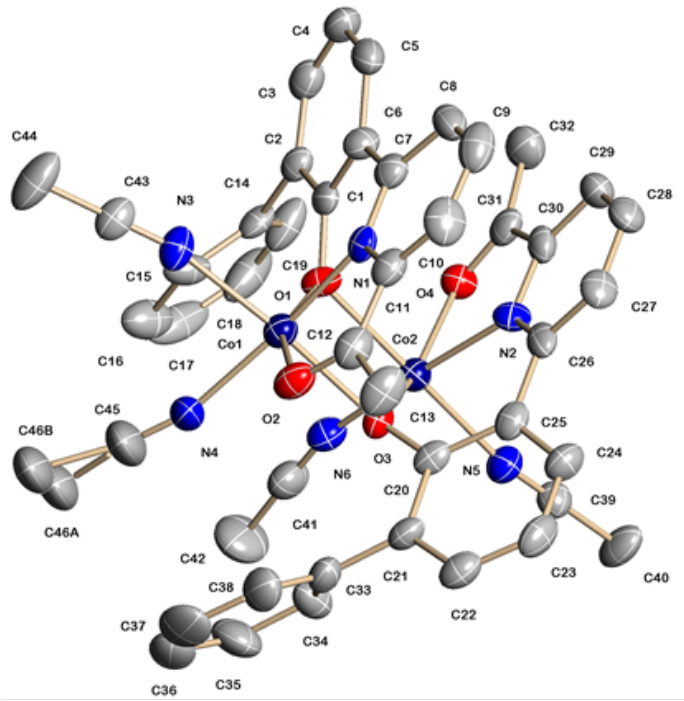

Figure 3.3.11: Molecular structure of **3.8**; the BF_4 counterions are omitted for clarity.

Table 3.3.9: Selected bond lengths and angles **3.8**.

Bond Lengths (Å)	
Co(1)-O(1)	1.971(4)
Co(1)-O(2)	2.137(4)
Co(1)-O(3)	2.171(4)
Co(2)-O(1)	2.167(4)
Co(2)-O(3)	1.953(4)
Co(2)-O(4)	2.108(4)
Co(1)-N(1)	2.109(5)
Co(2)-N(2)	2.088(5)
Co(1)-N(3)	2.129(5)
Co(1)···Co(2)	3.190
Bond Angles (°)	
N(1)-Co(1)-O(1)	85.81(17)
N(1)-Co(1)-O(2)	76.35(17)
N(1)-Co(1)-N(3)	89.51(18)
O(1)-Co(1)-O(3)	78.71(14)
Co(1)-O(1)-Co(2)	100.75(15)
C(13)-C(12)-N(2)	125.7(13)

3.3.2.2 Reactivity of **L2** and H**L4** towards $[Co(Py)_4(NCMe)_2][BF_4]_2$

The reactions of $[Co(Py)_4(NCMe)_2][BF_4]_2$ with bis(imino)pyridine **L2** and its derivative H**L4** were also explored. To allow solubilisation of the ligands, the reactions had to be conducted at reflux in a mixed solvent system composed of dry dichloromethane and acetonitrile (**Scheme 3.3.6**). After 16 hours the reactions were worked-up affording complexes $[(\mathbf{L2})Co(NCMe)_2(Py)][BF_4]_2$ (**3.9**) and $[(H\mathbf{L4})Co(NCMe)_2(HOBF_3)][BF_4]$ (**3.10**) in reasonable yield.

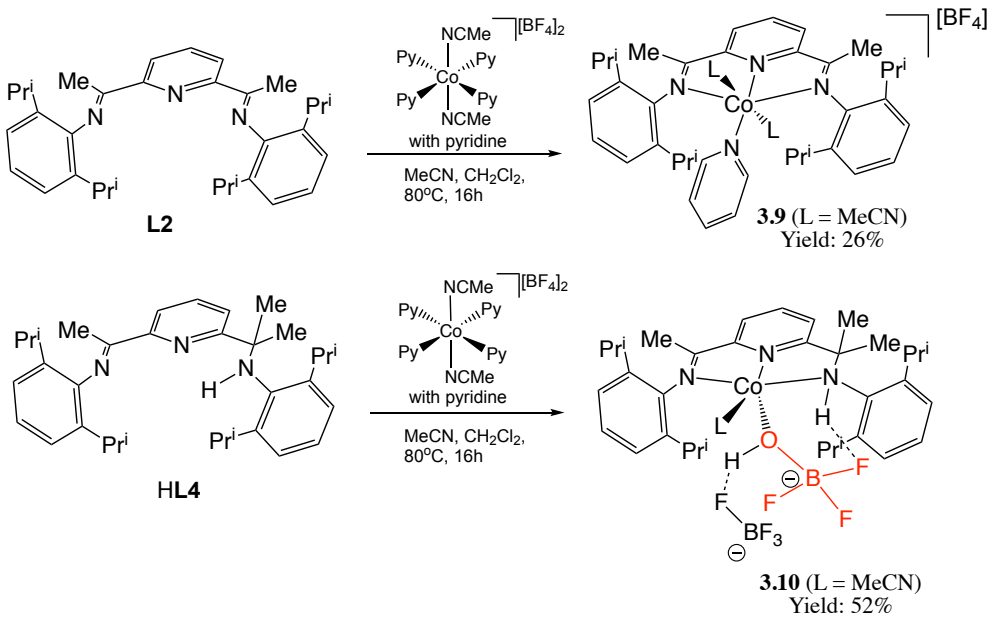

Scheme 3.3.6: Synthesis of **3.9** and **3.10**.

Both **3.9** and **3.10** have been characterised by ^{1}H, ^{19}F NMR spectroscopy, IR spectroscopy, mass spectrometry, elemental analysis and by single crystal X-ray diffraction. The stretching frequency of the coordinated imine had shifted to 1587 – 1579 cm^{-1} (**3.9** and **3.10**) from 1642 – 1650 cm^{-1} (**L2**, H**L4**), and the υ(N-H) stretches of **3.10** was observed at *ca.* 3300 cm^{-1}. In addition, analysis of **3.9** and **3.10** by FAB mass spectrometry showed strong fragmentation peaks at 540.8676 and 556.3104 which could be assigned to $[M\text{-}2MeCN\text{-}Py\text{-}2BF_4]^+$ (**3.9**) and $[M\text{-}MeCN\text{-}OHBF_3\text{-}BF_4]^+$ (**3.10**). Furthermore, the results of elemental analysis of both were consistent with the calculated elemental compositions.

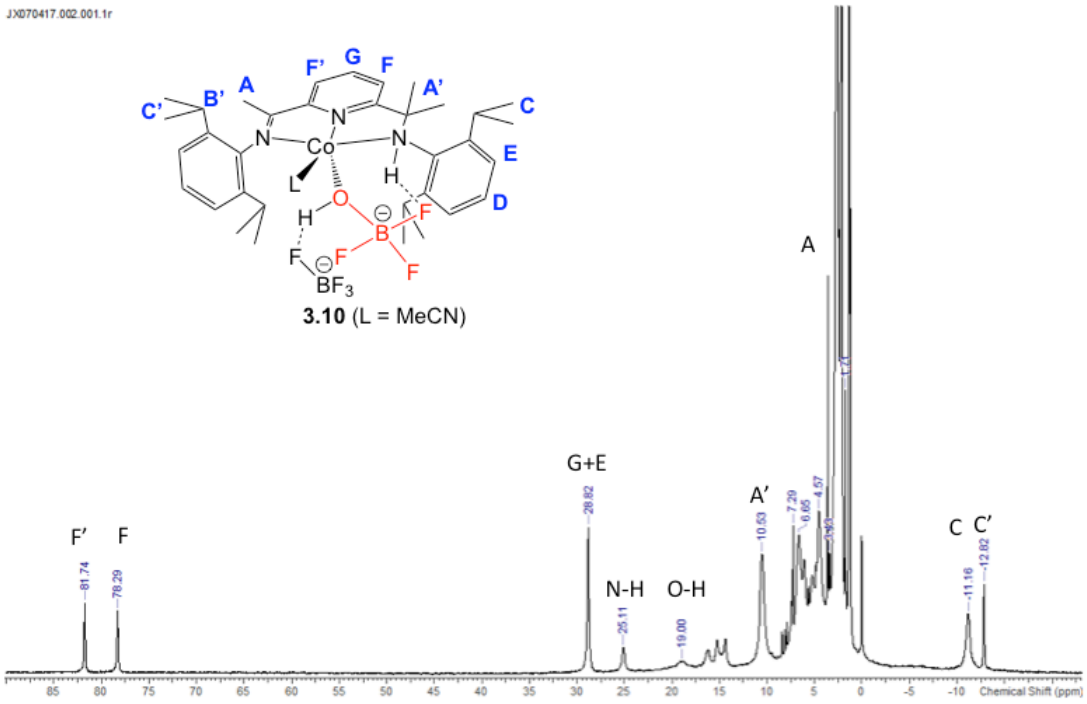

Figure 3.3.12: ^{1}H NMR spectrum of **3.10** in CD_3CN at room temperature.

The ^{1}H NMR spectrum of paramagnetic **3.9** proved too weak to allow a full assignment. On the other hand, some useful information was gained from the ^{1}H NMR spectrum of **3.10** (**Fig. 3.3.12)**. The inequivalent *meta*-pyridyl protons (**F**, **F'**) appeared downfield at δ 81.74 and δ 78.29, while the *para*-pyridyl and *meta*-aryl protons (**G**, **E**) can been seen more upfield at δ 28.82. The ketimine and ketamine methyl protons (**A** and **A'**) could be identified at δ 10.53 and δ 3.82, respectively. Furthermore, the isopropyl methyl protons (**C** and **C'**) were located at δ -11.16 and δ -12.82. Signals at δ 81.74 and 78.29 have been ascribed to the N-H and OH protons. The ^{19}F NMR spectra of both **3.9** and **3.10** showed one singlet for the tetrafluoroborate counterion at δ -150.95 (**3.9**) and δ -150.93 (**3.10**) respectively. Unfortunately, the signal corresponding to the hydrolysed $BF_3(OH)$ anion in **3.10** was not found in the ^{19}F NMR spectrum which is likely due to the paramagnetism of Co(II) centre. The effective magnetic moments (at 300 K) for **3.9** and **3.10** were determined to be μ_{eff} = 5.0 BM and 5.11 BM **3.10**, respectively. Evidently, replacing a chloride ligand by ligands that exert a stronger ligand field, such as CH_3CN, pyridine and $HOBF_3$, dis not affect the high-spin configuration of the metal centre.

Dark orange crystals of **3.9** and **3.10** were grown over a period of days from MeCN-Et_2O (1:10) solutions. **Figs 3.3.13** and **3.3.14** show the molecular structures of **3.9** and **3.10**; selected bond lengths and angles are compiled in **Tables 3.3.10** and **3.3.11**. The structures of **3.9** and **3.10** corroborate other spectroscopic date acquired and revealed mono-cobalt complexes that are charged balanced by the corresponding number of tetrafluoroborate counterions. Complex **3.9** displayed an octahedral geometry, supported by a *N,*N_{py}*,N*-ligand along with one pyridine and two MeCN ligands; the N-bound pyridine is coordinated *trans* to the pyridine unit in the *N,*N_{py}*,N*-ligand. The geometry observed in 3.9 is different from that seen in the related square pyramidal Zn(II) complex **2.7**. On the other hand, complex **3.10** adopted a distorted square pyramidal geometry similar to that seen in the Zn(II) analogue **2.8**, with an anionic $HOBF_3$ ligand, an acetonitrile and a neutral tridentate ligand making up the coordination sphere. In addition the structure was stabilised by hydrogen bonding between the amine proton belonging to *N,N,N*- ligand a fluoride substituent belonging to the coordinated $BF_3(OH)$ ligand (N(3)-H(3A)···F(1) 2.36 Å). Furthermore, a BF_4^- counterion underwent a hydrogen bonding interaction between one of its F substituents and the proton of the $HOBF_3$ (O(1)-H(1)···F(6) 1.86 Å). As a final point, the $BF_3(OH)^-$ unit was found to adopt a slightly distorted tetrahedral geometry with F-B-F and O-B-F bond angles in the range of 109.0(5)°-110.1(5)°.

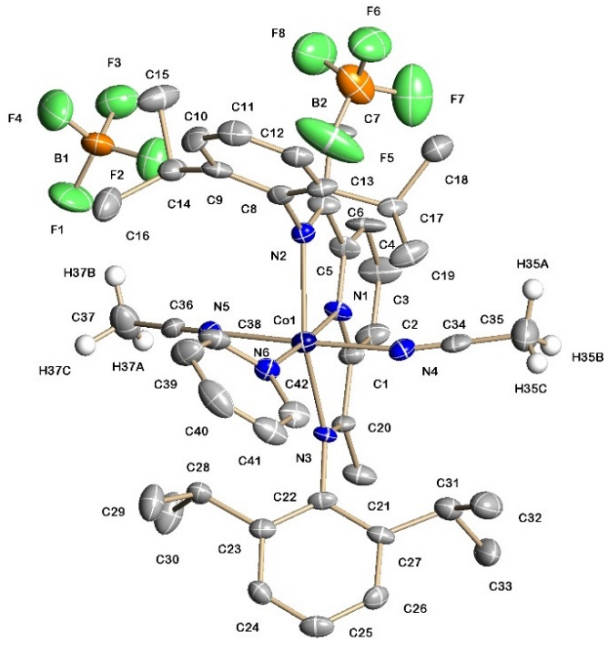

Figure 3.3.13: Molecular structure of **3.9**.

Table 3.3.10: Selected bond lengths and angles of **3.9**.

Bond Lengths (Å)	
Co(1)-N(1)	2.029(4)
Co(1)-N(2)	2.255(4)
Co(1)-N(3)	2.238(4)
Co(1)-N(5)	2.175 (4)
Co(1)-N(6)	2.050(4)
Bond Angles (°)	
N(1)-Co(1)-N(2)	75.31(16)
N(1)-Co(1)-N(3)	76.41(15)
N(5)-Co(1)-N(6)	94.56(16)
N(5)-Co(1)-N(4)	172.63(16)

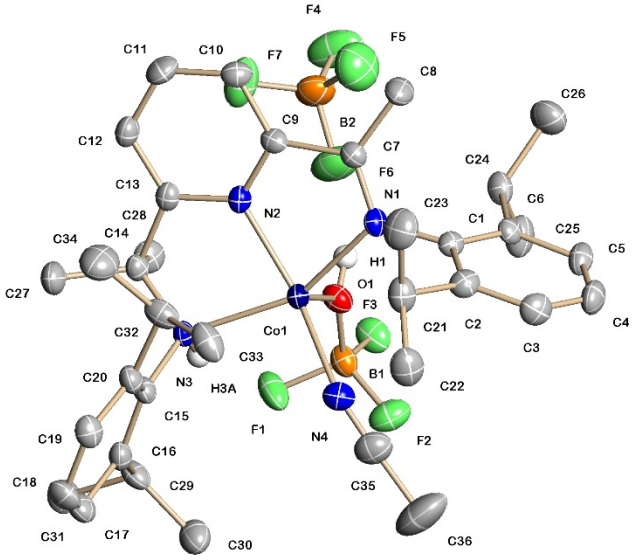

Figure 3.3.14: Molecular structure of **3.10**.

Table 3.3.11: Selected bond lengths and angles for **3.10**.

Bond Lengths (Å)	
Co(1)-O(1)	1.986(4)
Co(1)-N(1)	2.126(4)
Co(1)-N(2)	2.036 (4)
Co(1)-N(3)	2.207(4)
Co(1)-N(4)	2.028(5)
B(1)-O(1)	1.476(7)
B(1)-F(1)	1.392(7)
N(3)-H(3A)···F(1)	2.36

O(1)-H(1)···F(6)	1.86
Bond Angles (°)	
N(1)-Co(1)-N(2)	75.31(16)
N(1)-Co(1)-N(3)	76.41(15)
N(5)-Co(1)-N(6)	94.56(16)
N(5)-Co(1)-N(4)	172.63(16)

3.3.2.3 Attempted synthesis of Co(II) fluoride complexes by chloride/fluoride exchange.

With the aim to exchange the chloride ligands in (**L2**)$CoCl_2$ and **3.2c** with fluoride, two types of fluorinating reagents were explored for their potential in realising this transformation. Cesium fluoride was the first fluorinating reagent chosen as there is some discussion in the literature that this could be a suitable though underexplored to date.[55] Each complex was dissolved in at room temperature and 1.0 or 2.0 equivalents of CsF introduced. Periodic monitoring of the ^{1}H NMR spectrum showed no evidence for Co-F peaks in the ^{19}F NMR spectrum. Indeed, inspection of the ^{1}H NMR spectrum revealed that the complexes were decomposing to their free ligands after few hours (**Scheme 3.3.7**). The explanation for this unexpected reactivity remains unclear but it is likely that the low solubility of CsF in organic solvents and the hygroscopic nature of this alkali metal fluoride were a contributing factor – nevertheless it should be emphasised that the reactions were performed under dry and anaerobic conditions.

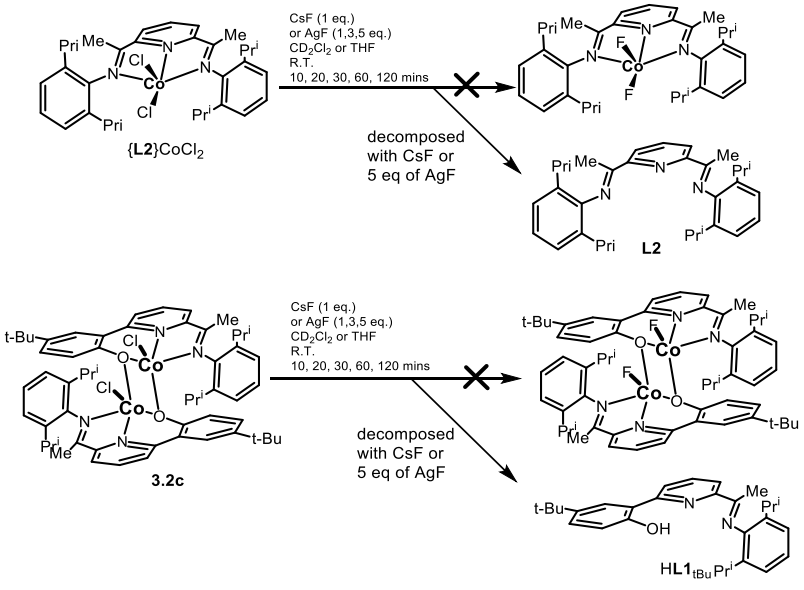

Scheme 3.3.7: Attempted synthesis of Co(II) fluoride complexes.

As alternative fluorinating agent, the use of AgF was also explored as a means to fluorinate (**L2**)$CoCl_2$ and **3.2c**. Typically, the reactions were performed on the small scale by treating the cobalt(II) complex with AgF in anhydrous THF. With regard to (**L2**)$CoCl_2$, the ^{1}H NMR spectrum showed that the fluorination did not occur after stirring at room temperature for 10 and 30 minutes or over more extended reaction times (60 and 120 minutes). Indeed, the ^{1}H NMR spectrum showed that the chloride complex had decomposed to free ligand following filtration of a dark grey precipitate. In addition, there was no cobalt-fluoride signal displayed in the ^{19}F NMR spectrum. It was considered that the paramagnetism of the Co(II) ion could possibly have affected the observation of the fluoride signal, or an unstable LCo(III)F_3 complex was formed during fluorination which then immediately decomposed to free ligand (**Scheme 3.3.8**). Unfortunately, the dark grey precipitate (assumed to be AgCl or CoF_3) was not soluble in a range of organic solvents. Likewise using **3.2c**, only signals corresponding to free ligand in the ^{1}H NMR spectrum were observed.

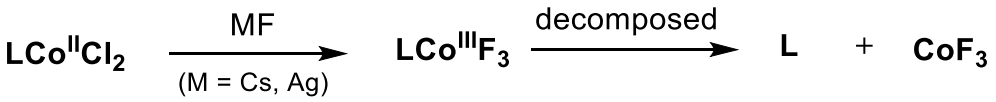

Scheme 3.3.8: Possible fluorination/decomposition pathway occurring when (**L2**)$CoCl_2$ was treated with CsF or AgF

3.3.3 Conclusions to Chapter 3

A range of novel cobalt(II) chloride pincer complexes **3.1a**, **3.1b**, **3.2a**, **3.2c**, **3.3** and **3.4**, have been successfully prepared by their reactions of the corresponding ligand (H$\mathbf{L1_H}$, H$\mathbf{L1_{Ph}}$, H$\mathbf{L1_{tBu}}$, $H_2\mathbf{L3_H}$ and H**L4**) with $CoCl_2$ (**Fig. 3.3.14**); the previously reported (**L2**)$CoCl_2$ was also re-synthesised. Complexes **3.1a**, **3.1b**, **3.3** and **3.4** all adopt mononuclear structures in which the tridentate ligand remains protonated. Deprotonation of the H$\mathbf{L1_H}$ ligand in **3.1a** has been demonstrated either thermally or by using a base leading to bimetallic **3.2a**. Complex **3.2a** as well as its t-butyl analogue, **3.2c**, contain a dicobalt core in which the *N,N,O*-ligand not only chelates the metal centres but also bridges through the $O_{phenoxy}$ unit. The structural difference is attributed to the different steric and electronic properties of the (pro)ligands.

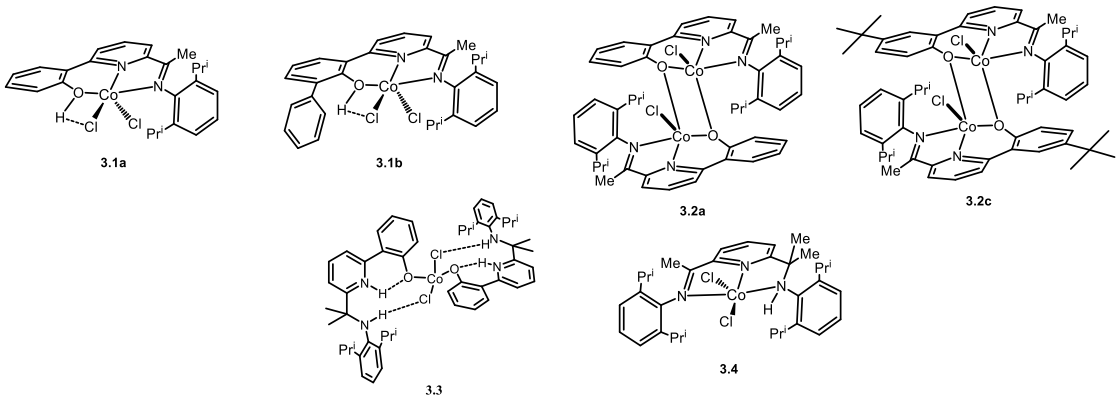

Figure 3.3.14: New cobalt(II) chloride complexes prepared in **Chapter 3**.

Subsequently, H**L1**$_{\mathbf{H}}$, H**L1**$_{\mathbf{Ph}}$, H**L1**$_{\mathbf{tBu}}$, **L2** and H**L4** were reacted with $[Co(Py)_4(NCMe)_2][BF_4]_2$ (**Fig. 3.3.15**). Two types of products were produced namely monocobalt (**3.7**, **3.9** and **3.10**) and dicobalt complexes (**3.5a**, **3.6c**) were formed in good yields. Furthermore, in order to investigate the steric properties of the pincer ligand, the *O,N,O(H)*-Ketone-Ph was additionally reacted with $[Co(Py)_4(MeCN)_2][BF_4]_2$ affording the dimeric cobalt complex **3.8**. In the solid state, the cobalt centres in **3.5a**, **3.6c** and **3.10** displayed distorted square pyramidal geometries, while in **3.7**, **3.8** and **3.9** octahedral geometries were exhibited. The unusual hydrolysis product **3.10** was also obtained from reaction between *N,N,N(H)* ligand **L4** and $[Co(Py)_4(MeCN)_2][BF_4]_2$; the zinc analogue **2.8** was reported in Chapter 2. Crystallisation of complex **3.7b** proved most challenging. It is worth noting that the phenol group of ligand H**L1**$_{\mathrm{Ph}}$ was not deprotonated and the proton formed a hydrogen bond with a nitrogen atom belonging to a molecule of pyridine.

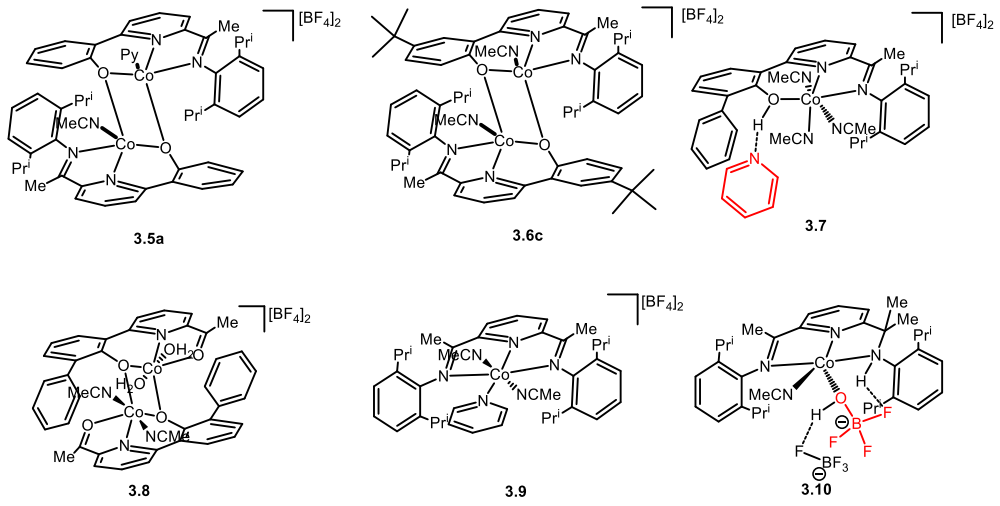

Figure 3.3.15: New cobalt(II) tetrafluoroborate complexes prepared in **Chapter 3**.

Chloride-fluoride exchange was attempted by using two different fluorinating reagents (CsF and AgF). The reactions of (**L2**)$CoCl_2$ and dicobalt **3.2c** were first investigated under a range of different conditions (*e.g.*, reaction time and number of equivalents of reagents etc). However, there was no evidence for the formation of a cobalt complex containing a Co-F bond by ^{1}H NMR or ^{19}F NMR spectroscopy. Indeed, the ^{1}H NMR spectrum revealed decomposition to free ligands. This finding is similar to that observed in Chapter 2 for the zinc(II) complexes. It is uncertain as to the origin of the decomplexation that is occurring in the presence of CsF or AgF.

References

1. V. C. Gibson and S. K. Spitzmesser, *Chem. Rev.,* 2003, **103**, 283-316.
2. G. J. P. Britovsek, V. C. Gibson and D. F. Wass, *Angew. Chem. Int. Ed*., 1999, **38**, 428-447.
3. S. D. Ittel, L. K. Johnson and M. Brookhart, *Chem. Rev.,* 2000, **100**, 1169-1203.
4. Z. Wang, G. A. Solan, W. Zhang and W. H. Sun, *Coord. Chem. Rev*., 2018, **363**, 91-108.
5. J. Yuwen, S. Chakraborty, W.W. Brennessel and W. D. Jones, *ACS Catal*. 2017, **7**, 3735-3740.
6. D. Srimani, A. Mukherjee, A. F. G. Goldberg, G. Leitus, Y. Diskin-Posner, L. J. W. Shimon, Y. Ben David and D. Milstein, *Angew. Chem., Int. Ed.* 2015, **54**, 12357-12360.
7. S. Fu, N. Y. Chen, X. Liu, Z. Shao, S. P. Luo and Q. Liu, *J. Am. Chem. Soc*., 2016, **138**, 8588-8594.
8. T. P. Lin and J. C. Peters, *J. Am. Chem. Soc.,* 2014, **136**, 13672-13638.
9. T. J. Korstanje, J. Ivar van der Vlugt, C. J. Elsevier and B. de Bruin, *Science,* 2015, **350**, 298-302.
10. H. Zhang and Z. Lu, *ACS Catal.* 2016, **6**, 6596-6600.
11. G. Zhang and S. K. Hanson, *Org. Lett.,* 2013, **15**, 650-653.
12. Y.-Y. Li, S.-L. Yu, W.-Y. Shen and J.-X. Gao, *Acc. Chem. Res*., 2015, **48**, 2587-2598.
13. P. Daw, S. Chakraborty, J. A. Garg, Y. B-David and D. Milstein, *Angew. Chem. Int. Ed.* 2016, **55**, 14373-14377.
14. V. C. Gibson and G. A. Solan, *Top. Organomet. Chem.,* 2009, **26**, 107-158.
15. W. Zhang, W.-H. Sun and C. Redshaw, *Dalton Trans.,* 2013, **42**, 8988-899.
16. S. C. Lee and R. H. Holm, *Inorg. Chem.,* 1993, **32**, 4745-4753.
17. Z. Flisak and W.-H. Sun, *ACS Catal.,* 2015, **5**, 4713-4724.
18. J. Ma, C. Feng, S. Wang, K. Q. Zhao, W.-H. Sun, C. Redshaw and G. A. Solan, *Inorg. Chem. Front.,* 2014, **1**, 14-34.
19. V. C. Gibson, C. Redshaw and G. A. Solan, *Chem. Rev.,* 2007, **107**, 1745-1776.
20. U. Matteoli, M. Blanchi, G. Menchi, P. Prediani and F. Piacenti, *J. Mol. Catal.,* 1984, **22**, 353-362.

21. U. Matteoli, G. Menchi, M. Bianchi and F. Piacenti*, J. Organomet. Chem.,* 1986, **299**, 233-238.
22. S. Elangovan, B. Wendt, C. Topf, S. Bachmann, M. Scalone, A. Spannenberg, H. J. Jiao, W. Baumann, K. Junge and M. Beller, *Adv. Synth. Catal*., 2016, **358**, 820-825.
23. T. Zell, Y. Ben-David and D. Milstein, *Angew. Chem., Int. Ed*., 2014, **53**, 4685-4689.
24. S. Werkmeister, K. Junge, B. Wendt, E. Alberico, H. J. Jiao, W. Baumann, H. Junge, F. Gallou and M. Beller, *Angew. Chem., Int. Ed.* 2014, **53**, 8722-8726.
25. S. Chakraborty, G. G. Dai, P. Bhattacharya, N. T. Fairweather, M. S. Gibson, J. A. Krause and H. R. Guan, *J. Am. Chem. Soc.,* 2014, **136**, 7869-7872.
26. R. Xu, S. Chakraborty, H. M. Yuan and W. D. Jones, *ACS Catal*., 2015, **5**, 6350-6354.
27. G. Q. Zhang, B. L. Scott and S. K. Hanson, *Angew. Chem., Int. Ed*. 2012, **51**, 12102-12106.
28. Q. Knijnenburg, A. D. Horton, H. van der Heijden, T. M. Kooistra, D. G. H. Hetterscheid, J. M. M. Smits, B. de Bruin, P. H. M. Budzelaar and A. W. Gal*, J. Mol. Catal. A: Chem*., 2005, **232**, 151-159.
29. G. Q. Zhang, K. V. Vasudevan, B. L. Scott and S. K. Hanson, *J. Am. Chem. Soc.* 2013, **135**, 8668-8681.
30. a) B. Gnanaprakasam, J. Zhang and D. Milstein, *Angew. Chem., Int. Ed*. 2010, **49**, 1468-1471. b) A. Maggi and R. Madsen, *Organometallics,* 2012, **31**, 451-455.
31. R. Halle, A. Bréhéret, E. Schulz, C. Pinel and M. Lemaire, Chiral Nitrogen-Metal Complexes for the Asymmetric Reduction of Ketones. Master's Dissertation, Xiamen University, 2003.
32. B. L. Small, M. Brookhart and A. M. A. Bennett, *J. Am. Chem. Soc*., 1998, **120**, 4049-4050.
33. G. J. P. Britovsek, V. C. Gibson, B.S. Kimberley, P. J. Maddox, S. J. McTavish, G. A. Solan, A. J. P. White and D. J. Williams, *Chem. Commum.,* 1998, 849-850.
34. G. J. P. Britovsek, M. Bruce, V. C. Gibson, B. S. Kimberley, P. J. Maddox, S. Mastroianni, S. J. Mctavish, C. Redshaw, G. A. Solan, S. Strömberg, A. J. P. White and D. J. Williams, *J. Am. Chem. Soc.*, 1999, **121**, 8728-8740.

35. Y. Chen, C. Qian and J. Sun, *Organometallics*, 2003, **22**, 1231-1236.
36. Y. Chen, R. Chen, C. Qian, X. Dong and J. Sun, *Organometallics,* 2003, **22**, 4312-4321.
37. W. A. Gobeze, V. A. Milway, B. Moubaraki, K. S. Murray and S. Brooker, *Dalton Trans*., 2012, **41**, 9708-9721.
38. J. Olguí, M. Kalisz, R. Clérac and S. Brooker, *Inorg. Chem.,* 2012, **51**, 5058-5069.
39. W. A. Gobeze, V. A. Milway, N. F. Chilton, B. Moubaraki, K. S. Murry and S. Brooker*, Eur. J. Inorg. Chem*., 2013, 4485-4498.
40. Y. I. Cho, M. L. Ward and M. J. Rose, *Dalton. Trans.,* 2016, **45**, 13466-13476.
41. W. L. Driessen, J. Reedijk, *Solid Solvates: The Use of Weak Ligands in Coordination Chemistry. Inorganic Synthesis,* 1992, **29,** 111-118.
42. M. A. Abadie, X. Trivelli, F. Medina, F. Capet, P. Roussel, F. Agbossou-Niedercorn and C. Michon, *ChemCatChem,* 2014, **6**, 2235-2239.
43. S. Chang-Kyo, K. Seong-Jin and K. Geon-Joong, *Tetrahedron Lett.,* 2004, **45**, 7429-7433.
44. M. Inomata and Y. Suenaga, *Acta Crystallogr., sect. E: Struct. Rep. Online,* 2014, **70**, m359-m360.
45. W. A. Gobeze, V. A. Milway, B. Moubaraki, K. S. Murry and S. Brooker, *Dalton Trans.,* 2012, **41**, 9708.
46. T. R. Musgrave and T. S. Lin*, J. Coord. Chem.,* 1973, **2**, 323-324.
47. M. A. Guichelaar, J. A. M. van Hest and J. Reedijk, *Inorg. Nucl. Chem. Lett.,* 1974, **10**, 999-1004.
48. D. F. Evans and D. A. Jakubovic. *J. Chem. Soc., Dalton Trans.,* 1988, 2927-2933.
49. D. F. Evans, *J. Chem. Soc.,* 1959, **36**, 2003-2005.
50. a) W. Zheng, W. Chai, W. H. Sun, X. Hu, C. Redshaw and X. Hao, *Organometallics,* 2012, **31**, 5039-5048. b) W.-H. Sun, S. Kong, W. Chai, T. Shiono, C. Redshaw, X. Hu, C. Gao and X. Hao, *Appl. Catal.,* A. 2012, 447-448, 67-73.
51. J. Ba, S. Du, E. Yue, X. Hu, Z. Flisak and W.-H. Sun. *RSC Adv.,* 2015, **5**, 32720-32729.

52. a) F. Huang, W. Zheng, E. Yue, T. Liang, X. Hu and W.-H. Sun, *Dalton Trans*, 2016, **45**, 657-666. b) F. Huang, W. Zheng, Y. Sun, X. Hu, G. A. Solan and W. H. Sun, *New. J. Chem*., 2016, **40**, 8012-8023.
53. V. K. Appukuttan, Y. Liu, B. C. Son, C. S. Ha, H. Suh and I. Kim, *Organometallics,* 2011, **30**, 2285-2294.
54. a) S. Du, W. Zheng, E. Yue, F. Huang, T. Liang and W. H. Sun, *Eur. J. Inorg. Chem.* 2016, **2016**, 1748-1755. b) S. Du, X. Wang, W. Zheng, Z. Filsak, Y. Sun and W. H. Sun, *Polym. Chem*., 2016, **7**, 4188-4197. c) C. Huang, S. Du, G. A. Solan, Y. Sun and W.-H. Sun, *Dalton Trans*, 2017, **46**, 6948-6957.
55. C. Bariashir, Z. Wang, S. Du, G. A. Solan, C. Huang, T. Liang and W. H. Sun, *J. Polym. Sci., Part A: Polym. Chem*, 2017, **55**, 3980-3989.
56. G. B. Nikiforov, H. W. Roesky and D. Koley, *Coord. Chem. Rev.,* 2014, **258**, 16-57.
57. a) C. Ludovici, R. Fröhlich, K. Vogtt, B. Mamat, M. Lübben, *Eur. J. Biochem*., 2002, **269**, 2630-2637. b) R. MacArthur, A. Sucheta, F. F. S. Chong, O. Einarsdóttir, *Pro. Natl. Acad. Sci. U.S.A.,* 1995, **92**, 8105-8109.
58. a) M. Zehnder, U. Thewalt, S. Fallab, *Helv. Chim. Acta* 1976, **59**, 2299-2310. B) U. Thewalt, G. Struckmeier, *Z. Anorg. Allg. Chem.,* 1976, **419**, 163-165. c) S. Fallab, M. Zehnder, U. Thewalt, *Helv. Chim. Acta.,* 1980, **63**, 1491-1495. d) H. Mäcke, M. Zehnder, U. Thewalt, S. Fallab, *Helv. Chim. Acta*., 1979, **62**, 1804-1806.

Chapter 4

Nickel(II) chloride and tetrafluoroborate complexes supported by *N,N,O*- and *N,N,N*-pincer ligands

4.1 Introduction

In last two chapters, the coordination chemistry of Zn(II) and Co(II) complexes bearing a range of N,N_{py},O and N,N_{py},N pincer ligands has been studied. As a continuation, the general target of this chapter is to synthesise a series of d^8 nickel(II) chloride and tetrafluoroborate complexes bearing the same pincer ligand frames. The propensity of the BF_4 anions to undergo *in-situ* B-F bond cleavage or hydrolysis in the presence of the nickel centre will be examined, while chloride to fluoride exchange reactions will be attempted with the chloride complexes. As a consequence, this introductory section will set the scene for the experimental work by reviewing applications of nickel-based pincer complexes, the use of BF_4^- counterions as a source of fluoride in nickel chemistry and other routes to nickel(II) fluorides.

4.1.1 Nickel(II) pincer complexes and their applications

Nickel-pincer complexes have been widely studied since the first examples were reported in 1976.[1] The low cost, reduced toxicity and relative abundance makes nickel particularly attractive for investigations concerned with targeting applications with pincer ligands. Indeed, many literature reports have shown that nickel(II)-pincer complexes are effective catalysts in a wide variety of reactions, such as the Kharasch addition [2,3], Kumada cross coupling [4], CO_2 reduction [5], alkene hydrogenation [6] and the polymerisation of olefins.[7-23]

The Kharasch addition is a well-known method for the generation of carbon-carbon bonds.[25] In 1997, van de Kuil *et al.* reported the addition reaction of polyhalogenated alkanes to alkanes (Kharasch addition reaction), which was catalysed under mild

reaction conditions (25 °C) by the aryl-nickel complexes of the type [Ni^{II}{2,6-$(CH_2NMe_2)_2$-4-RC_6H_2}] (R = H **1**, MeC(O) **2**, Cl **3**, MeO **4**, NH_2 **5**) affording a high selectivity for the 1:1 adduct (**Scheme 4.1.1: a**). Kinetic data obtained using **1** (abbreviated as [Ni(*N,C,N*)Br]), methyl methacrylate and CCl_4 revealed a rate of reaction that was first order in nickel and in the alkene. Furthermore, the reaction rate decreased with an increase in the steric congestion imparted by the *N*-donor of the [Ni(*N,C,N*)Br] catalyst (*i.e.*, NMe_2 > NEt_2 > NMe(^{i}Pr) > NMe(^{t}Bu)).[26] More recently Pandarus's group published the synthesis and characterisation of [{$(Pr^i_2POCH_2)_2$CH}$Ni^{III}Br_2$] (**6**) which was also explored in the Kharasch-type addition of CCl_4 to an olefin (**Scheme 4.1.1: b**). In contrast to van de Kuil's *N,C,N*-nickel system, **6** did not react at room temperature due to the greater steric bulk of the phosphinite moieties. In addition, the transformation had to be carried out in the absence of O_2 to prevent quenching of the intermediate organic radicals. Nonetheless, complex **6**, under the optimised set of conditions, showed effectiveness in promoting the Kharasch addition.[28]

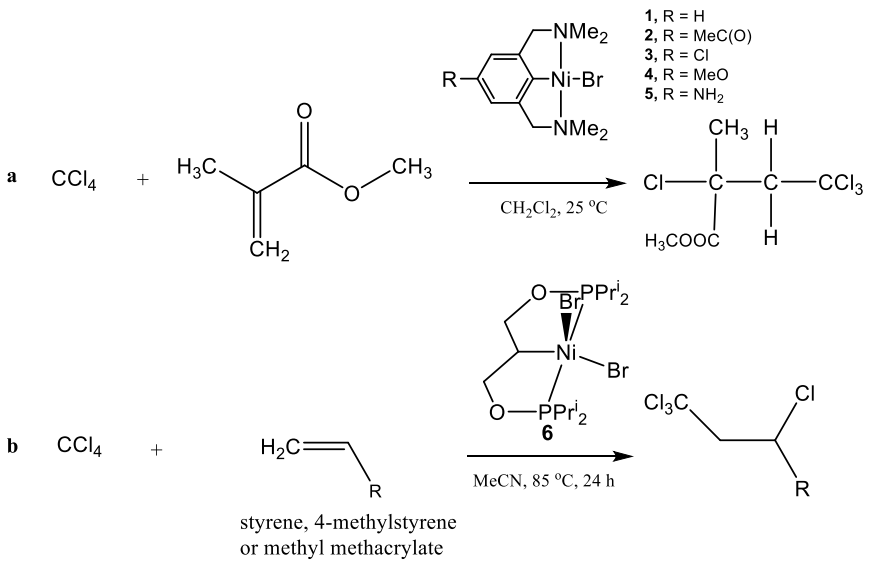

Scheme 4.1.1: (a) Kharasch addition reaction by using [Ni^{II}{2,6-$(CH_2NMe_2)_2$-4-RC_6H_2}] (**1 - 5**) as catalyst.[26] (b) Kharasch addition reaction by using {$(Pr^i_2POCH_2)_2$CH}$Ni^{III}Br_2$ (**6**) as catalyst.[27]

Another method for constructing C-C bonds is the alkyl-alkyl Kumada cross-coupling. Recently, the advantages of using nickel-mediated cross-coupling has attracted much attention. In 2012, the nickel(II) catalysed cross-coupling of 1,3- and 1,4-substituted cyclohexyl halides and tetrahydropyrans with alkyl Grignard reagents was reported by

Garcia's group (**Scheme 4.1.2**). The diastereoselectivity of the reactions between 4-methylcyclohexyl iodide and ^{n}BuMgCl using **7** as catalyst was very high (dr = 96:4). In addition, **7** was capable of delivering high diastereoselectivity (98:2) in the coupling of 3-methylcyclohexyl iodide with ^{n}BuMgCl.[28]

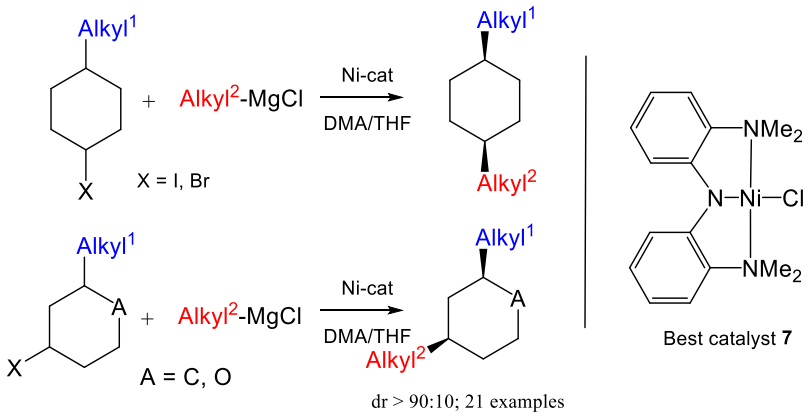

Scheme 4.1.2: Nickel catalysed Kumada coupling of alkyl halides.[28]

In recent years, the hydrogenation and hydroboration of CO_2 to methanol has gained attention due to CO_2 being a renewable, nontoxic and abundant feedstock for the synthesis of organic molecules.[29] Tridentate nickel complexes have also been explored for catalytic carbon dioxide reduction. The first nickel-catalysed hydrosilylation of CO_2 to methanol was achieved by Huaifeng and co-workers in 2018 by using a dearomatized *P,N,P*-nickel hydride complex.[30] The reaction was performed at 1 atm of CO_2 in DMF with Ph_2SiH_2 as the reductant under various conditions in the presence of three examples of *P,N,P*-Ni hydride catalyst (**8 - 10**) (**Scheme 4.1.3**). Overall, catalyst **8** showed the highest activity, with a loading as low as 0.02 mol%, with a TON of up to 4900 which is the highest value reported for the reduction of CO_2 with silane to methanol.[30] In addition, **8** also displayed notable reactivity and selectivity for the reductive methylation and formylation of amines with CO_2 with a very broad substrate scope.[30]

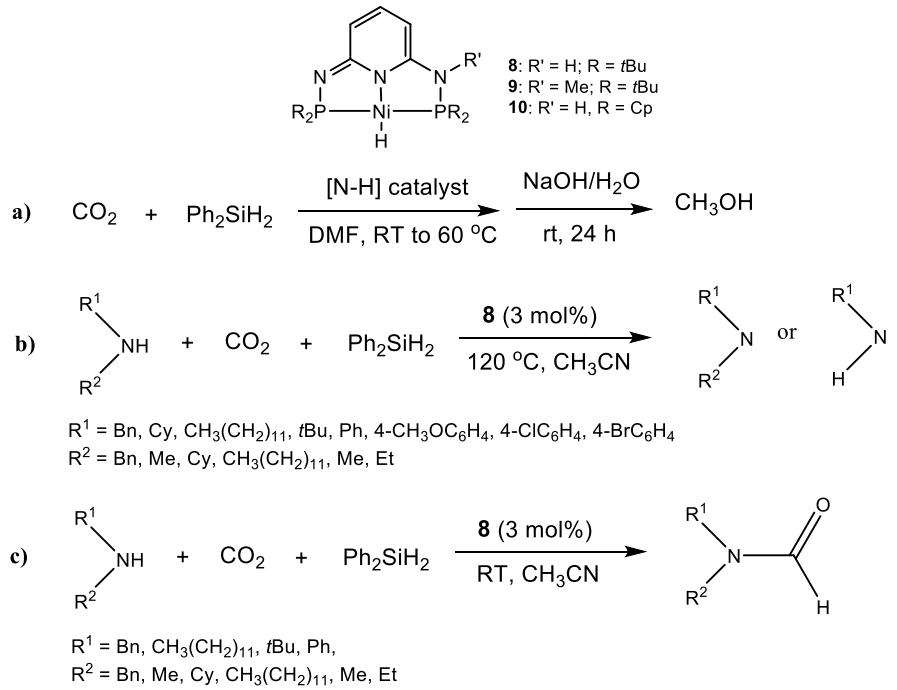

Scheme 4.1.3: a) Hydrosilylation of CO_2 with diphenylsilane catalysed by *P,N,P*-nickel hydride complexes (**8 - 10**). b) Methylation of various amines using CO_2 and Ph_2SiH_2 catalysed by **8**. c) Formylation of various amines using CO_2 and Ph_2SiH_2 catalysed by **8**.[30]

Nickel pincer complexes have also been gaining increasing attention as versatile and effective catalysts for alkene hydrogenation reactions.[31] In order to investigate metal-ligand cooperativity as a strategy for promoting nickel-catalyzed alkene hydrogenation, Vasudevan *et al*. reported the synthesis and characterization of cationic and neutral nickel(II) hydride complexes bearing the pincer ligand $PNHP^{Cy}$ {$PNHP^{Cy}$ = $HN[CH_2CH_2(Cy)_2]_2$}.[32] In particular, the hydride complex $[(PNHP^{Cy})Ni(H)][BPh_4]$ (**11**) was explored as a catalyst for the hydrogenation of styrene and 1-octene under mild conditions (**Scheme 4.1.4**). 100% conversion of styrene to ethylbenzene was observed after 24 hours at 80 ^oC with the hydrogen pressure at 4 atm. Moreover, mechanistic experiments involving catalyst **11** suggested that the hydrogenation reaction proceeded through a pathway involving initial insertion of the alkene into the Ni-H bond.[32]

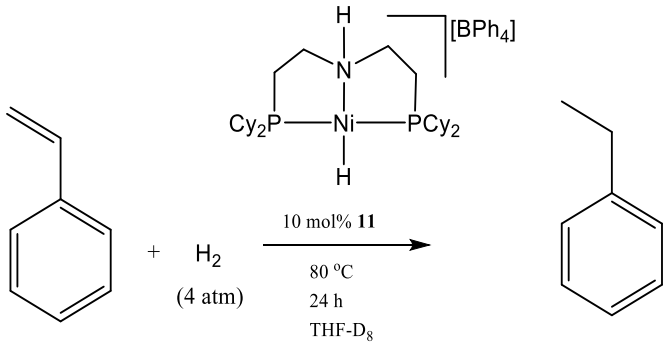

Scheme 4.1.4: Hydrogenation of styrene using cationic nickel hydride complex **11**.[32]

Although tridentate Ni(II) complexes tend to display lower activity for ethylene reactivity when compared to their bi-dentate nickel counterparts[24], Ni(II) systems bearing pincer-type ligands have shown promise as alternative ligand frames. For example, Sun and co-workers published the nickel complexes **14** and **15** (**Fig. 4.1.2**) bearing 2-imino-1,10-phenanthrolines and 2-imino-9-phenyl-1,10-phenanthrolines for ethylene oligomerisation catalysis. On activation with Et_2AlCl, it was evident that both the R substituents on the imino-carbon and on the N-aryl rings had a clear influence on the catalytic and distribution of oligomers which was attributed to the different electronic and steric properties of the ligand frame. Complex **14** gave moderate activities of up to 3.3×10^6 $g \cdot mol^{-1}(Ni) \cdot h^{-1}$,[33,34,35] while isopropyl-substituted **15f** showed the highest activity at 5.88×10^5 $g \cdot mol^{-1}(Ni) \cdot h^{-1}$.[35]

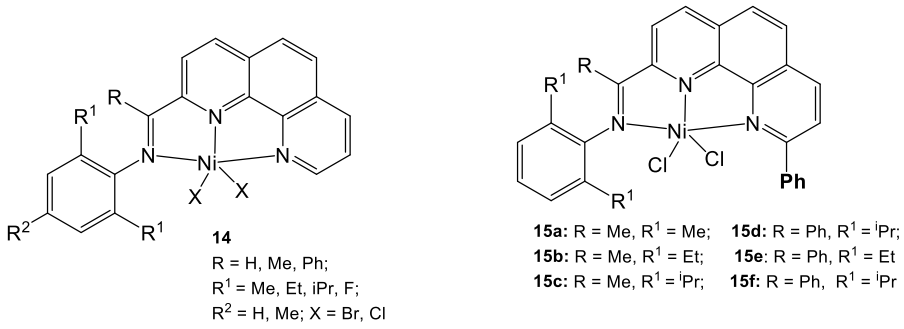

Figure 4.1.2: *N,N,N*-nickel complexes **14** and **15**.[33,34,35]

In addition, numerous *N,N,O*-nickel complexes such as **16 - 21** have also been explored for ethylene reactivity by the same group (**Figure 4.1.3**). Upon treatment with MAO, **16** revealed moderate catalytic activity for ethylene oligomerization and polymerisation.[36,37] The activity of **17** was higher than **18**, which was credited to the formation of an anionic amide ligand following deprotonation of the N-H group by the co-catalyst.[38,39] Nickel complex **20** showed high activity for ethylene dimerisation with

Et_2AlCl as co-catalyst, [40,41] while **21** exhibited higher catalytic activities and better thermal stability for ethylene oligomerisation.[42]

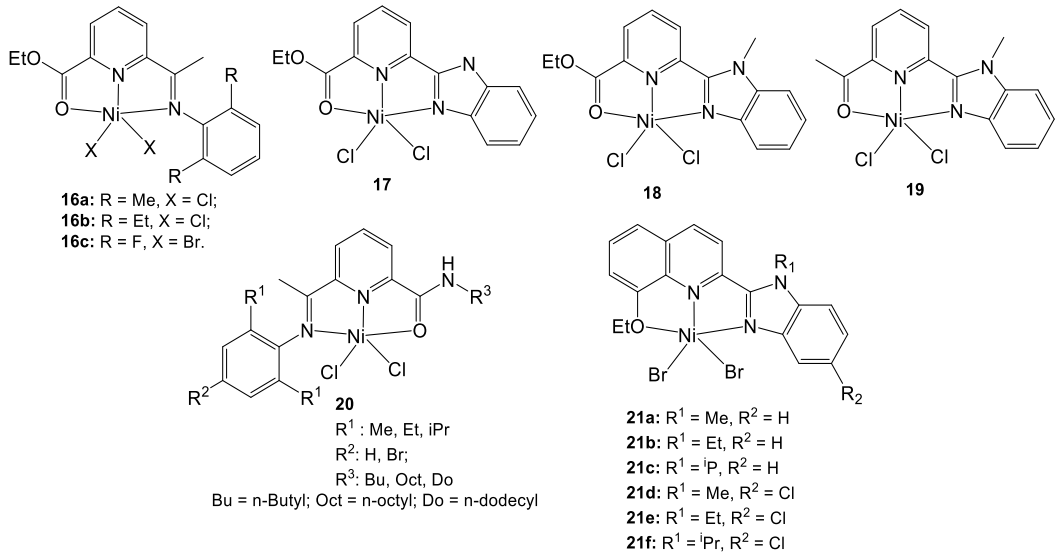

Figure 4.1.3: *N,N,O*-nickel precatalysts **16 – 21** for ethylene oligomerization.[36-42]

4.1.2 Nickel(II) tetrafluoroborate complexes and their applications

In the previous two chapters, the use of BF_4^- as a potential fluoride source has been discussed in the context of Zn(II) and Co(II) chemistry. As binary metal fluorides are insoluble in common organic solvents, tetrafluoroborate salts offer a promising means of providing a fluoride as their complexes are usually more soluble in organic media.[44] Moreover, such an approach avoids the use of external fluorinating agents that generate unwanted by-products.[44] However, the process of F abstraction form BF_4^- or PF_6^- is still not clearly understood.[44] The situation is made more complicated as the resulting complexes have, in some cases, been incorrectly characterised as their corresponding hydroxo compounds.[43] There are many key elements for fluoride abstraction to occur from a BF_4^- counterion such as the choice of the Lewis acid, the ligand capable of supporting the metal centre and the level of adventitious moisture present in the reaction mixture.[44] Therefore, part of the investigation conducted in this chapter, explores how nickel complexes containing tetrafluoroborate anions can act as a source of fluoride.

Kohl and co-workers published several examples of square-pyramidal nickel(II) tetrafluoroborate complexes that were synthesised by the reactions of pyridine-derived

tetraphosphane ligands $C_5H_3N[CMe(CH_2PMe_2)_2]_2$ (**L1**) and $C_5H_3N[CMe(CH_2PMe_2)_2][CMe_2(CH_2PMe_2)]$ (**L2**) with hexahydrate salts of nickel(II) tetrafluoroborate (**Scheme 4.1.5**). This study was carried out to investigate the effect of steric and electronic properties of the phosphanes ligated to the nickel center.[45] Notably in reaction **b**, the CH_3CN-coordinated complex **23** was formed by reacting ligand **L2** with $Ni(BF_4)_2{\cdot}6H_2O$ in acetonitrile. Conversely, when the reaction mixture was allowed to stand for several days, water initiated hydrolysis of the coordinated acetonitrile to give the acetamide complex **24** (**Scheme 4.1.5 b**).

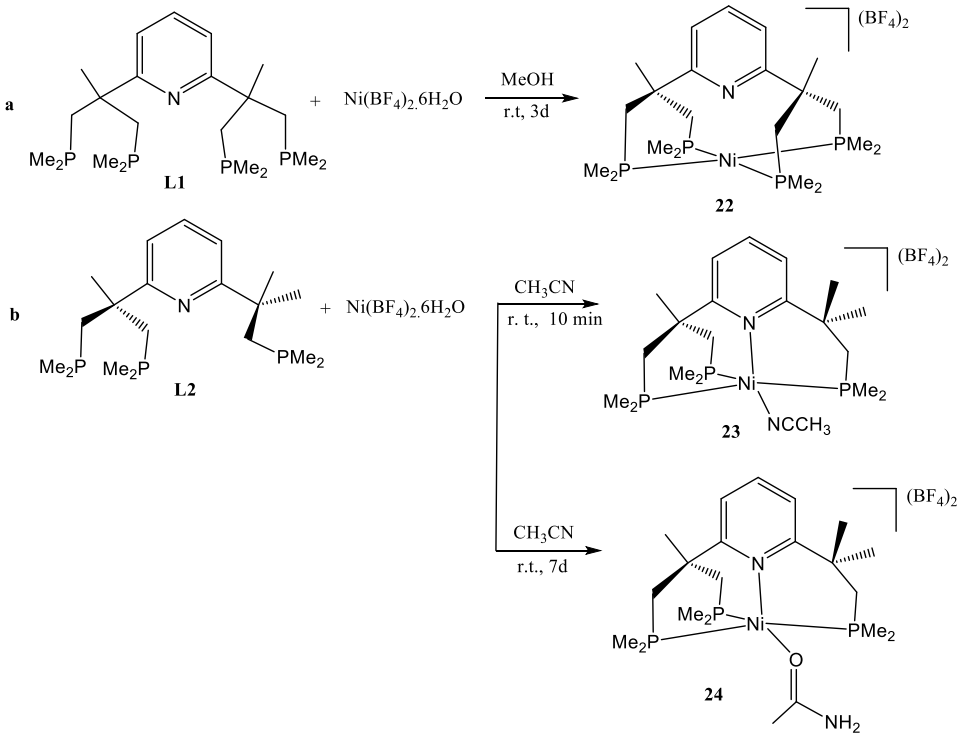

Scheme 4.1.5: Synthesis of nickel(II) complexes **22 - 24** bearing tripodal ligands **L1** and **L2**.[45]

Dinuclear nickel cationic complexes with tetrafluoroborate counterions have also received notable scientific interest as model systems for various metalloenzymes. In 2009, the first examples of dinuclear nickel(II) complexes bearing a bis(tripodal)amine ligand incorporating an *ortho*-phenylenlendiame bridging unit were reported by Hahn *et al*.[46] In particular, the binucleating octaamine ligand $\mathbf{H_6}$**-4** when reacted with $Ni(BF_4)_2{\cdot}6H_2O$ in the presence of the halide source, tetrabutylammonium chloride, afforded the dinuclear complex $[Ni_2(\mu\text{-}Cl)_2(\mathbf{H_6}\text{-}\mathbf{4})][BF_4]_2$ (**25**) (**Scheme 4.1.6**). Each nickel centre in **25** adopted a distorted octahedral geometry based on the four amine donor atoms of one tripodal unit and two Cl ligands, which additionally coordinated in a bridging mode to both the metal centres.

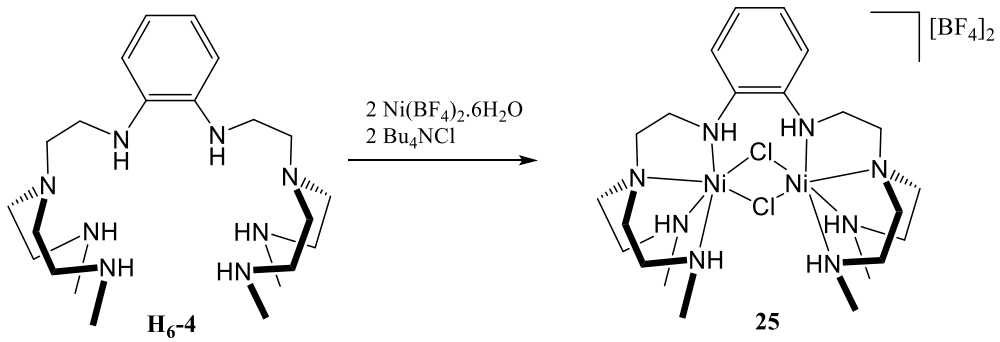

Scheme 4.1.6: Synthesis of the dinuclear nickel complex **25**.[46]

In recent years, interest in metal-fluoride compounds has increased as a consequence of metal-mediated C-F bond activation.[47] Elsewhere B-F activation of a BF_4^- anion can provide a F^- anion. For example, Regar and co-workers in 2006 showed the controlled release of F^- can be achieved by bimetallic activation of BF_4^-.[48] In addition, Das *et al*. reported the synthesis and characterization of the fluoro-bridged dinickel(II) compound $[Ni_2F_2(\mathbf{L_{Fe}})_4][BF_4]_2$ ($\mathbf{L_{Fe}}$ = [{(5,7-dimethyl-1,8-naphthyridin-2-yl)amino}carbonyl] ferrocene) (**26**) which was produced by fluoride abstraction from the BF_4^- anion in $[Ni(CH_3CN)_6][BF_4]_2$ (**Scheme 4.1.7**).[49] The choice of the ligand was based on three points: i) the naphthyridine (NP) unit was considered conducive to stabilising a dimetal core, ii) N-donor ligand could act as suitable acceptors for boron trifluoride, and iii) the amide functionalities could stabilise the metal fluorides by hydrogen-bonding interactions. The molecular structure of **26** consisted of two crystallographically unique nickel centres bridged by two fluorides, with each nickel centre revealing octahedral geometry. The ^{19}F NMR spectrum showed a resonance at δ -150.5 corresponding to the tetrafluoroborate anion. Owing to the paramagnetic behaviour of the complex, identification by ^1H NMR spectroscopy proved unsuccessful and no signal attributable to the fluoride bridges could be observed. It is worth noting that four N-H···F interactions were observed in the sold state that could account for the stability of the Ni_2F_2 core.[49]

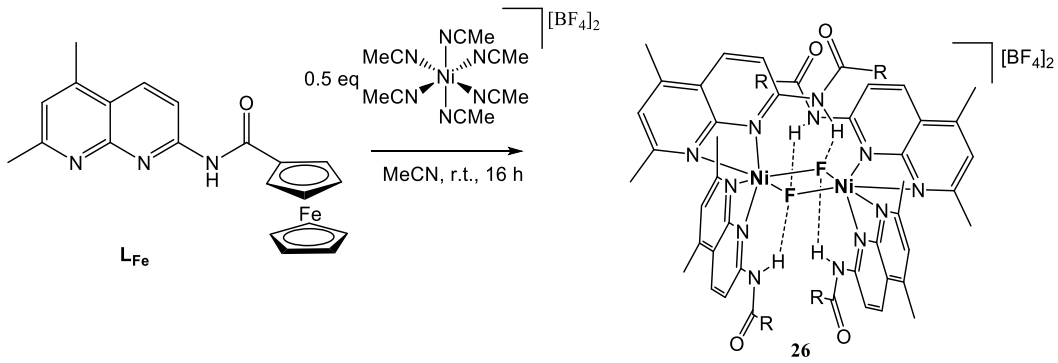

Scheme 4.1.7: Synthesis of the fluoro-bridged dinuclear nickel(II) compound $[Ni^{II}_2(\mu\text{-}F)_2(\mathbf{L_{Fe}})_4][BF_4]_2$ (**26**).[49]

Di-nickel tetrafluoroborate complexes bearing tridentate pincer ligands have also been recently investigated. In 2016, Xiang's group disclosed the synthesis and characterisation of a series of four-, five- and six-coordinate Ni(II) complexes bearing 2,6-bis(isopropylaminomethyl)pyridine (**L3**) and 2,6-bis(diethylaminomethyl)pyridine (**L4**).[50] Both mono-cationic $[Ni(\mathbf{L3})Cl][BF_4]$ (**28**) and di-cationic $[Ni(\mathbf{L3})(CH_3CN)_3][BF_4]_2$ (**29**) were formed by the metathesis of one or two Cl^- ions from **27** with one or two equivalents of $AgBF_4$ in THF or acetonitrile (**Scheme 4.1.8 A**). On the other hand, nickel(II) chloride complex **30** when reacted with one or two equivalents of $AgBF_4$ in THF or CH_3OH produced square planar $[Ni(\mathbf{L4})Cl][BF_4]$ (**31**) as well as the dinuclear Ni(II) fluoride complex $[Ni(\mathbf{L4}\text{-}H)(MeOH)F(\mu\text{-}F)]_2[BF_4]_2$ (**32**) in which two fluoride ligands bridged the two Ni(II) centres (**Scheme 4.1.8 B**). All structures were confirmed by single crystal X-ray diffraction. Since the synthesis of **32** was carried out under purified argon atmosphere in anhydrous solvents, hydroxide anions from water can be ruled out as the two bridging groups. Furthermore, the final R_1 and wR_2 crystallographic parameters were more consistent when the two bridging atoms being ascribed to fluoride rather than oxygen. It was considered that the highly electrophilic nature of the di-cationic Ni(II) centres promoted B-F bond cleavage of the coordinated BF_4^- in methanol resulting in fluoride-bridged **32**.[51]

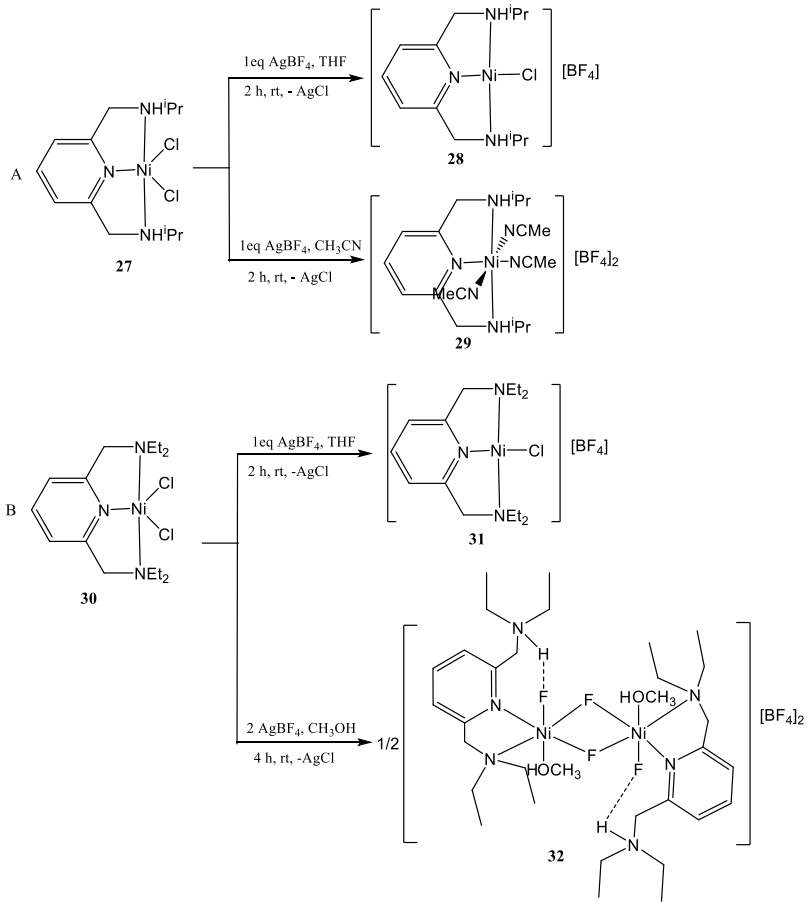

Scheme 4.1.8: Synthesis of [Ni(**L3**)Cl][BF_4] (**28**), [Ni(**L3**)$(NCCH_3)_3$][BF_4]$_2$ (**29**), [Ni(**L4**)Cl][BF_4] (**31**) and [Ni(**L4**-H)(MeOH)F(μ-F)$_2$(BF_4)$_2$] (**32**).[51]

4.2 Aims and objectives of chapter 4

In this Chapter, two novel classes of Ni(II) complexes will be targeted from the reactions of the *N,N$_{Py}$,O(H)* and *N,N$_{Py}$,N* (pro)ligands, H**L1$_R$**, **L2**, H**L4**, with $NiCl_2$(DME) and [$Ni(Py)_4(NCMe)_2$][BF_4]$_2$. In all cases, ^{1}H NMR and IR spectroscopy, mass spectrometry and elemental analysis will be used to identify the products. In addition, ^{19}F and ^{11}B NMR spectroscopies were used to additionally characterise the nickel tetrafluoroborate complexes and potential derivatives. Single crystal X-ray diffraction will be used, where possible, to explore their structural properties in the solid state. Furthermore, Cl-F exchange reactions using selected examples of nickel(II) chloride complexes will also be investigated by using nucleophilic fluorinating reagents.

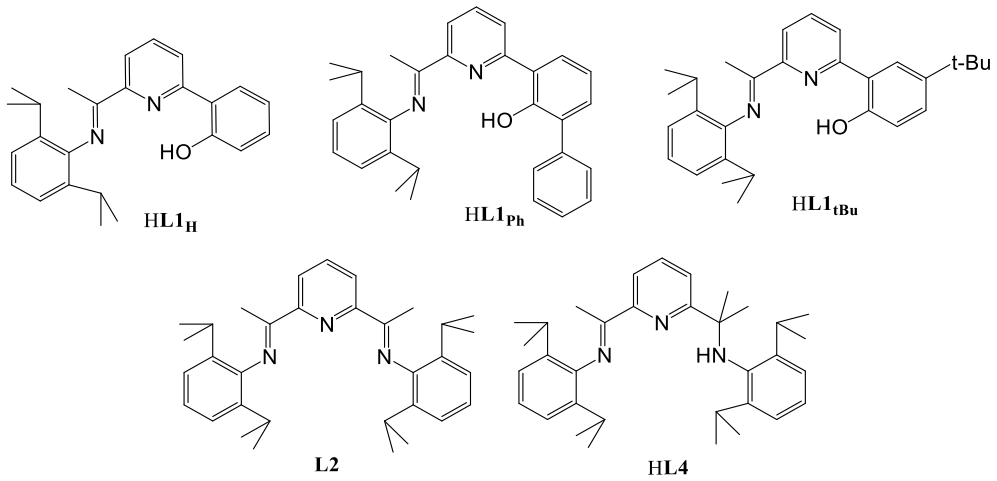

Figure 4.2.1: Types of pincer (pro)ligands to be employed in **Chapter 4**.

4.3 Results and discussion

4.3.1 Nickel(II) chloride complex synthesis

4.3.1.1 Reactivity of H**L1$_R$** towards nickel(II) chloride

The reactions of the *N,N,O(H)* (pro)ligands, H**L1$_H$**, H**L1$_{Ph}$** and H**L1$_{tBu}$**, with a slight excess of $NiCl_2$(DME) in THF at ambient temperature gave, on work-up, the mono-nickel chloride complexes (H**L1$_H$**)$NiCl_2$ (**4.1a**) and (**L1$_{Ph}$**)NiCl (**4.1b**) along with di-nickel (**L1$_{tBu}$**)$_2Ni_2Cl_2$ (**4.2c**) as orange powders in good yields (**Scheme 4.3.1**).

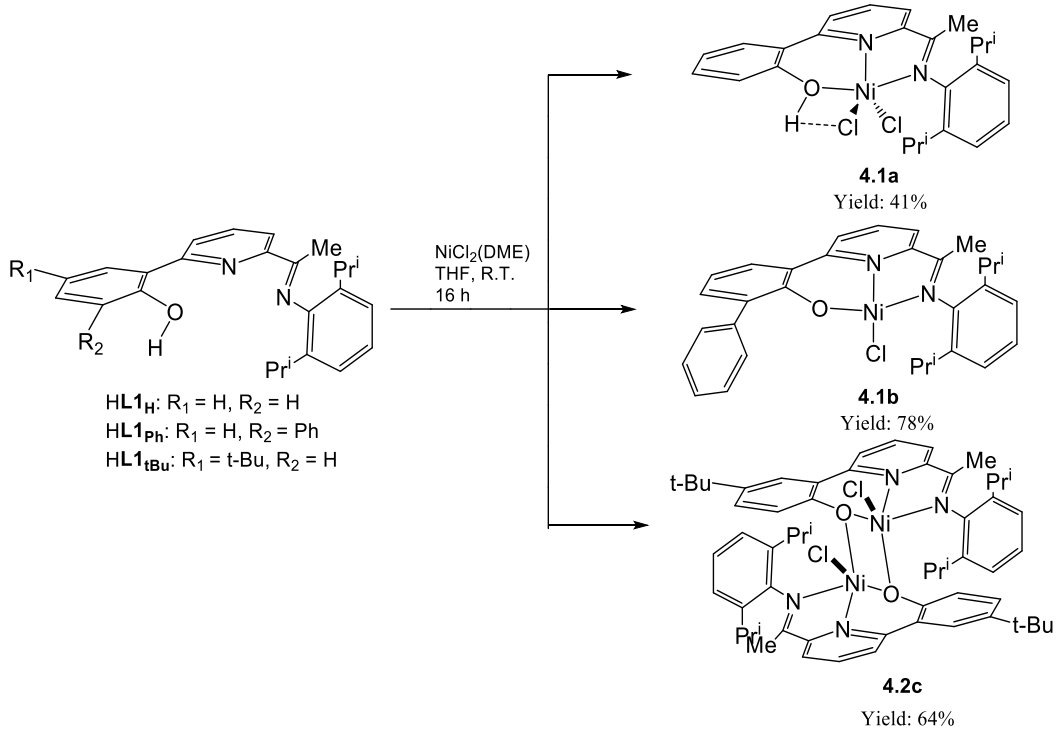

Scheme 4.3.1: Synthetic route to **4.1a**, **4.1b** and **4.2c.**

All complexes have been characterised by ^{1}H NMR spectroscopy, ESI MS, FAB MS, IR spectroscopy and elemental analysis. In addition, owing to the paramagnetic nature of **4.1a** and **4.2c**, magnetic measurements (Evans NMR) were also recorded. All data suggested that the complexation between the ligands and $NiCl_2$(DME) had been successful. By comparing the IR spectra of the complexes with those of the corresponding free ligands, the C=N absorption in the ligand had shifted to lower wavenumber (1580 - 1620 cm^{-1}), which was indicative of the successful coordination of the N_{imine} to the nickel. Meanwhile the μ_{eff} values of 2.9 BM (**4.1a**) and 4.6 BM (**4.2c**) were consistent with two unpaired electrons per nickel centre.[57] Moreover, broad paramagnetically shifted signals from δ -50 to 150 were a feature of their ^{1}H NMR

spectra. By contrast, **4.1b** gave sharp signals in its ^{1}H NMR spectrum in the conventional δ 1 – 8 window on account of its diamagnetic square planar geometry (**Fig. 4.3.1**).

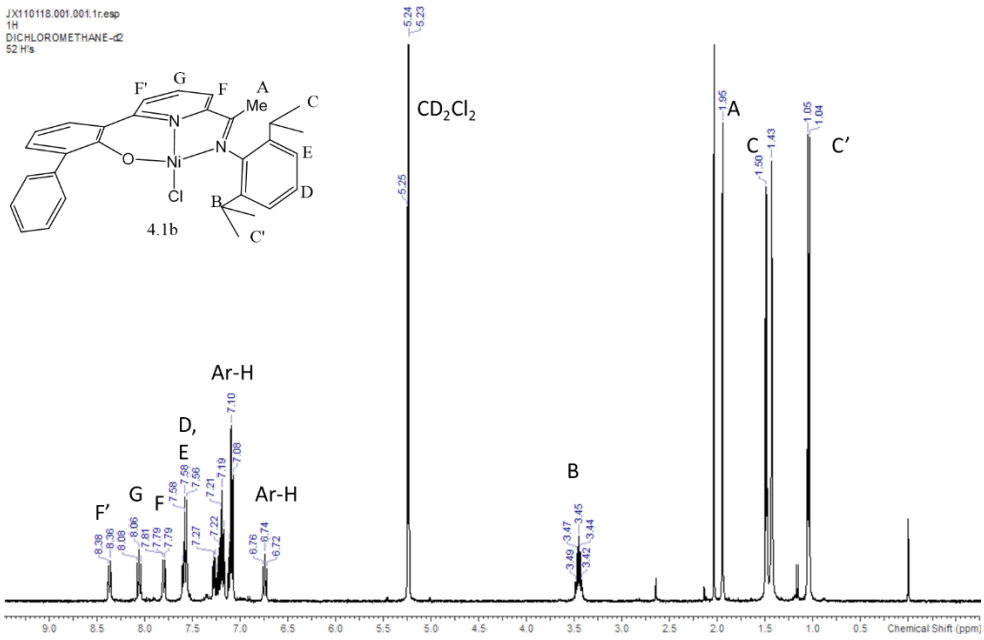

Figure 4.3.1: ^{1}H NMR spectrum of **4.1b** (recorded in CD_2Cl_2 at room temperature).

The ^{1}H NMR spectrum of **4.1b** displayed characteristic splitting of the isopropyl methyl signals (δ 1.05 and 1.50) into two distinct 6H doublets (**C**, **C'**), a feature that can be attributed to either two distinct Ar-CH*Me*$_2$ groups or to inequivalent CH*Me*^{A}*Me*^{B} methyl substituents. In addition the isopropyl protons (**B**: $CHMe_2$) were shifted to δ 3.46 from δ 2.70 (seen in (pro)ligand H**L1**$_{\mathbf{Ph}}$). On the other hand, analysis of **4.1a**, **4.1b** and **4.2c** by FAB mass spectrometry showed strong fragmentation peaks at *m/z* 429.6744, 505.1872 and 1011.4412 corresponding to the fragments $[M\text{-}HCl_2]^+$ (**4.1a**), $[M\text{-}Cl]^+$ (**4.1b**) and $[M\text{-}Cl_2\text{+}MeCN]^+$ (**4.2c**), respectively, which provided further support for complexation. Besides, the elemental analysis data was in accordance with the calculated elemental composition.

To allow structural characterisation, single crystals of **4.1a**, **4.1b** and **4.2c** suitable for X-ray determinations were grown by slow cooling of hot acetonitrile solutions containing the corresponding complex. Perspective views of the structures are shown in **Fig. 4.3.2** (**4.1a** and **4.1b**) and **Fig. 4.3.3** (**4.2c**); selected bond lengths and angles are collected in **Tables 4.3.1** and **4.3.2**.

The structure of **4.1a** revealed the nickel centre to be coordinated by an intact *N,N,O(H)* tridentate ligand along with two chlorides to form a distorted square-pyramidal geometry with Cl2 assuming the apical position; this is same geometry as observed for the cobalt analogue **3.1a**. In addition, intramolecular hydrogen bonding exists between one chloride and the hydroxyl group belonging to the *N,N,N,O(H)* ligand [O(1)-H(1)···Cl(2) 2.11 Å].

Unlike **4.1a**, the structure of **4.1b** reveals the hydroxyl group of the tridentate ligand to be deprotonated resulting in a square planar geometry at nickel. By comparison with the Co(II) chloride complex **3.1a**, the corresponding bond lengths and angles in **4.1a** are similar while the bond lengths for **4.1b** were noticeably shorter. In addition, the N-Ni-N and O-Ni-N angles within the 5- and 6-membered chelate rings of **4.1b** are close to 90°, which further highlights the square planar geometry. The difference in structure adopted by **4.1a** and **4.1b** is uncertain but could possibly be due to the substituents of the phenol group in H**L1**$_R$ affecting the coordination environment of the nickel centre.

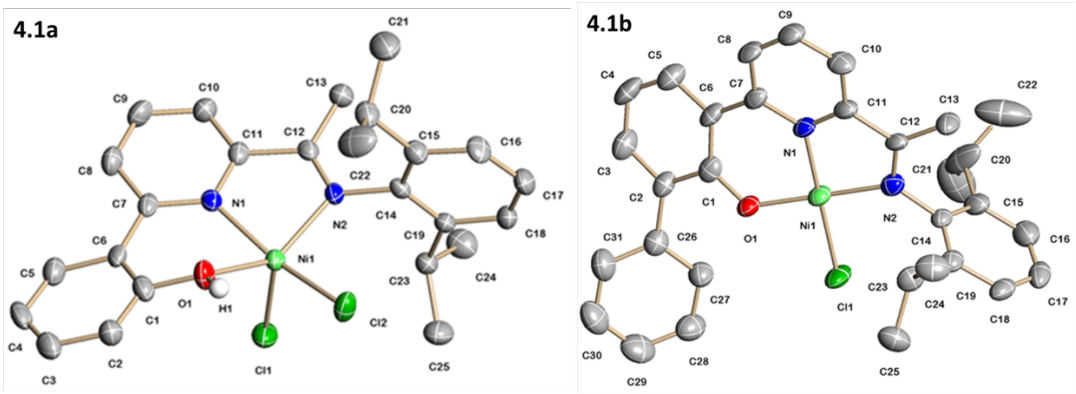

Figure 4.3.2: Molecular structures of **4.1a** and **4.1b**.

Table 4.3.1: Selected bond lengths and angles for **4.1a** and **4.1b**.

*Bond Lengths (Å) for **4.1a***		*Bond Lengths (Å) for **4.1b***	
Ni(1)-N(1)	2.038(3)	Ni(1)-N(1)	1.866(4)
Ni(1)-N(2)	2.033(3)	Ni(1)-N(2)	1.914(4)
Ni(1)-O(1)	2.059(3)	Ni(1)-O(1)	1.812(3)
Ni(1)-Cl(1)	2.263(12)	Ni(1)-Cl(1)	2.176(16)
O(1)-H(1)	0.9614		
O(1)-H(1)···Cl(2)	2.11		
*Bond Angles (°) for **4.1a***		*Bond Angles (°) for **4.1b***	
N(2)-Ni(1)-N(1)	80.37(13)	N(2)-Ni(1)-N(1)	84.88(19)
N(1)-Ni(1)-O(1)	82.86(12)	N(1)-Ni(1)-O(1)	93.41(17)
N(2)-Ni(1)-O(1)	143.46(12)	N(2)-Ni(1)-O(1)	176.20(17)
N(1)-Ni(1)-Cl(1)	95.01(9)	N(1)-Ni(1)-Cl(1)	177.84(15)
O(1)-Ni(1)-Cl(1)	106.46(9)	O(1)-Ni(1)-Cl(1)	87.68(11)

On the other hand, the molecular structure of **4.2c** is similar to that seen in the di-zinc (**2.2c**) and di-cobalt (**3.2c**) chloride complexes reported in **Chapters 2** and **3**, respectively. Specifically, **4.2c** consists of a dinickel species in which the two nickel centres are linked by a μ-$O_{phenolate}$ bridge belonging to the *N,N,O*-ligand. Square pyramidal geometries are adopted by each nickel centre with the *N,N,O*-ligand and one chloride forming the base and the second chloride the apex. The Ni(1)-O(1) bond distance is the shortest bond involving the tridentate ligand [1.993(3) Å] and is shorter when compared to that seen in the Zn(II) and Co(II) chloride comparators (**2.2c** and **3.2c**). The central Ni-$N_{pyridine}$ bond length [2.018(4) Å] is slightly shorter than the Ni-N_{imino} one [2.033(3) Å]. In addition, five- and six-membered chelate rings are a feature of the *N,N,O* ligand [N(2)-Ni(1)-N(1) 80.54(17)° and N(1)-Ni(1)-O(1) 88.37(16)°]. The Ni(1)···Ni(2) separation of 3.118 Å is close to those found in similar dinuclear nickel(II) complexes reported elsewhere.[52] Therefore, it is apparent that (pro)ligand H**L1**$_{\mathbf{tBu}}$ has a propensity to undergo deprotonation and form bimetallic products (see **2.2c**, **3.2c** and **4.2c**), which may be due to the electronic donating properties of the *t*-butyl group.

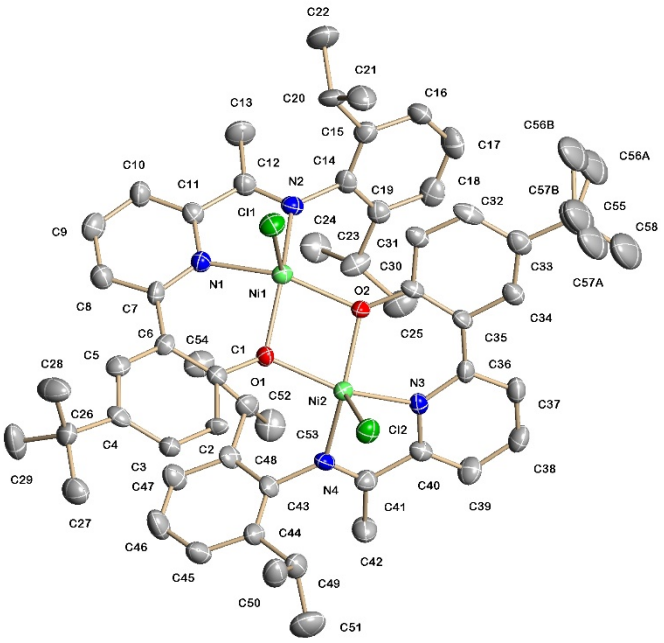

Figure 4.3.3: Molecular structure of **4.2c**.

Table 4.3.2: Selected bond lengths and bond angles for **4.2c.**

Bond Lengths (Å)	
Ni(1)-O(1)	1.993(3)

Ni(1)-O(2)	2.033(3)
Ni(2)-O(1)	2.040(3)
Ni(2)-O(2)	1.983(3)
Ni(1)-N(1)	2.018(4)
Ni(1)-N(2)	2.062(4)
Ni(1)-Cl(1)	2.2878(16)
Ni(1)···Ni(2)	3.118
Bond Angles (°)	
N(2)-Ni(1)-N(1)	80.54(17)
N(1)-Ni(1)-O(1)	88.37(16)
N(2)-Ni(1)-O(1)	147.84(16)
N(1)-Ni(1)-Cl(1)	92.60(13)
O(1)-Ni(1)-Cl(1)	114.07(11)
O(2)-Ni(1)-O(2)	78.06(14)
Ni(1)-O(2)-Ni(2)	101.28(15)

4.3.1.2 Reactivity of **L2** and H**L4** towards nickel(II) chloride

To complement the work conducted in the two previous chapters regarding *N,N,N* complexation, the previously reported nickel(II) chloride complex, [(**L2**)$NiCl_2$], was resynthesised from **L2**,[56] while its methylated derivative (H**L4**)$NiCl_2$ (**4.4**) was prepared for the first time in good yield by treating H**L4** with $NiCl_2$(DME) in THF at room temperature (**Scheme 4.3.2**). Novel complex **4.4** was characterised by ESI MS, FAB mass spectrometry, magnetic susceptibility, IR spectroscopy, ^{1}H NMR spectroscopy and single crystal X-ray diffraction.

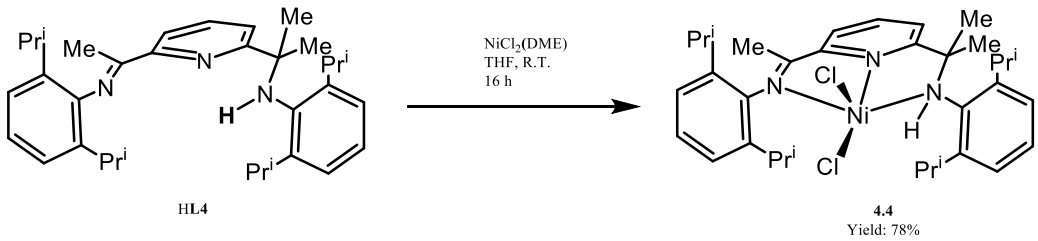

HL4 **4.4** Yield: 78%

Scheme 4.3.2: Synthesis of *N,N,N*-nickel(II) chloride **4.4**.

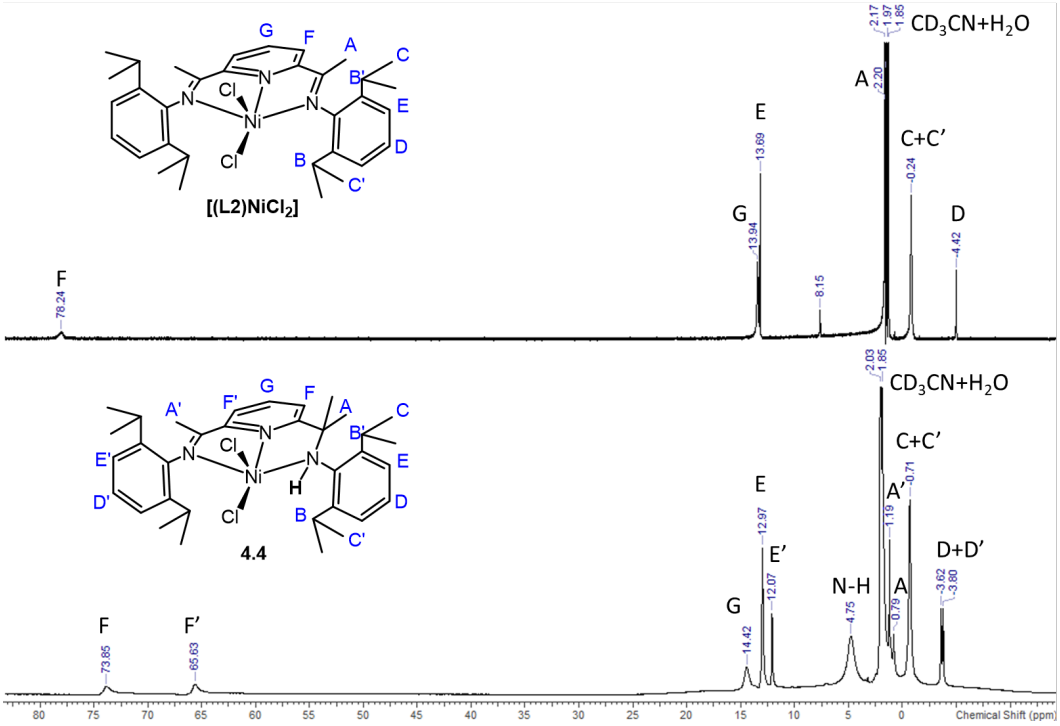

Figure 4.3.4: ^{1}H NMR spectra of (**L2**)$NiCl_2$ and **4.4** in CD_3CN at room temperature.

The IR spectrum of **4.4** displayed strong absorption bands around 1596 cm^{-1} and 3308 cm^{-1} consistent with a N-coordinated imine and a N-H stretch. Furthermore, the microanalytical data for the complex was in full agreement with an elemental composition of general formula (H**L2**)$NiCl_2$. Complex **4.4** also displayed fragmentation peaks in its FAB mass spectrum corresponding to *m/z*, $[M\text{-}Cl]^+$ 590.2831 and $[M\text{-}2Cl]^+$ 555.3183.

Characteristically broad paramagnetically shifted peaks were a further feature of the ^{1}H NMR spectrum of **4.4**, supportive of a high-spin ($S = 1$) state for the d^8 metal atom. The assignment of all the peaks in the ^{1}H NMR spectrum of **4.4** proved difficult but nevertheless some useful information could be obtained by comparison with data recorded for [(**L2**)$NiCl_2$], relative integration and proximity to the paramagnetic centre.[53] **Figure 4.3.4** shows the ^{1}H NMR spectrum of complexes [(**L2**)$NiCl_2$] and **4.4**. For **4.4**, two distinct downfield peaks for the *meta*-pyridyl protons (**F**, **F'**) at δ 73.93 and δ 65.69 were visible, while the *para*-pyridyl proton (**G**) and *meta*-aryl protons (**E**, E') can been seen more upfield at δ 14.42 and δ 12.52_{av}. By contrast, the ketamine and ketimine methyl protons (**A**, **A'**) can be seen at δ 1.19 and δ 0.79, while the isopropyl methyl protons (**C**, **C'**) appear at δ -0.71. In addition, the *para*-aryl protons (**D**, **D'**) can be seen at δ -3.62 and δ -3.80. The key differences between the **4.4** and

[(**L2**)$NiCl_2$] are the presence of two signals for the *meta*-pyridyl protons (**F** and **F'**), *meta*-aryl protons (**E** and **E'**) and the *para*-aryl protons (**D** and **D'**) in **4.4** respectively, while in [(**L2**)$NiCl_2$] only one singlet is observed (**F**, **E** and **D**). Furthermore, the amine proton (N-H) of **4.4** shows a broad peak at δ 4.75, while no such signal is present in [(**L2**)$NiCl_2$]. Moreover, two nickel complexes displayed magnetic moments of ~2.9 μ_B, consistent with two unpaired electrons.[57]

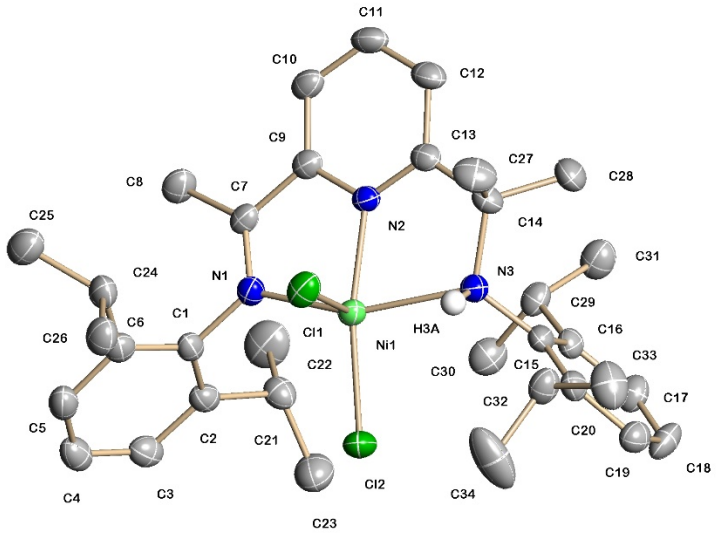

Figure 4.3.5: Molecular structure of **4.4**.

Table 4.3.3: Selected bond lengths and angles for **4.4**.

Bond Lengths (Å)	
Ni(1)-N(1)	2.125(2)
Ni(1)-N(2)	1.994(2)
Ni(1)-N(3)	2.248(2)
Ni(1)-Cl(1)	2.3025(9)
N(3)-H(3A)···Cl(1)	2.64
Bond Angles (°)	
N(2)-Ni(1)-N(1)	78.84 (10)
N(2)-Ni(1)-N(3)	154.51(10)
N(2)-Ni(1)-Cl(1)	101.04(7)
N(2)-C(12)-C(13)	119.7(3)

Single crystals of **4.4** suitable for an X-ray determination were grown from a hot concentrated acetonitrile solution. The molecular structure, selected bond lengths/angles are shown in **Fig 4.3.5** and **Table 3.3.3**, respectively. Within the structure, the nickel

centre adopted a distorted square pyramidal geometry in a manner similar to that previously reported for Zn(II) and Co(II) chloride complexes (**2.4** and **3.4**). The Ni-$N_{pyridyl}$ bond length is also shorter than the Ni-N_{imino} and Ni-N_{amino} lengths highlighting the superior donor properties of the pyridine. Double bond character is evident for the imino linkage N(1)-C(7) and single bond character for the amino linkage N(3)-C(14). The planes of the phenyl rings of both 2,6-diisopropylphenyl groups were oriented essentially orthogonally to the plane of the ligand [ranging between 79.2° and 77.9°. In addition, a hydrogen bond was observed between the amine proton and one chloride ligand.

4.3.2 Complexation with Ni(II) tetrafluoroborate salts

4.3.2.1 Reactivity of H**L1**$_{\mathbf{R}}$ towards $[Ni(Py)_4(NCMe)_2][BF_4]_2$

In last two chapters, we discussed the reactivity of H**L1**, **L2** and H**L4** towards Zn(II) and Co(II) tetrafluoroborate salts. Herein, we were interested in the reactions of these ligands with related nickel(II) tetrafluoroborate salts. Hence, reactions of H**L1**, **L2** and H**L4** with $[Ni^{II}(Py)_4(NCMe)_2][BF_4]_2$, $[Ni^{II}(3,5\text{-lutidine})_4(NCMe)_2][BF_4]_2$ and $[Ni^{II}(NCMe)_6][BF_4]_2$ in dry acetonitrile at 80 ^oC gave mono-nickel [(**L1**$_{\mathbf{H}}$)Ni(Py)][BF_4] (**4.5a**), [{**L1**$_{\mathbf{H}}$}Ni(3,5-lutidine)][BF_4]$_2$ (**4.6a**), [(**L1**$_{Ph}$)Ni(Py)][BF_4] (**4.7b**), [(**L1**$_{Ph}$)Ni(3,5-lutidine)][BF_4] (**4.8b**) and [(**L1**$_{Ph}$)Ni(NCMe)][BF_4] (**4.9b)** along with the dinickel complex [(**L1**$_{tBu}$)$_2$Ni$_2$(μ-BF_4)(NCMe)$_2$][BF_4] (**4.10c**) (**Scheme 4.3.3**).

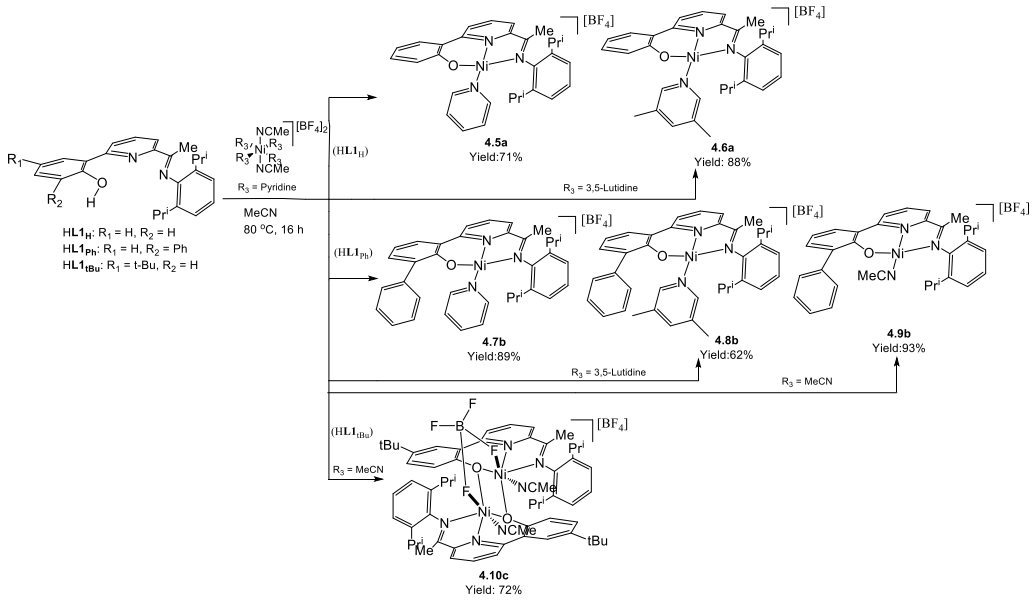

Scheme 4.3.3: Syntheses of **4.5a**, **4.6a**, **4.7b**, **4.8b**, **4.9b** and **4.10c**.

All complexes were characterised by ^{1}H NMR, ^{19}F NMR, IR spectroscopies, electrospray mass spectrometry (ESI-MS) and elemental analysis. With the exception of dinickel **4.10c**, all products were diamagnetic with sharp peaks observable between δ 0 and δ 10.0 in their ^{1}H NMR spectra, on account of the square planar geometry adopted. On the other hand, **4.10c** proved paramagnetic with broad and shifted peaks apparent in its ^{1}H NMR spectrum; magnetic measurements were also performed on **4.10c**.

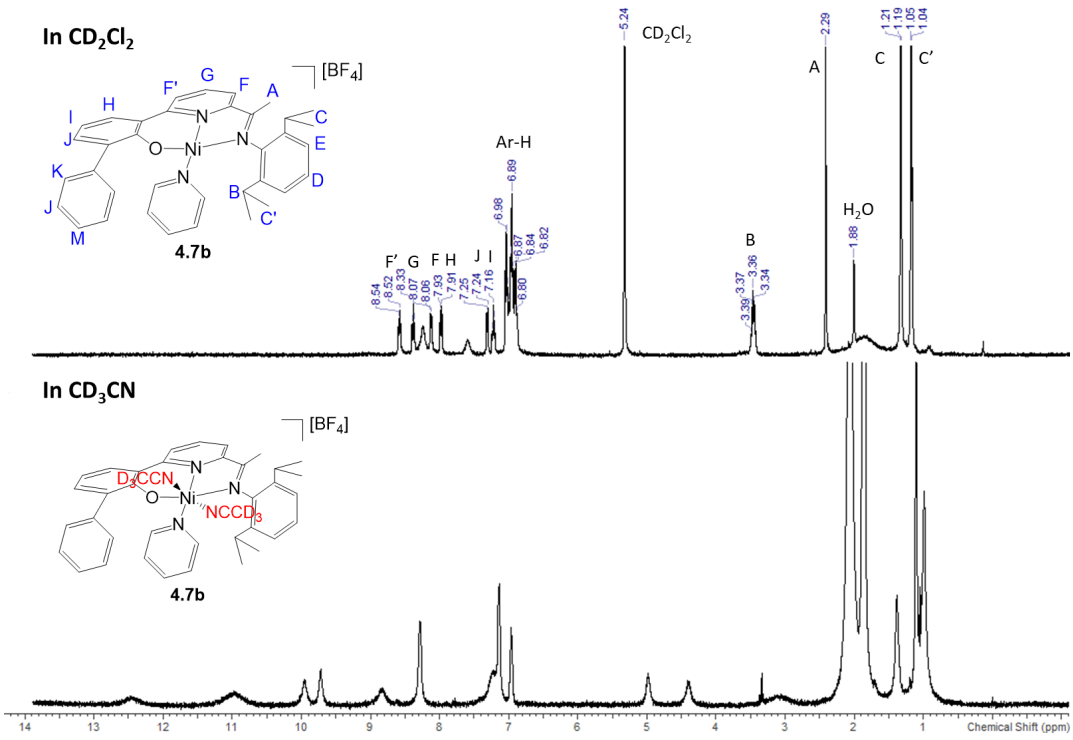

Figure 4.3.6: ^{1}H NMR spectra of **4.7b** in CD_2Cl_2 and CD_3CN; both recorded at room temperature.

The ^{1}H NMR spectrum for **4.7b** in CD_2Cl_2 shows two 6H doublets at δ 1.05 and δ 1.21 which can be assigned to the isopropyl methyl groups CH*Me*$_a$*Me*$_b$, this being a clear indication of complex formation (**Figure 4.3.6**). The septet peak for the isopropyl protons C*H*(Me)$_2$ was seen at δ 3.40 which is downfield from that seen in the proligand H**L1**$_{\mathbf{Ph}}$ (δ 2.70). In addition, the Py-*H*$_p$ proton shifted to δ 8.34 from δ 7.99 in the free ligand again supporting complexation. Interestingly, the ^{1}H NMR spectrum recorded in CD_3CN showed evidence for paramagnetic behaviour which likely arises on account of partial coordination of CD_3CN to **4.7b** (**Figure 4.3.6**). Re-recording the ^{1}H NMR spectrum of this sample in CD_2Cl_2 gave a spectrum identical to that recorded initially highlighting the lability of the acetonitrile ligands in **4.7b**·2CD_3CN. Similar observations were noted with **4.5a**, **4.6a**, **4.7b** and **4.8b**.

The IR spectra of **4.5a**, **4.6a**, **4.7b** and **4.8b** as well as **4.10c** displayed strong absorptions around 1586 - 1635 cm^{-1} which were assigned to the $\upsilon(C=N)_{imine}$ band which were shifted from about 1651 cm^{-1} in the corresponding free ligands. Furthermore, fragmentation peaks in their FAB mass spectra as well as the results of the elemental analysis were consistent with their formulations.

Single crystals of **4.5a**, **4.6a**, **4.7b**, **4.8b** and **4.10** suitable for the X-ray determinations were grown by slow diffusion of diethyl ether into an acetonitrile solution of the corresponding complex. As representative examples, the molecular structures of just **4.5a** and **4.7a** are shown in **Fig. 4.3.7**, while selected bond lengths and angles are presented in **Table 4.3.4**. The structures of all four complexes are similar and are based on a cation anion pair. Within the cationic unit a single nickel centre was surrounded by the corresponding *N,N,O*-ligand with either a pyridine (**4.5a**, **4.7b**) or 3,5-lutidine (**4.6a**, **4.8b**) filling the fourth coordination site to complete a distorted square planar geometry. A single tetrafluoroborate ion serves as the anionic unit. The bond lengths and angles between the four complexes are similar. Typically, the Ni(1)-O(1) bond represents the shortest bond length from the pincer ligand at *ca.* 1.798(2) Å on the account of the anionic component to the bonding, while the $Ni\text{-}N_{pyridine}$ bond lengths [1.861(4) Å (**4.5a**), 1.865(5) Å (**4.7b**)] were shorter than the $Ni\text{-}N_{imino}$ ones [1.882(2) – 1.893(5) Å]. On the other hand, the O(1)-Ni(1)-N(1) [94.98 (19)º (**4.5a**), 93.93 (17)º (**4.7b**)] and N(2)-Ni(1)-N(1) [84.3(2)º (**4.5a**), 85.8(2)º (**4.7b**)] angles within each six-membered and five-membered chelate rings are comparable to those seen for **4.1b**. The N(2)-C(12)-C(13) bond angle of around 125.2(5)° confirmed sp^2 hybridisation was retained by the imine unit. The planes of the phenyl rings of 2,6-diisopropylphenyl are oriented essentially orthogonally to the plane of the ligand backbone. The N-bound pyridine ligands are tilted with respect to the plane of the *N,N,O*-plane as borne out by the torsion angles 65.3(4)º (**4.5a**) and 68.5(5)º (**4.7a**).

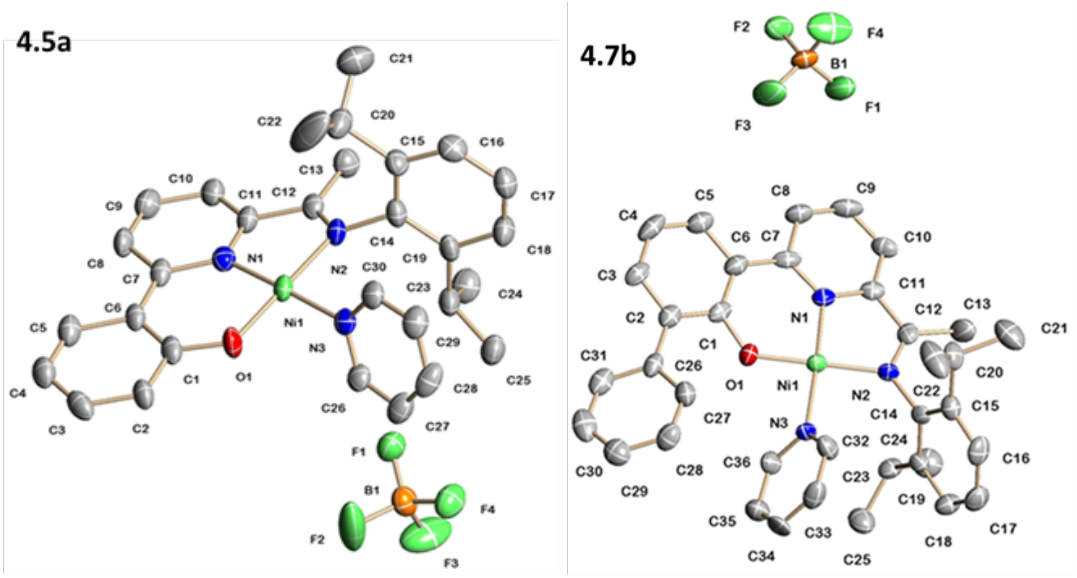

Figure 4.3.7: Molecular structures of **4.5a** and **4.7b.**

Table 4.3.4: Selected bond lengths and angles for **4.5a** and **4.7a.**

*Bond Lengths (Å) for **4.5a***		*Bond lengths (Å) for **4.7b***	
Ni(1)-O(1)	1.789(4)	Ni (1)-O(1)	1.802(4)
Ni (1)-N(1)	1.861(4)	Ni (1)-N(1)	1.865(5)
Ni(1)-N(2)	1.882(4)	Ni(1)-N(2)	1.893(5)
Ni(1)-N(3)	1.916(4)	Ni(1)-N(3)	1.911(4)
N(2)-C(12)	1.306(7)	N(2)-C(12)	1.288(6)
*Bond angles (°) for **4.5a***		*Bond angles (°) for **4.7b***	
O(1)-Ni(1)-N(1)	94.98(19)	O(1)-Ni(1)-N(1)	93.93(17)
O(1)-Ni(1)-N(3)	84.54(18)	O(1)-Ni(1)-N(3)	83.93(19)
N(2)-Ni(1)-N(1)	84.3(2)	N(2)-Ni(1)-N(1)	85.8(2)
N(2)-C(12)-C(13)	125.2(5)	N(2)-C(12)-C(13)	125.3(5)
*Torsion angles (°) for **4.5a***		*Torsion angles (°) for **4.7a***	
N(2)-Ni(1)-N(3)-C(30)	65.3(4)	N(2)-Ni(1)-N(3)-C(32)	68.5(5)
Ni(1)-N(2)C(14)-C(15)	-96.2(6)	Ni(1)-N(2)C(14)-C(15)	-94.2(5)

A view of **4.10c** is shown in **Fig 4.3.8**; selected bond lengths and angles are collected in **Table 4.3.5**. The structure of **4.10c** consists of a bimetallic cationic unit and a non-coordinating tetrafluoroborate anion. Within the cationic unit two nickel centres are triply bridged by two $O_{phenoxy}$ groups and a BF_4 group that makes use of two of its fluoride substituents to coordinate to each nickel centre. In addition each nickel centre is chelated by the *N,N,O*-ligand and a N-bound acetonitrile to complete a distorted

octahedral geometry. Such a bridging bonding mode for tetrafluoroborate is rare in nickel chemistry[54] but resembles that seen in the dizinc complex **2.6a'**. However, unlike **2.6a'** a stronger M···F contact is evident {Ni(1)-F(1) [2.337(4) Å] (**4.10c**) Zn(1)···F(1) [2.716(5) Å] (**2.6a'**)}. On the other hand, the two MeCN ligands on neighbouring nickel centres are configured *cis*. As has been noted elsewhere, the anionic Ni-O bond is the shortest involving the *N,N,O* ligand [O(1)-Ni(1) 1.963(7) Å] but longer than that seen in mono-nickel complexes **4.5** - **4.8** (range: 1.789-1.802 Å); the Ni-$O_{phenoxy}$ distances are, however, similar to other hexacoordinated nickel(II) complexes [1.971(2)-2.102(7) Å].[54,55] Meanwhile, the central Ni-$N_{pyridine}$ bond length [1.861(1) Å] is shorter than the Ni-N_{imino} one [1.882(4) Å]. The O(1)-Ni(1)-N(1) 89.54(15)º and N(2)-Ni(1)-N(1) 80.73(17)º angles within the six- and five-membered chelate rings are similar to that seen in **4.5** - **4.8**. The internuclear distance involving the two nickel centres is 3.091 Å and similar to that observed in the dicobalt complexes **3.5a** and **3.6c** [range: 3.099-3.118 Å].

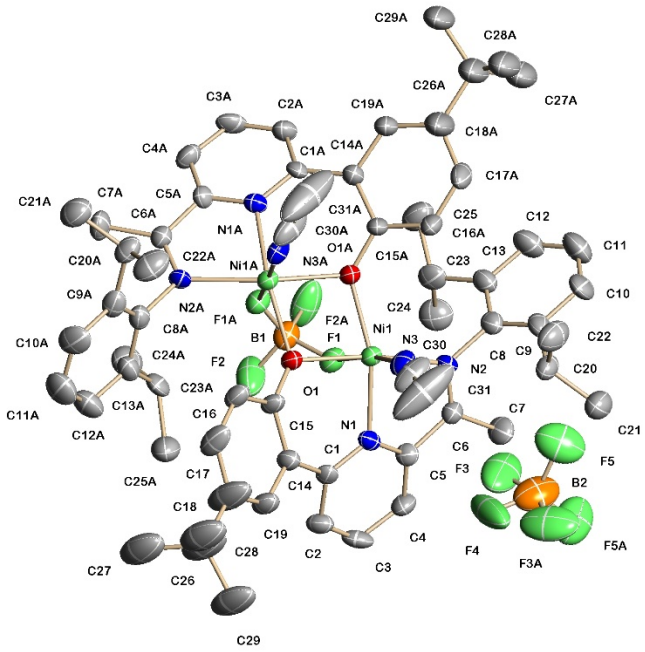

Figure 4.3.8: Molecular structure of **4.10c**.

Table 4.3.5: Selected bond lengths and angles in **4.10c**.

Bond Lengths (Å)	
Ni(1)-O(1)	1.963(7)
Ni(1)-O(1A)	2.007(3)

Ni(1A)-O(1)	2.007(3)
Ni(1A)-O(1A)	1.963(7)
Ni(1)-N(1)	2.047(4)
Ni(1)-N(2)	2.099(4)
Ni(1)-N(3)	2.040(6)
Ni(1A)-N(3A)	2.043(10)
Ni(1)-F(1)	2.338(4)
Ni(1A)-F(1A)	2.337(4)
B(1)-F(1)	1.401(7)
Ni(1)···Ni(1A)	3.091
Bond Angles (°)	
O(1)-Ni(1)-N(1)	89.54(15)
N(2)-Ni(1)-N(1)	80.73(17)
N(3)-Ni(1)-N(2)	98.07(18)
O(1)-Ni(1)-O(1A)	78.92(14)
Ni(1)-O(1)-Ni(1A)	100.69(14)
N(1)-Ni(1)-F(1)	76.86(15)
F(2)-B(1)-F(1)	110.0(2)

The atoms labelled with an 'A' have generated by symmetry

To explore, the steric control of the *N,N,O*-pincer ligand on the coordination chemistry of nickel(II), the reaction of the less hindered *O,N,O* precursor to H**L1**$_{Ph}$, Ketone-Ph, with $[Ni^{II}(Py)_4(NCMe)_2][BF_4]_2$ was also conducted under similar reaction conditions. On work-up, dicationic $[(O,N,O)_2Ni_2(MeCN)_4][BF_4]_2$ **4.11** was isolated in good yield (**Scheme 4.3.4**). Complex **4.11** has also been fully characterised by ^{1}H NMR, ^{19}F NMR and IR spectroscopies as well as by ESI, HR FAB mass spectrometry and elemental analysis.

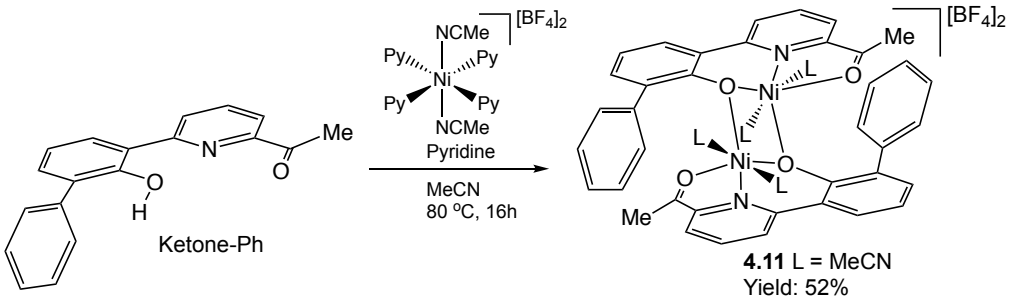

Scheme 4.3.4: Reaction of Ketone-Ph with $[Ni(Py)_4(NCMe)_2][BF_4]_2$

The ^{1}H NMR spectrum of **4.11** was difficult to fully assign due to its paramagnetic properties, but the *para*-pyridyl and *meta*-pyridyl protons were clearly identifiable at δ 22.77, δ 21.38 and δ 13.22. On the other hand, the ^{19}F NMR spectrum of **4.11** showed one singlet at δ -149.09 assignable to the non-coordinated BF_4^- anion. In the IR spectrum, the υ(C=O) absorption was observed at 1630 cm^{-1}, which was shifted to lower wavenumber by 41 cm^{-1} when compared to that seen in free Ketone-Ph. In addition, the FAB mass spectrometric and microanalytical data for the complex were in full agreement with the structure proposed.

Single crystals of **4.11** were also grown from MeCN/Et_2O solvent by using same method. A view of the molecular structure of **4.11** is shown in **Fig 4.3.9**, while selected bond distances and angles are compiled in **Table 4.3.6**. The structure resembles that seen in the corresponding cobalt complex **3.8** and is based on a dinickel cationic unit that is charge balanced by two tetrafluoroborate counterions. Each Ni(II) centre is coordinated by a *O,N,O*-ligand with each $O_{phenoxy}$ donor additionally acting as bridge. In addition, each nickel centre is surrounded by two MeCN ligands to complete a six-coordinate geometry. The Ni-$N_{Pyridine}$, Ni-$O_{Phenoxy}$ and Ni-O_{ketone} bond lengths in **4.11** are similar and compare favourably to those seen in **4.10c** as well as in the dicobalt complexes **3.2**-**3.8**. The metal-metal separation [Ni(1)···Ni(2) 3.124 Å] is longer than observed in **4.10c** (3.091 Å) but similar to that seen in the dinickel chloride complex **4.2c** (3.118 Å). As would be expected the *O,N,O*-angles within the 6- and 5-membered chelate rings showed some variation at 87.91(12)º and 79.04(13)º, respectively. Lastly, the two planes of *O,N,O*-ligands are aligned in parallel fashion and perpendicular to the Ni(1)-O(1)-Ni(1A)-O(3) plane.

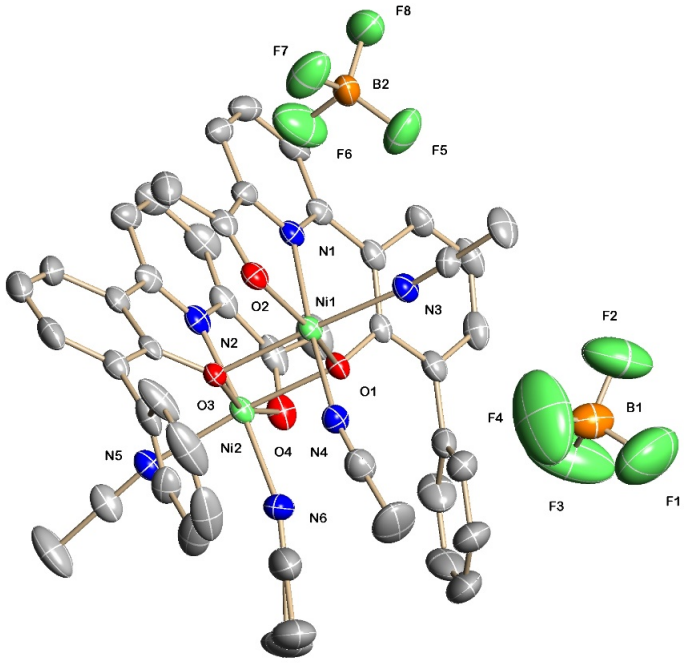

Figure 4.3.9: Molecular structure of **4.11**.

Table 4.3.6: Selected bond lengths and angles for **4.11.**

Bond Lengths (Å)	
Ni(1)-O(1)	1.983(3)
Ni(1)-O(2)	2.101(3)
Ni(1)-O(3)	2.094(3)
Ni(2)-O(1)	2.087(2)
Ni(2)-O(3)	1.982(3)
Ni(2)-O(4)	2.100(3)
Ni(1)-N(1)	2.043(3)
Ni(2)-N(2)	2.057(4)
Ni(1)-N(3)	2.096(4)
Ni(1)···Ni(2)	3.124
Bond Angles (°)	
N(1)-Ni(1)-O(1)	87.91(12)
N(1)-Ni(1)-O(2)	79.04(13)
N(1)-Ni(1)-N(3)	88.55(14)
O(1)-Ni (1)-O(3)	79.11(11)
Ni(1)-O(1)-Ni(2)	100.22(11)
C(13)-C(12)-O(2)	120.7(5)

4.3.2.2 Reactivity of **L2** and H**L4** towards $[Ni(Py)_4(NCMe)_2][BF_4]_2$

To allow a comparison with the *N,N,N* work disclosed in the previous chapters, the reactivity of the N,N_{Py},N-ligands, **L2** and H**L4**, towards $[Ni(Py)_4(NCMe)_2][BF_4]_2$ was also explored (**Scheme 4.3.5)**. The complexation reactions were carried out in a mixed solvent system composed of CH_2Cl_2 and MeCN at reflux affording, on work-up, [(**L2**)Ni(py)$(MeCN)_2][BF_4]_2$ (**4.12**) and [(H**L4**)Ni(η-$OHBF_3$)(MeCN)]$[BF_4]$ (**4.13d**) in good yields. In addition, the reaction of H**L4** with $[Ni(NCMe)_6][BF_4]_2$ in the absence of pyridine yielded the four-coordinate complex [(H**L4**)Ni(MeCN)]$[BF_4]_2$ (**4.14d**). All products have been characterised by ^{19}F NMR spectroscopy, IR spectroscopy, mass spectrometry and elemental analysis.

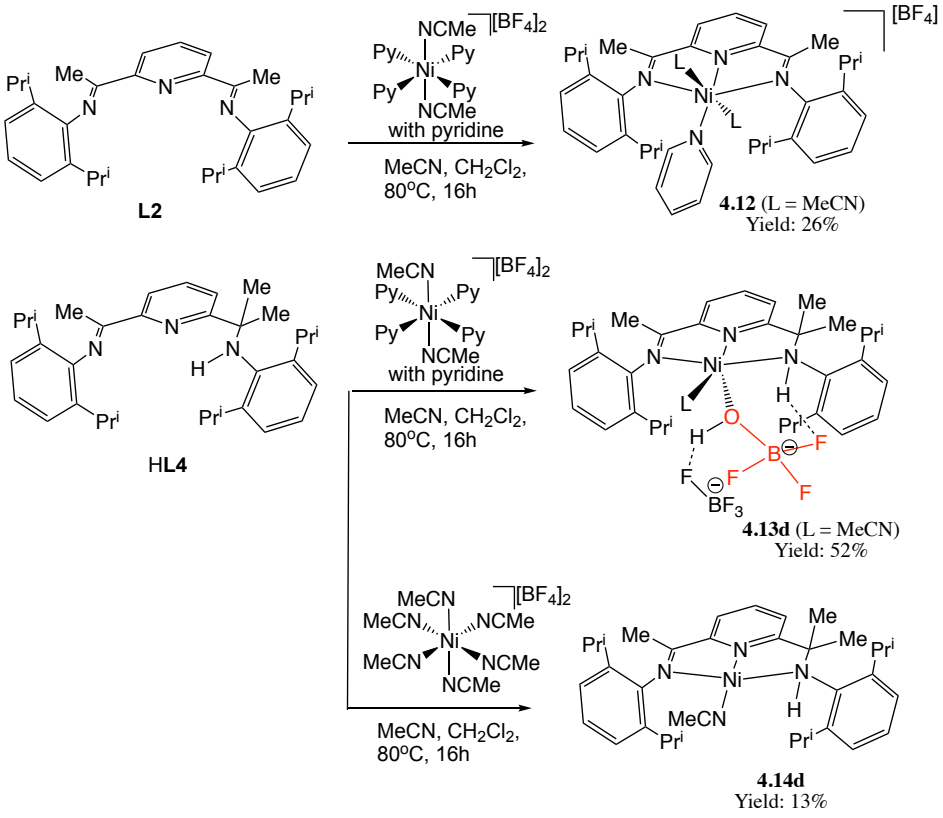

Scheme 4.3.5: Syntheses of **4.12**, **4.13d** and **4.14d.**

The ^1H NMR spectra of **4.12** and **4.13d** showed broad and paramagnetically shifted peaks while **4.14d** proved diamagnetic. The ^{19}F NMR spectra of **4.12**, **4.13d** and **4.14d** showed singlets at δ ~150.9 which corresponded to the BF_4^- anion. There was, however, no evidence for a signal for the $HOBF_3$ ligand in **4.13d** which could possibly be attributed to the paramagnetic properties of the nickel centre. Complex **4.12** displayed a

magnetic moment (μ_{eff}) of 2.9 BM while **4.13d** gave a value of 3.1 BM, both corresponding to two unpaired electrons. Square planar **4.14d** showed three doublets at δ 1.07 (6H), δ 1.12 (12H) and δ 1.19 (6H) in its ^{1}H NMR spectrum (recorded in CD_2Cl_2) which can be assigned to the isopropyl methyl groups. The two septet peaks for the isopropyl protons C*H*(Me)$_2$ were found at δ 3.40 and δ 3.50 which are downfield from that seen in the proligand H**L4** (δ 2.77 and δ 3.31). Moreover, the Py-H$_p$ protons shifted to δ 8.22 from δ 7.79 in the ligand. By contrast, **4.14d** displayed paramagnetic behaviour when its ^{1}H NMR spectrum was recorded in CD_3CN. In the IR spectra of **4.12**, **4.13d** and **4.14d,** the stretching frequency for the imine had shifted to 1567 - 1573 cm^{-1} when compared to 1642 – 1659 cm^{-1} in the free ligands, which is consistent with coordination of the imine nitrogen; a υ(N-H) stretch at *ca.* 3307 cm^{-1} in **4.13d** and **4.14d** was also clearly visible. Furthermore, analyses of all complexes by FAB mass spectrometry showed ions consistent with the proposed formulations. Likewise, elemental analysis of both complexes were consistent with the calculated elemental compositions.

The structure of **4.12** is similar to the Co(II) analogue **3.9**, and is based on a dicationic mono-nickel complex charged balanced by two tetrafluoroborate counterions. A view of **4.12** is illustrated in **Fig 4.3.10**; selected bond lengths and angles are given in **Table 4.3.7**. The structure consists of single nickel centre surrounded by a *N,N,N*-ligand along with one pyridine and two MeCN ligands, to complete a geometry that can be best described as distorted octahedral geometry.

By contrast, in **4.13d** it is evident that one of BF_4^- couterions has been hydrolysed to give a coordinated monoanionic $HOBF_3$ ligand, while the intact BF_4^- is involved in two types of hydrogen bonding interactions: one involving an NH proton [N(3)-H(3A)···F(1) 2.33Å] and the other an OH proton [O(1)-H(1)···F(6) 1.88 Å]. A similar observation was noted in the Zn(II) and Co(II) products **2.8** and **3.10**. As with its zinc and cobalt comparators a distorted square pyramidal geometry is a feature of the structure.

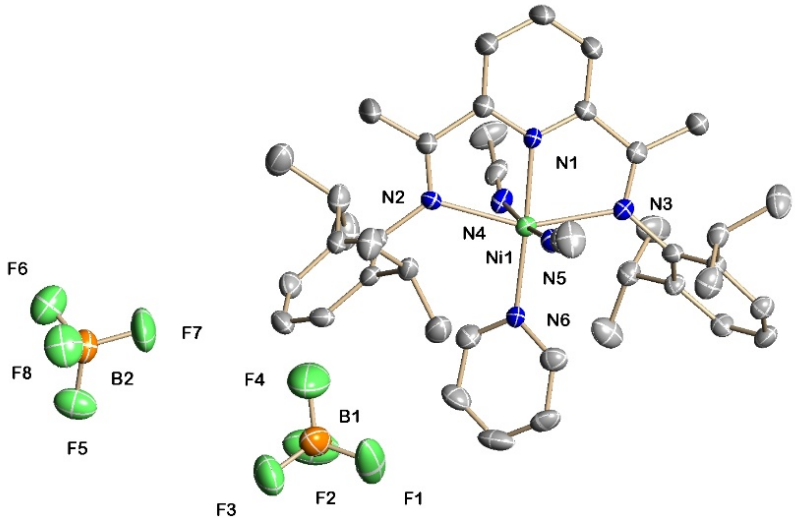

Figure 4.3.10: Molecular structure of **4.12.**

Table 4.3.7: Selected bond lengths and angles in **4.12**.

Bond Lengths (Å)	
Ni(1)-N(1)	1.966(3)
Ni(1)-N(2)	2.223(3)
Ni(1)-N(3)	2.202(3)
Ni(1)-N(4)	2.114(4)
Ni(1)-N(6)	2.029(3)
Bond Angles (°)	
N(1)-Ni(1)-N(2)	77.08(13)
N(1)-Ni(1)-N(3)	78.06(13)
N(1)-Ni(1)-N(5)	88.75(14)
N(2)-Ni(1)-N(6)	100.98(13)

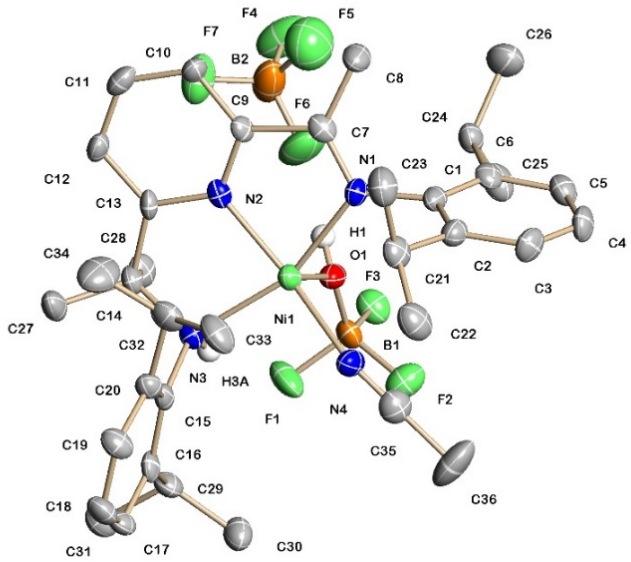

Figure 4.3.11: Molecular structure of **4.13d**.

Table 4.3.8: Selected bond lengths and angles for **4.13d**.

Bond Lengths (Å)	
Ni(1)-N(1)	2.098(4)
Ni(1)-N(2)	1.969(4)
Ni(1)-N(3)	2.133(4)
Ni(1)-N(4)	1.986(5)
Ni(1)-O(1)	1.992(4)
B(1)-O(1)	1.439(7)
B(1)-F(1)	1.407(7)
N(3)-H(3A)···F(1)	2.33
O(1)-H(1)···F(6)	1.88
Bond Angles (°)	
N(1)-Ni(1)-N(2)	79.22(18)
N(2)-Ni(1)-N(3)	80.70(17)
N(1)-Ni(1)-N(4)	98.44(18)
N(2)-Ni(1)-O(1)	102.87(15)
F(1)-B(1)-O(1)	112.3(5)
F(1)-B(1)-F(2)	106.3(5)

A view of **4.14d** is shown in **Fig 4.3.12**; selected bond distances and angles are collected in **Table 4.3.9**. Complex **4.14d** adopts a square planar geometry around nickel centre with two five-membered chelate rings forming internal N-Ni-N angles of 83.4(3)°

and 84.5(3)°. Of the three Ni-N distances involving the *N,N,N*-ligand, the Ni-$N_{pyridine}$ bond length is shortest [1.822(5) Å], followed by Ni-N_{imino} [1.887(6) Å] and then the Ni-N_{amino} [1.917(6) Å]. In general, the Ni-N bond lengths in **4.14d** [range: 1.822-1.917 Å] are similar to those seen in the square planar *N,N,O*-Ni(II) tetrafluoroborate complexes **4.5-4.8** [range: 1.861-1.916 Å]. In addition, the [N(1)-Ni(1)-N(2) 83.4(3)° and N(2)-Ni(1)-N(3) 84.5(3)° angles within the two five-membered chelate rings are similar to those in **4.5-4.8** [range:84.28-84.30 Å].

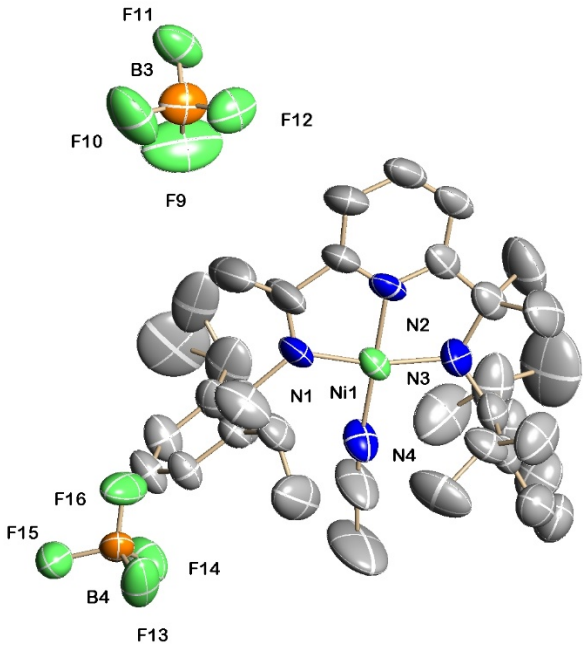

Figure 4.3.12: Molecular structure of **4.14d**.

Table 4.3.9: Selected bond lengths and angles for **4.14d**.

Bond Lengths (Å)	
Ni(1)-N(1)	1.887(6)
Ni(1)-N(2)	1.822(5)
Ni(1)-N(3)	1.917(6)
Ni(1)-N(4)	1.852(7)
B(1)-F(1)	1.440(12)
N(3)-H(3A)···F(1)	2.33
O(1)-H(1)···F(6)	1.88
Bond Angles (°)	
N(1)-Ni(1)-N(2)	83.4(3)
N(2)-Ni(1)-N(3)	84.5(3)
N(1)-Ni(1)-N(4)	97.0(3)

4.3.2.3 Attempted synthesis of Ni(II) fluoride complexes.

As in the previous two chapters, the use of fluorinating reagents was investigated as a potential means to allow the exchange of chloride for a fluoride ligand. In chapters 2 and 3, CsF proved an unsuitable fluorinating reagent. In this section we explore the use of silver fluoride. Indeed work by Martínea-Prieto and co-workers showed that the group 10 pincer halide complexes [(^{ipr}PCP)M-X] (M = Ni, X = Br; M = Pd, X = I) could be converted to [(^{ipr}PCP)M-F] by reaction with silver fluoride. To determine the best set of reaction conditions for this silver reagent, the reactivity of silver acetate towards **4.1b** was firstly examined under a range of different conditions. In particular, treatment of **4.1b**, on the small scale, with 1.1 equivalents of AgOAc in dry THF at room temperature in a completely photophobic environment resulted in full consumption (by ^{1}H NMR spectroscopy) of **4.1b** and the formation of **4.3b** (**Scheme 4.3.6**).

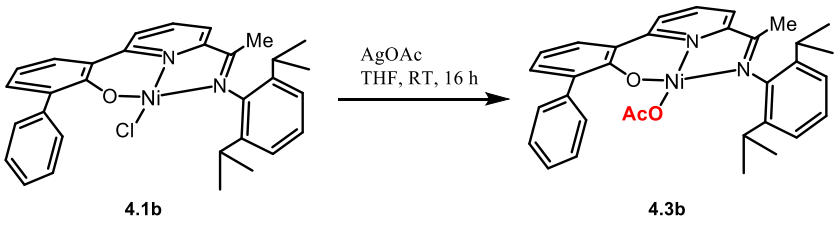

4.1b 4.3b

Scheme 4.3.6: Reaction of **4.1b** with AgOAc.

The structure of **4.3b** is depicted in **Fig 4.3.13**, while selected bond lengths and angles are compiled in **Table 4.3.10.** The structure reveals a nickel centre surrounded by an anionic *N,N,O*-ligand and a monodentate O-bound acetate to complete a distorted square planar geometry. The O(1)-Ni(1) bond length is the shortest bond length involving the pincer ligand, while all the N-Ni bonds are similar to those seen in **4.1b**, **4.7b** and **4.8b**. Similarly, then the O(1)-Ni(1)-N(1) 95.08(10)° and N(1)-Ni(1)-N(2) 85.09(10)° angles within each six- and five-membered chelate rings highlight the distortion within the square plane.

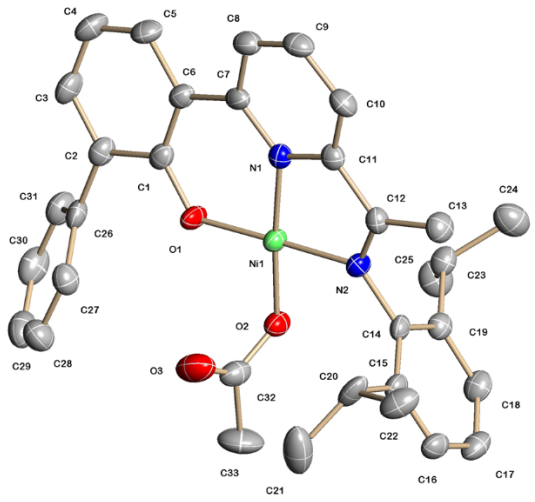

Figure 4.3.13: Molecular structure of **4.3b**.

Table 4.3.10: Selected bond lengths and bond angles for **4.3b.**

Bond Lengths (Å)	
Ni(1)-O(1)	1.820(19)
Ni(1)-O(2)	1.858(19)
Ni(1)-N(1)	1.864(2)
Ni(1)-N(2)	1.896(2)
Bond Angles (°)	
O(1)-Ni(1)-O(2)	88.38(9)
O(1)-Ni(1)-N(1)	95.08(10)
O(2)-Ni(1)-N(1)	175.72(10)
O(1)-Ni(1)-N(2)	178.49(10)
O(2)-Ni(1)-N(2)	91.53(9)
N(1)-Ni(1)-N(2)	85.09(10)

Therefore, on the basis of the conditions established using silver acetate, chloride exchange was explored using silver fluoride (**Scheme 4.3.7**). Periodic monitoring of the ^{1}H NMR spectrum showed some signals that did not belong to either proligand H**L1**$_{\mathbf{Ph}}$ nor **4.1b**. Furthermore, the ^{19}F NMR spectrum revealed a fluorine signal at δ -138 (*c.f.* AgF is -164 ppm) which suggested some type of fluorination reaction. Unfortunately, crystallisation of the product was not conducive to the formation of suitable single crystals for X-ray diffraction.

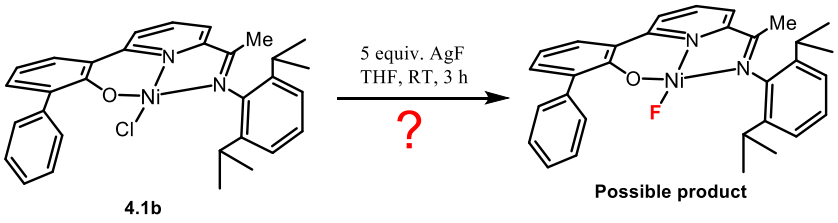

Scheme 4.3.7: Attempted synthesis of Ni(II) fluoride complex.

4.3.3 Conclusions to Chapter 4

The first objective of this chapter was to synthesise and characterise a series of novel nickel(II) chloride complexes from the reaction of the corresponding *N,N,O(H)* and *N,N,N* (pro)ligands with $NiCl_2$(DME) (**Fig. 4.3.14**). Using H**L1**$_{H}$ and H**L1**$_{Ph}$, the Ni(II) complexes **4.1a**, **4.2c**, **7** and **4.4** was formed and shown to adopt distorted square pyramidal geometries while **4.1b** exhibited a square planar arrangement. Conversely, the use of H**L1**$_{tBu}$ resulted in a binuclear chloride complex **4.2c** in which the two nickel centres were linked by two μ-$O_{phenoxy}$ bridges. In comparison with work detailed in previous chapters, (pro)ligand H**L1**$_{tBu}$ displayed a preference to form dimeric chloride complexes in Zn(II) **2.2c**, Co(II) **3.2c** and Ni(II) **4.2c**.

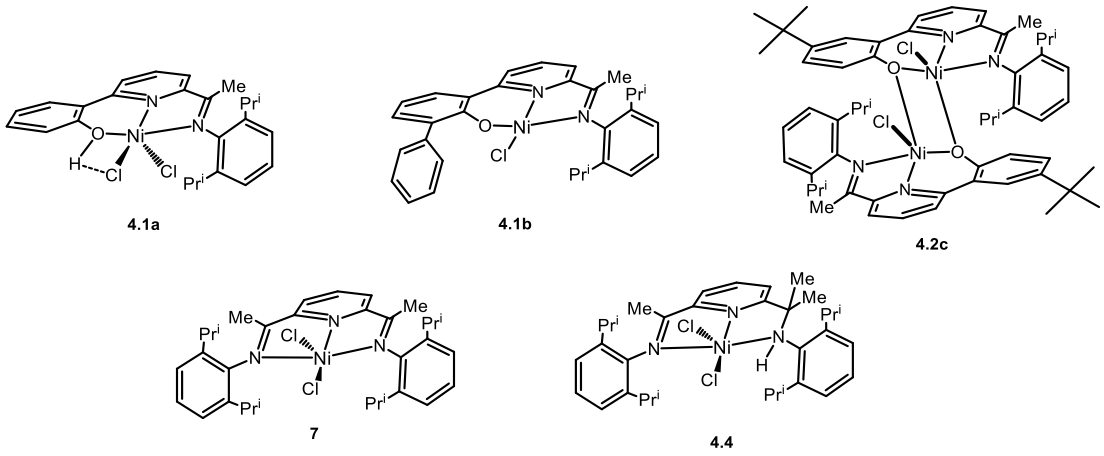

Figure 4.3.14: Ni(II) chloride complexes prepared in Chapter 4.

Secondly, a range of Ni(II) cationic complexes containing one or two tetrafluoroborate counterions were formed in good yields (**4.5a - 4.10c**) (**Fig. 4.3.15**). In addition, the *O,N,O*-ligand, Ketone-Ph, was also reacted with $[Ni(Py)_4(NCMe)_2][BF_4]_2$, affording the dimeric complex **4.11**. The X-ray structures of **4.5a**, **4.6a**, **4.7b** and **4.8b** showed the Ni(II) centres to adopt square planar geometries which was confirmed by their

diamagnetic ^{1}H NMR spectra (in CD_2Cl_2). However, it worth noting that **4.5** - **4.8** gave paramagnetic shifts in CD_3CN, which can be attributed by CD_3CN ligating to the nickel centre in solution. In dimeric **4.10c**, the capacity of BF_4^- to act as a bridging ligand was shown. On the other hand in **4.13d** the ability of BF_4^- to undergo hydrolysis was apparent on reaction of imine-amine ligand H**L4** with $[Ni(Py)_4(NCMe)_2][BF_4]_2$. By contrast, by performing the reaction in the complete absence of pyridine, non-hydrolysed **4.14d** was formed. Therefore, it would be appear moisture present within pyridine employed is the possible reason for forming the hydrolysed product.

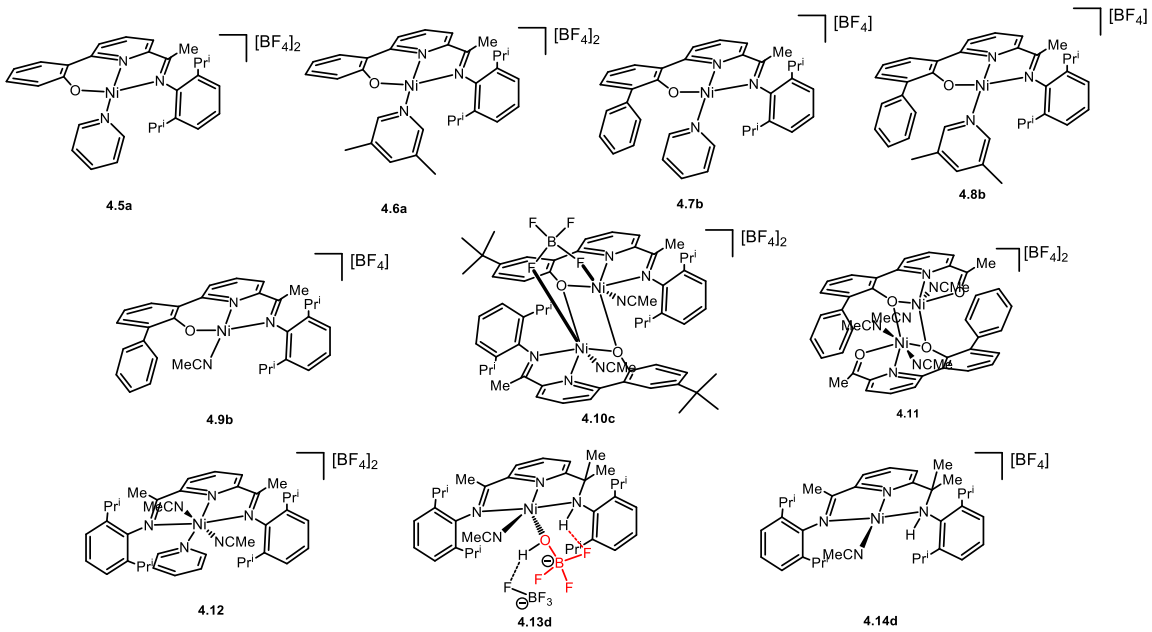

Figure 4.3.15: Nickel(II) tetrafluoroborate complexes prepared in **Chapter 4**.

Chloride exchange reactions in **4.1b** using the silver salts, silver acetate and silver fluoride, were also attempted. In the case of silver acetate, the reaction proceeded smoothly forming **4.3b** in good yield (**Fig. 4.3.16**). However, reaction of **4.1b** with AgF under the same reaction conditions was less clear.

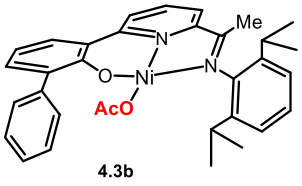

Figure 4.3.16: Nickel-acetate complex **4.3b**.

References

1. C. J. Moutlon and B. L. Shaw, *Dalton Trans.,* 1976, **11**, 1020-1024.
2. D. M. Grove, G. van Koten, H. J. C. Ubbels and R. Zoet, *Organometallics,* 1984, **3**, 1003-1009.
3. V. Pandarus and D. Zargarian, *Chem. Commun.,* 2007, **9**, 978-980.
4. P. M. P. Garcia, T. Di Franco, A. Orsino, P. Ren and X. L. Hu, *Org. Lett*., 2012, **14**, 4286-4289.
5. S. Chakraborty, J. Zhang, J. A. Krause and H. Guan, *J. Am. Chem. Soc.,* 2010, **132**, 8872-8873.
6. K. V. Vasudevan, B. L. Scott and S. K. Hanson, *Eur. J. Inorg. Chem.,* 2012, 4898-4906.
7. G. J. P. Britovsek, V. C. Gibson and D. F. Wass, *Angew. Chem, Int. Ed*., 1999, **28**, 428-447.
8. S. D. Ittel, L. K. Johnson and M. Brookhart, *Chem. Rev.,* 2000, **203**, 325-351.
9. S. Mecking, *Coord. Chem. Rev*., 2000, **203**, 325-351.
10. S. Mecking, *Angew. Chem. Int. Ed.,* 2001, **30**, 534-540.
11. C. W. Coates, P. D. Hustad and S. Reinartz, *Angew. Chem. Int. Ed*. 2002, **41**, 2236-2257.
12. V. C. Gibson and S. K. Spitzmesser, *Chem. Rev*. 2003, **103**, 283-315.
13. J. Zhang, X. Wang and G.-X. Jin, *Coord. Chem. Rev.,* 2006, **250**, 95-109.
14. G. J. Domakia, J. M. Rosea, G. W. Coates, A. D. Bolig and M. Brookhart, *Prog. Polym. Sci.,* 2007, **32**, 30-92.
15. T. M. J. Anselment, S.–I. Vagin and B. Rieger, *Dalton Trans*., 2008, 4537-4548.
16. F. M. Bauers and S. Mecking, *Macromolecules.,* 2001, **34**, 1165-1171.
17. A. Bastero, G. Franci, W. Leitner and S. Mecking, *Chem. Eur. J.,* 2006, **12**, 6110-6116.
18. I. Göttker-Schnetmann, P. Wehrann, C. Röhr and S. Mecking, *Organometallics.,* 2007, **26**, 2348-2362.
19. P. Wehrmann and S. Mecking, *Organometallics*, 2008, **27**, 13899-1408.
20. A. Nakamura, S. Ito and K. Nozaki, *Dalton Trans.,* 2012, **41**, 13807-13809.
21. D. Guironnet, T. Friedberger and S. Mecking, *Dalton Trans*., 2009, 8929-2934.
22. S. Ito, Y. Ota and K. Nazaki, *Dalton Trans.,* 2012, **41**, 13807-13809.

23. T. Friedberger, P. Wucher and S. Mecking., *J. Am. Chem. Soc.,* 2012, **124**, 1010-1018.
24. L. K. Johnson, C, M, Killian and M. Brookhart, *J. Am. Chem. Soc.,* 1995, **117**, 6414-6415.
25. a) M. S. Kharasch, H. Engelmann and F. R. Mayo, *J. Org. Chem.,* 1938, **2**, 288-302. b) M. S. Kharasch, E. V. Jensen and W. H. Urry, *J. Am. Soc.* 1945, **67**, 1626-1626. c) M. S. Kharasch, E. V. Elwood and W. H. Urry, *J. Am. Chem. Soc,* 1947, **69**, 1100-1105. d) M. S. Kharasch and H. N. Friedlander, *J. Org. Chem.,* 1949, **14**, 239-247. e) M. S. Kharasch and M. Sage*, J. Org. Chem.,* 1949, **1**, 79-83. f) M. S. Kharasch, E. Simon and W. Nudenberg, *Ibid.,* 1953, **18**, 328-336.
26. L. A. van de Kuil, D, M, Grove, R. A. Gossage, J. W. Zwikker, L. W. Jenneskens, W. Drenth and G. van Koten, *Organometallics*, 1997, **16,** 4985-4994.
27. V. Pandarus and D. Zargarian, *Chem. Commun*., 2007, **9**, 978-980.
28. P. M. Perez Garci, T. D. Franco, A. Orsino, O. Ren and X. L. Hu, *Org. Lett.,* 2012, **14**, 4286-4289.
29. a) T. Sakakura, J.-C. Choi and H. Yasuda, *Chem. Rev*. 2007, **107**, 2365-2387; b) S. N. Riduan and Y. Zhang, *Dalton Trans.,* 2010, **39**, 3347-3357; c) M. Aresta, Carbon dioxide as chemical feedstock, Wiley-VCH, Weinheim, 2010, p. 394; p.xix; d) M. Aresta, A. Dibenedetto and A. Angelini, *Chem. Rev*., 2014, **114**, 1709-1742; e) C. Maeda, Y. Miyazaki and T. Ema, *Catal. Sci. Technol*., 2014, **4**, 1482-1497; f) Q. Liu, L. Wu, R. Jackstell and M. Beller, *Nat. Commun*., 2015, **6**,1-15.
30. H. -F. Li, T. P. Gonçalves, Q.-Y. Zhao, D. Gong, Z. P. Lai, Z. X. Wang, J. R. Zheng and K.-W. Huang, *Chem. Commun.,* 2018, **54**, 11395-11398.
31. a) I. M. Angulo, E. Bouwman, R. van Gorkum, S. M. Lok, M. Lutz and A. L. Spek, *J. Mol. Catal. A*. 2003, **202**, 97-106. b) C. Gonzalez-Arellano, E. Gutierrea-Puebla, M. Iglesias and F. Sanchez, *Eur. J. Inorg. Chem*., 2004, 1955-1962. c) A. Flores-Gaspar, P. Pinedo-Gonzalez, M. G. Crestani, M. Munoz-Hernandez, D. Morales-Morales, B. A. Warsop, W. D. Jones and J. J. Garcia, *J. Mol. Catal. A*. 2009, 309, 1-11.
32. K. V. Vasudevan, B. L. Scott and S. K. Hanson, *Eur. J. Inorg. Chem.,* 2012, 4898-4906.

33. L. Wang, W. H. Sun, L. Han, H. Yang, Y. Hu and X. Jin, *J. Organomet, Chem,* 2002, **658**, 62-70.
34. W. H. Sun, S. Zhang, S. Jie, W. Zhang, Y. Li, H. Ma, J. Chen, K. Wedeking and R. Fröhlich, *J. Organoment. Chem*., 2006, **691**, 4196-4203.
35. S. Jie, S. Zhang and W. H. Sun, *Eur. J. Inorg. Chem.,* 2007, 5584-5598.
36. P. Hao, S. Zhang, W. H. Sun, Q. Shi, S. Adewuyi, X. Lu and P. Li., *Organometallics,* 2007, **26**, 2439-2446.
37. X. Tang, W. H. Sun, T. Gao, J. Hou, J. Chen and W. Chen, *J. Organomet. Chem*., 2005, **690**, 1570-1580.
38. W. Zhang, W. H. Sun, S. Zhang, J. Hou, K. Wdeking, S. Schultz, R. FröHlich and H. Song, *Organometallics*, 2006, **25**, 1961-1969.
39. D. S. McGuinness, P. Wasserscheid, D. H. Morgan and J. T. Dixon, *Organometallics*, 2005, **24**, 522-556.
40. M. D. Leatherman, S. A. Svejda, L. K. Johnson and M. Brookhart, *J. Am. Chem. Soc.* 2003, **125**, 3068-3081.
41. H. S. Schrekker, V. Kotov, P. Preoshuber-Pflugl, P. White and M. Brookhart, *Macromolecules,* 2006, **39**, 6341-6354.
42. H. Liu, L. Zhang, L. Chen, C. Redshaw, Y. Li and W. H. Sun, *Dalton Trans*, 2011, **40**, 2614-2621.
43. S. C. Lee and R. H. Holm, *Inorg. Chem.,* 1993, **32**, 4745-4753.
44. R. K. Das, T. Ghatak, R. C. Samanta and J. K. Bera, *India J. Chem.*, 2011, **50A**, 1350-1355.
45. S. W. Kohl, F. W. Heinemann, M. Hummert, H. Weiβhoff and A. Grohmann, *Eur. J. Inorg. Chem.*, 2006, 3901-3910.
46. F. E. Hahn, H. Schröder and T. Pape, *Eur. J. Inorg. Chem.,* 2009, 4373-4377.
47. a) T. G. Richmond, Metal Reagents for Activation and Functionalization of Carbon-Fluorine Bonds, in Activation of Unreactive bonds in Organic Synthesis; edited by S Murai, (Springer, Berlin), 1999, p. 243; b) J. L. Kiplinger, T. G. Richmond and C. E. Osterberg, *Chem Rev.,* 1994, **94**, 373-431; c)J. Vela, J. M. Smith, Y. Yu, N. A. Keterer, C. J. Flaschenriem, R. J. Lachicotte and P. L. Holland, *J. Am. Chem. Soc.,* 2005, **127**, 7857-7870; d) D. Viets, E. Lork, P. G. Watson and R. Mews, *Angew. Chem. Int. Ed. EngI*., 1997, **36**, 623-624; e) G. B. Nikiforov, H. W. Roesky, P. G. Jones, J. Magull, A. Ringe and R. B. Oswald, *Inorg. Chem.* 2008, **47**, 2171-2179.

48. D. L. Reger, R. P. Watson, J. R. Gardinier, M. D. Smith and P. J. Pellechia, *Inorg. Chem*., 2006, **45**, 10088-10097.
49. R. K. Das, T. Ghatak, R. C. Samanta and J. K. Bera, *India J. of Chem*., 2011, **50A**, 1350-1355.
50. W. J. Xiang, Q. Luo, H, Jiang, X. G. Meng, R. J. Li, J. Zhang and T. Y. Peng, *J. Coord. Chem*., 2016, **69**, 2353-2363.
51. a) J. Reedijk, *Comments Inorg. Chem*., 1982, **1**, 379-389. b)F. S. Keij, R. A. G. Degraaffm J. G. Haasnoot, A. J. Oosterling, E. Pendersen and J. Reedijk, *J. Chem. Soc*., *Chem. Commun*., 1988, **6**, 423-425. c) M. Ghiladi, C. J. McKenzie, A. Meier, A. K. Powell, J. Ulstrup and S. Wocadlo, *Dalton Trans*., 1997, **21**, 4011- 4018.
52. a) K. K. Nanda, K. Kenkatsubramanian, D. Majundar and K. Nag, *Inorg. Chem.,* 1994, **33**, 1581-1582. b) H. Amdams, S. Clunas and D. E. Fenton, *Inorg. Chem. Commun*., 2001, **4**, 667-670. c) K. K. Nada, R. Das, L. K. Thompson, K. Venkatsubramanian, P. Paul and K. Nag, *Inorg. Chem.,* 1994, **33**, 1188-1193.
53. A. A. Antonov, N. V. Semikolenova, V. A. Zakharov, W. J. Zhang, Y. H. Wang, W. H. Sun, E. P. Talsi and K. P. Bryliakov, *Organimetallics*, 2012, **31**, 1143-1149.
54. L. Rodríguez, E. Labisbal, A. Sousa-Pedrares, J. A. García-Vázquez, J. Romero, M. L. Durán, J. A. Real and A. Sousa, *Inorg. Chem.,* 2006, **45**, 7903-7914.
55. a) D. Kong, X. Ouyang, J. Relbenspies, A. Clearfield and A. E. Martell, *Inorg. Chem. Commun*., 2002, **5**, 873-878. b) E. V. Rybak-Akimova, N. W. Alcock and D. H. Busch, *Inorg. Chem*. 1998, **37**, 1563-1574. c) H. Lou, J. M. Lo, P. E. Fanwich, J. G. Stowell and M. A. Green, *Inorg. Chem.,* 1999, **38**, 2071-2078. d) S. Mohanta, K. K. Namda, R. Werner, W. Haase, A. K. Mukherjee, S. H. Dutta and K. K. Nag, *Inorg. Chem.,* 1999, **38**, 2071-2078. e) R. Mattes and T. Z. Enrian, *Anorg. Allg. Chem*., 2003, **629**, 2298-2304.
56. R.-Q. Fan, D.-S. Zhu, Y. Mu, G.-H. Li, Q. Su, J.-G. Ni, S.-H, Feng, *Chem. Res. Chin. Univ.,* 2005, **21**, 496-500.
57. a) D. F. Evans, *J. Chem. Soc.* 1959, 2003-2005. b) D. F. Evanse, G. V. Fazakerley, P. R. F. Phillips. *J. Chem, Soc.,* A, 1971, 1931-1934.

Chapter 5

N,N,O- and *N,N,N*-iron(II) pincer complexes; applications as precatalysts in ethylene polymerisation

5.1 Introduction

In last three chapters, the capacity of a range of $N,N_{py},O(H)$ and N,N_{py},N compounds to act as pincer ligands have been explored for Zn(II), Co(II) and Ni(II) chloride and tetrafluoroborate complexes. This chapter extend this study to d^6 iron(II) with a view to probing the coordination chemistry of this first row d-block metal ion. In addition, the ability of two examples of *N,N,N*-iron(II) tetrafluoroborate complex to act as precatalysts is also investigated for ethylene polymerisation and compare their performance with the well-studied (**L2**)$FeCl_2$ precatalyst.[24,25] To set the scene for the experimental work, the use of iron pincer complexes in homogeneous catalysis is first surveyed and then review applications of iron(II) tetrafluoroborate complexes.

5.1.1 Iron(II) complexes and their applications

Iron complexes have a well-established track record as catalysts for organic reactions.[1] In terms of historical development 1891 saw the birth of organo-iron chemistry with Mond and Berthelot's discovery of pentacarbonyl-iron.[2] In 1951, the report of ferrocene and iron-catalysed Reppe synthesis represent further milestones.[3,4] In 1971, the iron-catalysed cross-coupling of Grignard reagents with organic halides was published by Kochi and coworkers.[5] With respect to oxidation state, the most common for iron is +2 and +3. In air, most iron(II) compounds are readily oxidised to their corresponding iron(III) analogues, which represents the most stable iron species.[6] Nevertheless, iron(II) chemistry has rapidly developed in recent years and in particular with regard to iron(II) pincer complexes.

Many literature reports have shown that iron(II) complexes can serve as effective catalysts in a broad range of reactions, such as oxidation of alkanes [7], alkene

hydroboration [8], hydrogenation of esters [9], C-N bond formation [10], ring opening polymerisation and olefin polymerisation.[11,24,25] In recent years, many non-heme iron-based catalysts for the oxidation of alkanes with H_2O_2 have been reported.[12] Britovsek and co-workers investigated a series of Fe(II) pincer complexes (**Scheme 5.1.1**: complexes **1** and **2**) containing tridentate bis(imino)pyridine and bis(amino)pyridine ligands and weakly coordinating triflate (OTf^-) or non-coordinating SbF_6^- anions. These Fe(II) complexes showed good catalytic activity in the catalytic oxidation of alkanes, which was attributed to Fenton-type free radical auto-oxidation.[7]

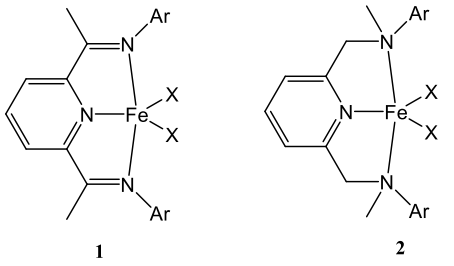

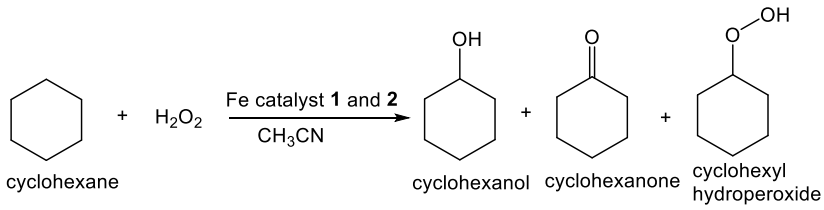

Scheme 5.1.1: Iron pincer complexes **1** and **2** and their use in the catalytic oxidation of cyclohexane.[7]

Alkylboronic acid derivatives are now widely used as intermediates in organic synthesis, as they can be readily isolated, purified and stored in air.[14] Wilkinson's catalyst [$RhCl(PPh_3)_3$] has been extensively used for the hydroboration of a wide range of alkenes (*e.g.*, allylamine[15a], allylimines[15a], functionalised olefins[15b,c] etc)[15] However, side reactions such as dehydrogenative borylation and alkene hydrogenation always occur resulting in low regioselectivity and extreme sensitivity to impurities.[16] Therefore, earth-abundant and inexpensive iron complexes have received more attention in this area. Zhang *et al.* reported the first example of an electron-rich pincer iron complex that can catalyse alkene hydroboration using pinacolborane.[8] After comparing with known bidentate iron complexes, the results showed that the tridentate ligand is necessary for iron-catalysed alkene hydroboration (**Scheme 5.1.2:** complexes **3**, **4** and **5**).[8] The highest activity and yield was achieved by **5** containing Milstein's

P,N,N ligand that bears *tert*-butyl-substituted phosphino groups (**Scheme 5.1.2**). The system was so active that the reaction afforded 99% of product in 10 minutes even with 0.25 mol% loading of **5.** In addition, this paper also reported that this iron catalyst system displayed remarkably good yield and activity for alkene hydroboration with a variety of different alkenes.[8]

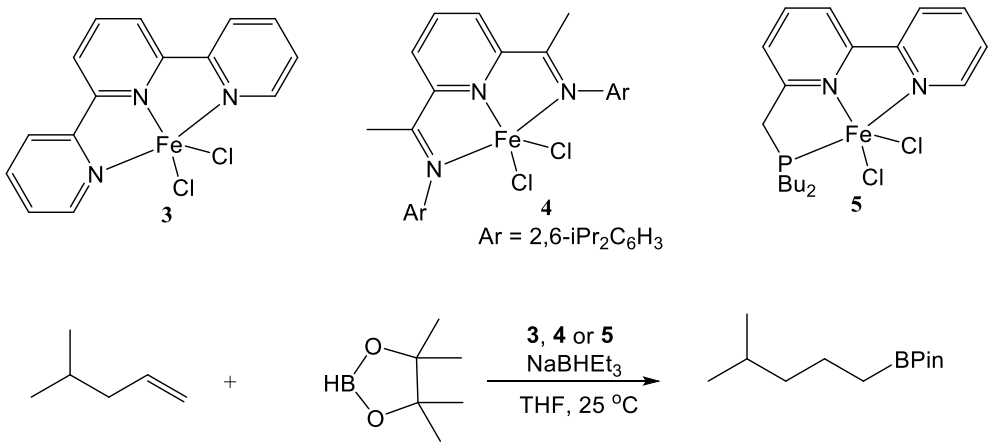

Scheme 5.1.2: Tridentate pincer iron precatalysts **3**, **4** and **5** and their use in the hydroboration of 4-methyl-1-pentene.[8]

Hydrogenation of esters is an important reaction in the Chemical Industry for the production of alcohols, especially fatty alcohols that find broad applications in consumer products.[17,18] More recently, iron catalysts have attracted attention due to their low cost and low impact on environment.[19] In 2014, Chakraborty *et al.* reported a series of *P,N,P*-iron pincer complexes (**Scheme 5.1.3:** complexes **6**, **7** and **8**) as efficient catalysts for the hydrogenation of many types of esters (**Scheme 5.1.3**: **A**).[9] Under optimal conditions, **7** gave the best activity and yield without any added base and led to the highest selectivity for alcohol formation. As a result, **7** was explored for the hydrogenation of the commercially used ester, CE-1027, which is derived from coconut oils and consists of methyl laurate (C12, 73%), methyl myristate (C14, 26%) and a small amount of C10 and C16 methyl esters (1%) (**Scheme 5.1.3**: **B**).[9] CE-1270 was fully converted in 3 hours by using 1 mol% of iron catalyst **7**, generating a mixture of fatty alcohols in combined GC yield of 99%.[9]

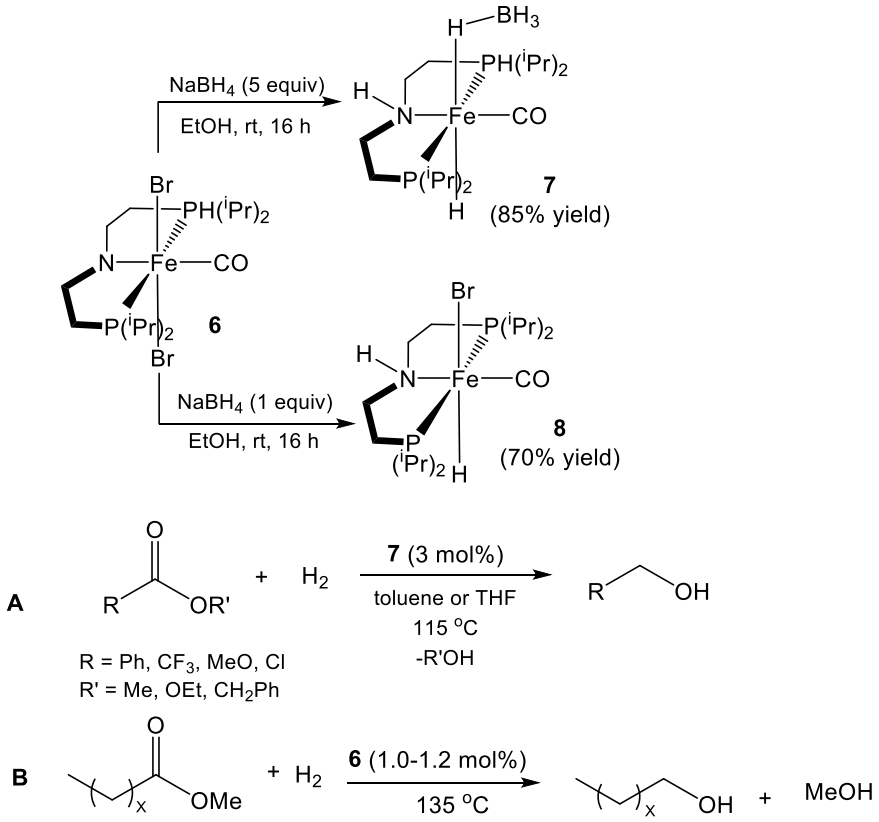

Scheme 5.1.3: *P,N,P*-iron pincer complexes **6, 7** and **8**; **A**) hydrogenation of esters catalysed by **7**; **B**) catalytic hydrogenation of CE-1270 using **6**.[9]

Another important challenge in organic synthesis is the construction of C-N bonds on account of the widespread presence of nitrogen-containing compounds in a broad range of synthetic and natural organic molecules.[20] To avoid the use of precious metal such as iridium, rhodium and palladium, cheap and more easily accessible catalysts based on iron has seen some developments. Sinha and co-workers published a series of iron pincer complexes based on redox non-innocent 2-(arylazo)-1,10-phenanthroline ligands (**5.11** - **5.14**).[10] These iron catalysts were used for the C-N bond forming reactions between 1H-pyrazole and iodobenzene; the best performance was achieved by **5.11** in DMSO at 120 °C using 10 mol% of **5.11** in the presence of 2.0 equivalents of KO^{t}Bu.[10]

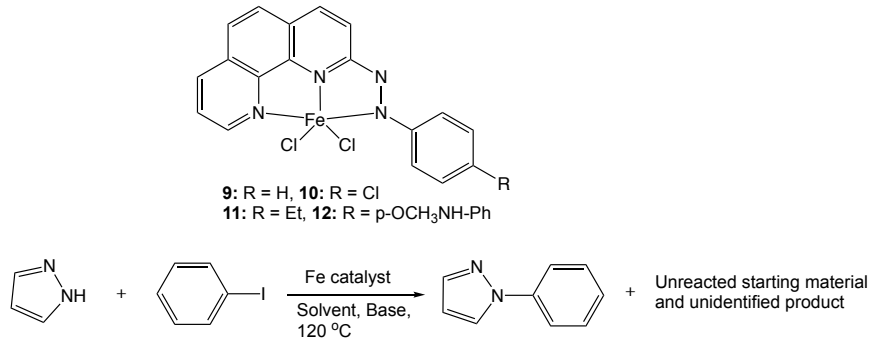

Scheme 5.1.4: C-N bond forming reactions using iron catalysts **9** - **12**.[10]

Iron-based complexes are also appealing in ring-opening polymerisation (ROP) reactions.[21] So far iron catalysts have tended to only display low activities and yielded broad molecular weight distributions.[22] Nevertheless, iron-based complexes remain attractive as they provide unique opportunities for tuning the iron spin state, overall charge and oxidation state. Cramer and co-workers reported a series of iron-alkoxide catalysts (**5.15** - **5.18**) bearing the bis(imino)pyridine framework for the ROP of ε-caprolactone.[11] Furthermore, this group also studied the electronic structure of these iron catalysts and their reaction mechanism (**Scheme 5.1.5: B**). These computation results offered significant mechanistic insights that were helpful for understanding the ROP process and improving the design of more efficient, selective and switchable catalysis.[11] Notably, the Fe(I) complex **5.15** proved the most active catalyst for the polymerisation of lactones, with 99% conversion at room temperature in 10 minutes with a 0.05 mol% catalyst loading.

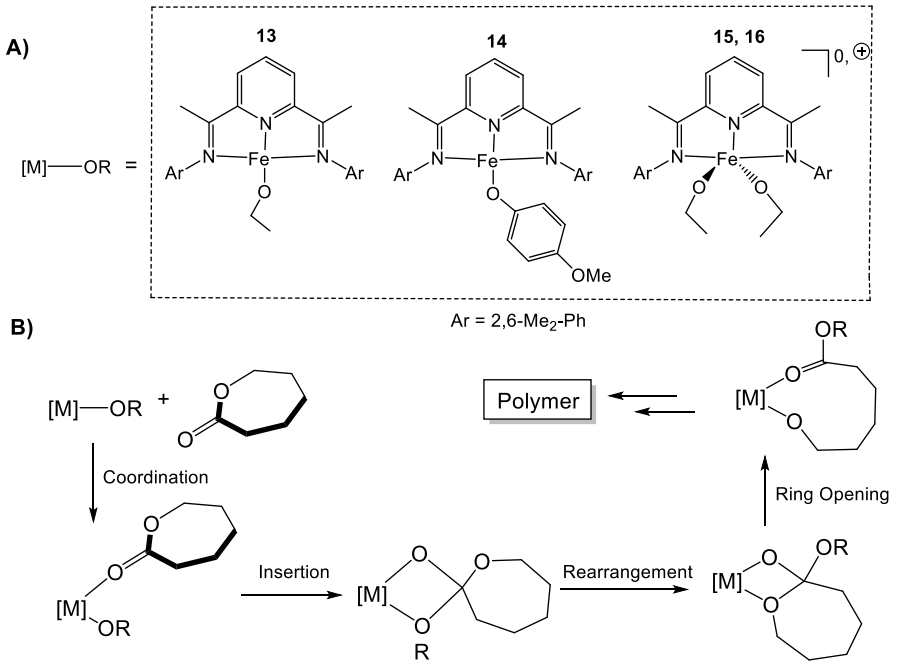

Scheme 5.1.5: A) Iron-pincer catalysts **13 - 16**; **B**) general coordination-insertion mechanism for the ROP of ε-caprolactone.[11]

Over the last 22 years, iron-based polymerisation catalysts have developed rapidly because of the low environmental impact of iron, cost effectiveness and tolerance to heteroatom functionalities[23] The main milestones have been the development of well characterised bulky bis(arylimino)pyridine iron(II) precatalysts for the polymerisation/oligomerisation of olefins (mainly ethylene).[24] In 1998, the Brookhart[25a] and Gibson[25b] groups independently disclosed that 2,6-bis(arylimino)pyridine-iron(II) pincer complexes on activation with methylaluminoxane (MAO) gave effective catalysts (up to 206.0 × 10^6 g PE mol^{-1} (Fe) h^{-1}) for the conversion of ethylene into either high density polyethylene (HDPE) or into α-olefins with Schulz-Flory distributions (**Scheme 5.1.6:** complex **17**).[25] More recently, Sun and his group have found that the fusion of cycloalkyl units to the central pyridine can be influential on the chelation properties of the ligand and as a result impact on the activity of the catalyst and the properties of the resulting polymeric material.[26] Elsewhere, Gibson, Redshaw and Solan studied the activity of *N,N,O*-iron(II) chloride precatalysts bearing 2-imine-6-(methylalcohol)pyridines in ethylene polymerisation (**Scheme 5.1.6:** complex **18**).[28] The highest activity was obtained by **18b** at 276 h $mmol^{-1}$ h^{-1} bar^{-1} using 500 equivalents of MAO as activator. Nonetheless, the activities of **18a** and **18b** can be regarded as moderate and significantly lower than the aforementioned bis(arylimino)pyridine iron systems.[28]

In 2019, Zheng *et al*. published the preparation of five ferrous chloride complexes, **19a-19e** (**Scheme 5.1.6**), which differed in the steric and electronic properties of the *N*-aryl groups.[27] These iron complexes displayed exceptionally high catalytic activity at 50 ^oC with MAO and MMAO as co-catalysts forming highly linear polyethylenes (T_m ≈ 131 ^oC) with broad distributions. Notably, the least sterically hindered **19a** (R^1 = Me) and **19d** (R^1 = Me) showed higher activity than their bulkier counterparts **19b** (R^1 = Et), **19c** (R^1 = i-Pr) and **19e** (R^1 = Et). The most hindered **19c** (R^1 = i-Pr) displayed the lowest activity, but formed the highest molecular weight of polyethylene. By contrast, oxo-bridged **19'** showed the lowest activity and produced the lowest molecular weight of polyethylene (**Scheme 5.1.6**).[27]

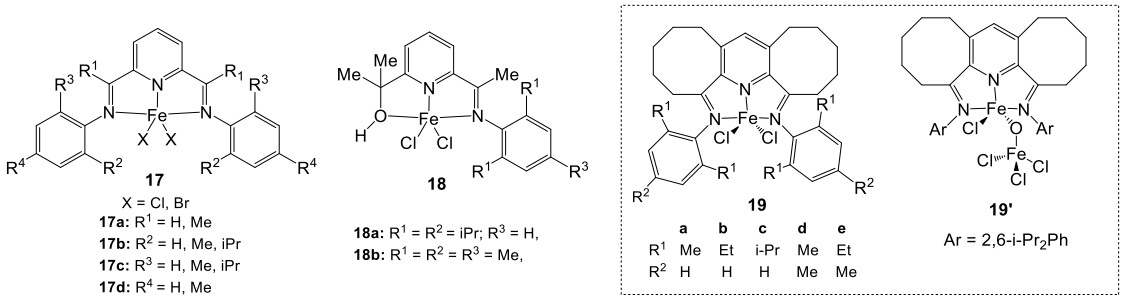

Scheme 5.1.6: *N,N,N*- and *N,N,O*-iron(II) halide precatalysts (**17** - **19**) for ethylene polymerisation.[24-28]

5.1.2 Iron(II) tetrafluoroborate complexes and their applications

In 2011, Gentschow and co-workers reported the mononuclear iron(II) tetrafluoroborate complex **20** which was readily formed from reaction of iron(II) tetrafluoroborate hexahydrate with the triphosphane $C_5H_3N\{2\text{-}[[CMe(CH_2PMe_2)_2]]\}\{CMe_2(CH_2PMe_2)\}$ and diethylphosphane (Et_2PH) (**Scheme 5.1.7**).[29] Treatment of **20** with excess CO produced two complexes **21** and **22** in an approximate ratio 40:1. In the formation of **21**, the agostic methyl group and the diethylphosphane ligand in **20** were replaced by two equivalents of CO, while in **22** P-C bond formation had occurred.[29]

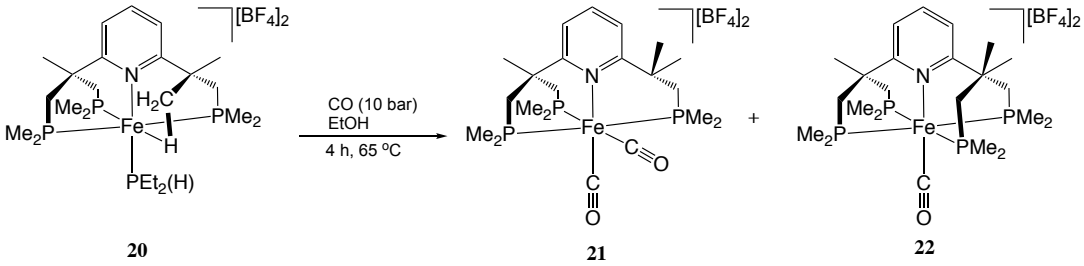

Scheme 5.1.7: Iron(II) complex **20** bearing a tetrapodal ligand and its with CO to give **21** and **22**.[29]

In 2017, Dammers *et al.* reported that the reaction of the dinucleating ligand susan$^{6\text{-Me}}$ with $Fe(BF_4)_2{\cdot}6H_2O$ gave the homovalent $Fe^{II}Fe^{II}$ complex cation $[(susan^{6\text{-Me}})\{Fe^{II}(\mu\text{-}F)_2Fe^{II}\}]^{2+}$ (**23**) along with the mixed-valence $Fe^{II}Fe^{III}$ complex cation $[(susan^{6\text{-Me}})\{Fe^{II}F(\mu\text{-}F)FFe^{III}\}]^{2+}$ (**24**), depending on the absence or presence of dioxygen, respectively (**Scheme 5.1.8**).[30] Notably, **24** was the first example of a mixed-valence complex bearing fluoride bridges that derive from fluoride abstraction from the BF_4^- counterion.

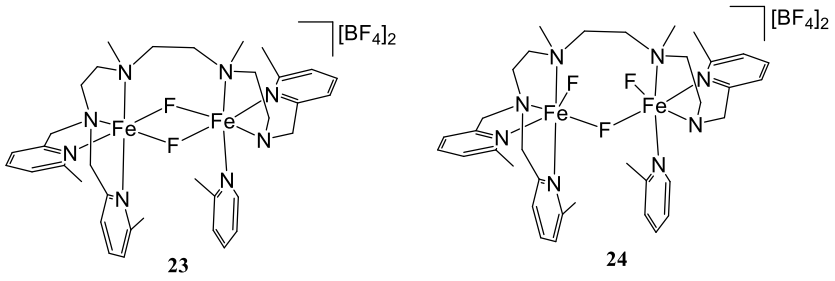

Scheme 5.1.8: Two examples of fluoride-bridged diiron complexes **23** and **24**.[30]

Iron(II) tetrafluoroborate complexes have also been used as catalysts for many types of reactions. In 2007, two iron(II) complexes of the types $[Fe(P,N,P)(CO)(CH_3CN)][BF_4]_2$ (**Scheme 5.1.9:** complexes **25** and **26**) were prepared and characterised by Benito-Garagorri and co-workers. Both iron complexes acted as efficient catalysts for the coupling of aromatic aldehydes with ethyldiazoacetate (EDA) to give 3-hydroxyacrylates (**Scheme 5.1.9: A**).[31] The most effective catalyst was found to be *cis*-$[Fe(PNP\text{-}^{i}Pr)(CO)(CH_3CN)][BF_4]_2$ (**27**). More recently, Zuo and Morris published a protocol for the synthesis of the *trans*-[amine(imine)diphosphine]chlorocarbonyl-iron(II) tetrafluoroborate complex **28**, which was used as a precatalyst for the asymmetric transfer hydrogenation of ketones and imines with good yields and enantio-enrichment (**Scheme 5.1.9: B**).[32]

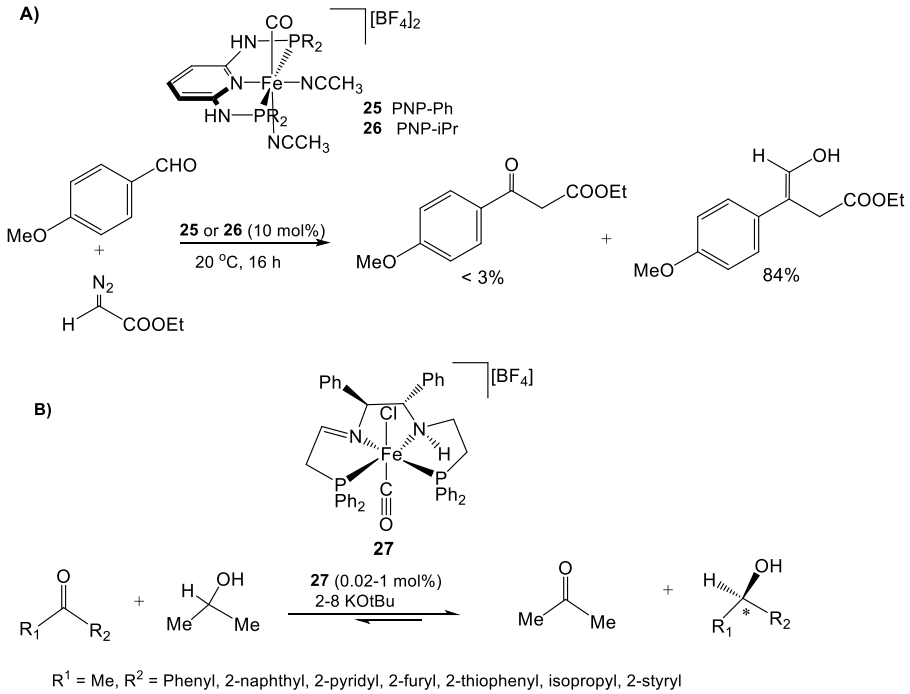

R^1 = Me, R^2 = Phenyl, 2-naphthyl, 2-pyridyl, 2-furyl, 2-thiophenyl, isopropyl, 2-styryl

Scheme 5.1.9: A) [Fe(*P,N,P*)(CO)(CH_3CN)][BF_4]$_2$ (**25**, **26**) and its use as a catalyst in the coupling reaction of aromatic aldehydes; **B**) iron(II) catalyst **27** and its use in the asymmetric transfer hydrogenation for the synthesis of enantio-enriched alcohols and amines.[31,32]

5.2 Aims and objectives of Chapter 5

In this Chapter, the main focus is on preparing and characterising iron(II) tetrafluoroborate complexes of the *N,N,N*-ligands **L2** and H**L4** (**Fig. 5.3.1**) with view to screening these as precatalysts for ethylene polymerisation. To allow a comparison to be made of their catalytic performance and the resulting polymer properties, the prototypical iron(II) chloride precatalyst, **L2**$FeCl_2$[24-28] will be also screened under the same conditions. In addition, the synthetic chemistry associated with the reactions of i) the N,N_{py},O (pro)ligand, H**L1$_{Ph}$**, with $FeCl_2Py_4$, and (ii) N,N_{py},N-containing **L2** and H**L4** with $[Fe(Py)_4(NCMe)_2][BF_4]_2$ will be discussed.

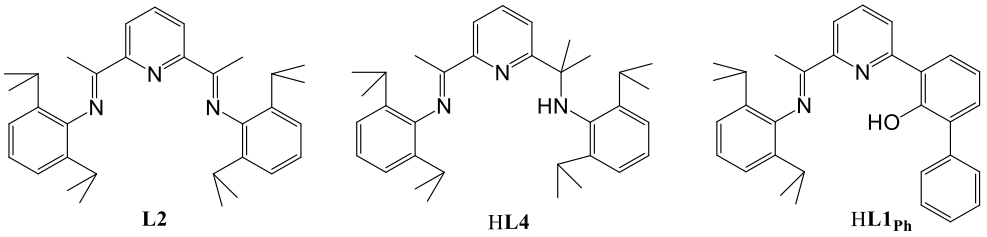

Figure 5.2.1: Types of pincer (pro)ligands to be employed in this Chapter.

5.3 Results and discussion

5.3.1 Fe(II) chloride complex synthesis

5.3.1.1 Reactivity of H**L1$_{Ph}$** towards iron(II) chloride

As a variation to that described in the last two chapters, NaH was employed as a base to deprotonate the proligand H**L1$_{Ph}$** and the resulting sodium salt, Na**L1**$_{Ph}$ then reacted with $FeCl_2Py_4$ in THF at room temperature. On work-up, the mono-iron(II) chloride complex (**L1**$_{Ph}$)Fe(Py)Cl (**5.1**) was formed as a dark blue powder in good yield (**Scheme 5.3.1**).

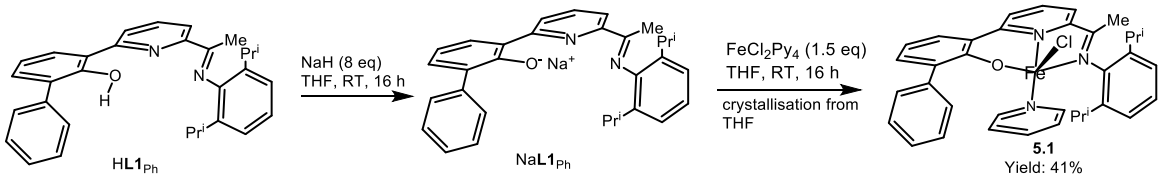

Scheme 5.3.1: Synthetic route to **5.1**.

Complex **5.1** was characterised by IR spectroscopy, elemental analysis and by magnetic measurements (Evans NMR). In the IR spectrum of **5.1**, the $C{=}N_{imine}$ absorption was observed at 1576 cm^{-1} which compared to 1640 cm^{-1} in free H**L1**$_{Ph}$. Meanwhile the μ_{eff} value of 4.8 BM was consistent four unpaired electrons and hence a high spin configuration. Furthermore, ^{1}H NMR spectrum showed broad paramagnetically shifted signals between δ -50 and δ 150. Additional confirmation of the structure of **5.1** was provided by a single crystal X-ray diffraction study.

Crystals of **5.1** suitable for the X-ray determination were grown from a concentrated THF solution. A view of **5.1** is given in **Fig. 5.3.1** while selected bond lengths and angles are collected in **Table 5.3.1**. The structure of **5.1** consisted of an iron centre bound by an monoanionic *N,N,O* tridentate ligand, an N-bound pyridine along and a chloride to complete a five-coordinate geometry. The geometry can be best described as square-based pyramidal with Cl(1) occupying the apical site; this geometry notably differs from the corresponding nickel(II) chloride complex **4.1b** which adopted a square planar geometry. Unexpectedly, the X-ray determination revealed electron density close to the carbon atom (C4); this was modelled as a chloride (Cl(2)) with shared occupancy with a hydrogen atom; it is unclear as to the origin of the chloride atom. The Fe(1)-O(1) bond distance is the shortest bond belonging to the pincer ligand [1.945(3) Å] which is shorter than in a related complex [2.173(6) Å].[28] Conversely, the $Fe\text{-}N_{pyridine}$ bond length [2.190(5) Å] is longer than the $Fe\text{-}N_{imine}$ distance [2.138(6) Å], the latter being shorter than that typically seen in related species.[25] The N(1)-Fe(1)-O(1) 83.3(2)° and N(2)-Fe(1)-N(1) 75.2(2)° angles within each six-membered and five-membered chelate rings are similar to those seen with other metal complexes presented in this thesis.

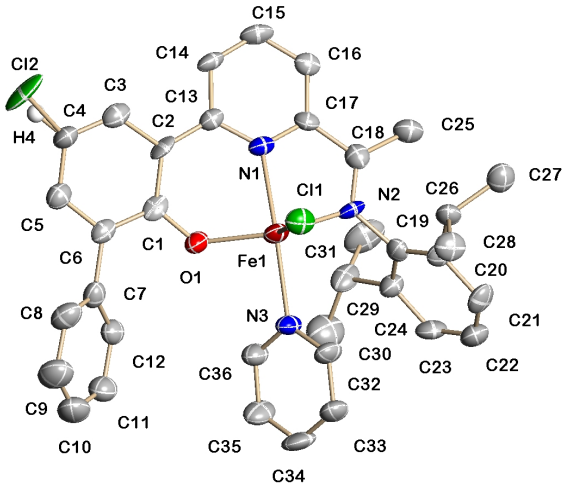

Figure 5.3.1: Molecular structure of **5.1**.

Table 5.3.1: Selected bond lengths and bond angles for **5.1.**

Bond Lengths (Å)	
Fe(1)-O(1)	1.945(3)
Fe(1)-N(1)	2.190(5)
Fe(1)-N(2)	2.138(6)
Fe(1)-N(3)	2.184(5)
Fe(1)-Cl(1)	2.297(2)
Bond Angles (°)	
N(2)-Fe(1)-N(1)	75.2(2)
N(1)-Fe(1)-O(1)	83.3(2)
N(1)-Fe(1)-Cl(1)	102.13(15)
N(1)-Fe(1)-N(3)	157.9(2)

The reactions of the other two *N,N,O* (pro)ligands, H**L1**$_{H}$ and H**L1**$_{tBu}$, with $FeCl_2Py_4$ were also attempted. However, their products did not prove conducive to crystallisation. In addition, the reactions of H**L1**$_{Ph}$ (along with H**L1**$_{H}$ and H**L1**$_{tBu}$) with $[Fe(Py)_4(NCMe)_2][BF_4]_2$ gave products of unknown composition. Despite multiple efforts at attempting to crystallise these products, no crystals suitable for X-ray could be grown.

5.3.2 Complexation with Fe(II) tetrafluoroborate salts

5.3.2.1 Reactivity of **L2** and H**L4** towards $[Fe(Py)_4(NCMe)_2][BF_4]_2$

As discussed earlier, Dammers *et al.* reported the preparation of of $[LFe^{II}(\mu\text{-}F)_2Fe^{II}][BF_4]_2$ and the mixed-valence $Fe^{II}Fe^{III}$ complex $[LFe^{II}F(\mu\text{-}F)Fe^{II}][BF_4]_2$

from the reaction of the corresponding ligand with $Fe(BF_4)_2{\cdot}6H_2O$ in methanol under an argon atmosphere (see **Scheme 5.1.7 B**).[30] However, both **L2** and H**L4** proved insoluble in methanol, thus the reactions in this work were carried out in a mixture of acetonitrile and dichloromethane under an inert gas atmosphere. Hence, **L2** and H**L4** were reacted with $[Fe^{II}(MeCN)_6][BF_4]_2$ (prepared *in-situ* from the reaction of $Fe(BF_4)_2{\cdot}6H_2O$ with acetonitrile) in the mixed solvent system affording, on work-up, [(**L2**)Fe(NCMe)$_2$L][BF$_4$]$_2$ (L = MeCN or H_2O, **5.2**) and [(H**L4**)Fe(NCMe)(OHBF$_3$)][BF$_4$]$_2$ (**5.3**) in 87% and 16% yield, respectively (**Scheme 5.3.2**). Both complexes were characterised by a combination IR spectroscopy and elemental analysis, while **5.2** was additionally the subject of a single crystal X-ray diffraction study.

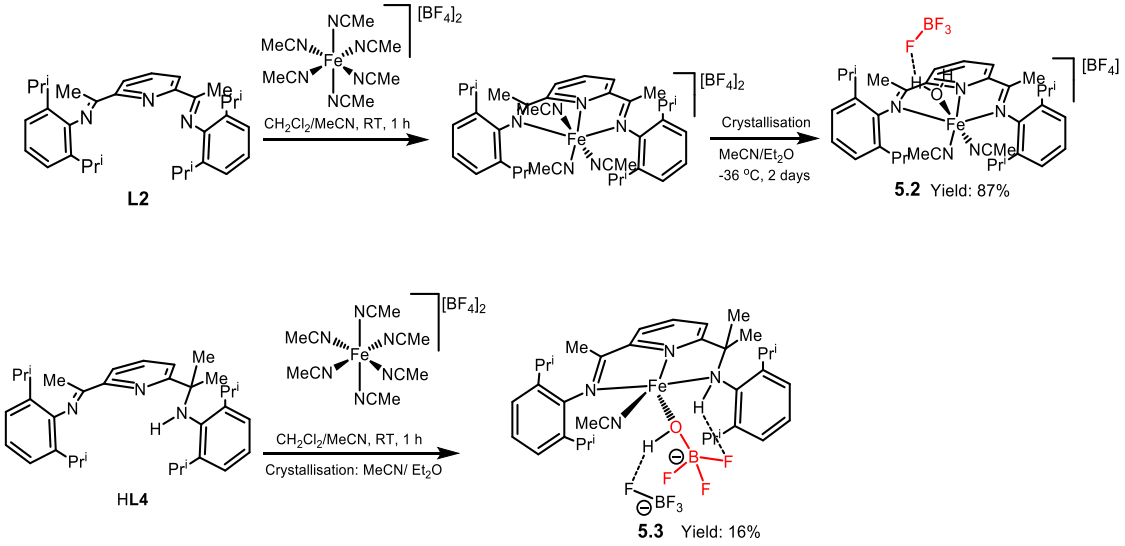

Scheme 5.3.2: Synthesis of *N,N$_{py}$,N*-iron(II) complexes **5.2** and **5.3**.

The crystallisation of complexes **5.2** and **5.3** proved extremely challenging due to the amenability of these iron(II) complexes to undergo oxidation. Indeed, many attempts were made with the most effective method being the slow diffusion of diethyl ether into an acetonitrile solution of the corresponding complex. While suitable crystals of **5.3** proved elusive for the X-ray determination, red crystals of **5.2** could be grown and a dataset was obtained for **5.2** at a temperature of 150 K. Unfortunately, the data for **5.2** proved to be of relatively poor quality as the result of the crystal decomposing in the X-ray beam after about 4 hours. Attempts to collect the data for **5.2** at lower temperature (*e.g.* 100 K) or at room temperature showed no improvement. Nonetheless, the gross structure of **5.2** could still be identified and indicated a 50:50 mixture of

[(**L2**)Fe(NCMe)$_3$][BF$_4$]$_2$ (molecule A) and [(**L2**)Fe(NCMe)$_2$(OH$_2$)][BF$_4$]$_2$ (molecule B). It should emphasised that the structure was highly disordered.

A view of molecule B in **5.2** is shown in **Fig. 5.3.2**, while selected bond lengths and angles are collected in **Table 5.3.2**. The structure consisted of a cationic unit and a tetrafluoroborate counterion. Within the cationic unit a single iron centre is surrounded by a *N,N$_{py}$,N* ligand, two MeCN ligands and one H$_2$O ligand, forming a distorted octahedral geometry. Meanwhile one of the F atoms belonging to a BF_4^- counterion formed an interaction with the coordinated water [O(1)-H(1C)···F(6) 2.842 Å]. With regard to the Fe-N distances, the Fe-N$_{pyridine}$ bond length was the shortest [range: 2.071(9) – 2.274(6) Å] and slightly longer than that seen in the corresponding Ni(II) complex **4.12** [range: 1.969 - 2.113 Å]. There are also two five-membered chelate rings formed with internal N(2)-Fe(1)-N(1) and N(3)-Fe(1)-N(1) angles of 74.21(16)º and 89.57(17)º, respectively.

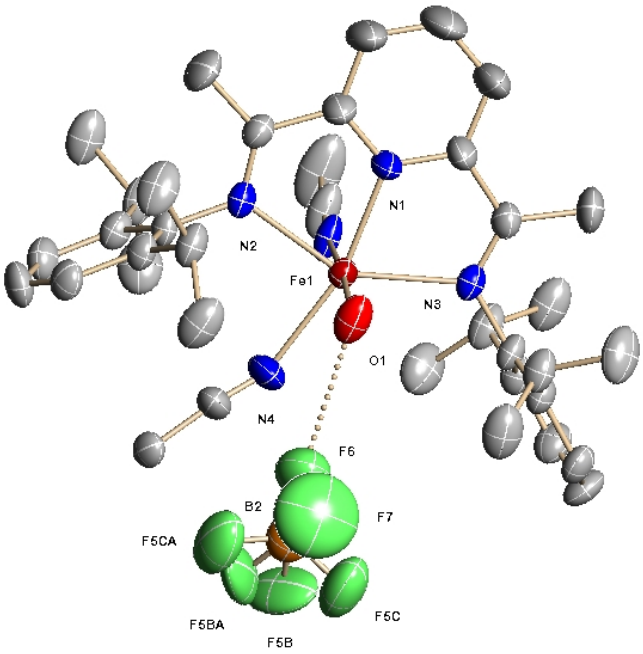

Figure 5.3.2: Molecular structure of **5.2** (molecule B).

Table 5.3.2: Selected bond lengths and angles for **5.2** (molecule B).

Bond Lengths (Å)	
Fe(1)-N(1)	2.071(9)
Fe(1)-N(2)	2.274(6)

Fe(1)-N(3)	2.123(9)
Fe(1)-N(4)	2.192(14)
Fe(1)-O(1)	2.099(8)
O(1)-H(1C)···F(6)	2.842
Bond Angles (°)	
N(2)-Fe(1)-N(1)	74.21(16)
O(1)-Fe(1)-N(1)	92.10(17)
N(3)-Fe(1)-N(1)	89.57(17)
O(1)-Fe(1)-N(3)	173.9(4)

5.3.3 Ethylene polymerisation evaluation

In previously reported studies, iron(II) chloride complexes have been shown to exhibit their optimal catalytic performance in the presence of either methylaluminoxane (MAO) or modified MAO (MMAO) as co-catalyst.[24-28] Hence, this investigation focused on these two co-catalysts using tetrafluoroborate-containing **5.2** as the test precatalyst. Once the optimal reaction temperature, Al:Fe molar ratio and reaction time were independently established for **5.2**/MAO and **5.2**/MMAO, the corresponding set of conditions were also used to screen **5.3** and previously reported (**L2**)$FeCl_2$.[24-28] All polymeric materials were characterised by gel permeation chromatography (GPC) and differential scanning calorimetry (DSC), while the microstructural properties of the selected samples were examined using high-temperature ^{13}C NMR spectroscopy.

5.3.3.1 Ethylene polymerisation with MAO as the co-catalyst

In the first instance, the effect of the temperature on the polymerisation using **5.2**/MAO was investigated with the Al:Fe molar ratio set at 2000:1 (**Scheme 5.3.3**). Typically, the runs were performed in toluene under 10 atm of ethylene pressure over 30 minutes (entries 1 - 6, **Table 5.3.3**).

On raising the temperature from 30 to 80 ºC, the best activity for **5.2**/MAO was observed at 13.48 × 10^6 g PE mol^{-1} (Fe) h^{-1} at 60 ºC (entry 4, **Table 5.3.3**). Above 60 ºC, the activity steadily reduced reaching a minimum at 80 ºC of 4.26 × 10^6 g PE mol^{-1} (Fe) h^{-1}. This lowering in the activity could be attributed to partial catalyst deactivation and also to the lower solubility of ethylene at higher temperature. [25c,33,34,35] Nevertheless,

the activity recorded at 80 °C can still be regarded as good, which highlights the good thermal stability of this catalyst system. **Fig. 5.3.3** shows the GPC traces recorded for the polymers at 30, 40, 50, 60, 70 and 80 °C. A broad bimodal molecular weight distribution was observed at 30 °C with a low molecular weight fraction and high molecular weight fraction. On increasing the temperature the lower molecular fraction dropped in intensity leading to more unimodal-like distribution at higher temperature; this was accompanied by a steady decrease in molecular weight from 193.74 kg mol^{-1} at 30 °C to 74.97 kg mol^{-1} at 80 °C. This lowering in the molecular weight can likely be attributed to increased chain transfer to aluminium or chain termination by β-H elimination at the high temperature (**Scheme 5.3.4**).[44,35,45] Meanwhile, the molecular weight distribution saw a considerable narrowing over the temperature range (M_w/M_n range: 39.4 at 30 °C to 6.5 at 80 °C).

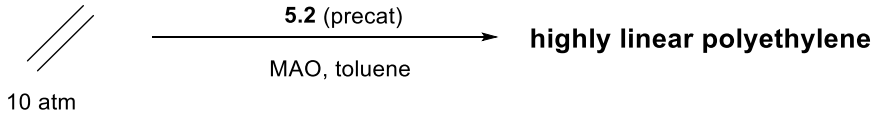

Scheme 5.3.3: Ethylene polymerisation using **5.2** with MAO as co-catalyst.

Table 5.3.3: Effects of temperature on ethylene polymerisation using **5.2**/MAO[a]

Entry	T (ºC)	Mass (g)	Activity[b]	M_w[c]	M_w/M_n[c]	T_m[d] (ºC)
1	30	2.50	2.50	193.74	39.4	134.2
2	40	4.31	4.31	183.41	31.7	133.5
3	50	5.41	5.41	168.33	27.6	133.8
4	60	13.48	13.48	113.72	14.3	133.7
5	70	12.03	12.03	90.62	12.1	133.6
6	80	4.26	4.26	74.97	6.5	131.3

[a] Conditions: 2.0 μmol of **5.2**; 100 mL toluene, 10 atm ethylene; 2000:1 Al:Fe molar ratio; 30 minute run time. [b] Values in units of 10^6 g(PE) mol^{-1} (Fe) h^{-1}. [c] Determined by GPC, and M_w: 10^3 g mol^{-1}. [d] Determined by DSC.

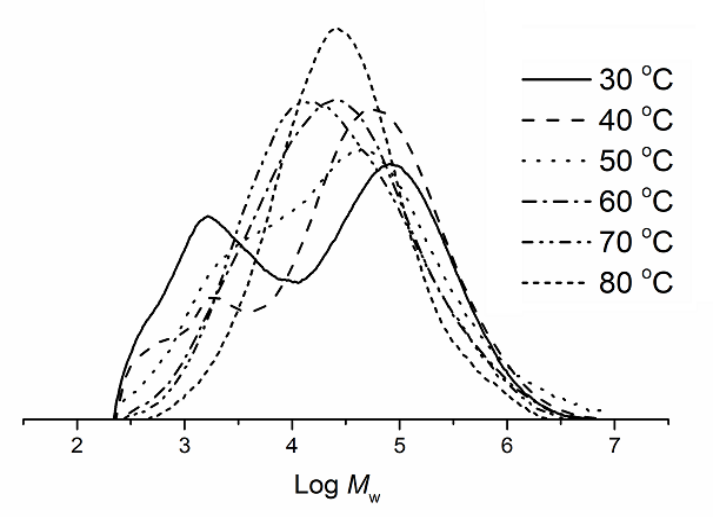

Figure 5.3.3: GPC traces of the polyethylenes obtained using **5.2**/MAO at different run temperatures (entries 1 – 6, **Table 5.3.3**).

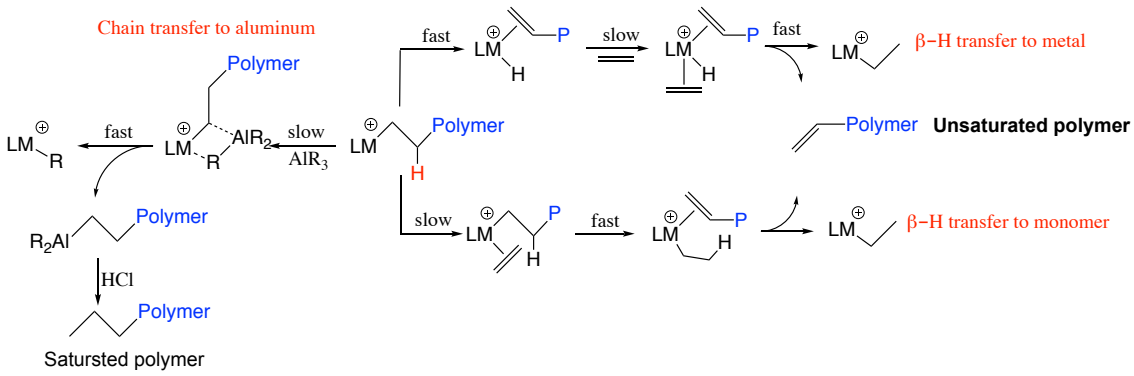

Scheme 5.3.4: Possible mechanisms for chain termination.

Secondly, the effect of the molar ratio of Al:Fe on the catalytic performance of **5.2**/MAO was explored. Due to the optimal activity being identified earlier at 60 °C, the subsequent runs were carried out at 60 °C over 30 minutes with the ratio varied between 1000:1 and 3000:1 (entries 1 - 5, **Table 5.3.4**). The peak activity of 13.48 × 10^6 g (PE) mol^{-1} (Fe) h^{-1} was observed at a molar ratio of 2000:1 (entry 3, **Table 5.3.4**). The molecular weight of the polymer was seen to decrease from 148.12 to 90.34 kg mol^{-1} on changing the ratio from 1000:1 to 3000:1 which can likely be ascribed to increased chain transfer from iron to aluminum with the larger amounts of aluminium co-catalyst.[25c,36,37] The GPC curves further illustrate this behaviour (**Figure 5.3.4**). At 1000 equivalents of MAO a broad unimodal molecular weight distribution was observed. As the Al:Fe ratio was increased to 2000:1 a broader distribution was apparent. Above 2000 equivalents, a lower molecular weight shoulder appeared that

became more prominent at higher molar equivalents. In addition, the molecular weight distribution remained broad across the range in Al:Fe molar ratios (M_w/M_n = 17.2 - 10.1) suggesting multiple active species.

Table 5.3.4: Effects of Al:Fe molar ratio on the polymerisation using **5.2**/MAO[a]

Entry	Al:Fe	t (min)	Mass (g)	Activity[b]	M_w[c]	M_w/M_n[c]	T_m[d] (°)
1	1000	30	9.75	9.75	148.12	17.2	134.1
2	1500	30	11.75	11.75	113.82	10.4	133.9
3	2000	30	13.48	13.48	113.72	14.3	133. 7
4	2500	30	12.65	12.65	94.52	10.2	132.8
5	3000	30	12.12	12.12	90.34	10.1	131.9

[a] Conditions: 2.0 μmol of **5.2**; 100 mL toluene, 10 atm ethylene; 60 °C run temperature. [b] Values in units of 10^6 g(PE) mol^{-1} (Fe) h^{-1}. [c] Determined by GPC, and M_w: 10^3 g mol^{-1}. [d] Determined by DSC.

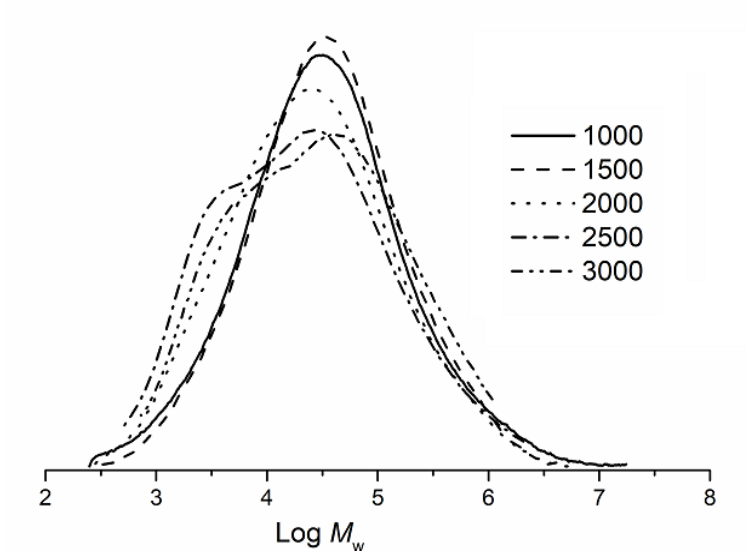

Figure 5.3.4: GPC traces of the polyethylenes obtained using **5.2**/MAO with various Al:Fe molar ratios (entries 1 – 5, **Table 5.3.4**).

The reaction time can have a significant effect on productivity, molecular distribution, and the polymer end groups. Therefore, the lifetime of **5.2**/MAO was explored by carrying out the polymerisations over 5, 15, 30, 45 and 60 minute run times (entries 1 - 6, **Table 5.3.5**). The highest activity (43.20 × 10^6 g (PE) mol^{-1} (Fe) h^{-1}) was achieved after 5 minutes which can be attributed to the active species being rapidly formed after the addition of MAO and then gradually deactivating (entry 1, **Table 5.3.5**).[36a,38] Nevertheless, there were sufficient active species over the longer run times leading to

longer chains and in-turn a gradual increase in the molecular weight of the resulting polymeric material. Their GPC curves further illustrate this behaviour (**Fig. 5.3.5**). The molecular weight distribution remained broad (M_w/M_n = 7.8 to 14.7) over more extended run times consistent with multiple active species.

The ethylene pressure also can have a profound influence on both the yield and the molecular weight distribution of the polymer. In this study, lowering the ethylene pressure from 10 to 5 atm with 2000 molar equivalents of MAO, a dramatic drop in catalytic activity was evident (entry 3 vs 6, **Table 5.3.5**) while the M_w lowered form 113.72 kg mol^{-1} to 81.43 kg mol^{-1}. However even at lower pressure (1 atm) some polymer was detectable (entry 7, **Table 5.3.5**). In general, the activity of catalyst, the yield of polyethylene and the molecular weight increased linearly with ethylene pressure.

Table 5.3.5: Effects of reaction time and ethylene pressure on **5.2**/MAO[a]

Entry	t (min)	Mass (g)	Activity[b]	M_w[c]	M_w/M_n[c]	T_m[d] (℃)
1	5	7.20	43.20	42.13	7.8	132.5
2	15	10.08	20.16	83.21	11.5	132.9
3	30	13.48	13.48	113.72	14.3	133.7
4	45	14.45	9.60	118.32	14.2	134.9
5	60	14.48	7.24	123.22	14.7	135.1
6[e]	30	4.48	4.48	81.34	8.8	132.8
7[f]	30	0.45	0.45	37.95	6.3	107.7

[a] Conditions: 2.0 μmol of **5.2**; 100 mL toluene, 10 atm ethylene; 2000:1 Al:Fe molar ratio; 60 °C run temperature. [b] Values in units of 10^6 g(PE) mol^{-1} (Fe) h^{-1}. [c] Determined by GPC, and M_w: 10^3 g mol^{-1}. [d] Determined by DSC. [e] 5 atm ethylene. [f] 1 atm ethylene.

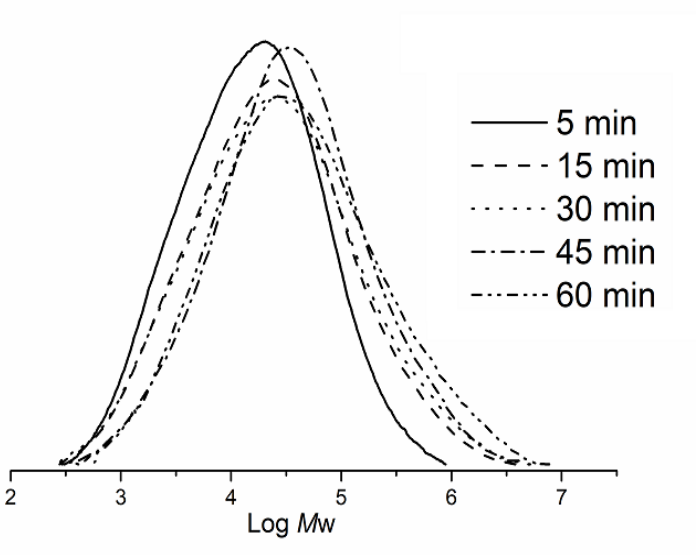

Figure 5.3.5: GPC traces for the polyethylenes obtained using **5.2**/MAO at different run times (**Table 5.3.4**).

Finally, **5.3** and (**L2**)$FeCl_2$[24-28] were screened for ethylene polymerisation employing the optimised conditions established for **5.2**/MAO (*viz*., Al:Fe = 2000:1, run temperature = 60 °C, reaction time = 30 minutes). Collectively, all the iron catalysts exhibited high activities (range: 1.21 – 13.48 × 10^6 g (PE) mol^{-1} (Fe) h^{-1}) and were found to decrease in the order **5.2** > (**L2**)$FeCl_2$ > **5.3** (**Table 5.3.6**). In addition, the molecular weight of the polymer generated using **5.2** was much higher than these observed for (**L2**)$FeCl_2$. By contrast, **5.3** showed the lowest activity and the lowest molecular weight polymer. In terms of polymer's dispersity, that obtained using **5.2** and **5.3** was broader (M_w/M_n = 14.3 and 13.7) than seen using (**L2**)$FeCl_2$ (M_w/M_n = 8.1).

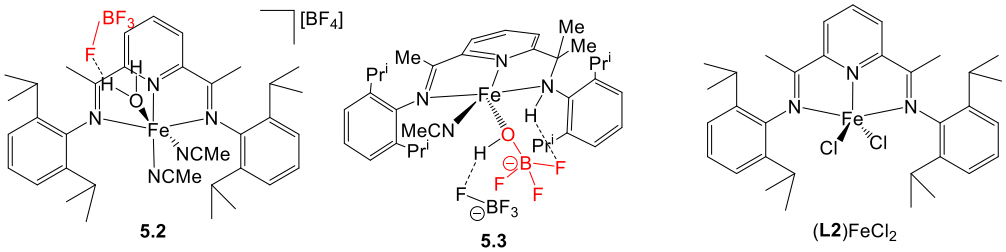

Table 5.3.6: Comparative performance of **5.2**, **5.3** and (**L2**)$FeCl_2$ using MAO as co-catalyst[a]

Entry	Precat.	Mass (g)	Activity[b]	M_w[c]	M_w/M_n[c]	T_m[d] (℃)
1	**5.2**	13.48	13.48	113.72	14.3	133.7
2	**5.3**	1.20	1.20	62.69	13.7	131.9
3	(**L2**)$FeCl_2$[24]	9.89	9.89	92.37	8.1	134.1

[a] Conditions: 2.0 µmol of iron precatalyst; 100 mL toluene; 10 atm ethylene; 2000:1 Al:Fe molar ratio; 60 °C run temperature; 30 minute run time. [b] Values in units of 10^6 g(PE) mol^{-1} (Fe) h^{-1}. [c] Determined by GPC, and M_w: 10^3 g mol^{-1}. [d] Determined by DSC. [e] 5 atm ethylene. [f] 1 atm ethylene.

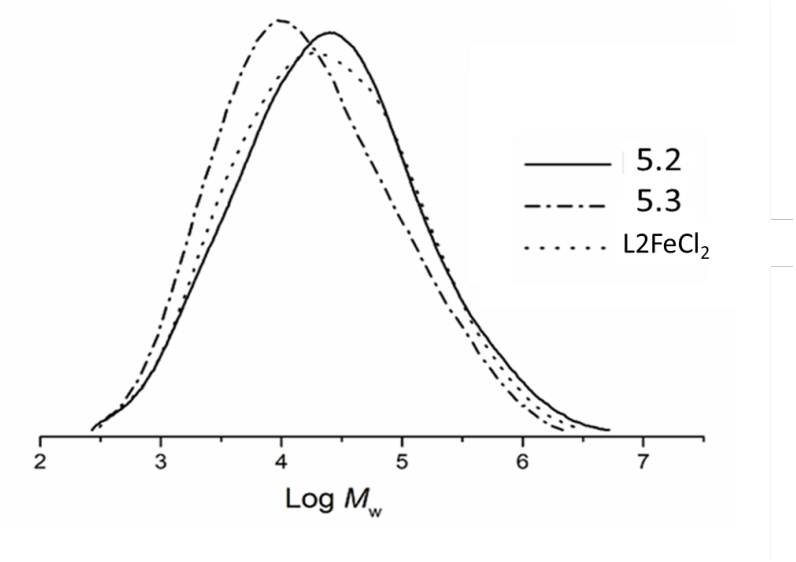

Figure 5.3.6: GPC traces of the polyethylenes obtained using **5.2**, **5.3** and (**L2**)$FeCl_2$ with MAO as co-catalyst.

In order to investigate the microstructural properties of the polyethylene generated using **5.2, 5.3** and (**L2**)$FeCl_2$, both DSC and high temperature ^{13}C NMR spectroscopic measurements were recorded. The high melting temperature (~ 135 ºC) for the polymers obtained from all runs (with sharp endotherm peaks in their DSC trances) were characteristic of highly linear materials (**Figure 5.3.7**). To support this conclusion, a sample of the polyethylene obtained using **5.2**/MAO (entry 4, **Table 5.3.2**) was characterised by ^{13}C NMR spectroscopy (recorded in 1,1,2,2-[d_2]tetrachloroethane at 135 ºC). The spectrum revealed a broad singlet peak around δ 30.00 assignable to the -$(CH_2)_n$- repeat unit of a linear polyethylene (**Figure 5.3.8**).[39, 40, 36c] Unfortunately, no peaks could be detected for the polymer end groups, presumably as a consequence of the high molecular weight.

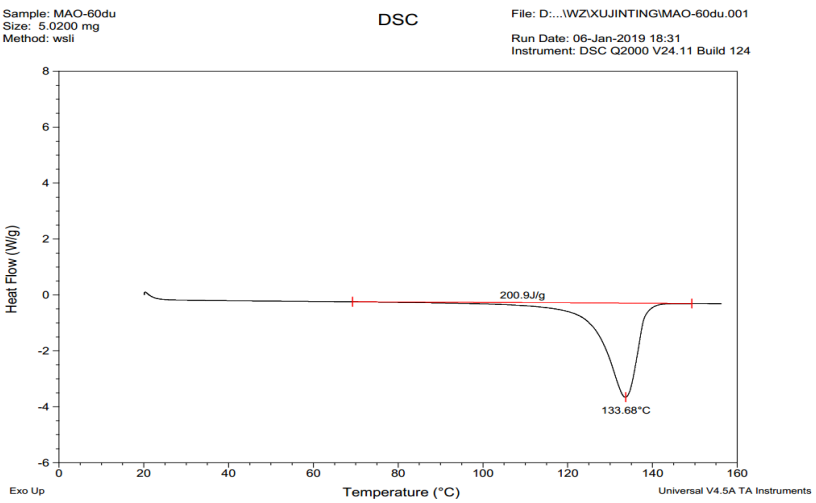

Figure 5.3.7: DSC thermogram of the polyethylene obtained using **5.2**/MAO at 60 ^{o}C (Al:Fe molar ratio = 2000:1, **Table 5.3.1**, entry 4)

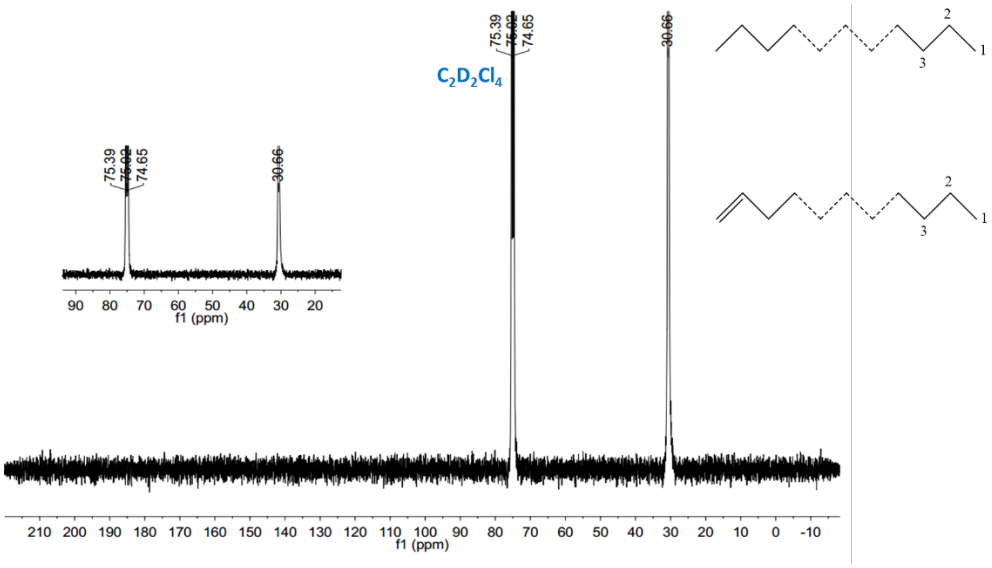

Figure 5.3.8: ^{13}C NMR spectrum of the polyethylene obtained using **5.2** /MAO at 60 °C - recorded in 1,1,2,2-tetrachloroethane-d_2 (δ C 74.2) at 135 ºC.

5.3.3.2 Ethylene polymerisation with MMAO as the co-catalyst

To explore the effect of co-catalyst, the polymerisation runs were also conducted using MMAO as co-catalyst (**Scheme 5.3.5**). Complex **5.2** was also used as the test precatalyst and the optimisation of the polymerisation conditions was performed with the pressure of ethylene in the initial screen set at 10 atm and the Al:Fe molar ratio fixed at 2000:1 and the run time at 30 minutes. On varying the reaction temperature

from 30 to 80 ºC (entries 1 - 6, **Table 5.3.7**), the highest activity of 8.65 × 10^6 g (PE) mol^{-1} (Fe) h^{-1} was again achieved at 60 ºC (entry 4, **Table 5.3.7**), which is notably lower than that seen with MAO (13.48 × 10^6 g (PE) mol^{-1} (Fe) h^{-1}). Furthermore, the molecular weight of the polymer at this run temperature [90.77 kg mol^{-1}] was found to be less than that achieved using MAO at the same temperature [113.72 kg mol^{-1}]. On increasing the temperature of the run from 60 ^oC to 80 ^oC saw the molecular weight decrease sharply from 90.77 to 18.32 kg mol^{-1} which was accompanied by a broadening in the molecular weight distribution (M_w/M_n = 9.6 to 21.3). These observation may be attributed to either increased chain transfer to aluminium or chain termination by β-H elimination at higher temperature.[44,45] Unlike the polymers generated using **5.2**/MAO, the GPC curves obtained using **5.2**/MMAO indicated the molecular weight distribution to be more bimodal at run temperatures ≤ 70 ^oC (**Fig. 5.3.9**). By contrast, at 80 ^oC the distribution exhibited a more unimodal shape with the lower molecular weight fraction becoming the major component at high temperature; similar behavior have been previously reported for related catalysts.[44e] These observations can be attributed to the difference in rates of chain termination of the two likely competing processes.

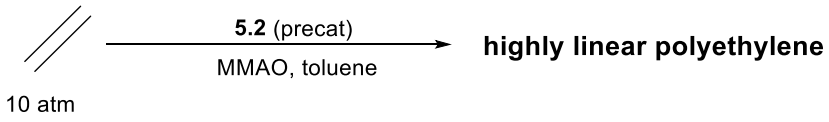

Scheme 5.3.5: Ethylene polymerisation using **5.2** with MMAO as co-catalyst.

Table 5.3.7: Effects of temperature on the polymerisation using **5.2**/MMAO[a]

Entry	T (ºC)	Mass (g)	Activity[b]	M_w[c]	M_w/M_n[c]	T_m[d] (ºC)
1	30	3.28	3.28	26.95	21.4	124.7
2	40	4.23	4.23	31.33	17.2	126.0
3	50	5.96	5.96	40.47	15.0	128.3
4	60	8.65	8.65	90.77	21.3	131.9
5	70	8.25	8.25	80.96	23.1	131.1
6	80	4.75	4.75	18.32	9.6	129.3

[a] Conditions: 2.0 μmol of **5.2**; 100 mL toluene, 10 atm ethylene; 30 minute run time; 2000:1 Al:Fe molar ratio. [b] Values in units of 10^6 g(PE) mol^{-1} (Fe) h^{-1}. [c] Determined by GPC and M_w: 10^3 g mol^{-1}. [d] Determined by DSC.

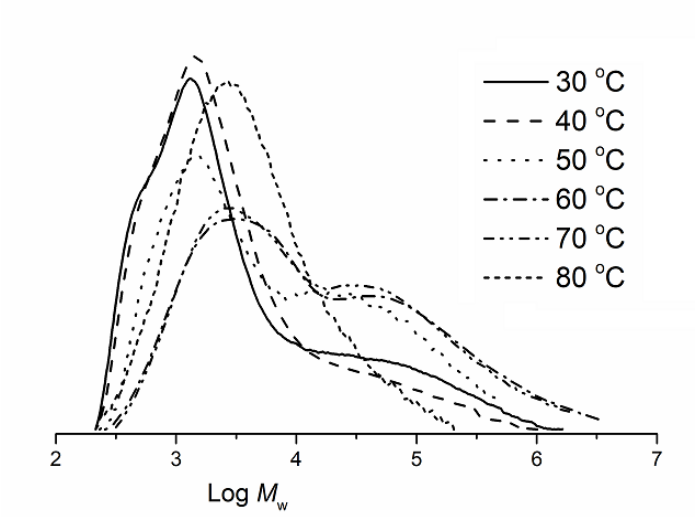

Figure 5.3.9: GPC traces for the polyethylenes obtained using **5.2**/MMAO at different run temperatures (entries 1 – 6, **Table 5.3.6**).

Subsequently, the effect of varying the Al:Fe molar ratio was explored from 1000:1 to 3000:1 with the temperature fixed at 60 °C and the run time at 30 minutes (entries 1 - 5, **Table 5.3.8**). It was found that a maximum in catalytic activity of 8.65 × 10^6 g (PE) mol^{-1} (Fe) h^{-1} was observed with the ratio at 2000:1 (entry 3, **Table 5.3.8**). It was also noted that the molecular weight of the resulting polymers decreased by about a quarter from 118.82 to 30.70 kg mol^{-1} when the Al:Fe molar ratio increased from 1000:1 to 3000:1. This observation can likely be attributed to increasing chain transfer from the iron center to aluminium with larger amounts of MMAO; similar performance characteristics have been reported elsewhere.[44f,44a-e,46] In comparison with the results obtained with **5.2**/MAO, these MMAO-promoted polymerisations were found to produce polymers slightly broader distributions over the range in molar ratios (M_w/M_n = 13.9 - 21.3). A further striking feature was the gradual appearance of a bimodal distribution as the Al:Fe ratio was increased from 1000:1 to 2000: 1 (**Figure 5.3.10**). Indeed, as the molar ratio was increased to 3000:1 the intensity of the lower molecular fraction noticeably became the most prominent. Surprisingly, this finding was not observed with the runs using **5.2**/MAO (see **Fig 5.3.4**). A reasonable explanation for this difference is behavior may derive from higher amounts of $AlMe_3$ that are present in commercial samples of MMAO as compared to that in MAO. This higher concentration would then lead to an increase in the rate of chain transfer and in turn a reduction in chain propagation and lower in turn lower molecular weight polymer. These results are consistent with chain transfer to aluminum playing an important role in the generation of the lower molecular weight fraction.[25c, 41]

Table 5.3.8: Effects of Al:Fe molar ratio on the polymerisation using **5.2**/MMAO[a]

Entry	Al:Fe	Mass (g)	Activity[b]	M_w[c]	M_w/M_n[c]	T_m[d] (℃)
1	1000	7.10	7.10	118.82	18.9	133.4
2	1500	8.15	8.15	108.19	13.5	131.2
3	2000	8.65	8.65	90.77	21.3	131.9
4	2500	8.25	8.25	79.82	19.9	130.9
5	3000	6.20	6.20	30.70	13.9	130.7

[a] Conditions: 2.0 μmol of **5.2**; 100 mL toluene, 10 atm ethylene; 60 °C run temperature; 30 minute run time. [b] Values in units of 10^6 g(PE) mol^{-1} (Fe) h^{-1}. [c] Determined by GPC, and M_w: 10^3 g mol^{-1}. [d] Determined by DSC.

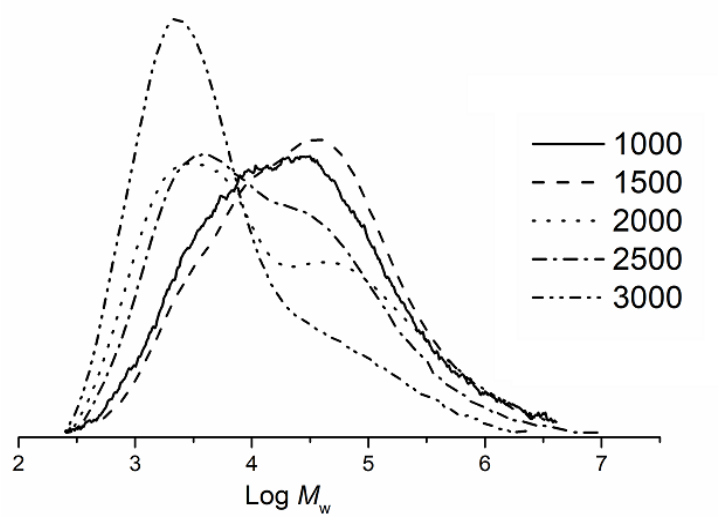

Figure 5.3.10: GPC traces of the polyethylenes obtained using **5.2**/MMAO at various Al:Fe ratios (entries 1-5, **Table 5.3.8**).

To explore the lifetime of the active species derived form **5.2**/MMAO, the polymerisation runs were conducted over 5, 15, 30, 45 and 60 minutes (entries 1-5, **Table 5.3.9**) with the Al:Fe molar ratio at 2000:1 and the temperature at 60 °C. The highest activity was found at 22.8 × 10^6 g (PE) mol^{-1} (Fe) h^{-1} after 5 minutes (entry 1, **Table 5.3.9**). It was noted that the activity after 5 minutes more than twice than observed after 30 minutes (8.65 × 10^6 g (PE) mol^{-1} (Fe) h^{-1}), which highlights both the rate at which the active species was generated after MMAO addition and the onset of catalyst deactivation over time.[36a,38,42] Again, the molecular weight increased on extending the reaction time with broad bimodal distributions observed for all the polymers with the higher molecular weight fraction becoming the major component with more extended run times (**Figure 5.3.11**). With regard to the ethylene pressure, the activity was found to drop by more than a half (from 8.65 to 3.20 × 10^6 g(PE) mol^{-1} (Fe)

h^{-1}) when lowered from 10 to 5 atm (entries 3 *vs* 6, **Table 5.3.9**); at 1 atm, only trace amounts of polymer could be isolated (entry 7, **Table 5.3.9**). This behavior is likely be credited to the lower ethylene concentration at lower pressure.[35, 41, 44a-b, 45a,d,e]

Table 5.3.9: Effects of reaction time and ethylene pressure on the polymerisation using **5.2**/MMAO[a]

Entry	t (min)	Mass (g)	Activity[b]	M_w[c]	M_w/M_n[c]	T_m[d] (℃)
1	5	3.80	22.80	41.65	14.1	127.0
2	15	6.80	13.60	82.71	19.5	130.1
3	30	8.65	8.65	90.77	21.3	131.9
4	45	10.45	6.96	107.23	24.3	133.4
5	60	11.28	5.64	117.34	14.7	133.9
6[e]	30	3.20	3.20	81.34	8.8	132.8
7[f]	30	trace	trace	-	-	-

[a] Conditions: 2.0 μmol of **5.2**; 100 mL toluene, 10 atm ethylene; 60 °C run temperature; 2000:1 Al:Fe molar ratio. [b] Values in units of 10^6 g(PE) mol^{-1} (Fe) h^{-1}. [c] Determined by GPC and M_w: 10^3 g mol^{-1}. [d] Determined by DSC. [e] 5 atm ethylene. [f] 1 atm ethylene.

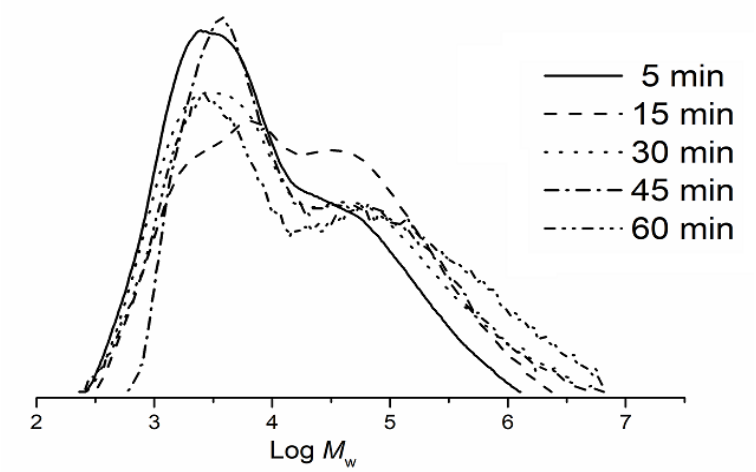

Figure 5.3.11: GPC curves for the polyethylenes obtained using **5.2**/MMAO at different run times (entries 1-5, **Table 5.3.10**).

Using the optimised conditions established for **5.2**/MMAO (*i.e.*, Al:Fe molar ratio = 2000:1, run temperature = 60 °C, run time = 30 minutes), **5.3** and (**L2**)$FeCl_2$[24] were additionally explored for ethylene polymerisation. All these MMAO-promoted systems showed high activities 8.65 - 1.12 × 10^6 g (PE) mol^{-1} (Fe) h^{-1} (**Table 5.3.10**) but were lower than that observed with MAO as co-catalyst (13.48 – 1.21 × 10^6 g (PE) mol^{-1} (Fe) h^{-1}) (**Table 5.3.10**). In terms of their relative catalytic performance, the activities

were found to fall in the order **5.2** > (**L2**)$FeCl_2$ > **5.3**, which is same as that seen with MAO. Notably, **5.2** and **5.3** produced lower molecular weight polymers than that reported with MAO. In addition, unlike the polymers obtained using MAO as co-catalysts, the GPC curves obtained using **5.2** and (**L2**)$FeCl_2$/MMAO displayed broad bimodal molecular weight distributions (M_w/M_n = 21.3 and 31.1).

The melt temperatures of all the polymers were found to fall in the range of 124.7 – 133.9 °C, values which are quite typical of highly linear polyethylenes. On comparison of the DSC traces of the polymers obtained using MAO, the melting endotherm of the MMAO-derived polymers exhibit, in most cases, slightly broader endotherms; this is consistent with these polymers displaying broader molecular weight distributions.

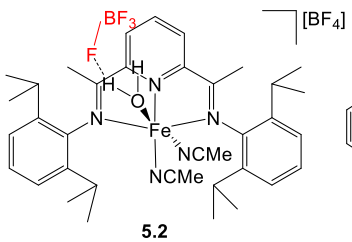

5.2

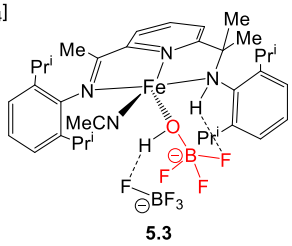

5.3

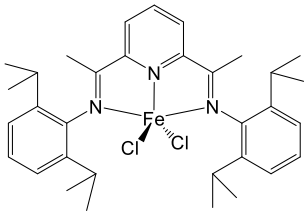

(**L2**)$FeCl_2$

Table 5.3.10: Comparative performance of **5.2**, **5.3** and (**L2**)$FeCl_2$ using MMAO as co-catalyst[a]

Entry	Precat.	Mass (g)	Activity[b]	M_w[c]	M_w/M_n[c]	T_m[d] (℃)
1	**5.2**	8.65	8.65	90.77	21.3	131.9
2	**5.3**	1.12	1.23	26.23	10.2	128.8
3	**L2**$FeCl_2$[24]	7.20	7.20	96.91	31.1	131.6

[a] Conditions: 2.0 µmol of iron precatalyst; 100 mL toluene, 10 atm ethylene; 2000:1 Al:Fe molar ratio; 60 °C run temperature; 30 minute run time. [b] Values in units of 10^6 g(PE) mol^{-1} (Fe) h^{-1}. [c] Determined by GPC, and M_w: 10^3 g mol^{-1}. [d] Determined by DSC. [e] 5 atm ethylene. [f] 1 atm ethylene.

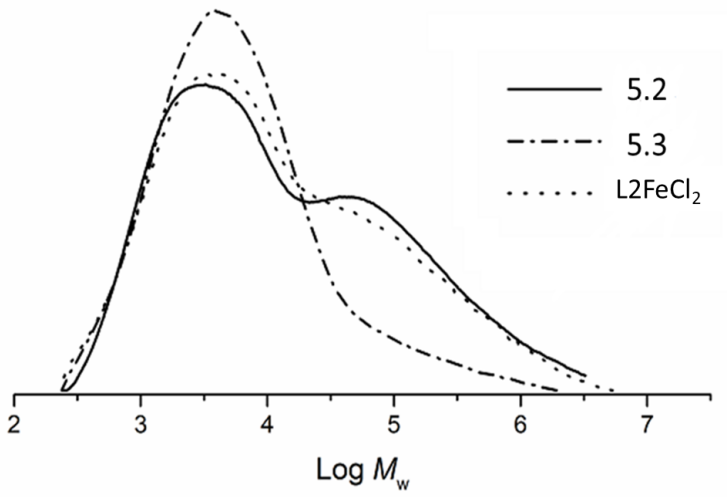

Figure 5.3.12: GPC traces of the polyethylenes obtained using **5.2**, **5.3** and **L2**$FeCl_2$ with MMAO as the co-catalyst.

Further support for the linearity of the polymeric materials was provided by the high temperature ^{13}C NMR spectroscopic data for the sample obtained using **5.2**/MMAO (entry 4, **Table 5.3.7**). In particular, a high intensity singlet at δ 30.60 supports the presence of equivalent -$(CH_2)_n$- repeat units (**Figure 5.3.13**).[34-42] It worth noting that, lower intensity peaks at δ 32.84 (3), 23.54 (2) and 14.77 (1) corresponding to n-propyl end groups were also detectable. By contrast, there was no evidence for peaks corresponding to iso-butyl end groups, precluding chain transfer to $Al(^iBu)_3$ and its derivatives present in MMAO.[43] Furthermore, no peaks attributable to unsaturated chain ends could be identified which may suggest the absence of termination via *β*-H elimination.

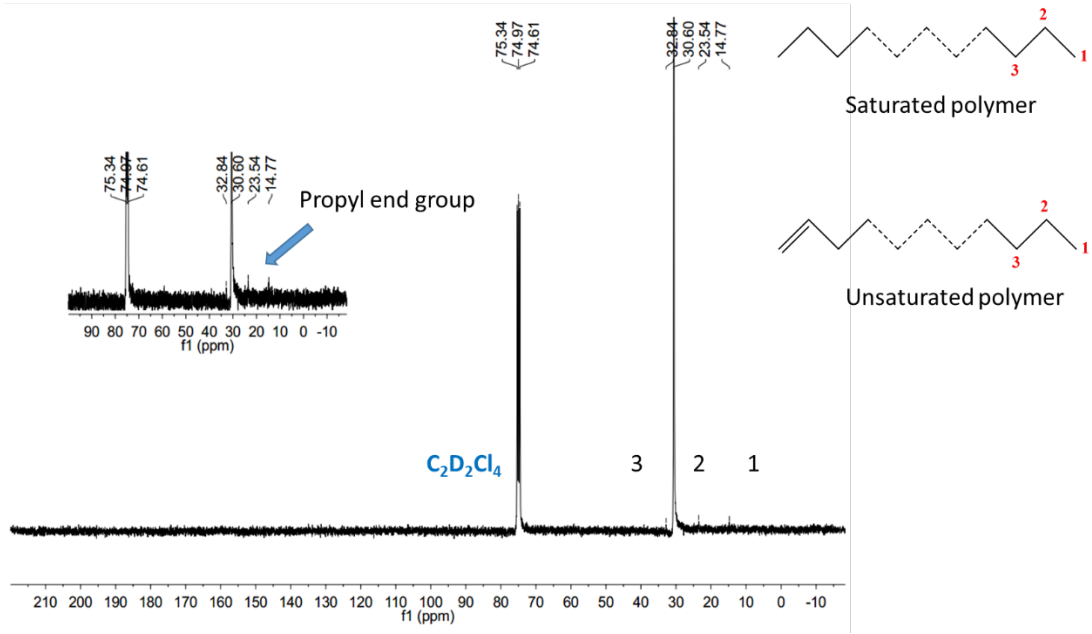

Figure 5.3.13: ^{13}C NMR spectrum of the polyethylene obtained using **5.2** /MMAO at 60 °C; recorded in 1,1,2,2-tetrachloroethane-d_2 (δ C 74.2) at 135 ºC.

5.3.4 Conclusion to Chapter 5

Two new iron(II) tetrafluoroborate complexes (**5.2** and **5.3**), each bearing *N*,N_{py},*N* tridentate pincer ligands, have been successfully synthesised. The X-ray structure of **5.2** showed a distorted octahedral geometry for the complex cation with a coordinated water molecule undergoing a hydrogen bonding interaction with one of the BF_4^-

counterions. The structure of **5.3** was deduced based on that observed for the corresponding zinc, cobalt and nickel complexes. The *N,N,O* complex **5.1** has also been synthesised and structurally characterised. On activation with MAO or MMAO, **5.2** and **5.3** exhibited high activity toward ethylene polymerisation and produced highly linear polyethylenes. Meanwhile, the well-known (**L2**)$FeCl_2$[24-27] was also prepared and screened to allow a comparison.

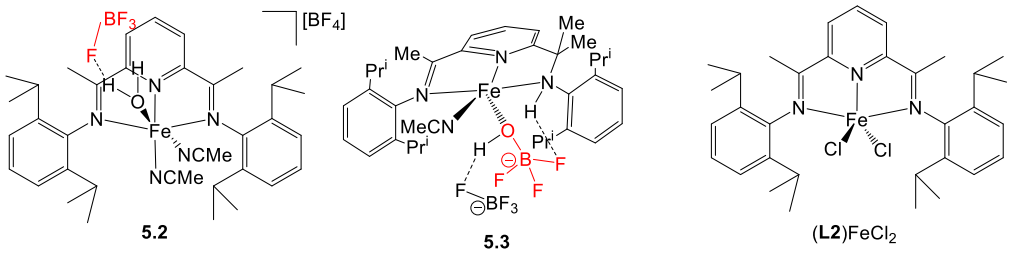

Figure 5.3.14: Iron(II) precatalysts **5.2**, **5.3** and (**L2**)$FeCl_2$ investigated.[24]

Catalyst **5.2**/MAO exhibited the highest activity of up to 13.48 × 10^6 g PE mol^{-1} (Fe) h^{-1} and the highest molecular weight of polymers while **5.3**/MAO showed the lowest (1.20 × 10^6 g PE mol^{-1} (Fe) h^{-1}). In general, the MAO-activated systems gave higher molecular weights than their MMAO counterparts. By contrast, the **5.2**/MMAO, **5.3**/MMAO and (**L2**)$FeCl_2$/MMAO showed lower activities than **5.2**/MAO, **5.3**/MAO and (**L2**)$FeCl_2$/MAO, and displayed broader and in many cases slightly bimodal distributions.

References

1. a) A. J. Pearon, *Metallo-organic Chemistry*, Wiley, Chichester, 1985; b) J. P. Collman, L. S. Hegedus, J. R. Northon and R. G. Finke, *Principles and Application of Organotransition metal chemistry, University Science Books, Mill Valley,* CA, 1987; c) S. G. Dacies, *Organotransition Metal Chemistry: Application to Organic Synthesis, Pergamon Press, Oxford,* 1989; d) L. S. Hegedus, *Transition Metals in the Synthesis of Complex Organic Molecules, 2nd edn., University Science Books, Sausalito, CA.* 1999; e) J. Tsuji, *Transition Metal Reagents and Catalysts, Innovations in Organic Synthesis, Wiley, Chichester,* 2000.

2. a) L. Mond and F. Quinke, *J. Chem. Soc.,* 1891, **59**, 604-607; b) M. Berthelot. *C. R. Hebd. Seances Acad. Sci*., 1891, **112**, 1343-1349.

3. T. J. Kealy and P. L. Pauson, *Nature,* 1951, **168**, 1039-1040.

4. W. Reppe, H. Vetter and J. Liebigs, *Ann. Chem*. 1953, **582**, 133-163.

5. a) M Tamura and J. Kochi, *Synthesis,* 1971, 303-308; b) M. Tamura and J. Kochi, *J. Am. Chem. Soc.*, 1971, **93**, 1487-1489.

6. I. Bauer and H.-J. Knölker, *Iron catalysis in Organic Chemistry: Reactions and Applications, Chapter 1 Iron complexes in organic chemistry,* 2008.

7. G. J. P. Britovsek, J. England. S. K. Spitzmesser, A. J. P White and J. Williams, *Dalton Trans.*, 2005, 945-955.

8. L. Zhang, D. Peng, X. Leng and Z. Huang*, Angew. Chem. Int. Ed.,* 2013, **52**, 3676-3680.

9. S. Chakraborty, H. Dai, P. Bhattacharya, N. T. Fairweather, M. S. Gibson, J. A. Krause and H. Guan, *J. Am. Chem. Soc.,* 2014, **136**, 7869-7872.

10. S. Sinha, R. Sikari, U. Jash, S. Das, P. Brandão, S. Demeshko, F. Meyer, B. de Bruin and N. D. Paul, *Inorg. Chem*., 2019, **58**, 1935-1948.

11. a) M. A. Ortuño, B. Dereli, K. R. D. Chiaie, A. B. Biernesser, M. Qi, J. A. Byers and C. J. Cramer, *Inorg. Chem*., 2019, **57**, 2064-2071.

12. a) M. Costas, M. P. Mehn, M. P. Jensen and L. Que, *Jr.*, *Chem. Rev*., 2004, **104**, 939; b) M Costas, K. Chen and L. Que, Jr., *Coord. Chem. Rev*., 2000, **200-202**, 517-544.

13. a) J. Kim, R. G. Harrison, C. Kim and L. Que, Jr., *J. Am. Chem. Soc.,* 1996, **118**, 4373-4379; b) G. Roelfes, M. Lubben, R. Hage, L. Que, Jr. and B. L. Feringa, *Chem. Eur. J.,* 2000, **6**, 2152-2159; c) K. Chen and L. Que, Jr., *Chem. Commun.,* 1999, 1375-1376.

14. a) Boronic acids: Preparation and Applications in Organic Synthesis and Medicine (Ed.: D. G. Hall), Wiley-VCH, Wein-Heim, 2005; b) C. M. Crudden and D. Edwards, *Eur. J. Org. Chem.*, 2003, 4695-4712.

15. a) C. M. Vogels, P. E. O'Connor, T. E. Phillips, K. J. Eaton, M. P. Shaver, P. G. Hayes and S. A. Westcott, *Can, J. Chem.* 2001, **79**, 1898-1905; b) S. Colin, L. Vaysse-Ludot, J. P. Lecouve and J. Maddaluno, *J. Chem. Soc*., *Perkin Trans*. 1, 2000, 4505-4511; c) P. V. Ramachandran, M. P. Jennings and H. C. Brown, *Org. Lett*., 1999, **1**, 1399-1402; d) S. Pereira and M. Srebnik, *J. Am. Chem. Soc*., 1996, **118**, 909-910.

16. a) D. A. Evans, G. C. Fu and A. H. Hoveyda, *J. Am. Chem. Soc.*, 1992, **114**, 6671-6679; b) D. A. Evans, G. C. Fu and B. A. Anderson, *J. Am. Chem. Soc*., 1992, **114**, 6679-6685; c) K. Burgess, W. A. Van der Donk, S. A. Westcott, T. B. Marder, R. T. Baker and J. C. Calabrese, *J. Am. Chem. Soc*., 1992, **114**, 9350-9359.

17. J. Zhang, G. Leitus, Y. Ben-David and D. Milstein, *Angew. Chem., Int. Ed.*, 2006, **45**, 1113-1115.

18. a) L. Saudan, P. Dupau, J. J. Riedhauser, P. Wyss (Firmenich SA), Patent WO 2006106483 and WO 2006106484, 2006; b) L. A. Saudan, C. M. Saudan, C. Debieus and P. Wyss, *Angew. Chem., Int. Ed.* 2007, **46**, 7473-7376.

19. B. Plietker., Ed. Iron Catalysis in Organic Chemistry: Reactions and applications; Wiley-VCH: D. Milstein, *Angew. Chem., Int. Ed*. 2014, **53**, 4685-4689.

20. a) R. Hili and A. K. Yudin, *Nat. Chem. Biol.,* 2006, **2**, 284-287; b) F. Ullmann, *Ber. Dtsch. Chem. Ges.,* 1906, **39**, 1691-1692; c) I. Goldberg, *Ber. Dtsch. Chem. Ges.,* 1906, **39**, 1691-1692; d) D. H. R. Barton, K. Nakanishi and O. Meth-Cohn, Comprehensive Natural Products Chemistry, Elsevier: Oxford, 1999; Vol.4.

21. A. Fürstner, *ACS Cent. Sci.*, 2016, **2**, 778-789.

22. a) B. J. O'Keefe, L. E. Breyfogle, M. A. Hillmyer and W. B. Tolman, *J. Am. Chem. Soc.*, 2002, **124**, 4384-4393; b) V. C. Gibson, E. L. Marshall, D. Navarro-Llobet, A.

J. P. White and D. J. A. Williams*, J. Chem. Soc., Dalton Trans.,* 2002, 4321-4322; c) M. Stolt and A. Södergard, *Macromolecules,* 1999, **32**, 6412-6417; d) B. J. O'Keefe, S. M. Monnier, M. A. Hillmyer and W. B. Tolman, *J. Am. Chem. Soc*., 2001, **123**, 339-340.

23. A. Leblance, E. Grau, J. P. Broyer, C. Boisson and R. Spitz, *Macromolecules,* **44**, 3293-3301.

24. V. C. Gibson and G. A. Solan, *Top. Organomet. Chem.,* 2009, **26**, 107-158.

25. a) B. L. Small, M. Brookhart and A. M. A. Bennett, *J. Am. Chem. Soc*., 1998, **120**, 4049-4050; b) B. L. Small, M. Brookhart, *Macromolecules*, 1999, **32**, 2120-2130; c) B. L. Small and M. Brookhart, *J. Am. Chem. Soc.,* 1998, **120**, 7143-7144. d) G. J. P. Britovsek, V. C. Gibson, B. S. Kimberley, P. J. Maddox, S. J. Mctavish, G. A. Solan, A. J. P. White and D. J. Williams, *Chem. Commum.,* 1998, 849-850; e) G. J. P. Britovsek, V. C. Gibson, B. S. Kimberley, P. J. Maddox, S. Mastroianni, S. J. McTavish, C. Redshaw, G. A. Solan, S. Stromberg, A. J. P. White and D. J. Williams, *J. Am. Chem. Soc*., 1999, **121**, 8728-8740.

26. a) Y. Zhang, H. Suo, F. Huang, T. Liang, X. Hu and W. H. Sun, *J. Polym. Sci., Part A*: *Polym. Chem*., 2017, **55**, 830-842; b) F. Huang, W. Zhang, Y. Sun, X. Hu, G. A. Solan and W. H. Sun, *New J. Chem.,* 2016, **40**, 8012-8023; c) W. Zhang, W. Chai, W. H. Sun, X. Hu, C. Redshaw and X. Hao, *Organometallics*, 2012, **31**, 5039-5048; d) W. H. Sun, S. Kong, W. Chi, T. Shiono, C. Redshaw, X. Hu, C. Guo and X. Hao, *Appl. Catal. A*., 2012, **67-73**, 447-449.

27. Z. Wang, R. Zhang, W. Zhang, G. A. Solan, Q. Liu, T. Liang and W. H. Sun, *Catal. Sci. Technol.*, 2019, **9**, 1933-1943.

28. V. C. Gibson, C. Redshaw, G. A. Solan, A. J. P. White and D. J. Williams, *Organometallics*, 2007, **26**, 5119-5123.

29. S. A. Gentschow, S. W. Kohl, W. Bauer, M. Hummert and A. Grohmann, *Eur. J. Inorg. Chem*., 2011, 556-566.

30. S. Dammers, T. P. Zimmermann, S. Walleck, A. Stammler, H. Bögge, E. Bill and T. Glaser, *Inorg. Chem.,* 2017, **56**, 1779-1782.

31. D. Benito-Garagorri, J. Wiedermann, M. Pollak, K. Mereiter and K. Kirchner, *Organometallics,* 2007, **26**, 217-222.

32. W. Zuo and R. H. Morris, *Nature Protocols.,* 2015, **10**, 241-257.

33. M. Zhang, P. Hao, W. Zuo, S. Jie and W.-H. Sun*, J. Organomet. Chem.*, 2008, **639**, 483-491.

34. F. Huang, W. Zhang, Y. Sun, X. Hu, G. A. Solan and W.-H. Sun, *New J. Chem.,* 2016, **40**, 8012-8023.

35. Y. Zhang, H. Suo, F. Huang, T. Liang, X. Hu and W.-H. Sun, *J. Polymer. Sci., Part A: Polym. Chem.*, 2017, **55**, 830-840.

36. a) S. Du, W. Zhang, E. Yue, F. Huang, T. Liang and W.-H. Sun, *Eur. J. Inorg. Chem*., 2016, 2016, 1748-1755; b) S. Du, X. Wang, W. Zhang, Z. Flisak, Y. Sun and W.-H. Sun, *Polym. Chem*., 2016, **7**, 4188-4197; c) C. Huang, S. Du, G. A. Solan, Y. Sun and W.-H. Sun, *Dalton Trans.,* 2017, **46**, 6948-6957.

37. a) D. J. Jones, V. C. Gibson, S. M. Green, P. J. Maddox, A. J. P. White and D. J. Williams, *J. Am. Chem. Soc.,* 2005, **127**, 11037-11046; b) A. K. Tomov, V. C. Gibson, G. J. P. Britovsek, R. J. Long, M. van Meurs, D. J. Jones, K. P. Tellmann and J. J. Chirinos, *Organometallics*, 2009, **28**, 7033-7040.

38. T. Xiao, P. Hao, G. Kehr, X. Hao, G. Erker and W.-H. Sun, *Organometallics*, 2011, **30**, 4847-4853.

39. Y. Zhang, C. Huang, X. Hao, X. Hu and W.-H. Sun, *RSC Adv.,* 2016, **6**, 91401-91408.

40. V. K. Appukuttan, Y. Liu, B. C. Son, C.-S. Ha, H. Suh and I. Kim, *Organometallics*, 2011, **30**, 2285-2294.

41. W. Zhang, W. Chai, W.-H. Sun, X. Hu, C. Redshaw and X. Hao, *Organometallics*, 2012, **31**, 5039-5048.

42. a) J. Yu, W. Huang, L. Wang, C. Redshaw and W.-H. Sun, *Dalton Trans.*, 2011, **40**, 10209-10214; b) J. Lai, W. Zhao, W. Yang, C. Redshaw, T. Liang, Y. Liu and W.-H. Sun, *Polymer Chem.*, 2012, **3**, 787-793.

43. N. V. Semikolenova, W.-H. Sun, I. E. Soshnikov, M. A. Mastsko, O. V. Kolesova, V. A. Zakharov and K. P. Bryliakov, *ACS Catal.*, 2017, **7**, 2868-2877.

44. a) W. Zhang, S. Wang, S. Du, C.-Y. Guo, X. Hao and W.-H. Sun, *Macromol. Chem. Phys.,* 2014, **215**, 1797-1809; b) S. Wang, B. Li, T. Liang, C. Redshaw, Y. Li and W.-H. Sun, *Dalton Trans.,* 2013, **42**, 9188-9197; c) T. M. Smit, A. K. Tomov, G. J. P. Britovsek, V. C. Gibson, A. J. P. White and D. J. Williams, *Catal. Sci. Technol.,* 2012, **2**, 643-655; d) W. Zhao, J. Yu, S. Song, W. Yang, H. Liu, X. Hao, C. Redshaw and W.-H. Sun, *Polymer*, 2012, **53**, 130-137; e) X. Cao, F. He, W. Zhao, Z. Cai, X. Hao, T. Shiono, C. Redshaw and W.-H. Sun, *Polymer,* 2012, **53**, 1870-1880; f) J. Lai, W. Zhao, W. Yang, C. Redshaw, T. Liang, Y. Liu and W.-H. Sun, *Polym. Chem.,* 2012, **3**, 787-793; g) N. E. Mitchell, W. C. Anderson and B. K. Long, *J. Polym. Sci., Part A: Polym. Chem.*, 2017, **55**, 3990-3996.

45. a) W. Zhang, W. Chai, W.-H. Sun, X. Hu, C. Redshaw and X. Hao, *Organometallics,* 2012, **31**, 5039-5048; b) J. Ba, S. Du, E. Yue, X. Hu, Z. Flisak and W.-H. Sun, *RSC Adv.,* 2015, **5**, 32720-32729; c) Y. Zhang, C. Huang, X. Hao, X. Hu and W.-H. Sun, *RSC Adv.,* 2016, **6**, 91401-91408; d) S. Du, X. Wang, W. Zhang, Z. Flisak, Y. Sun and W.-H. Sun, *Polym. Chem.,* 2016, **7**, 4188-4197; e) F. Huang, Q. Xiong, T. Liang, Z. Flisak, B. Ye, X. Hu, W. Yang and W.-H. Sun, *Dalton Trans.,* 2014, **43**, 16818-16829.

46. a) D. J. Jones, V. C. Gibson, S. M. Green, P. J. Maddox, A. J. P. White and D. J. Williams, *J. Am. Chem. Soc*., 2005, **127**, 11037-11046. b) A. K. Tomov, V. C. Gibson, G. J. P. Britovsek, R. J. Long, M. van Meurs, D. J. Jones, K. P. Tellmann and J. J. Chirinos, *Organometallics*, 2009, **28**, 7033-7040.

Chapter 6
Experimental

6.1 General experimental

All manipulations were performed under an inert atmosphere of nitrogen using standard glove-box and Schlenk line techniques unless stated otherwise. Solvents were distilled under nitrogen from appropriate drying agents. Dichloromethane (DCM), diethyl ether (Et_2O), toluene and tetrahydrofuran (THF) were distilled under nitrogen from the appropriate drying agents immediately prior to use. Nuclear magnetic resonance (NMR) spectra were recorded on Bruker DPX 400 (^{1}H, 400 MHz; ^{13}C, 100 MHz; ^{19}F, 376.46 MHz; ^{11}B, 128 MHz) or a Bruker Avance III 500 spectrometer (^{1}H, 500 MHz; ^{13}C, 125 MHz) instrument at ambient temperature unless otherwise stated, using deuterated chloroform ($CDCl_3$), deuterated dichloromethane (CD_2Cl_2) and deuterated acetonitrile (CD_3CN). Chemical shifts (δ) were determined with the use of the residual proton absorption of chloroform-d_1 at δ 7.26 (H) and 77.23 (C) and dichloromethane-d_2 δ 5.32 (H) and 53.5 (C) in parts per million (ppm), *J* values are given in Hz. Spectral data is reported as follows: chemical shift, integration, multiplicity with the following abbreviations for the observed peaks (s = singlet, d = doublet, dd = doublet of doublets, t = triplet, q = quartet, sept = septet, m = multiplet), coupling constant(s) and assignment. Magnetic moments for all paramagnetic complexes was measured by Evans' NMR method and recorded in CD_3CN solvent.[10-12] Column chromatography was carried out using Merck Kieselgel 60 (230-400 mesh). IR spectroscopy was carried out using a Perkin Elmer® Spectrum One FT-IR Spectrometer with a Universal ATR attachment accessory as neat films. Vibrational frequencies (ν_{max}) are reported in wavenumbers (cm^{-1}). Melting points (M.p.) were determined using a Gallenkamp melting point apparatus (model MFB-595). Electrospray mass spectrometry (ESI-MS) was recorded using a micromass Quattro LC mass spectrometer with methanol (MeOH) or acetonitrile (MeCN) as solvent. FAB mass spectra were recorded on a Kratos Concept spectrometer with *m*-nitrobenzyl alcohol (NBA) as matrix. Elemental analyses were performed at the Science Technical Support Unit, London Metropolitan University. The compounds, 2-bromo-6-acetylpyridine,[1]

bis(2,6-diisopropylphenylimino)pyridine (**L2**),[6] (**L2**)$ZnCl_2$,[7] (**L2**)$CoCl_2$,[5] (**L2**)$NiCl_2$,[7] (**L2**)$FeCl_2$,[6] H**L1**$_{Phmes}$,[4] $NiCl_2(DME)$,[13] $Pd(PPh_3)_4$[14] and $FeCl_2Py_4$[15] were made by literature procedures. All other reagents used were purchased from SigmaAldrich®, Fisher Scientific® or Alfa Aesar® and used without further purification.

6.2 Experimental procedures for Chapter 2

6.2.1 Synthesis of 3-bromobiphenyl-2-ol[2]

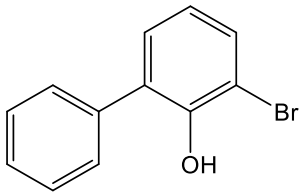

An oven dried three-necked round bottomed flask (500 mL) equipped with a magnetic stir bar and Soxhlet apparatus was charged with 2-phenylphenol (10.00 g, 58.75 mmol) and *N*-bromosuccinimide (10.45 g, 58.75 mmol, 1 eq). The system was then evacuated and backfilled with nitrogen before the addition of diisopropylamine (0.83 mL, 5.87 mmol, 0.1 eq) and freshly distilled dichloromethane (200 mL). The reaction mixture was stirred and heated to reflux for 16 h. During this period of time all the N-bromosuccinimide was gradually consumed. After cooling to room temperature, the reaction mixture was treated with 2M H_2SO_4 (200 mL). The organic phase was isolated and the aqueous layer extracted with diethyl ether (4 × 50 mL). The combined organic layers were washed with water (2 × 30 mL) and brine (2 × 30 mL) and dried over $MgSO_4$. Following filtration, the solvent was removed on the rotary evaporator to give the crude product as white oil. The product was purified in two steps. Firstly, column chromatography (petroleum ether: dichloromethane as the eluting solvent system 80:20) was used to remove the unreacted 2-phenylphenol starting material. Secondly, the resulting oil was then dissolved in the minimum quantity of hexane and the solution cooled to -30 °C overnight to form needle-like crystals. The flask was then left to warm to room temperature (*ca.* 1 h) and the remaining solid filtered affording pure mono-brominated 3-bromobiphenyl-2-ol as a white crystalline solid. This purification/separation can be repeated to obtain more of the desired mono-brominated species (12.41 g, 83%). ^{1}H NMR (400 MHz, $CDCl_3$): δ 7.51 (dd, 2H, $^3J_{HH}$ = 8.1, 1.2 Hz, Ar-H), 7.45 (dd, 2H, $^3J_{HH}$ = 7.2, 3.6 Hz, Ar-H), 7.37 (m, 2H, Ar-H, Py-H), 7.24

(dd, 1H, $^3J_{HH}$ = 7.6, 1.6 Hz, Py-H_m), 6.87 (t, 1H, $^3J_{HH}$ = 7.8 Hz, Py-H_p), 5.66 (s, 1H, OH). M.p.: 53 – 54 °C. The data collected was consistent with the literature report.[2]

6.2.2 Synthesis of 2-hydroxyphenylboronic acid (**boronic acid-a**)[2]

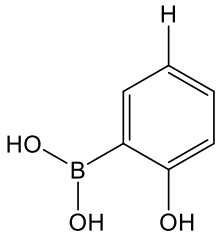

An oven dried three necked round bottom flask equipped with a stirrer bar and nitrogen inlet was evacuated and backfilled with nitrogen. 2-Bromophenol (2.64 g, 15.2 mmol) and dry diethyl ether (100 mL) were added and the solution cooled to -90 °C. *n*-BuLi (20 mL, 32.0 mmol, 2.1 eq) was added *via* syringe slowly over a period of 20 min to the cooled (-90 °C) solution. The reaction mixture was then allowed to warm to room temperature and stirred for 2 h under nitrogen. The flask was cooled back to -90 ^oC and a solution of triisopropylborate (5.86 mL, 25 mmol, 1.67 eq) was added rapidly. The reaction was left to stir for 0.5 h at -90 °C and then brought to room temperature and allowed to stir for 15 h under nitrogen to form a white precipitate. The mixture was cooled to 0 °C and 2M HCl (13 mL) slowly added and the reaction mixture left to stir for a further 0.5 h resulting in complete dissolution of the white precipitate. All the solvent including the aqueous layer were removed under reduced pressure affording **boronic acid-a** as a white solid (1.68 g, 80%). ^1H NMR (400 MHz, MeOD): Multiple resonances in the aromatic region were observable that could not be assigned. Nonetheless, this crude product was used without further purification.

6.2.3 Synthesis of 2-hydroxy-biphenyl-3-yl boronic acid (**boronic acid-b**)[1]

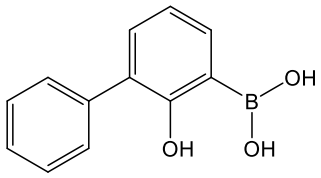

An oven dried three-necked round bottomed flask (500 mL) equipped with magnetic stir bar was evacuated and backfilled with nitrogen before 3-bromobiphenyl-2-ol (6.0 24.11 mmol) and dry diethyl ether (160 mL) were added. The solution was stirred and cooled to -90 °C before *n*-BuLi (30 mL, 48 mmol, 2.1 eq) was added dropwise. The

solution was then allowed to warm to room temperature and stirred for 2 h producing a milky white precipitate. The reaction mixture was then cooled to -90 °C with continuous stirring and a solution of triisopropyl borate (8.82 mL, 38.8 mmol, 1.67 eq) rapidly added. The reaction was cooled to 0 °C in an ice bath and 2M HCl (26 mL) was gradually added and the reaction mixture stirred for further 30 min until the white emulsion had become clear. The organic phase was isolated and the aqueous layer was washed with diethyl ether (3×50 mL). The combined organic extracts were dried over $MgSO_4$ and filtered. The filtrate was collected and solvent removed under reduced pressure affording a gummy grey solid. The solid was then washed with petroleum ether (40:60) forming **boronic acid-b** as a free flowing white solid (4.52 g, 92%). ^{1}H NMR (400 MHz, MeOD): Multiple resonances in the aromatic region were observable that could not be assigned. Nonetheless, this crude product was used without further purification.

6.2.4 Synthesis of 2-hydroxy-4-*tert*-butylphenylboronic (**boronic acid-c**)

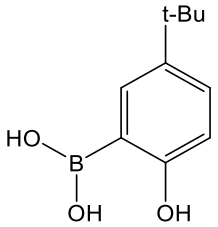

A similar procedure to that outlined for **boronic acid-a** and **boronic acid-b** was followed using 2-bromo-4-*tert*-butyphenol (3.317 g, 14.5 mmol) affording **boronic acid-c** as a creamy white solid (2.714 g, 98%). ^{1}H NMR (400 MHz, $CDCl_3$): δ 7.17 (s, br, 1H, Ar-H), 7.11 (dd, 1H, $^3J_{HH}$ = 7.8 Hz, $^4J_{HH}$ = 3.0 Hz, Ar-H), 6.70 (dt, 1H, $^3J_{HH}$ = 7.8 Hz, $^5J_{HH}$ = 2.6 Hz, Ar-H), 1.22 (s, 9H, Ar-C$(CH_3)_3$). No further characterisation data was recorded and the crude sample was used in the subsequent Suzuki cross coupling reaction.

6.2.5 Synthesis of **ketone-a**[2]

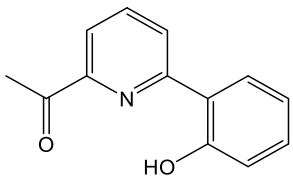

An oven dried Schlenk flask equipped with a stir bar was evacuated and backfilled with nitrogen. The flask was charged with 2-bromo-6-acetyl pyridine (0.894 g, 4.47 mmol), $Pd(PPh_3)_4$ (0.109 g, 0.094 mmol 0.02 eq), dry toluene (20 mL) and an aqueous 2M solution of potassium carbonate (4.45 mL, 8.94 mmol, 2 eq). The solution was then stirred at room temperature for 15 min before a solution of **boronic acid-a** (0.800 g, 5.89 mmol, 1.3 eq) in ethanol (11 mL) was added. After heating to reflux for 42 h, the mixture was left to cool to room temperature and 30% hydrogen peroxide (0.4 mL) added. The mixture was left to stir at room temperature for 30 min and the product extracted with diethyl ether (2 × 100 mL), washed with saturated sodium chloride solution and water (3 × 30 mL) to give an orange organic layer. The aqueous layers was washed repeatedly with chloroform until the extracts were colourless. The organic extracts were combined and dried with $MgSO_4$ and all volatiles removed under reduced pressure to five an orange brown residue. The residue was then recrystallised from methanol to give **ketone-a** as a yellow solid (0.762 g, 80%). ^{1}H NMR (400 MHz, $CDCl_3$): δ 13.65 (s, 1H, OH), 8.07 (dd, 1H, $^3J_{HH}$ = 7.0, $^4J_{HH}$ = 2.0 Hz, Py-H_m), 7.97 (m, 2H, Py-H_m), 7.79 (dd, 1H, $^3J_{HH}$ = 8.0 Hz, $^4J_{HH}$ = 1.6 Hz, Ar-H), 7.32 (td, 1H, $^3J_{HH}$ = 7.0 Hz, $^4J_{HH}$ = 2.0 Hz, Py-H_p), 7.02 (dd, 1H, $^3J_{HH}$ = 8.4 Hz, $^4J_{HH}$ = 1.2 Hz Ar-H), 6.92 (td, 1H, $^3J_{HH}$ 8.4, $^4J_{HH}$ = 1.6 Hz, Ar-H), 2.71 (s, 3H, CH_3). ^{13}C {^{1}H} NMR (100 MHz, $CDCl_3$): δ 196.4 (MeC=O), 158.5 (C), 156.2 (C), 149.0 (C), 137.75 (CH), 131.1 (CH), 121.8 (CH), 118.8 (CH), 118.3 (CH), 117.6 (CH), 117.3 (C), 25.1 (CCH_3=O). IR (cm^{-1}): 750 (Orthosub'd-Ar), 1225 (Ar-OH), 1588 (Ar-C=C), 1692 (C=O). ESIMS (+ve, MeOH): *m/z* 214 $[M+H]^+$, ESIMS (-ve, MeOH): *m/z* 212 $[M-H]^-$. HRMS: (TOF): Calculated for $C_{13}H_{12}NO_2$ $[M+H]^+$ 214.0868, found: 214.0868. M.p.: 100-104 ℃.[2]

6.2.6 Synthesis of **ketone-b**[3]

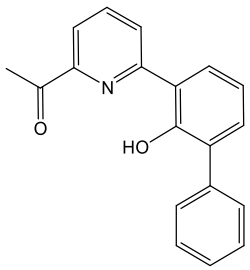

An oven-dried large size Schlenk vessel containing a magnetic stirring bar was evacuated, backfilled with nitrogen and charged with 2-bromo-6-acetyl pyridine (1.144 g, 7.22 mmol), $Pd(PPh_3)_4$ (0.166 g, 0.144 mmol, 0.02 eq), toluene (20 mL) and an aqueous 2M solution of potassium carbonate (7.23 mL, 14.45 mmol, 2 eq). The solution was stirred at ambient temperature for 15 min before the addition of **boronic acid-b** (1.320 g, 10.84 mmol, 1.5 eq) in ethanol (10 mL). The mixture was then stirred and heated to 90 °C for 72 h. On cooling to room temperature 30% hydrogen peroxide (0.5 mL) was added. The mixture was stirred at room temperature for further half hour. The organic phase was separated and the aqueous phase washed with diethylether (4 × 50 mL). The aqueous phase was extracted and washed continually with chloroform until the extracts become clear. The combined organic extracts were then washed with brine (30 mL) and water (2×30 mL) and dried over $MgSO_4$ and filtered. The solvent was removed under reduced pressure giving a brown residue. The residue was then recrystallised from methanol affording **ketone-b** as a yellow solid (1.61 g, 80%). ^{1}H NMR (400 MHz, $CDCl_3$): δ 14.03 (s, 1H, OH), 8.18 (dd, 1H, $^3J_{HH}$ = 9.2 Hz, $^4J_{HH}$ = 1.6Hz, Py-H_p,), 8.02 (d, 1H, $^3J_{HH}$ = 7.8 Hz, Py-H_p), 8.01 (dd, 1H, $^3J_{HH}$ = 9.8, $^4J_{HH}$ = 2.0 Hz, Py-H_m), 7.85 (dd, 1H, $^3J_{HH}$ = 9.6 Hz, $^4J_{HH}$ = 1.5 Hz, Ar-H), 7.66 (dd, 2H, $^3J_{HH}$ = 0.8 Hz, Ar-H), 7.44 (t, 2H, $^3J_{HH}$ = 7.2 Hz, Ar-H), 7.30 (dd, $^3J_{HH}$ = 1.5 Hz, Ar-H), 7.37 (tt, 1H, $^3J_{HH}$ = 1.2 Hz , Ar-H), 7.04 (t, 1H, $^3J_{HH}$ = 6.3 Hz, Ar-H), 2.75 (s, 3H, COMe). ^{13}C {^{1}H} NMR (100 MHz, $CDCl_3$): 197.6 (C=O), 157.5 (CH), 156.8 (CH), 149.9 (CH), 138.8 (CH), 138.2 (CH), 135.2 (CH), 133.3 (C), 129.5 (CH), 128.2 (C), 127.7 (CH), 126.1 (CH), 123.3 (CH), 119.8 (CH), 119.1 (CH), 118.6 (C), 26.3 (CH_3). IR (cm^{-1}): 3055 (C-H), 2565 (O-H), 1698 (C=O), 1585 ($C=N_{pyridine}$), 1250 and 1104 ($C-O_{phenol}$). ESIMS (+ve, MeOH): *m/z* 290 $[M+H]^+$, 312 $[M+Na]^+$. HRMS (TOF): calculated for $C_{19}H_{16}NO_2$ $[M+H]^+$ 290.1181, found: 290.1169. M.p.: 115-116 ℃. [3]

6.2.7 Synthesis of **ketone-c**

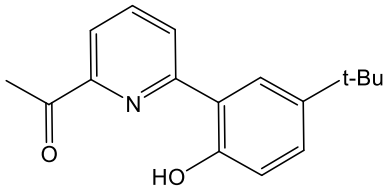

A similar procedure to that outlined for **ketone-a** and **ketone-b** was followed using 2-bromo-6-acetylpyridine (0.893 g, 4.47 mmol), $Pd(PPh_3)_4$ (0.106 g, 0.092 mmol 0.02 eq), dry toluene (20 mL), an aqueous 2M solution of potassium carbonate (4.45 mL, 8.94 mmol 2 eq) and **boronic acid-c** (1.128 g, 5.80 mmol) in ethanol (11 mL). Following work-up **ketone-c** was obtained as a pale yellow solid (0.700 g, 59%). ^{1}H NMR (400 MHz, $CDCl_3$): δ 13.38 (s, 1H, OH), 8.06-8.08 (dd, 1H, $^3J_{HH}$ = 7.8 Hz, $^4J_{HH}$ = 1.4Hz, Py-H_p), 7.89-7.96 (m, 2H, Py-H_m), 7.74-7.76 (d, 1H, $^3J_{HH}$ = 8.4 Hz, Ar-H), 7.34-7.36 (dd, 1H, $^3J_{HH}$ = 8.8 Hz, $^4J_{HH}$ = 2.4 Hz, Ar-H), 6.93-6.96 (d, 1H, $^3J_{HH}$ = 8.4 Hz Ar-H), 2.70 (s, 3H, CCH_3=O), 1.30 (s, 9H, C-$(CH_3)_3$). ^{13}C {^{1}H} NMR (100 MHz, $CDCl_3$): δ 196.6 (MeC=O), 156.7 (C), 156.1 (C), 149.1 (C), 140.9 (C), 137.7 (CH), 128.6 (CH), 121.9 (CH), 121.8 (CH), 118.6 (CH), 118.6 (CH), 117.1(CH), 116.5 (C), 30.5 (C-$(CH_3)_3$), 25.1 (CCH_3=O). IR (cm^{-1}): 1201 (Ar-OH), 1455, 1493, 1588 (Ar C=C), 1702(C=O). HRMS (TOF): calculated for $C_{16}H_{20}NO_2$ $[M+H]^+$ 270.1505, found: 270.1505. ESIMS (+ve, MeOH): *m/z* 270 $[M+H]^+$. ESIMS (-ve, MeOH): *m/z* 268 $[M-H]^-$. M.p.: 111-113 ℃.

6.2.8 Synthesis of H**L1**$_H$ [3]

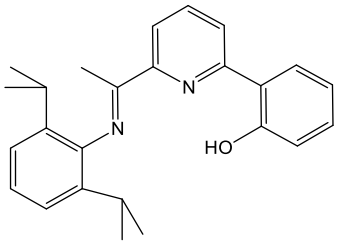

A 50 mL round bottom flask, equipped with a stir bar and reflux condenser, was charged with a solution of **ketone-a** (0.465 g, 2.18 mmol) in methanol (*ca.* 3-4 mL) and 2,6-diisopropylaniline (0.584 g, 3.27 mmol, 1.5 eq). The reaction was stirred at reflux for 5 min before the addition of 2-4 drops of formic acid. After the solution was left under reflux for two days, the reaction mixture was cooled to room temperature and

then left to stand for 3 h. The resulting suspension was filtered, washed with cold methanol and dried to give H**L1**$_{\mathbf{H}}$ as yellow solid (0.630 g, 78%). ^{1}H NMR (400 MHz, $CDCl_3$): δ 14.16 (s, 1H, OH), 8.24-8.25 (d, 1H, $^{3}J_{HH}$ = 7.7 Hz, Py-H$_m$), 7.97-7.99 (d, 1H, $^{3}J_{HH}$ = 7.7 Hz, Py-H$_m$), 7.89-7.93 (t, 1H, $^{3}J_{HH}$ = 7.7 Hz, Py-H$_p$), 7.79-7.82 (dd, 1H, $^{3}J_{HH}$ = 8.0 Hz, $^{4}J_{HH}$ = 1.6 Hz, Ar-H), 7.26-7.30 (td, $^{3}J_{HH}$ = 8.4 Hz, $^{4}J_{HH}$ = 1.6 Hz, Ar-H), 7.12 (d, 1H, $^{3}J_{HH}$ = 1.6 Hz, Ar-H), 7.10 (s, 1H, Ar-H), 7.03-7.05 (t, 1H, $^{3}J_{HH}$ = 8.0 Hz, Ar-H), 6.97-6.99 (d, 1H, $^{3}J_{HH}$ = 8.0 Hz, Ar-H), 6.88-6.92 (t, 1H, $^{3}J_{HH}$ = 7.6 Hz, Ar-H), 2.62-2.71 (sept, 2H, $^{3}J_{HH}$ = 6.8 Hz, CH-$(CH_3)_2$), 2.19 (s, 3H, N=CCH_3), 1.07-1.09 (d, 12H, $^{3}J_{HH}$ = 7.6 Hz, CH-$(CH_3)_2$). ^{13}C{^{1}H} NMR (100 MHz, $CDCl_3$): δ 164.8 (C=N), 159.6 (C), 156.9 (C), 153.2 (C), 146.0 (C), 138.4 (CH), 135.7 (C), 131.8 (CH), 126.5 (CH), 124.0 (CH), 123.1 (CH), 120.4 (CH), 119.4 (CH), 119.2 (CH), 118.8 (C), 118.5 (CH), 28.4 (H-C-$(CH_3)_2$), 23.2 (H-C-$(CH_3)_2$), 22.9 (H-C$(CH_3)_2$), 17.4 (N=C-CH_3). IR (cm^{-1}): 791 (Orthosub'd-Ar), 1222 (Ar-OH), 1457, 1503, 1587 (Ar C=C), 1640 (C=N). ESIMS (+ve, MeOH): *m/z* 373 $[M+H]^+$, ESIMS (-ve, MeOH): *m/z* 371 $[M-H]^-$. M.p.: 181-183 °C.[3]

6.2.9 Synthesis of H**L1**$_{Ph}$ [3,4]

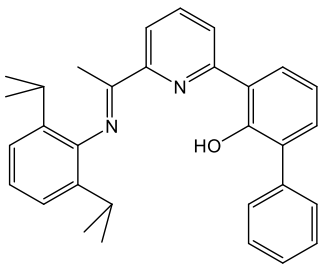

A 50 mL round bottomed flask equipped with a magnetic stirrer bar and reflux condenser, was charged with **ketone-b** (0.404 g, 1.39 mmol), methanol (10 mL) and distilled 2,6-diisopropylaniline (0.367 g, 1.38 mmol, 1.5 eq). The solution mixture was stirred at reflux for 5 min, prior to the addition of 1-2 drops of formic acid. The reaction was then heated to reflux for 72 h. On cooling to room temperature a precipitate was formed that was filtered, washed with cold methanol and dried under reduced pressure. The product, H**L1**$_{Ph}$, was isolated as white-yellow solid (0.700 g, 99%). ^{1}H NMR (400 MHz, $CDCl_3$): δ 14.44 (s, 1H, OH), 8.33 (dd, 1H, $^{3}J_{HH}$ 7.7, $^{4}J_{HH}$ 0.8 Hz, Py-H$_m$), 8.08 (dd, 1H, $^{3}J_{HH}$ 8.1, $^{4}J_{HH}$ 0.6 Hz, Py-H$_m$), 7.99 (t, 1H, $^{3}J_{HH}$ 7.9 Hz, Py-H$_p$), 7.87 (dd, 1H, $^{3}J_{HH}$ = 9.7 Hz, $^{4}J_{HH}$ = 1.6 Hz, Ar-H), 7.66 (dd, 2H, $^{3}J_{HH}$ = 9.4 Hz, $^{4}J_{HH}$ = 1.3 Hz,

Ar-H), 7.43 (t, 2H, $^{3}J_{HH}$ = 7.5 Hz, Ar-H), 7.40 (dd, $^{3}J_{HH}$ = 9.0 Hz, $^{4}J_{HH}$ = 1.5 Hz, Ar-H), 7.33 (tt, $^{3}J_{HH}$ = 8.0 Hz, $^{4}J_{HH}$ = 1.2 Hz, Ar-H), 7.16 (m, 3H, Ar-H), 7.05 (t, 1H, $^{3}J_{HH}$ = 7.7 Hz, Ar-H), 2.70 (sept, 2H, $^{3}J_{HH}$ = 6.8 Hz, $CH(CH_3)_2$), 2.23 (s, 3H, $C=NCH_3$), 1.13 (m, 12H, $CH(CH_3)_2$). $^{13}C\{^{1}H\}$ NMR (100 MHz, $CDCl_3$); δ 164.8 (C=N), 157.1 (C), 156.9 (C), 153.0 (C), 145.9 (C), 138.4 (CH), 135.7 (C), 132.9 (CH), 131.2 (C), 129.5 (CH), 128.1 (CH), 127.0 (CH), 126 (CH), 123.2 (CH), 123.0 (CH), 120.8 (C), 119.4 (CH), 119.1 (CH) , 118.9 (CH), 28.3 (CH), 23.1 (CH_3), 22.8 (CH_3), 17.5 (CH_3). IR (cm^{-1}): 3058 (C-H str. For CH_3), 1625 ($C=N_{imine}$), 1591 ($C=N_{pyridine}$). ESIMS: *m/z* 449 $[M+H]^{+}$. M.p: 196-197 ℃.[3,4]

6.2.10 Synthesis of H**L1**$_{tBu}$

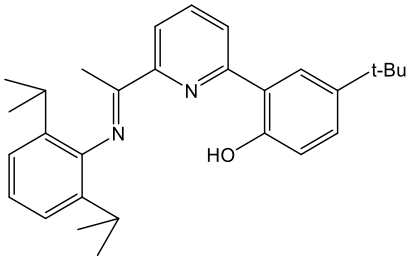

A similar procedure to that outlined for H**L1**$_{H}$ was followed using **ketone-c** (1.00 g, 3.72 mmol) methanol (*ca*. 10 mL) and 2,6-diisopropylaniline (0.989 g, 5.58 mmol, 1.5 eq) producing H**L1**$_{tBu}$ as a yellow solid (1.402 g, 88%). ^{1}H NMR (400 MHz, $CDCl_3$): δ 13.85 (s, 1H, OH), 8.21-8.23 (dd, 1H, $^{3}J_{HH}$ = 7.6 Hz, $^{4}J_{HH}$ = 0.8 Hz, Py-H), 7.97-7.99 (d, 1H, $^{3}J_{HH}$ = 7.6Hz, Py-H), 7.89-7.93 (t, 1H, $^{3}J_{HH}$ = 7.6Hz, Py-H), 7.77 (d, 1H, $^{3}J_{HH}$ = 2.4 Hz, Ar-H,), 7.31-7.34 (dd, 1H, $^{3}J_{HH}$ = 8.4 Hz, $^{4}J_{HH}$ = 2.5 Hz, Ar-H), 7.11-7.12 (d, 1H, $^{3}J_{HH}$ = 1.6 Hz, Ar-H), 7.02-7.06 (m, 1H, Ar-H), 6.91-6.93 (d, 1H, $^{3}J_{HH}$ = 8.4 Hz, Ar-H), 2.06-2.07 (sept, 2H, $^{3}J_{HH}$ = 6.8 Hz, $CH\text{-}(CH_3)_2$), 2.18 (s, 3H, $N=CCH_3$), 1.31 (s, 9H, $C\text{-}(CH_3)_3$), 1.07-1.09 (dd, 12H, $^{3}J_{HH}$ = 6.8 Hz, $^{4}J_{HH}$ = 2.0 Hz, $CH\text{-}(CH_3)_2$), ^{13}C $\{^{1}H\}$ NMR (100 MHz, $CDCl_3$): δ 163.9 (C=N), 156.2 (C), 156.2 (C), 152.2 (C), 140.7 (C), 116.9 (CH), 33.2 ($C(CH_3)_3$), 30.5 ($C(CH_3)_3$), 28.7 (C), 27.3 ($H\text{-}C\text{-}(CH_3)_2$), 22.2 ($H\text{-}C\text{-}(CH_3)_2$), 21.8 ($H\text{-}C\text{-}(CH_3)_2$), 16.3 ($N=C\text{-}CH_3$). IR ($cm^{-1}$): 1226 (Ar-OH), 1459 1566, 1584 (Ar C=C), 1648 $(C=N)_{imine}$. HRMS (TOF): calculated: 429.2906, found: 429.2900. ESIMS (+ve, MeOH): *m/z* 429 $[M+H]^{+}$. ESIMS (-ve, MeOH): *m/z* 427 $[M-H]^{-}$. M.p: 158-161℃.[5]

6.2.11 Synthesis of H_2**L3**$_H$ [3]

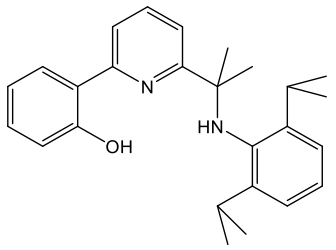

An oven dried Schlenk flask equipped with a magnetic stir bar was evacuated and backfilled with nitrogen. To the flask was added H**L1**$_H$ (601 mg, 2.70 mmol) and toluene (20 mL) followed by the syringed addition of two equivalents of $AlMe_3$ (3.4 mL, 6.07 mmol, 2M solution in toluene). The reaction mixture was stirred and heated to 110 ℃ for 12 h. On cooling to room temperature all volatiles were removed under reduced pressure. Petroleum ether (40-60) (20 mL) was added and the flask cooled to 0 ℃. Water (20 mL) was carefully added dropwise and the suspension stirred at room temperature for a further 3 h. The combined organic phases were dried over $MgSO_4$. Following filtration the volatiles were removed under reduced pressure to give H**L3**$_H$ as a brown oil (549 mg, 80%). ^{1}H NMR (400 MHz, $CDCl_3$): δ 7.76 (m, 3H, CH), 7.59 (dd, 1H, $^3J_{HH}$ = 7.3 Hz, $^4J_{HH}$ = 1.4 Hz, CH), 7.22 (dt, 1H, $^3J_{HH}$ = 1.7 Hz, CH), 6.92-6.98 (m, 4H, CH), 6.85 (dt, 1H, $^3J_{HH}$ =7.6 Hz, $^4J_{HH}$ = 1.2 Hz, CH), 3.35 (broad s, 1H, OH), 2.92 (sept, 2H, $^3J_{HH}$ = 7.0 Hz, C*H*Me$_2$), 1.48 (s, 6H, NC*Me*$_2$), 0.98 (d, 12H, $^3J_{HH}$ = 7.0 Hz, CH*Me*$_2$). ^{13}C NMR (100 MHz, $CDCl_3$): δ 165.1 (C), 159.0 (C), 155.5 (C), 144.3 (C), 138.7 (C), 137.0 (C), 130 3 (C), 125.3 (C), 123.5 (C), 122.1 (2C), 118.1 (C), 117.7 (C), 117.4 (C), 117.2 (C), 115.7 (C), 58.1 (1C, N*C*Me$_2$), 28.2 (2C, NC*Me*$_2$), 27.4 (CHMe$_2$), 22.8 (CHMe$_2$). IR (cm^{-1}): 1596 (C=N$_{pyridine}$), 3352 (N-H). ESIMS (+ve, MeOH): *m/z* 389 $[M+H]^+$.[3]

6.2.12 Synthesis of H**L4**[6]

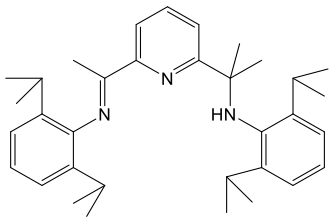

A Schlenk vessel was evacuated and backfilled with nitrogen. The vessel was charged with a solution of **L2** (0.40 g, 0.83 mmol) in dry toluene (40 mL) and trimethylaluminium (0.83 ml, 1.66 mmol, 2M solution in toluene) added dropwise. The resulting solution was stirred and heated to reflux overnight. On cooling to room temperature, the volatiles were removed under reduced pressure. The residue was then dissolved in hot dry acetonitrile (*ca.* 15 mL) and transferred by cannular filtration into a second Schlenk vessel under nitrogen. On standing at room temperature overnight golden blocks of the aluminium-containing intermediate were formed. The solvent was then removed by cannular and the crystals dried under reduced pressure. Bench diethyl ether (30 mL) was added to the crystals followed by the careful addition of water (20 mL). After stirring for 3 h, the aqueous layer was separated and extracted with diethyl ether (3 × 30 mL). The combined organic extracts were dried over $MgSO_4$, filtered and the volatiles removed under pressure to give H**L4** as yellow powder (0.38 g, 71%). ^{1}H NMR (400 MHz, $CDCl_3$,): δ 8.25 (d, 1H, $^3J_{HH}$ = 7.7 Hz, Py-H_m), 7.79 (app. t, 1H, $^3J_{HH}$ = 7.7 Hz, Py-H_p), 7.59 (d, 1H, Py-H_m), 7.2-7.0 (m, 6H, Ar-H), 4.47 (s, br, 1H, NH), 3.31 (sept, 2H, $^3J_{HH}$ = 6.7 Hz,C*H*Me_2), 2.77 (sept, 2H, $^3J_{HH}$ = 6.7 Hz, C*H*Me_2), 2.24 (s, 3H, N=CMe), 1.51 (s, 6H, N-C*Me*$_2$), 1.17 (d, 12H, $^3J_{HH}$ = 6.2 CH*Me*$_2$), 1.07 (d, 12H, $^3J_{HH}$ = 6.8 CH*Me*$_2$). IR (cm^{-1}): 1599 (C=$N_{pyridine}$), 3362 (N-H). ESIMS (+ve, MeOH): *m/z* 498 $[M+H]^+$. The data were consistent with that previously reported.[6]

6.2.13 Synthesis of (H**L1**$_H$)$ZnCl_2$ (**2.1a**)

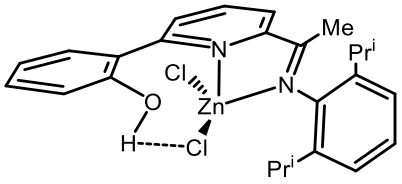

A small oven dried Schlenk flask, equipped with a magnetic stir bar, was evacuated and backfilled with nitrogen and then charged with anhydrous $ZnCl_2$ (13.15 mg, 0.097 mmol, 1.2 eq) and H**L1**$_H$ (30 mg, 0.080 mmol). Dry THF (10 mL) was then added to the flask and the reaction mixture stirred at room temperature for 16 h. The solvent was removed under reduced pressure and residue recrystallised from hot acetonitrile to give, after several days, **2.1a** as yellow crystals (47.67 mg, 70%). ^{1}H NMR (400 MHz, CD_3CN, 298 K): δ 8.35 (t, 1H, $^3J_{HH}$ = 7.7 Hz, Py-H$_p$), 8.29 (d, 1H, $^3J_{HH}$ = 7.6 Hz, Py-H$_m$), 8.16 (d, 1H, $^3J_{HH}$ = 7.9 Hz, Py-H$_m$), 7.72 (d, 1H, $^3J_{HH}$ = 6.0 Hz, Ar-H), 7.59 (t, 1H, $^3J_{HH}$ = 6.0 Hz, Ar-H), 7.49 (t, 1H, $^3J_{HH}$ = 6.3 Hz, Ar-H), 7.40 (t, 1H, $^3J_{HH}$ = 6.9 Hz, $^4J_{HH}$ = 1.2 Hz, Ar-H), 7.31 (s, 2H, Ar-H), 7.12 (t, 1H, $^3J_{HH}$ = 6.8 Hz, $^4J_{HH}$ = 1.1 Hz, Ar-H), 5.67(s, 1H, OH), 2.88 (sept, 2H, $^3J_{HH}$ = 6.6 Hz, C*H*(Me)$_2$), 2.39 (s, 3H, N=C*Me*), 1.21 (d, 6H, $^3J_{HH}$ = 7.0, CH*Me*$_2$), 1.09 (d, 6H, $^3J_{HH}$ = 6.7, CH*Me*$_2$), IR (cm^{-1}): 1246 (C-O), 1431 (C=N$_{py}$), 1618 (C=N$_{imine}$), 3379 (Ar-OH). ESIMS (+ve, MeCN): 471 [M-Cl]$^+$. TOFMS (ASAP): *m/z* calculated for $C_{25}H_{28}N_2OZnCl$ [M-Cl]$^+$ 471.8300， $C_{25}H_{27}N_2OZn$ [M-HCl$_2$]$^+$ 436.1500; found 471.1151, 436.1584. Anal. Calc for ($C_{25}H_{28}N_2OZnCl_2$): C 58.96, H 5.50, N 5.50%. Found C 58.79, H 5.46, N 5.28%.

6.2.14 Synthesis of (H**L1**$_{Ph}$)$ZnCl_2$ (**2.1b**)

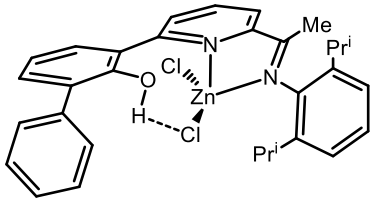

A small oven dried Schlenk flask equipped with a magnetic stir bar was evacuated and backfilled with nitrogen and then charged with anhydrous $ZnCl_2$ (10.93 mg, 0.08 mmol, 1.2 eq) and H**L1**$_{Ph}$ (30 mg, 0.0682 mmol), Following this addition, dry THF (10 mL) was added and the contents of the flask stirred at room temperature for 16 h. The solvent was removed under reduced pressure and the residue recrystallised from a hot

acetonitrile affording yellow crystals of **2.1b** after few days (26.29 mg, 66%). ^{1}H NMR (400 MHz, $CDCl_3$, 298K): δ 8.20 (t, 1H, $^{3}J_{HH}$ = 8.0 Hz, Py-H_p), 8.02 (d, 1H, $^{3}J_{HH}$ = 6.6 Hz, Py-H_m), 7.98 (d, 1H, $^{3}J_{HH}$ = 6.0 Hz, Py-H_m), 7.60 (dd, 1H $^{3}J_{HH}$ = 12.0 Hz, $^{4}J_{HH}$ = 1.2 Hz, Ar-H), 7.50 (d, 2H, $^{3}J_{HH}$ = 8.0 Hz, Ar-H), 7.40 (t, 2H, $^{3}J_{HH}$ = 8.0 Hz, Ar-H), 7.38 (dd, 1H, $^{3}J_{HH}$ = 8.0 Hz, $^{4}J_{HH}$ = 1.2 Hz, Ar-H), 7.34(t, 1H, $^{3}J_{HH}$ = 8.0 Hz, Ar-H), 7.24 (m, 3H, Ar-H), 7.15 (t, 1H, $^{3}J_{HH}$ = 8.0 Hz, Ar-H), 5.71 (s, 1H, OH), 2.93 (sept, 2H, $^{3}J_{HH}$ = 6.83 Hz, C*H*Me_2), 2.37 (s, 3H, N=C*Me*), 1.24(d, 6H, $^{3}J_{HH}$ = 6.8 Hz, CH*Me*$_2$), 0.99 (d, 6H, $^{3}J_{HH}$ = 7.0, CH*Me*$_2$). IR (cm^{-1}): 1460 (C=N_{py}), 1621 (C=N_{imine}), 3229 (Ar-OH). ESIMS (+ve, MeCN): *m/z* 547 $[M\text{-}Cl]^+$. TOFMS (ASAP): *m/z* calculated for $C_{31}H_{32}N_2OZnCl$ $[M\text{-}Cl]^+$ 547.1534, $C_{31}H_{31}N_2OZn$ $[M\text{-}HCl_2]^+$ 513.1893; found 547.5542, 513.7654. Anal. Calc for ($C_{31}H_{32}N_2OZnCl_2$): C 63.67, H 5.48, N 4.29. Found C 63.38, H 5.54, N 4.84%.

6.2.15 Synthesis of (**L1**$_{tBu}$)$_2Zn_2Cl_2$ (**2.2c**)

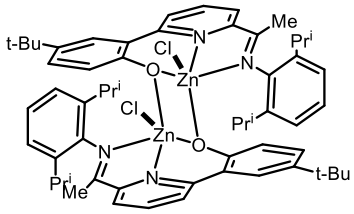

A small oven dried Schlenk flask equipped with a magnetic stir bar was evacuated and backfilled with nitrogen and then charged with anhydrous $ZnCl_2$ (11.46 mg, 0.084 mmol, 1.2 eq) and H**L1**$_{tBu}$ (30 mg, 0.070 mmol). Dry THF (10 mL) was then added and the mixture stirred at room temperature for 16 h. The solvent was removed under reduced pressure and the residue recrystallised from a hot acetonitrile affording after several days **2.2c** as yellow crystals (58.46 mg, 79%). IR (cm^{-1}): 1257 (C-O) 1464(C=N_{Py}), 1595 (C=N_{imine}), 2961 (CH_3), ESIMS (+ve, MeCN): *m/z* 1021 $[M\text{-}Cl]^+$. TOFMS (ASAP): *m/z* calculated for $C_{58}H_{70}N_4O_2ZnCl$ $[M\text{-}Cl]^+$, 1021.2123, found 1021.3727. Anal. Calc for ($C_{58}H_{70}N_4O_2ZnCl_2 \cdot 2H_2O$): C 63.75, H 6.78, N 5.13. Found C 63.68, H 6.92, N 5.62%.

6.2.16 Synthesis of (**L2**)$ZnCl_2$ [7]

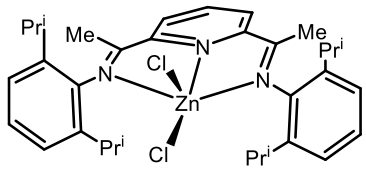

A similar procedure to that outlined for **2.1** and **2.2** was followed using **L2** (30 mg, 0.062 mmol), $ZnCl_2$ (10.20 mg, 0.075 mmol, 1.2 eq) and dry THF (10 mL). Recrystallisation from a mixture of acetonitrile and dichloromethane (2:1) gave (**L2**)$ZnCl_2$ as yellow needle-like crystals (31.19 mg, 81%). The spectroscopic data were consistent with that previously reported.[47] ^{1}H NMR (500 MHz, DMSO-d_6): δ 8.45 (d, 2H, $^3J_{HH}$ = 8.0 Hz, Py-H_m), 8.15 (t, 1H, $^3J_{HH}$ = 8.0 Hz, Py-H_p), 7.19-7.06 (m, 6H, Ar-H), 2.69 (sept, 4H, $^3J_{HH}$ = 6.5 Hz, C*H*Me$_2$), 2.21 (s, 6H, N=C*Me*), 1.11 (dd, 24H, $^4J_{HH}$ = 6.5 Hz, $^3J_{HH}$ = 1.3 CH*Me*$_2$). IR (cm^{-1}): 1579 (C=N_{imine}), 1421(C=N_{Py}), 770 (C-H). Anal. Calc. for ($C_{33}H_{43}N_3Cl_2Zn$): C 64.13, H 7.01, N 6.80. Found: C 64.30, H 6.91, N 6.65%.[7]

6.2.17 Synthesis of (H**L4**)$ZnCl_2$ (**2.3**)

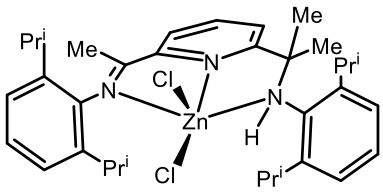

A similar procedure to that outlined for **2.1** and **2.2** was followed using H**L4** (30 mg, 0.0604 mmol), $ZnCl_2$ (16.45 mg, 0.0724 mmol, 1.2 eq.) and dry THF (10 mL). Recrystallisation of the residue from a mixture of acetonitrile and dichloromethane gave **2.3** as a pale yellow powder (32.09 mg, 32%). IR (cm^{-1}): 1464 (C=N_{Py}), 1624 (C=N_{imine}), 2961 (CH_3), 3298 (N-H). ESIMS (+ve, MeCN): *m/z* 561 $[M\text{-}2Cl]^{2+}$. TOFMS (ASAP): *m/z* calculated for $C_{34}H_{47}N_3Zn$ $[M\text{-}2Cl]^{2+}$561.3800; found 561.1287.

6.2.18 Synthesis of bis(ligand) complex (**2.4)** (Ar = 2,4,6-$Me_3C_6H_2$)

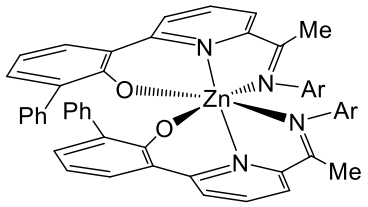

A small oven dried Schlenk flask equipped with a magnetic stir bar was evacuated and backfilled with nitrogen and then charged with 2-((2'-OH-C_6H_4)-6-(CMe=N(2,4,6-$Me_3C_6H_2$))C_5H_3N (H**L1**$_{Phmes}$) (50 mg, 0.123 mmol) and dissolved in dry toluene (10 mL). After stirring at room temperature for 10 min, the solution was cooled to -78 ^oC before the addition of a $ZnEt_2$ solution (0.26 mL, 0.135 mmol, 2.1 eq.; 1.0 M in hexanes) resulting in an immediate colour from yellow to red. The tap of the Schlenk flask was left open to the nitrogen bubbler to allow release of the eliminated ethane. After stirring at room temperature for 12 h, the red solution became gradually orange. All volatiles were removed under reduced pressure and the orange residue crystallised from dry acetonitrile affording **2.4** as bright orange cube-like crystals (51.78 mg, 52%). IR (cm^{-1}): 2961 (CH_3), 1628 ($C=N_{imine}$), 1501 ($C=N_{Py}$), 1102 (C-O).

6.2.19 Synthesis of [(**L1**$_H$)$_2$$Zn_2$(Py)(MeCN)][$BF_4$]$_2$ (**2.5a**)

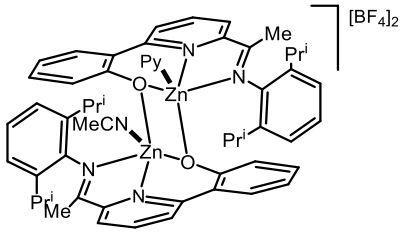

Two small oven dried Schlenk flasks equipped with magnetic stir bars were evacuated and backfilled with nitrogen. In one of the flasks, zinc(II) tetrafluoroborate hydrate (38.45 mg, 0.161 mmol, 1.2 eq) was dissolved in dry acetonitrile (5 mL) and three drops of distilled pyridine added dropwise. The solution was stirred for half hour at room temperature forming a colourless solution containing [$Zn(Py)_4(NCMe)_2$][BF_4]$_2$. The solution of this zinc intermediate was then added dropwise by cannula to the second flask containing H**L1**$_H$ (50 mg, 0.134 mmol) in acetonitrile (5 mL) forming a yellow solution. After stirring and heating to 80 ^oC for 16 h, the reaction mixture was

allowed to cool to room temperature. All volatiles were removed under reduced pressure and the residue then dissolved in dry acetonitrile (1 mL) (heating if necessary), layered with diethyl ether (8 mL) and left to stand at room temperature affording **2.5a** as yellow cube-like crystals after three to four days (101.59 mg, 65%). ^{1}H NMR (400 MHz, CD_3CN, 298 K): δ 8.44 (t, 2H, $^{3}J_{HH}$ = 7.9 Hz, Py-H_p), 8.26 (d, 2H, $^{3}J_{HH}$ = 6.6 Hz, Py-H_m), 8.17 (s br, 2H, Py-H_m), 7.41-7.76 (m, 4H, Ar-H), 7.22 (d, 2H, $^{3}J_{HH}$ = 6.8 Hz Ar-H), 7.09 (t, 2H. $^{3}J_{HH}$ = 7.0 Hz, Ar-H), 6.83 (d, 2H, $^{3}J_{HH}$ = 7.0 Hz, Ar-H), 6.67 (d, 4H, $^{3}J_{HH}$ = 6.7 Hz Ar-H), 2.73 (sept, 2H, $^{3}J_{HH}$ = 6.53 Hz, C*H*Me_2), 2.59 (sept, 2H, $^{3}J_{HH}$ = 6.60 Hz, C*H*Me_2), 2.50 (s, 6H, N=C*Me*), 0.89 (d, 12H, $^{3}J_{HH}$ = 6.9 Hz CH*Me*$_2$), 0.48 (d, 12H, $^{3}J_{HH}$ = 6.9 Hz CH*Me*$_2$). ^{19}F{^{1}H} NMR (CD_3CN, 376 MHz): δ -151.82 (s, $^{11}BF_4$), -151.71 (s, $^{10}BF_4$). ^{11}B NMR (CD_3CN, 128 MHz): δ -1.19 (s, BF_4^-). IR (cm^{-1}): 1270 (C-O), 1463 (C=N_{py}), 1595 (C=N_{imine}), 1015 (B-F). ESIMS (+ ve, MeCN): *m/z* 437 $[M/2\text{-MeCN}]^+$, 479 $[M/2\text{-}BF_4]^+$. TOFMS (ASAP): *m/z* calculated for $C_{27}H_{32}N_3O_2Zn$ [(M-2BF_4)/2-Py+MeCN+H_2O] 494.3800, $C_{50}H_{53}N_4O_2Zn_2$ [M-2BF_4-Py-MeCN] 870.7600; found 494.3881, 870.7612. Anal Calc. for ($C_{57}H_{62}B_2F_8N_6O_2Zn_2$): C 58.64, H 5.38, N 7.20%. Found: C 58.48, H 5.46, N 7.06%.

6.2.20 Synthesis of [(**L1**$_H$)$_2$Zn$_2$(MeCN)$_2$(μ-BF_4)][BF_4] (**2.5a'**)

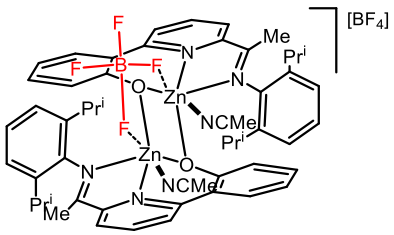

Two small oven dried Schlenk flasks equipped with magnetic stir bars were evacuated and backfilled with nitrogen. In one of the flasks, zinc(II) tetrafluoroborate hydrate (38.45 mg, 0.161 mmol, 1.2 eq) was dissolved in dry acetonitrile (5 mL). The solution was stirred for half hour forming a colourless solution containing $[Zn(NCMe)_6][BF_4]_2$. The solution of this zinc intermediate was then added dropwise by cannular to the second flask containing H**L1**$_H$ (50 mg, 0.134 mmol) in acetonitrile (5 mL) forming a yellow solution. After stirring and heating to reflux for 16 h, the reaction mixture was allowed to cool to room temperature. All volatiles were removed under reduced pressure and the residue then dissolved in dry acetonitrile (1 mL) (heating if necessary),

layered with diethyl ether (8 mL) and left to stand at room temperature affording **2.5a'** as yellow cube-like crystals after four to seven days (127.0 mg, 84%). ^{1}H NMR (400 MHz, CD_2Cl_2, 298K): δ 8.22 (t, 2H, $^{3}J_{HH}$ = 7.9 Hz, Py-H_p), 8.10 (d, 2H, $^{3}J_{HH}$ = 6.5 Hz, Py-H_m), 7.99 (d, 2H, $^{3}J_{HH}$ = 6.0 Hz, Py-H_m), 7.89 (dd, 2H, $^{3}J_{HH}$ = 6.7 Hz, $^{4}J_{HH}$ = 1.7 Hz, Ar-H), 7.43 (d, 2H, $^{3}J_{HH}$ = 7.9 Hz, Ar-H), 7.32 (t, 2H, $^{3}J_{HH}$ = 8.1 Hz, Ar-H), 7.13 (m, 2H, Ar-H), 6.98 (m, 2H, Ar-H), 6.77 (t, 4H, $^{3}J_{HH}$ = 8.0 Hz, Ar-H), 3.47 (sept, 2H, $^{3}J_{HH}$ = 6.8 Hz, C*H*Me_2), 2.65 (sept, 4H, $^{3}J_{HH}$ = 6.7 Hz, C*H*Me_2), 2.21 (s, 6H, N=C*Me*) 0.74 (d, 12H, $^{3}J_{HH}$ = 6.6 Hz, CH*Me*$_2$), 0.39 (d, 12H, $^{3}J_{HH}$ = 6.6 Hz, CH*Me*$_2$). ^{19}F{^{1}H} NMR (CD_3CN, 375 MHz): -147.26 (s, μ-BF_4), -151.84 (s, $^{11}BF_4$), -151.70 (s, $^{10}BF_4$). ^{11}B NMR (CD_3CN, 128 MHz): δ 0.54 (s br, μ-BF_4), -1.19 (s, $^{11}BF_4$). IR (cm^{-1}): 1463 ($C{=}N_{py}$), 1595 ($C{=}N_{imine}$), 1045 (B-F), 1033 (B-F). ESIMS (+ve, MeCN): *m/z* 870 $[M\text{-}2BF_4\text{-}2MeCN]^+$, 435 $[(M\text{-}2BF_4\text{-}2MeCN)/2]^+$. TOFMS (ASAP): *m/z* calculated for $C_{50}H_{54}N_4O_2Zn_2$ $[M\text{-}2BF_4\text{-}2MeCN]^+$ 870.7600 found 870.7667. Anal Calc. for ($C_{54}H_{60}B_2F_8N_6O_2Zn_2$): C 57.43, H 5.32, N 7.44%. Found: C 57.44, H 5.75, N 7.63%.

6.2.21 Synthesis of [{**L1**$_{Ph}$(BF_3)}Zn(MeCN)(Py)][BF_4] (**2.6b**)

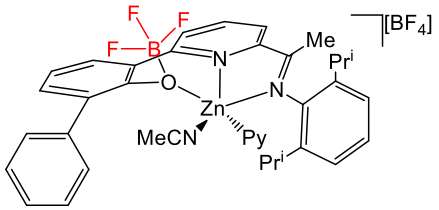

Two small oven dried Schlenk flasks equipped with magnetic stir bars were evacuated and backfilled with nitrogen. In one of the flasks, zinc(II) tetrafluoroborate hydrate (19 mg, 0.080 mmol, 1.2 eq) was dissolved in dry acetonitrile (5 mL) and two drops of pyridine added. The solution was stirred for half hour forming a colourless solution containing $[Zn(Py)_4(NCMe)_2][BF_4]_2$. The solution of this zinc intermediate was then added dropwise by cannular to the second flask containing H**L1**$_{Ph}$ (30 mg, 0.067 mmol) in acetonitrile (5 mL) forming a yellow solution. After stirring and heating to reflux for 16 h, the reaction mixture was allowed to cool to room temperature. All volatiles were removed under reduced pressure and the residue then dissolved in dry acetonitrile (1 mL) (heating if necessary), layered with diethyl ether (8 mL) and left to stand at room temperature affording **2.6b** as yellow cube-like crystals after four to seven days.(10.36 mg, 43%). ^{1}H NMR (400 MHz, CD_3CN, 298K): δ 8.49 (t, 1H, $^{3}J_{HH}$ = 7.8 Hz, Py-Hp),

8.20-8.31 (m, 2H, Py-Hm), 8.15 (d, 1H, $^{3}J_{HH}$ = 6.5 Hz, Ar-H), 7.76 (t, 1H, $^{3}J_{HH}$ = 8.0 Hz, Ar-H), 7.68 (d, 1H, $^{3}J_{HH}$ = 7.9 Hz, Ar-H), 7.50-7.59 (m, 2H, Ar-H), 7.12-7.39 (m, 5H, Ar-H), 6.67 (d, $^{3}J_{HH}$ = 7.7 Hz, Ar-H), 3.04 (sept, 2H, $^{3}J_{HH}$ = 6.3 Hz, C*H*Me$_2$), 2.50 (s, 3H, N=C*Me*), 1.09 (d, 6H, $^{3}J_{HH}$ = 7.0 Hz, CH*Me*$_2$), 0.91 (d, 6H, $^{3}J_{HH}$ = 6.9 Hz, CH*Me*$_2$). ^{19}F{^{1}H} NMR (CD$_3$CN, 375 MHz): δ -145.39 (s br, –OBF$_3$), -151.81 (s, ^{11}BF$_4$), -151.69 (s, ^{10}BF$_4$). ^{11}B NMR (CD$_3$CN, 128MHz): δ 19.89 (s br, –OBF$_3$), -1.19 (s, ^{11}BF$_4$). IR (cm^{-1}): 1460 (C=N$_{Py}$), 1596 (C=N$_{imine}$), 1254 (C-O), 1033 (B-F), 1031 (B-F). ESIMS (+ve, MeCN): *m/z* 569 [M-BF$_4$-Py-BF$_3$]$^{+}$. TOFMS (ASAP): *m/z* calculated for C$_{32}$H$_{32}$N$_2$OZn [M-BF$_4$-BF$_3$-MeCN-Py]$^{+}$ 511.1721 found 511.1735. Anal Calc. for (C$_{39}$H$_{43}$B$_2$F$_7$N$_4$OZn): C 58.28, H 5.35, N 6.97. Found C 58.44, H 5.75, N 7.03%.

6.2.22 Synthesis of [{**L1$_{tBu}$**(BF$_3$)}Zn(MeCN)(Py)][BF$_4$] (**2.7c**)

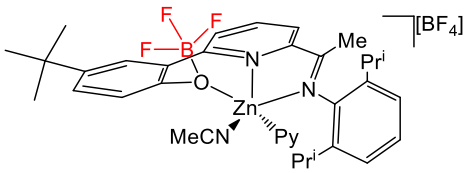

A similar procedure to that outlined for **2.6b** was followed using zinc(II) tetrafluoroborate hydrate (20 mg, 0.0841 mmol, 1.2 eq), H**L1**$_{tBu}$ (30 mg, 0.070 mmol), dry acetonitrile (5 mL) and two drops of pyridine. Following work-up yellow cube-like crystals of **2.7c** were formed by layering an acetonitrile solution of the complex with diethylether (31.19 mg, 88%). ^{1}H NMR (400 MHz, CD$_3$CN, 298 K): δ 8.35 (t, 1H, $^{3}J_{HH}$ = 8.0 Hz, Py-H$_p$), 8.22 (d, 1H, $^{3}J_{HH}$ = 6.6 Hz, Py-H$_m$), 7.94 (t, 1H, $^{3}J_{HH}$ = 6.0 Hz, Py-H$_m$), 7.21 (s, 1H, Ar-H), 7.05 (t, 1H, $^{3}J_{HH}$ = 8.0 Hz, Ar-H), 6.75 (d, 1H, $^{3}J_{HH}$ = 8.0 Hz, Ar-H), 6.65 (s, 1H, Ar-H), 5.95 (s, 1H, Ar-H), 2.81 (sept, 2H, $^{3}J_{HH}$ = 6.77 Hz, C*H*Me$_2$), 2.68 (sept, 2H, $^{3}J_{HH}$ = 6.7 Hz, C*H*Me$_2$) 2.51(s, 3H, N=C*Me*), 1.25 (s, 9H, tBu), 1.15(d, 3H, $^{3}J_{HH}$ = 6.7, CH*Me*$_2$), 0.49 (d, 3H, $^{3}J_{HH}$ = 6.8, CH*Me*$_2$), 1.09 (d, 3H, $^{3}J_{HH}$ = 7.0, CH*Me*$_2$), 0.84 (d, 3H, $^{3}J_{HH}$ = 6.9, CH*Me*$_2$). ^{19}F{^{1}H} NMR (CD$_3$CN, 375 MHz): δ -146.84 (q, $^{1}J_{BF}$ = 7.6 Hz, –OBF$_3$), -151.84 (s, ^{11}BF$_4$), -151.70 (s, ^{10}BF$_4$). ^{11}B NMR (CD$_3$CN, 128 MHz): δ 19.88 (s br, –OBF$_3$), -1.19 (s, ^{11}BF$_4$). IR (cm^{-1}): 1460 (C=N$_{py}$), 1593 (C=N$_{imine}$), 1229 (C-O), 1045 (B-F). TOFMS (ASAP): *m/z* calculated for C$_{29}$H$_{35}$N$_2$OZn [M-BF$_4$-BF$_3$-2MeCN] 491.2049, C$_{31}$H$_{38}$N$_3$OZn [M-BF$_3$-BF$_4$-MeCN]

532.1017; found 491.2041, 532.1024. Anal Calc. for ($C_{39}H_{43}B_2F_7N_4OZn$): C 54.30, H 5.62, N 7.69. Found C 54.49, H 5.77, N 7.54%.

6.2.23 Synthesis of [(**L2**)Zn(Py)(MeCN)(η^1-FBF_3)][BF_4] (**2.8**)

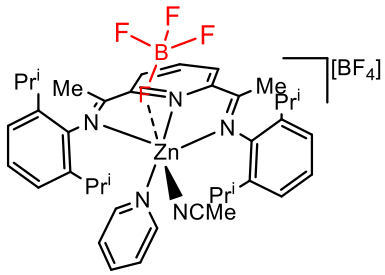

Two small oven dried Schlenk flasks equipped with magnetic stir bars were evacuated and backfilled with nitrogen. In one of the flasks, zinc(II) tetrafluoroborate hydrate (39.0 mg, 0.125 mmol, 1.2 eq) was dissolved in dry acetonitrile (5 mL) and two drops of pyridine added. The solution was stirred for half hour forming a colourless solution containing $[Zn(Py)_4(NCMe)_2][BF_4]_2$. The solution of this zinc intermediate was then added dropwise by cannular to the second flask containing **L2** (50.0 mg, 0.104 mmol) in dry dichloromethane (5 mL) forming a yellow solution. After stirring and heating to reflux for 16 h, the reaction mixture was allowed to cool to room temperature. All volatiles were removed under reduced pressure and the residue then dissolved in dry acetonitrile (1 mL) (heating if necessary), layered with diethyl ether (8 mL) and left to stand at room temperature affording **2.8** as yellow cube-like crystals after three to four days (58.53 mg, 67%).^{1}H NMR (400 MHz, CD_3CN, 298 K): δ 8.82 (dd, 1H, $^3J_{HH}$ = 12.0 Hz, $^4J_{HH}$ = 1.2 Hz, Py-H_p), 8.71 (t, 2H, $^3J_{HH}$ = 8.0 Hz, Py-H_m), 8.25 (d, 2H, $^3J_{HH}$ = 8.0 Hz, Py-H_m), 8.19 (tt, 1H, $^3J_{HH}$ = 8.0 Hz, Py-H_p), 7.65 (t, 2H, $^3J_{HH}$ = 8.0 Hz, Py-H_m), 7.35 (m, 6H, Ar-H), 2.59 (s, 6H, N=C*Me*), 2.52 (sept, 4H, $^3J_{HH}$ = 6.83 Hz, C*H*Me_2), 1.53 (d, 12H, $^3J_{HH}$ = 6.8, CH*Me*$_2$), 0.95 (d, 12H, $^3J_{HH}$ = 6.7, CH*Me*$_2$). ^{19}F{^{1}H} NMR (CD_3CN, 375 MHz): δ -147.71 (s br, η^1-BF_4), -151.45 (s, $^{11}BF_4$), -151.31 (s, $^{10}BF_4$). ^{11}B NMR (CD_3CN, 128 MHz): δ 0.52 (s br, η^1-BF_4), -1.19 (s, $^{11}BF_4$). IR (cm^{-1}): 1643 ($C{=}N_{imine}$), 1455 ($C{=}N_{Py}$), 1044 (B-F). ESIMS *m/z* 546 $[M\text{-}2BF_4\text{-}Py\text{-}MeCN\text{-}H]^+$. TOFMS (ASAP): *m/z* calculated for $C_{33}H_{43}N_3Zn$ $[M\text{-}2BF_4\text{-}Py\text{-}MeCN\text{-}H]^+$ 545.2700 found 545.2790. Anal Calc. for ($C_{40}H_{51}B_2F_8N_5Zn{\cdot}2H_2O$): C 54.79, H 6.28, N 7.99. Found: C 55.18, H 6.80, N 7.46%.

6.2.24 Synthesis of [(H**L4**)Zn(η^1-OHBF$_3$)(MeCN)][BF$_4$] (**2.9**)

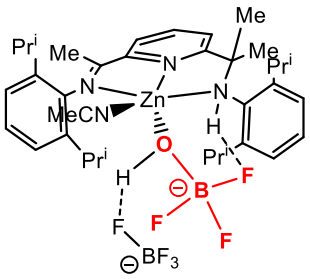

A similar procedure to that outlined for **2.8** was followed using zinc(II) tetrafluoroborate hydrate (23 mg, 0.097 mmol, 1.2 eq) and H**L4** (40 mg, 0.0805 mmol). On crystallisation of the residue from a mixture of acetonitrile and diethylether, yellow cube-like crystals of **2.9** were formed after several days (33.06 mg, 53%). ^{1}H NMR (400 MHz, CD_3CN, 298 K): δ 8.56 (t, 1H, $^3J_{HH}$ = 8.0 Hz, Py-H$_p$), 8.41 (d, 1H, $^3J_{HH}$ = 6.0 Hz, Py-H$_m$), 8.21 (d, 1H, $^3J_{HH}$ = 6.9 Hz, Py-H$_m$), 7.39 (m, 6H, Ar-H), 5.57 (sept, 2H, $^3J_{HH}$ = 6.5 Hz, C*H*Me$_2$), 4.83 (sept, 1H, $^3J_{HH}$ = 6.8 Hz, C*H*Me$_2$), 2.67 (sept, 1H, $^3J_{HH}$ = 6.7 Hz, C*H*Me$_2$), 2.55 (s, 3H, N=C*Me*), 2.31 (s, 6H, NH-C*Me*$_2$), 1.23 (m, 24H, CH*Me*$_2$). ^{19}F{^{1}H} NMR (375 MHz, CD_3CN): δ -144.56 (quartet, 3F, $^1J_{BF}$ = 7.1 Hz, η^1-OHBF$_3$), -151.85 (s, ^{11}BF$_4$), -151.77 (s, ^{10}BF$_4$). ^{11}B NMR (128 MHz, CD_3CN): δ -0.34 (quartet, $^1J_{BF}$ = 7.6 Hz, η^1-OHBF$_3$), -1.19 (s, ^{11}BF$_4$). IR (cm^{-1}): 3431 (O-H), 3588 (N-H), 1627 (C=N$_{imine}$), 1599 (C=N$_{Py}$), 1050 (B-F). ESIMS (+ve, MeCN): *m/z* 606 [M-BF$_4$-OBF$_3$-H]$^+$, 562 [M-BF$_4$-OBF$_3$-MeCN-H]$^+$, 80 [BF$_2$O$_2$]$^+$. ESIMS (-ve, MeCN): *m/z* 87 [BF$_4$]$^-$, 65 [BF$_2$O]$^-$. TOFMS (ASAP): *m/z* calculated for $C_{38}H_{53}N_5Zn$ [M-BF$_4$-OBF$_3$+MeCN]$^+$ 643.3600 found 643.3629. Anal Calc. for ($C_{36}H_{51}B_2F_7N_4OZn\cdot 3H_2O$): C 52.11, H 6.88, N 6.75. Found: C 52.54, H 6.44, N 6.54%.

6.2.25 Attempted reactions of (H**L1**$_H$)ZnCl$_2$ (**2.1a**) with CsF in CD_2Cl_2

An NMR tube was charged with **2.1a** (6.0 mg, 0.012 mmol) and then transferred to the glove box. CsF (1.8 mg, 0.012 mmol, 1.0 eq or 3.6 mg, 0.024 mmol, 2.0 eq) was added to the NMR tube under an atmosphere of nitrogen. After removal from the glovebox, CD_2Cl_2 (1 mL) was added to the NMR tube and the contents agitated using sonication at room temperature. The ^{1}H NMR and ^{19}F NMR spectra were both monitored at 10 min, 20 min, 30 min, 60 min and 120 min. The ^{1}H NMR spectra revealed peaks

consistent with free H**L1**$_{\mathbf{H}}$; there was no evidence of zinc fluoride formation by ^{19}F NMR spectroscopy.

6.2.26 Attempted reaction of (**L1**$_{tBu}$)$_2$Zn$_2$Cl$_2$ (**2.2c**) with CsF in CD_2Cl_2

A similar procedure to that outlined above for **2.1a** with CsF was followed using **2.2c** (6.0 mg, 0.006 mmol), CsF (1.4 mg, 0.006 mmol, 1.0 eq or 1.7 mg, 0.011 mmol, 2.0 eq) and CD_2Cl_2 (1 mL). The ^{1}H NMR spectra revealed peaks consistent with free H**L1**$_H$; there was no evidence of zinc fluoride formation by ^{19}F NMR spectroscopy.

6.2.27 Attempted reaction of (H**L1**$_H$)ZnCl$_2$ (**2.1a**) with AgF in THF

An oven dry small Schlenk flask equipped with stirred bar was evacuated and backfilled with nitrogen. The flask was loaded with **2.1a** (10 mg, 0.0197 mmol) and then placed under reduced pressure for 30 min. The flask was then backfilled with nitrogen and AgF (2.5 mg, 0.0197 mmol, 1.0 eq) and dry THF (5 mL) added. Aluminium-foil was used to surround the Schlenk flask in order to ensure the reaction proceeded in a photophobic environment. After stirring at room temperature for 15 min, 30 min and 60 min, the solution was filtered through celite in the air and washed with THF. The solvent was removed under reduced pressure affording a green powder, which was identified by ^{1}H NMR spectroscopy as unreacted **2.1a**. The procedure was repeated with 3 eq AgF (7.5 mg, 0.0590 mmol) and 5 eq AgF (12.5 mg, 0.0984 mmol). With 3 eq of AgF, the ^{1}H NMR spectrum showed no while with 5 eq. of AgF, the ^{1}H NMR spectrum showed free H**L1**$_H$ after stirring at room temperature for 30 min.

6.2.28 Attempted reaction of (**L1**$_{tBu}$)$_2$Zn$_2$Cl$_2$ (**2.2c**) with AgF in THF

A similar procedure to that outlined above for **2.1a** with AgF was followed using **2.2c** (10 mg, 0.0095 mmol), AgF (1.2 mg, 0.0095 mmol, 1.0 eq or 3.6 mg, 0.0284 mmol, 3.0 eq; 6.0 mg, 0.0474 mmol, 5 eq) and dry THF (5 mL). No signals consistent with zinc fluoride formation could be detected by ^{1}H and ^{19}F NMR spectroscopy for any of the molar ratios. Indeed, the ^{1}H NMR spectrum recorded using 5 eq. of AgF showed only H**L1**$_{tBu}$.

6.3 Experimental procedures for Chapter 3

6.3.1 Synthesis of (H**L1**$_H$)$CoCl_2$ (**3.1a**)

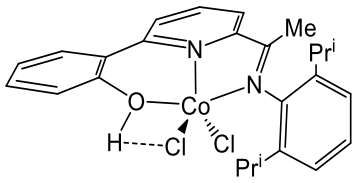

A small oven-dried Schlenk flask equipped with a magnetic stir bar was evacuated and backfilled with nitrogen. The flask was charged with anhydrous $CoCl_2$ (52 mg, 0.40 mmol), dry THF (10 mL) and H**L1**$_H$ (149 mg, 0.40 mmol). After stirring at room temperature for 24 h, the reaction mixture was concentrated under reduced pressure (to *ca.* 1-2 mL of solvent). Hexane was added to induce precipitation and this suspension was stirred overnight, filtered in the air, washed with hexane (2 × 30 mL) and dried under reduced pressure to give a green solid. Recrystallisation from a hot acetonitrile gave green crystals of **3.1a** (112 mg, 74%). IR (cm^{-1}): 3430 (OH), 2963 (CH_3), 1620 ($C{=}N_{imine}$), 1251 (C-O). ESIMS (+ve, MeCN): *m/z* 430 $[M\text{-}HCl_2]^+$. HRMS (TOF): *m/z* calculated for $C_{25}H_{27}N_2OCo$ $[M\text{-}HCl_2]^+$ 430.1455, found 430.1463. Anal. Calc for ($C_{25}H_{28}N_2OCoCl_2$): C 59.72, H 5.60, N 5.72. Found C 59.77, H 5.62, N 5.58%. μ_{eff} = 4.6 BM.

6.3.2 Synthesis of (**L1**$_H$)$_2Co_2Cl_2$ (**3.2a**)

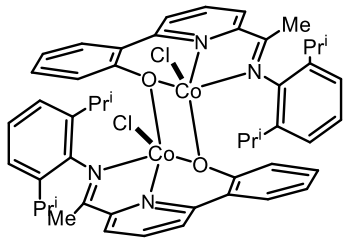

An oven-dried small Schlenk flask equipped with a magnetic stir bar was evacuated and backfilled with nitrogen. The flask was charged with $CoCl_2$ (36 mg, 0.28 mmol) and dry n-butanol (10 mL) and the reaction mixture stirred and heated to 90 ^oC to allow dissolution. H**LI**$_H$ (93 mg, 0.25 mmol) was introduced and the reaction mixture stirred for further 2 h at 90 ^oC. On cooling to room temperature the reaction mixture was concentrated to half volume and hexane (*ca.* 30 mL) added to induce precipitation of a green powder. The green suspension was stirred overnight, filtered, washed with hexane

(2 x 30 mL) and dried under reduced pressure. Recrystallisation from hot acetonitrile solution gave green crystals of **3.2a** (98 mg, 80%). ^{1}H NMR (400 MHz, CD_3CN, 298 K): δ 65.54 (s, 2H, Py-H_m), 47.22 (s, 2H, Py-H_m), 32.24 (s, 2H, Ar-H), 28.71 (s, 2H, Py-H_p), 24.76 (s, 2H, Ar-H), 20.60 (s, 2H, Ar-H), 19.14 (s, 4H, Ar-H), 4.36 (s, 6H, N=C*Me*), -13.20 (s, 2H, Ar-H), -16.33 (s, 12H, CH*Me*$_2$), -18.93 (s, 12H, CH*Me*$_2$), -34.71 (s, 4H, C*H*Me$_2$). IR (cm^{-1}): 1619 (C=N_{imine}), 1591 (C=$N_{pyridine}$), 1231 (C-O). HRMS (FAB): *m/z* calculated for $C_{50}H_{54}N_4O_2Co_2Cl$ $[M\text{-}Cl]^+$, $C_{25}H_{27}N_2OCo$ $[M/2\text{-}Cl]^+$ 895.2631, 430.1531; found 895.2602, 430.1529. Anal. Calc. for ($C_{50}H_{54}N_4O_2Co_2Cl_2$): C 64.45, H 5.83, N 6.01. Found C 64.52, H 5.83, N 6.01%. μ_{eff} = 6.36 BM.

6.3.3 Synthesis of (H**L1**$_{Ph}$)$CoCl_2$ (**3.1b**)

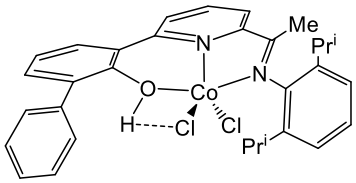

A small oven-dried Schlenk flask equipped with a magnetic stir bar was evacuated and backfilled with nitrogen. The flask was charged with anhydrous $CoCl_2$ (29 mg, 0.22 mmol), dry THF (10 mL) and H**L1**$_{Ph}$ (99 mg, 0.22 mmol). After stirring at room temperature for 24 h, the reaction mixture was concentrated (to *ca.* 1-2 mL of solvent) and hexane added to induce precipitation. The suspension was stirred overnight, filtered in the air, washed with hexane (2 × 30 mL) and dried under reduced pressure to give a green powder. The solid was recrystallised by the slow cooling of a hot acetonitrile solution affording **3.1b** as green crystals (108 mg, 85%). IR (cm^{-1}) 1604 (C=N_{imine}), 1586 (C=N_{py}), 1243 (C-O). HRMS (FAB): *m/z* calculated for $C_{31}H_{32}N_2OCoCl$ $[M\text{-}Cl]^+$ 542.1573, $C_{31}H_{31}N_2OCo$ $[M\text{-}HCl_2]^+$ 506.2234; found 542.1554, 506.2232. μ_{eff} = 4.7 BM.

6.3.4 Synthesis of $(\mathbf{L1}_{tBu})_2Co_2Cl_2$ (**3.2c**)

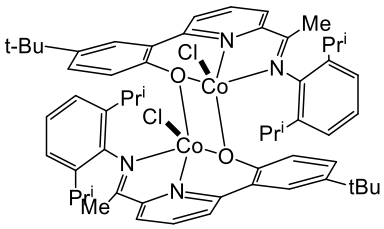

A small oven-dried Schlenk flask equipped with a magnetic stir bar was evacuated and backfilled with nitrogen. The flask was charged with anhydrous $CoCl_2$ (29 mg, 0.22 mmol), dry THF (10 mL) and H$\mathbf{L1}_{tBu}$ (94 mg, 0.22 mmol). After stirring at room temperature for 24 h, the reaction mixture was concentrated to a minimal volume of solvent and hexane added to induce precipitation. The resulting suspension was stirred for 3 h, filtered, washed with hexane (2 × 30 mL) and dried under reduced pressure. Green crystals of **3.2c** were obtained by the slow cooling of a hot acetonitrile solution (104 mg, 76%). ^{1}H NMR (400 MHz, CD_3CN, 298 K): δ 63.71 (s, 2H, Py-H_m), 44.19 (s, 2H, Py-H_m), 29.37 (s, 2H, Py-H_p), 25.71 (s, 2H, Ar-H), 21.39 (s, 2H, Ar-H), 20.30 (s, 4H, Ar-H), 19.44 (s, 2H, Ar-H), 5.01 (s, 3H, N=C*Me*), -13.16 (s, 2H, Ar-H), -16.91 (s, 24H, CH*Me*$_2$). IR (cm^{-1}): 1599 (C=N_{imine}), 3431 (CH_3), 1261 (C-O). HRMS (FAB): *m/z* calculated for $C_{58}H_{71}N_4Co_2Cl$ $[M\text{-}2HCl]^+$ 486.1100, found 486.0012. Anal. Calc. for ($C_{58}H_{72}N_4Co_2Cl_2$): C 66.75, H 6.71, N 5.37. Found C 66.24, H 6.12, N, 5.82%. μ_{eff} = 6.0 BM.

6.3.5 Synthesis of $(H_2\mathbf{L3}_H)_2CoCl_2$ (**3.3**)

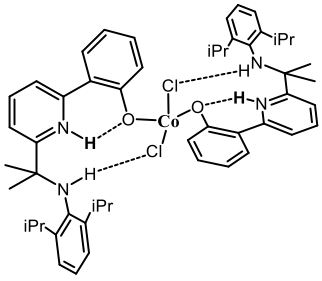

A small oven-dried Schlenk flask equipped with a magnetic stir bar was evacuated and backfilled with nitrogen. The flask was charged with anhydrous $CoCl_2$ (8.36 mg, 0.064 mmol), dry THF (10 mL) and H$\mathbf{L3}_H$ (50 mg, 0.128 mmol). After stirring at room temperature for 24 h, the reaction mixture was concentrated (to *ca.* 1-2 ml of solvent) and hexane added to induce precipitation. The green suspension was stirred overnight, filtered, washed with hexane (2 × 30 mL) and dried under reduced pressure.

Recrystallisation of the solid from a hot acetonitrile gave **3.3** as green crystals (107 mg, 70%). IR (cm^{-1}): 3301 (N-H), 3219 (Ar-OH), 1458 ($C=N_{py}$). HRMS (FAB): *m/z* calculated for $C_{26}H_{31}N_2OCo$ $[M\text{-}H\mathbf{L3}_H\text{-}2Cl]^+$ 446.4822, found 446.4817. Anal Calc. for ($C_{52}H_{64}N_4O_2CoCl_2 \cdot 6H_2O$): C 61.58, H 7.48, N 5.53. Found C 62.00, H 7.51, N 5.62%.

6.3.6 Synthesis of (H**L4**)$CoCl_2$ (**3.4**)

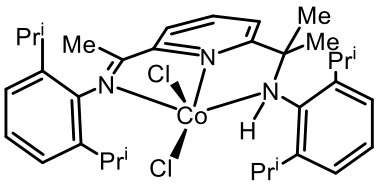

A similar procedure to that outlined for **3.1a** was followed using H**L4** (50 mg, 0.100 mmol), $CoCl_2$ (12.97 mg, 0.100 mmol) and dry THF (10 mL). On crystallisation of the resulting solid from hot acetonitrile gave green needle-like crystals of **3.4** (50.1 mg, 78%). ^1H NMR (500 MHz, CD_2Cl_2): δ 117.51 (s, 1H, Py-H_m), 95.86 (s, 1H, Py-H_m), 32.28 (s, 1H, Py-H_p), 5.29 (s, 3H, N=C*Me*), -5.71 (br, s, 1H, N-H), -11.84 (s, 4H, Ar-H_m), -13.84 (s, 2H, Ar-H_p), -21.12 (s, 24H, 2×CH*Me*$_2$), -22.53 (br, s, 2H, C*H*Me_2), -28.20 (br, s, 2H, C*H*Me_2). IR (cm^{-1}): 1593 ($C=N_{imine}$), 1577 ($C=N_{py}$) 3300 (N-H). HRMS (FAB): *m/z* calculated for $C_{34}H_{47}N_3CoCl$ $[M\text{-}Cl]^+$ 591.2810, $C_{34}H_{46}N_3Co$ $[M\text{-}2Cl\text{-}H]^+$ 555.3100; found 591.2819, 555.3147. Anal Calc. for ($C_{34}H_{47}N_3CoCl_2 \cdot H_2O \cdot 2MeCN$): C 62.73, H 7.56, N 9.63. Found C 62.74, H 7.43, N 9.59%. μ_{eff} = 4.6 BM.

6.3.7 Synthesis of $[(\mathbf{L1}_H)_2Co_2(Py)(MeCN)][BF_4]_2$ (**3.5a**)

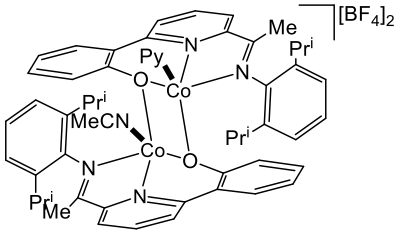

Two small oven dried Schlenk flasks equipped with magnetic stir bars were evacuated and backfilled with nitrogen. In one of the flasks, cobalt(II) tetrafluoroborate hexahydrate (55.1 mg, 0.161 mmol, 1.2 eq) was dissolved in dry acetonitrile (5 mL) and

five drops of pyridine added. The solution was stirred for half hour forming an orange/pink solution containing $[Co(Py)_4(NCMe)_2][BF_4]_2$. The solution of this cobalt intermediate was then added dropwise by cannular to the second flask containing H**L1$_H$** (50 mg, 0.134 mmol) in acetonitrile (5 mL) forming a dark orange solution. After stirring and heating to reflux for 16 h, the reaction mixture was allowed to cool to room temperature. The solution was filtered by cannular and the filtrate concentrated (to *ca.* 2 mL of solvent), layered with diethyl ether (10 mL) and left to stand at room temperature affording **3.5a** as dark brown crystals after several days (96 mg, 62%). ^{1}H NMR (400 MHz, CD_3CN, 298 K): δ 61.69 (s, 2H, Py-H_m), 58.70 (br s, 1H, Pyridine-H_p), 58.20 (s, 2H, Py-H_m), 32.49 (s, 2H, Py-H_p), 31.03 (s, 4H, Pyridine-H), 23.17 (br s, 2H, Ar-H), 19.39 (s, 4H, Ar-H), 17.90 (s, 2H, Ar-H), 10.58 (s, 4H, Ar-H), -4.39 (s, 2H, Ar-H), -11.75 (s, 24H, CH*Me*$_2$), -22.23 (s, 4H, C*H*Me$_2$). ^{19}F{^{1}H} NMR (375 MHz, CD_3CN): δ -150.93 (s, $^{11}BF_4$), -150.70 (s, $^{10}BF_4$). IR (cm^{-1}): 1593 ($C{=}N_{Py}$), 1609 ($C{=}N_{imine}$), 1215 (C-O), 1039 (B-F), 1046 (B-F). HRMS (FAB): *m/z* calculated for $C_{50}H_{54}N_4O_2Co_2$ $[M\text{-}2BF_4\text{-Py-MeCN-H}]^+$ 860.2612, found 860.2645. Anal Calc. for ($C_{57}H_{62}B_2F_8N_6O_2Co_2 \cdot 2H_2O \cdot$ MeCN): C 57.53, H 5.61, N 7.96. Found C 57.44, H 5.75, N 7.63%. μ_{eff} = 6.24 BM.

6.3.8 Synthesis of $[(H\mathbf{L1_{Ph}})Co(Py)(MeCN)_2][BF_4]_2$ (**3.7**)

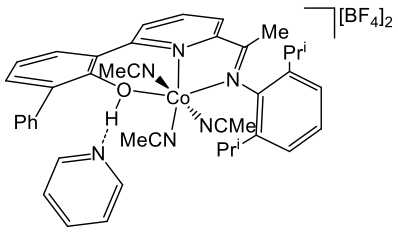

Two small oven dried Schlenk flasks equipped with magnetic stir bars were evacuated and backfilled with nitrogen. In one of the flasks, cobalt(II) tetrafluoroborate hexahydrate (54 mg, 0.161 mmol, 1.2 eq) was dissolved in dry acetonitrile (5 mL) and five drops of pyridine added. The solution was stirred for half hour forming an orange/pink solution containing $[Co(Py)_4(NCMe)_2][BF_4]_2$. The solution of this cobalt intermediate was then added dropwise by cannular to the second flask containing H**L1$_{Ph}$** (50 mg, 0.134 mmol) in acetonitrile (5 mL) forming a dark orange solution. After stirring and heating to reflux for 16 h, the reaction mixture was allowed to cool to

room temperature. The solution was filtered by cannular and the filtrate concentrated (to *ca.* 2 mL of solvent), layered with diethyl ether (10 mL) and left to stand at room temperature affording **3.7** as dark brown crystals after several days (96 mg, 12%). $^{19}F\{^{1}H\}$ NMR (CD_3CN, 375 MHz): δ -151.60 (s, $^{11}BF_4$), -151.37 (s, $^{10}BF_4$). IR (cm^{-1}): 3100 (O-H), 1588 ($C{=}N_{imine}$), 1568 ($C{=}N_{Py}$), 1031 (B-F). HRMS (FAB): *m/z* calculated for $C_{31}H_{32}N_2OCo$ $[M\text{-}2BF_4\text{-}3MeCN\text{-}Py]^+$ 507.1821, found 507.1843. Anal Calc. for ($C_{42}H_{46}B_2F_8N_6OCo{\cdot}2H_2O$): C 54.86, H 5.44, N 9.14. Found C 54.76, H 5.32, N 9.31%.

6.3.9 Synthesis of $[(\mathbf{L1}_{tBu})_2Co_2(MeCN)_2][BF_4]_2$ (**3.6c**)

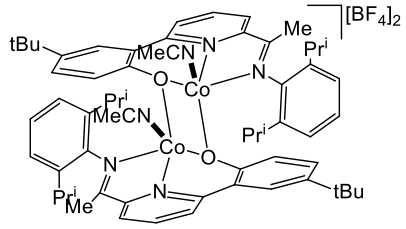

Two small oven dried Schlenk flasks equipped with magnetic stir bars were evacuated and backfilled with nitrogen. In one of the flasks, cobalt(II) tetrafluoroborate hexahydrate (60 mg, 0.176 mmol, 1.2 eq) was dissolved in dry acetonitrile (5 mL) and three drops of pyridine added. The solution was stirred for half hour, forming an orange/pink solution containing $[Co(Py)_4(NCMe)_2][BF_4]_2$. The solution of this cobalt intermediate was then added dropwise by cannular to the second flask containing $H\mathbf{L1}_{tBu}$ (50 mg, 0.147 mmol) in acetonitrile (5 mL) forming a dark orange solution. After stirring and heating to reflux for 16 h, the reaction mixture was allowed to cool to room temperature. The solution was filtered by cannular and the filtrate concentrated (to *ca.* 2 mL of solvent), layered with diethyl ether (10 mL) and left to stand at room temperature affording **3.6c** as dark brown crystals after several days (0.093 g, 72%). ^{1}H NMR (400 MHz, CD_3CN, 298 K): δ 62.58 (s, 2H, Py-Hm), 61.77 (s, 2H, Py-Hm), 49.41-34.80 (Pyridine signals), 33.97 (s, 2H, Py-Hp), 20.49 (s, 2H, Ar-H), 18.88 (s, 2H, Ar-H), 16.76 (s, 2H, Ar-H), 10.12 (s, 4H, Ar-H), -3.57 (s, 2H, Ar-H), -11.69 (s, 24H, $CH\mathit{Me}_2$), -22.50 (s, 4H, $C\mathit{H}Me_2$). $^{19}F\{^{1}H\}$ NMR (CD_3CN, 400 MHz): δ -150.93 (s, $^{11}BF_4$), 150.70 (s, $^{10}BF_4$). IR (cm^{-1}): 1588 ($C{=}N_{Py}$), 1609 ($C{=}N_{imine}$), 1208 (C-O), 1039 (B-F). HRMS (FAB): *m/z* calculated for $C_{58}H_{70}N_4O_2Co_2$ $[M\text{-}2BF_4\text{-}2MeCN]^+$ 972.4200,

$C_{29}H_{35}N_2OCo$ $[(M\text{-}2BF_4\text{-}2MeCN)/2]^+$ 486.2100 found 972.4209, 486.2134. Anal Calc. for ($C_{62}H_{76}B_2Co_2F_8N_6O_2$): C 60.61, H 6.19, N 6.84. Found C 60.03, H 6.05, N 6.11%. μ_{eff} = 6.17 BM.

6.3.10 Synthesis of $[(O,N,O)_2Co_2(MeCN)_4][BF_4]_2$ (**3.8**)

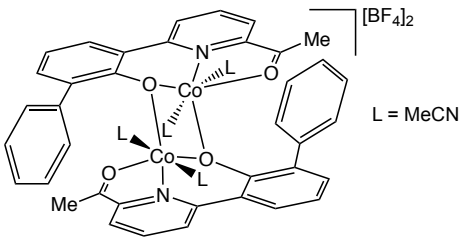

Two small oven dried Schlenk flasks equipped with magnetic stir bars were evacuated and backfilled with nitrogen. In one of the flasks, cobalt(II) tetrafluoroborate hexahydrate (54 mg, 0.161 mmol, 1.2 eq) was dissolved in dry acetonitrile (5 mL) and five drops of pyridine added. The solution was stirred for half hour, forming an orange/pink solution containing $[Co(Py)_4(NCMe)_2][BF_4]_2$. The solution of this cobalt intermediate was then added dropwise by cannular to the second flask containing Ketone-Ph (50 mg, 0.134 mmol) in acetonitrile (5 mL) forming a dark orange solution. After stirring and heating to reflux for 16 h, the reaction mixture was allowed to cool to room temperature. The solution was filtered by cannular and the filtrate concentrated (to *ca.* 2 mL of solvent), layered with diethyl ether (10 mL) and left to stand at room temperature affording **3.8** as dark brown crystals after several days (96 mg, 52%). $^{19}F\{^1H\}$ NMR (CD_3CN, 375 MHz): δ -150.97 (s, $^{11}BF_4$), -150.74 (s, $^{10}BF_4$). IR (cm^{-1}): 1593 ($C{=}N_{Py}$), 1654 (C=O), 1224 (C-O), 1015 (B-F). HRMS (FAB): calculated for $C_{46}H_{40}N_5O_4Co_2$ $[M\text{-}2BF_4]^+$ 858.1800 found 858.1821. Anal Calc. for ($C_{46}H_{40}B_2Co_2F_8N_6O_4$): C 51.10, H 3.85, N 5.68. Found C 51.30, H 3.73, N 5.74%. μ_{eff} = 6.05 BM.

6.3.11 Synthesis of [(**L2**)Co(Py)(MeCN)$_2$][BF$_4$]$_2$ (**3.9**)

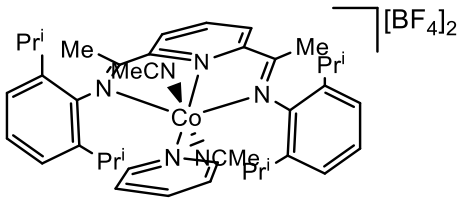

Two small oven dried Schlenk flasks equipped with magnetic stir bars were evacuated and backfilled with nitrogen. In one of the flasks, cobalt(II) tetrafluoroborate hexahydrate (39 mg, 0.125 mmol, 1.2 eq) was dissolved in dry acetonitrile (5 mL) and three drops of pyridine added. The solution was stirred for half hour, forming an orange/pink solution containing [Co(Py)$_4$(NCMe)$_2$][BF$_4$]$_2$. The solution of this cobalt intermediate was then added dropwise by cannular to the second flask containing **L2** (50 mg, 0.104 mmol) in acetonitrile (5 mL) forming a dark orange solution. After stirring and heating to reflux for 16 h, the reaction mixture was allowed to cool to room temperature. The solution was concentrated (to *ca.* 2 mL of solvent), layered with diethyl ether (25 mL) and left to stand at room temperature affording **3.9** as orange crystals after several days (18.95 mg, 26%). ^{19}F{^{1}H} NMR (CD$_3$CN, 375 MHz): δ -150.98 (s, ^{11}BF$_4$), -150.75 (s, ^{10}BF$_4$). IR (cm^{-1}): 1620 (C=N$_{imine}$), 1587 (C=N$_{py}$), 1035 (B-F). HRMS (FAB): calculated for $C_{39}H_{52}N_6Co$ [M-2BF$_4$-Py-2MeCN]$^+$ 540.8600; found 540.8676. Anal Calc. for ($C_{42}H_{54}N_6CoB_2F_8$): C 57.57, H 6.17, N 9.60. Found C 57.29, H 6.24, N 9.28%. μ_{eff} = 5.0 BM.

6.3.12 Synthesis of [(H**L4**)Co(η^1-OHBF$_3$)(MeCN)][BF$_4$] (**3.10**)

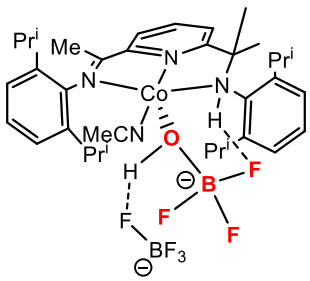

Two small oven dried Schlenk flasks equipped with magnetic stir bars were evacuated and backfilled with nitrogen. In one of the flasks, cobalt(II) tetrafluoroborate hexahydrate (41 mg, 0.121 mmol, 1.2 eq) was dissolved in dry acetonitrile (5 mL) and three drops of pyridine added. The solution was stirred for half hour, forming an orange/pink solution containing [Co(Py)$_4$(NCMe)$_2$][BF$_4$]$_2$. The solution of this cobalt

intermediate was then added dropwise by cannular to the second flask containing H**L4** (50 mg, 0.101 mmol) in acetonitrile (5 mL) forming a dark orange solution. After stirring and heating to reflux for 16 h, the reaction mixture was allowed to cool to room temperature. The solution was filtered by cannular and the filtrate concentrated (to *ca.* 2 mL of solvent), layered with diethyl ether (10 mL) and left to stand at room temperature affording **3.10** as dark brown crystals after several days (0.036 g, 52%). ^{1}H NMR (400 MHz, CD_3CN, 298 K): δ 81.74 (s, 1H, Py-H_m), 78.29 (s, 1H, Py-H_m), 28.82 (s, 5H, Py-H_p and Ar-H), 25.11 (br s, N-H), 19.00 (br s, 1H, OH), 10.53 (s, 6H, NH-C*Me*$_2$), 3.43 (s, 3H, N=C*Me*), 11.16 (s, 12H, CH*Me*$_2$), 12.82 (s, 12H, CH*Me*$_2$). ^{19}F{^{1}H} NMR (CD_3CN, 375 MHz): δ -150.93 (s, $^{11}BF_4$), -150.71 (s, $^{10}BF_4$). IR (cm^{-1}): 1619 (C=N_{imine}), 1586 (C=N_{Py}), 3310 (N-H), 1033 (B-F), 1045 (B-F). HRMS (FAB): calculated for $C_{34}H_{47}N_3Co$ [M-OHBF$_3$-BF$_4$-MeCN]$^+$ 556.3100 found 556.3104. Anal Calc. for ($C_{36}H_{51}B_2F_7N_4CoO\cdot 4H_2O$): C 51.39, H 7.02, N 6.66. Found C 51.56, H 7.32, N 6.51%. μ_{eff} = 5.11 BM.

6.3.13 Attempted reaction of (**L2**)$CoCl_2$ with CsF in CD_2Cl_2

A NMR tube was charged with (**L2**)$CoCl_2$ (6.0 mg, 0.00984 mmol) and then transferred to the glove box. The CsF (1.4 mg, 0.0098 mmol, 1.0 eq or 2.9 mg, 0.0197 mmol, 2.0 eq) was added to the NMR tube under an atmosphere of nitrogen. After removal from the glovebox, CD_2Cl_2 (1 mL) was added to the NMR tube and the contents agitated using sonication at room temperature. The ^{1}H NMR and ^{19}F NMR spectra were both monitored after 10 min, 20 min, 30 min, 60 min and 120 min. The ^{1}H NMR spectra revealed peaks consistent with free **L2**; there was no evidence of zinc fluoride formation by ^{19}F NMR spectroscopy.

6.3.14 Attempted reaction of (**L1**$_{tBu}$)$_2Co_2Cl_2$ (**3.2c**) with CsF in CD_2Cl_2

A similar procedure to that outlined for (**L2**)$CoCl_2$ with CsF was followed using **3.2c** (6.0 mg, 0.00575 mmol), CsF (1.4 mg, 0.0058 mmol, 1.0 eq or 1.7 mg, 0.0115 mmol, 2.0 eq) and CD_2Cl_2 (1 mL). The ^{1}H NMR spectra revealed peaks consistent with free H**L1**$_{tBu}$; there was no evidence of zinc fluoride formation by ^{19}F NMR spectroscopy.

6.3.15 Attempted reaction of (**L2**)$CoCl_2$ with AgF in THF

An oven dry small Schlenk flask equipped with stirred bar was evacuated and backfilled with nitrogen. The flask was loaded with (**L2**)$CoCl_2$ (10 mg, 0.0164 mmol) and then placed under reduced pressure for 30 min. The flask was then back-filled with nitrogen and AgF (2.1 mg, 0.0164 mmol, 1.0 eq) and dry THF (5 mL) introduced. Aluminium-foil was used to surround the Schlenk flask in order to ensure the reaction proceeded in a photophobic environment. After stirring at room temperature for 15 min, 30 min and 60 min. The solution was filtered through celite in the air and washed with THF. The solvent was removed under reduced pressure affording a green powder, which was identified by ^{1}H NMR spectroscopy as unreacted (**L2**)$CoCl_2$. The procedure was repeated with 3 eq and 5 eq AgF. In the case of 3 eq, the ^{1}H NMR spectrum again showed no reaction. On the other hand, with 5 eq of AgF only free **L2** could be identified after stirring at room temperature for 30 mins.

6.3.16 Attempted reaction of (**L1**$_{tBu}$)$_2Co_2Cl_2$ (**3.2c**) with AgF in THF

A similar procedure to that outlined for the reaction of (**L2**)$CoCl_2$ with AgF was followed using **3.2c** (10 mg, 0.0096 mmol), AgF (1.2 mg, 0.0096 mmol, 1.0 eq; 3.6 mg, 0.0287 mmol, 3.0 eq; 6.1 mg, 0.0481 mmol, 5 eq) and anhydrous THF (5 mL). Once again there was no evidence for zinc fluoride formation by ^{1}H and ^{19}F NMR spectroscopy. Indeed, formation of free H**L1**$_{tBu}$ was observed after 30 min when the reaction was performed in the presence of 5 eq of AgF.

6.4 Experimental procedures for Chapter 4

6.4.1 Synthesis of (H**L1**$_H$)$NiCl_2$ (**4.1a**)

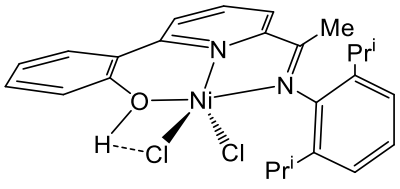

A small oven-dried Schlenk flask equipped with a magnetic stir bar was evacuated and backfilled with nitrogen. The flask was charged with $NiCl_2$(DME) (35.05 mg, 0.161 mmol), dry THF (10 mL) and H**L1**$_H$ (50 mg, 0.134 mmol). After being stirred at room temperature for 24 h, the reaction mixture was concentrated (to *ca.* 1-2 mL of solvent)

and hexane added to induce precipitation. The orange suspension was stirred for several hours, filtered, washed with hexane (2 × 30 mL) and dried under reduced pressure. Recrystallisation of the resulting solid from hot acetonitrile gave dark red crystals of **4.1a**. (27.56 mg, 41%). IR (cm^{-1}): 3430 (OH), 2963 (CH_3), 1620 ($C{=}N_{imine}$). HRMS (FAB): calculated for $C_{25}H_{28}N_2ONiCl$ $[M\text{-}Cl]^+$ 465.1206, $C_{25}H_{27}N_2ONi$ $[M\text{-}HCl_2]^+$ 429.6754; found 465.1254, 429.6744. Anal Calc. for ($C_{25}H_{28}N_2ONiCl_2$): C, 59.81; H, 5.58; N, 5.58. Found: C, 59.82; H, 5.62; N, 5.86. μ_{eff} = 2.9 BM.

6.4.2 Synthesis of (**L1$_{Ph}$**)NiCl (**4.1b**)

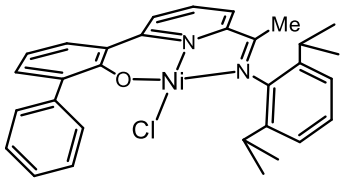

A small oven-dried Schlenk flask equipped with a magnetic stir bar was evacuated and backfilled with nitrogen. The flask was charged with $NiCl_2$(DME) (29.36 mg, 0.133 mmol), dry THF (10 mL) and H**L1**$_{Ph}$ (50 mg, 0.111 mmol). After being stirred at room temperature for 24 h, the reaction mixture was concentrated (to *ca.* 1-2 mL of solvent) and hexane added to induce precipitation. The orange suspension was stirred overnight, filtered, washed with hexane (2 × 30 mL) and dried under reduced pressure. Recrystallisation of the resulting solid from a hot acetonitrile gave dark orange crystals of **4.1b** (46.85 mg, 78%). ^{1}H NMR (400 MHz, CD_2Cl_2, 298 K): δ 8.38 (d, 1H, $^3J_{HH}$ = 8.0 Hz, Py-H_m), 8.04 (t, 1H, $^3J_{HH}$ = 8.0 Hz Py-H_p), 7.79 (d, 1H, $^3J_{HH}$ = 8.0 Hz, Py-H_m), 7.61 (m, 3H, Ar-H), 7.19 (m, 7H, Ar-H), 6.73 (t, 1H, $^3J_{HH}$ = 8.0 Hz, Ar-H), 3.45 (sept, 2H, $^3J_{HH}$ = 6.8 Hz, C*H*Me$_2$), 1.92 (s, 3H, N=C*Me*), 1.49 (d, 6H, $^3J_{HH}$ = 6.7 Hz, CH*Me*$_2$), 1.05 (d, 6H, $^3J_{HH}$ = 6.8 Hz, CH*Me*$_2$). ^{1}H NMR (400 MHz, CD_3CN, 298 K): δ 8.25 (d, $^3J_{HH}$ = 8.0 Hz, 1H, Py-H_m), 8.07 (t, 1H, $^3J_{HH}$ = 8.0 Hz, Py-H_p), 7.92 (t, $^3J_{HH}$ = 6.0 Hz, 2H, Py-H_m and Ar-H), 7.55 (d, $^3J_{HH}$ = 8.0 Hz, 3H, Ar-H), 7.39 (m, 5H, Ar-H), 7.05 (m, 2H, Ar-H), 3.30 (sept, 1H, $^3J_{HH}$ = 6.2 Hz, C*H*Me$_2$), 2.97 (sept, 1H, $^3J_{HH}$ = 6.2 Hz, C*H*Me$_2$), 2.58 (s, 3H, N=C*Me*), 1.13 (d, 3H, $^3J_{HH}$ = 4.0 Hz, CH*Me*$_2$), 1.04(d, 3H, $^3J_{HH}$ = 8.0 Hz, CH*Me*$_2$), 0.80 (d, $^3J_{HH}$ = 8.1 Hz, 3H, CH*Me*$_2$), IR (cm^{-1}): 2963 (CH_3), 1620 ($C{=}N_{imine}$), 1579 ($C{=}N_{py}$), 1208 (C-O). HRMS (FAB): calculated for $C_{31}H_{31}N_2ONi$ $[M\text{-}Cl]^+$ 505.1820, found 505.1872. Anal Calc. for ($C_{31}H_{31}N_2ONiCl{\cdot}2H_2O$): C 65.45, H 6.06, N 4.45. Found: C 65.39, H 6.12, N 4.53%.

6.4.3 Synthesis of (**L1**$_{tBu}$)$_2$Ni$_2$Cl$_2$ (**4.2c**)

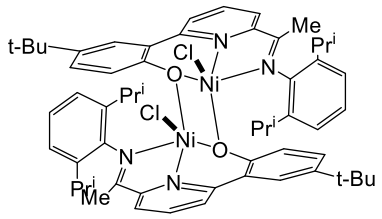

A small oven-dried Schlenk flask equipped with a magnetic stir bar was evacuated and backfilled with nitrogen. The flask was charged with $NiCl_2$(DME) (30.80 mg, 0.140 mmol, 1.2 eq), dry THF (10 mL) and H**L1**$_{tBu}$ (50 mg, 0.117 mmol). After being stirred at room temperature for 24 h, the reaction mixture was concentrated (to *ca.* 1-2 mL of solvent) and hexane added to induce precipitation. The orange suspension was stirred overnight, filtered, washed with hexane (2 × 30 mL) and dried under reduced pressure. Recrystallisation of the resulting solid from a hot acetonitrile gave green crystals of **4.2c** (78.05 mg, 64%). IR (cm^{-1}): 1580 (C=N$_{imine}$), 1561 (C=N$_{py}$), 1221 (C-O). HRMS (FAB): calculated for $C_{60}H_{73}N_5O_2Ni_2$ [M-Cl_2+MeCN]$^+$ 1011.4412, found 1011.4450. Anal Calc. for ($C_{58}H_{70}N_4O_2Ni_2Cl_2$): C 66.78, H 6.72, N 5.37. Found: C 66.71, H 6.93, N 5.46%. μ_{eff} = 4.6 BM.

6.4.4 Synthesis of (**L2**)$NiCl_2$ [7]

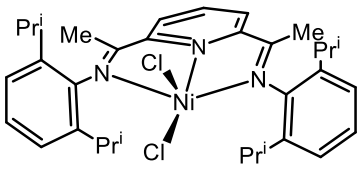

A similar procedure to that outlined for **4.1** was followed using **L2** (50 mg, 0.104 mmol), $NiCl_2$(DME) (27.41 mg, 0.125 mmol, 1.2 eq) and dry THF (10 mL). Recrystallisation of the resulting solid from hot acetonitrile gave (**L2**)$NiCl_2$ as orange needle-like crystals (57.15 mg, 90%). ^{1}H NMR (CD_3CN, 400 MHz): δ 78.24 (s, 2H, Py-H$_m$), 13.94 (s, 1H, Py-H$_p$), 13.69 (s, 4H, Ar-H$_m$), 2.20 (s, 6H, N=CCH_3), -0.24 (s, 24H, ^{i}Pr-Me), -4.42 (s, 2H, Ar-H$_p$). ^{1}H NMR ($CDCl_3$, 400 MHz): δ 117.1 (2H, Py-H$_m$), 49.91 (1H, Py-H$_p$), 10.07 (4H, Ar-H$_m$), 4.56 (6H, N=CCH_3), -8.75 (2H, Ar-H$_p$), -17.51 (12H, ^{i}Pr-Me), -18.51 (12H, ^{i}Pr-Me). IR (cm^{-1}): 1593 (C=N$_{imine}$), 3308 (N-H). IR (cm^{-1}): 1601 (C=N$_{imine}$), 1559 (C=N$_{py}$), 1231 (C-O). HRMS (FAB): calculated for $C_{33}H_{43}N_3NiCl$ [M-Cl]$^+$ 574.2512, found 575.8703. μ_{eff} = 3.01 BM.[7]

6.4.5 Synthesis of (H**L4**)$NiCl_2$ (**4.4**)

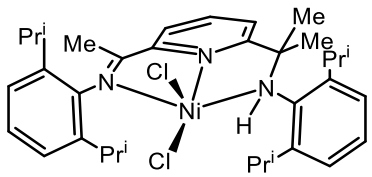

A similar procedure to that outlined for **4.1** was followed using H**L4** (50 mg, 0.101 mmol), $NiCl_2$(DME) (26.53 mg, 0.121 mmol, 1.2 eq) and dry THF (10 mL). Recrystallisation of the resulting solid from hot acetonitrile gave **4.4** as orange needle-like crystals (44.29 mg, 70%). ^{1}H NMR (CD_3CN, 400 MHz): δ 73.85 (s, 1H, Py-H_m), 65.63 (s, 1H, Py-H_m), 14.42 (s, 1H, Py-H_p), 12.97 (s, 2H, Ar-H_m), 12.07 (s, 2H, Ar-H_m), 4.75 (s, 1H, N-H), 1.19 (s, 6H, NH-CMe_2), 0.79 (s, 3H, N=C*Me*), -0.71 (s, 24H, ^{i}Pr-Me), -3.62 (s, 1H, Ar-H_p), -3.80 (s, 1H, Ar-H_p). IR (cm^{-1}): 3308 (N-H), 1593 (C=N_{imine}), 1586 (C=N_{py}). HRMS (FAB): calculated for $C_{34}H_{47}N_3NiCl$ $[M\text{-}Cl]^+$, $C_{34}H_{47}N_3Ni$ $[M\text{-}2Cl]^+$ 590.2811, 555.3121 found 590.2831, 555.3183. Anal Calc. for ($C_{25}H_{28}Cl_2N_2NiO$): C, 59.81; H, 5.58; N, 5.58. Found: C, 59.82; H, 5.62; N, 5.86%. μ_{eff} = 2.92 BM.

6.4.6 Synthesis of [(**L1$_H$**)Ni(Py)][BF_4] (**4.5a**)

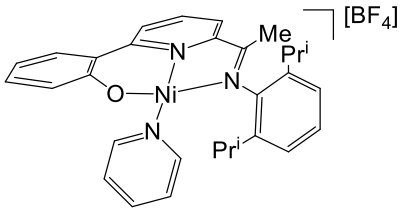

Two small oven dried Schlenk flasks equipped with magnetic stir bars were evacuated and backfilled with nitrogen. In one of the flasks, nickel(II) tetrafluoroborate hexahydrate (54.75 mg, 0.161 mmol, 1.2 eq) was added and dried under reduced pressure for 2 h. The flask was back-filled with nitrogen and dry acetonitrile (5 mL) and three drops of pyridine added. The solution was stirred for half hour, forming a pale violet/purple solution containing $[Ni(Py)_4(NCMe)_2][BF_4]_2$. The solution of this nickel intermediate was then added dropwise by cannular to the second flask containing H**L1$_H$** (50 mg, 0.134 mmol) in acetonitrile (5 mL) forming a violet solution. After stirring and heating to reflux for 16 h, the reaction mixture was allowed to cool to room temperature. All volatiles were removed under reduced pressure and the residue dried for a further

0.5 h. The residue was then dissolved in dry MeCN (1 mL) (heating if necessary) and layered with diethyl ether (8 mL) and left to stand at room temperature. After several days of standing dark brown crystals of **4.5a** were formed (56.65 mg, 71%). ^{1}H NMR (400 MHz, CD_2Cl_2, 298 K): δ 9.88 (br s, 2H, Pyridine-H_m), 8.98(d, 1H, $^{3}J_{HH}$ = 8.1 Hz, Py-H_m), 8.69 (d, 1H, $^{3}J_{HH}$ = 8.0 Hz, Py-H_m), 8.45 (t, 1H, $^{3}J_{HH}$ = 8.0 Hz, Py-H_p), 8.13 (d, 2H, $^{3}J_{HH}$ = 8.1 Hz, Pyridine-H_m), 7.87 (t, 1H, $^{3}J_{HH}$ = 8.0 Hz, Pyridine-H_p), 7.07 (m, 3H, Ar-H), 6.45 (t, 2H, $^{3}J_{HH}$ = 8.0 Hz, Ar-H), 3.29 (sept, 2H, $^{3}J_{HH}$ = 6.5 Hz, C*H*Me$_2$), 2.31(s, 3H, N=C*Me*), 1.22 (d, 6H, $^{3}J_{HH}$ = 7.0 Hz, CH*Me*$_2$), 1.06 (d, 6H, $^{3}J_{HH}$ = 6.9 Hz, CH*Me*$_2$). ^{19}F{^{1}H} NMR (CD_3CN, 375 MHz): δ -150.61 (s, $^{11}BF_4$), -150.38 (s, $^{10}BF_4$). IR (cm^{-1}): 1593 (C=N_{imine}), 1544 (C=N_{Py}), 1220 (C-O), 1039 (B-F). ESIMS *m/z* 472 [M$^+$-Py+MeCN]$^+$, 593 [M+MeCN]$^+$. HRMS (FAB): calculated for $C_{25}H_{27}N_2NiO$ [M-Py]$^+$ 429.1457, $C_{27}H_{30}N_3ONi$ [M-Py+MeCN]$^+$ 470.1730; found 429.1477, 470.1742. Anal. Calc for ($C_{30}H_{32}BF_4N_3NiO{\cdot}2H_2O{\cdot}$MeCN): C 57.09, H 5.84, N 8.32. Found: C 57.03, H 5.74, N 8.55%.

6.4.7 Synthesis of [(**L1**$_H$)Ni(3,5-lutidine)][BF_4]$_2$ (**4.6a**)

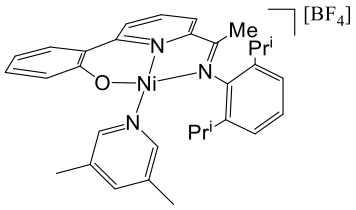

A similar procedure to that outlined for **4.1** was followed using nickel(II) tetrafluoroborate hexahydrate (54.75 mg, 0.161 mmol, 1.2 eq), H**L1**$_H$ (50 mg, 0.134 mmol), dry acetonitrile (5 mL) and two drops of pyridine. Crystallisation of the resulting solid from a mixture of acetonitrile and diethylether gave **4.6a** as cube-like dark red crystals (73.52 mg, 88%).^{1}H NMR (400 MHz, CD_2Cl_2, 298 K): δ 10.45 (br s, 2H, 3,5-lutidine-H_m), 9.13 (d, 1H, $^{3}J_{HH}$ = 8.0 Hz, Py-H_m), 9.02 (d, 1H, $^{3}J_{HH}$ = 8.0 Hz, Py-H_m), 8.51 (br s, 1H, 3,5-lutidine-H_p), 8.22 (t, 1H, $^{3}J_{HH}$ = 8.0 Hz, Py-H_p), 7.67 (d, 1H, $^{3}J_{HH}$ = 8.0 Hz, Ar-H), 7.10 (t, 2H, $^{3}J_{HH}$ = 8.2 Hz, Ar-H), 6.98 (m, 2H, Ar-H), 6.24 (t, 2H, $^{3}J_{HH}$ = 7.6 Hz, Ar-H), 3.22 (m, 5H, C*H*Me$_2$ and N=CCH_3), 2.37 (s, 6H, 3,5-lutidine-(Me)$_2$), 1.24 (d, 6H, $^{3}J_{HH}$ = 6.8 Hz, CHMe$_2$), 1.07 (d, 6H, $^{3}J_{HH}$ = 6.9 Hz, CHMe$_2$). ^{19}F{^{1}H} NMR (CD_3CN, 375 MHz): δ -150.68 (s, $^{11}BF_4$), -150.48 (s, $^{10}BF_4$). IR (cm^{-1}): 1603 (C=N_{imine}), 1565 (C=N_{py}), 1219 (C-O), 1046 (B-F). ESIMS *m/z* 429

$[M^+\text{-Py}]^+$, 470 $[M^+\text{-Py+MeCN}]^+$, 536 $[M]^+$. HRMS (FAB): calculated for $C_{25}H_{27}N_2NiO$ $[M\text{-}BF_4\text{-Py}]^+$ 429.1500. Found 429.1520. Anal. Calc for ($C_{32}H_{36}N_3NiOBF_4$): C 61.59, H 5.77, N 6.71. Found C 61.91, H 5.48, N 6.72 %.

6.4.8 Synthesis of [(**L1**$_{Ph}$)Ni(Py)][BF_4] (**4.7b**)

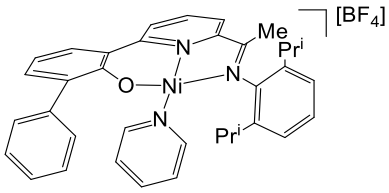

A similar procedure to that outlined for **4.1** was followed using nickel(II) tetrafluoroborate hexahydrate (45.48 mg, 0.134 mmol, 1.2 eq), H**L1**$_{Ph}$ (50 mg, 0.111 mmol), dry acetonitrile (5 mL) and two drops of pyridine. Crystallisation of the resulting solid from a mixture of acetonitrile and diethylether gave **4.7b** as cube-like dark red crystals (66.34 mg, 89%). ^{1}H NMR (400 MHz, CD_2Cl_2, 298 K): δ 8.53 (d, 1H, $^3J_{HH}$ = 8.0 Hz, Py-H_m), 8.34(t, 1H, $^3J_{HH}$ = 6.1 Hz, Py-H_p), 8.07 (d, 1H, $^3J_{HH}$ = 8.0 Hz, Py-H_m), 7.93 (d, 1H, $^3J_{HH}$ = 12.0 Hz, Ar-H), 7.25 (d, 1H, $^3J_{HH}$ = 8.0 Hz, Ar-H), 7.17 (t, 1H, $^3J_{HH}$ = 8.1 Hz, Ar-H), 6.96 (m, 8H, Ar-H), 3.34 (sept, 2H, $^3J_{HH}$ = 6.5 Hz, C*H*Me_2), 2.29 (s, 3H, N=C*Me*), 1.21 (d, 6H, $^3J_{HH}$ = 8.1 Hz, CHMe_2), 1.05 (d, 6H, $^3J_{HH}$ = 8.2 Hz, CH*Me*$_2$). ^{19}F{^{1}H} NMR (CD_3CN, 375 MHz): δ -151.76 (s, $^{11}BF_4$), -151.53 (s, $^{10}BF_4$). IR (cm^{-1}): 1602 ($C{=}N_{imine}$), 1554 ($C{=}N_{Py}$), 1212 (C-O), 1032 (B-F). ESIMS *m/z* 547 $[M^+\text{-Py+MeCN+H}]^+$. HRMS (FAB): calculated for $C_{33}H_{34}N_3ONi$ $[M\text{-}BF_4\text{-Py+MeCN}]^+$ 546.7250 found 546.7243. Anal. Calc for ($C_{36}H_{36}N_3ONiBF_4$): C 60.77, H 5.36, N 6.25. Found C 60.62, 5.24, 6.19%.

6.4.9 Synthesis of [(**L1**$_{Ph}$)Ni(3,5-lutidine)][BF_4] (**4.8b**)

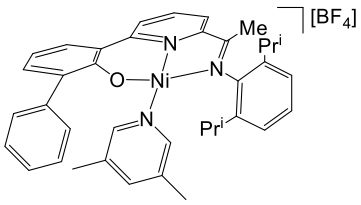

A similar procedure to that outlined for **4a** was followed using nickel(II) tetrafluoroborate hexahydrate (45.48 mg, 0.134 mmol, 1.2 eq), H**L1**$_{Ph}$ (50 mg, 0.111

mmol), dry acetonitrile (5 mL) and two drops of 3,5-lutidine. Crystallisation of the resulting solid from a mixture of acetonitrile and diethylether gave **4.8b** as cube-like dark red crystals (48.14 mg, 62%). ^{1}H NMR (400 MHz, CD_2Cl_2, 298 K): δ 8.68 (d, 1H, $^{3}J_{HH}$ = 8.2 Hz, Py-H_m), 8.56 (s br, 2H, 3,5-lutidine-H_m), 8.46 (t, 1H, $^{3}J_{HH}$ = 6.1 Hz, Py-H_p), 8.23 (d, 1H, $^{3}J_{HH}$ = 8.1 Hz, Py-H_m), 8.16 (s, 1H, 3,5-lutidine-H_p), 8.07 (d, $^{3}J_{HH}$ = 8.1 Hz, Ar-H_m), 7.42 (d, $^{3}J_{HH}$ = 8.0 Hz, 1H, Ar-H_p), 7.29 (m, 2H, Ar-H), 7.12 (m, 6H, Ar-H), 3.48 (sept, 2H, $^{3}J_{HH}$ = 6.9 Hz, C*H*Me_2), 2.58 (s, 6H, 3,5-lutidineMe_2), 2.42 (s, 3H, N=CMe), 1.32 (d, 6H, $^{3}J_{HH}$ = 4.2 Hz, CH*Me*$_2$), 1.17 (d, $^{3}J_{HH}$ = 8.0 Hz, 6H, $CHMe_2$). ^{19}F{^{1}H} NMR (CD_3CN, 375 MHz): δ -151.67 (s, $^{11}BF_4$), 151.44 (s, $^{10}BF_4$). IR (cm^{-1}): 1593 (C=N_{imine}), 1533 (C=N_{Py}), 1222 (C-O), 1041 (B-F). ESIMS (+ve, MeCN): *m/z* 614 $[M\text{-}BF_4]^+$, 546 $[M\text{-}BF_4\text{-}Py\text{+}MeCN]^+$. HRMS (FAB): *m/z* calculated for $C_{33}H_{34}N_3NiO$ $[M\text{-}BF_4\text{-}Py\text{+}MeCN]^+$ 546.7250, found 546.7213. Anal. Calc for ($C_{38}H_{40}BF_4N_3NiO$): C 65.19, H 5.72, N 6.00. Found C 64.98, H 5.81, N 6.14%.

6.4.10 Synthesis of [(**L1**$_{Ph}$)Ni(NCMe)][BF_4] (**4.9b**)

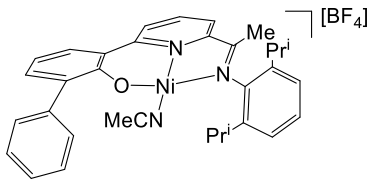

A similar procedure to that outlined for **4.1** was followed using nickel(II) tetrafluoroborate hexahydrate (45.48 mg, 0.134 mmol, 1.2 eq), H**L1**$_{Ph}$ (50 mg, 0.111 mmol) and dry acetonitrile (5 mL). Crystallisation of the resulting solid from a mixture of acetonitrile and diethylether gave **4.9b** as cube-like dark red crystals (65.39 mg, 93%). ^{19}F{^{1}H} NMR (CD_3CN, 375 MHz): δ -151.36 (s, $^{11}BF_4$), -151.12 (s, $^{10}BF_4$). IR (cm^{-1}): 1609 (C=N_{imine}), 1577 (C=N_{Py}), 1202 (C-O), 1019 (B-F). ESIMS (+ve, MeCN): *m/z* 547 $[M+H]^+$, 506 $[M^+\text{-}MeCN]^+$. HRMS (FAB): *m/z* calculated for $C_{33}H_{34}BF_4N_3NiO$ $[M\text{-}BF_4]^+$ 546.7250 found 546.7237. Anal. Calc for ($C_{33}H_{34}BF_4N_3NiO$): C 62.51, H 5.37, N 6.63. Found C 62.76, H 5.12, N 6.61%.

6.4.11 Synthesis of [(**L1**$_{tBu}$)$_2$Ni$_2$(μ-BF$_4$)(NCMe)$_2$][BF$_4$] (**4.10c**)

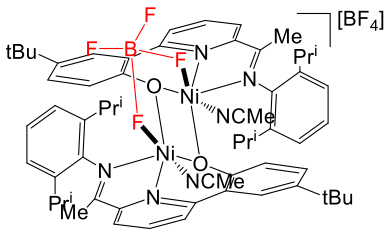

A similar procedure to that outlined for **4.1** was followed using nickel(II) tetrafluoroborate hexahydrate (28.63 mg, 0.0841 mmol, 1.2 eq), H**L1**$_{tBu}$ (30 mg, 0.0701 mmol), dry acetonitrile (5 mL) and two drops of pyridine. Crystallisation of the resulting solid from a mixture of acetonitrile and diethylether gave **4.10c** as cube-like dark brown crystals (47 mg, 93%). ^{19}F{^{1}H} NMR (CD$_3$CN, 400 MHz): δ -150.93 (s, ^{11}BF$_4$), -150.70 (s, ^{10}BF$_4$). IR (cm^{-1}): 1635 (C=N$_{imine}$), 1586 (C=N$_{py}$), 1231 (C-O), 1015 (B-F). ESIMS (+ve, MeCN): *m/z* 972 [M-2BF$_4$-2MeCN+H]$^+$, [M-2BF$_4$+H]$^+$ 1054. HRMS (FAB): calculated for C$_{60}$H$_{73}$N$_5$Ni$_2$O$_2$ [M-2BF$_4$-2MeCN]$^+$ 1011.4500, found 1011.4565. Anal. Calc for (C$_{62}$H$_{76}$B$_2$F$_8$N$_6$Ni$_2$O$_2$·6H$_2$O): C 55.31, H 6.69, N 6.32. Found C 55.26, H 6.76, N 6.25%.

6.4.12 Synthesis of [(*O,N,O*)$_2$Ni$_2$(MeCN)$_4$][BF$_4$]$_2$ (**4.11**)

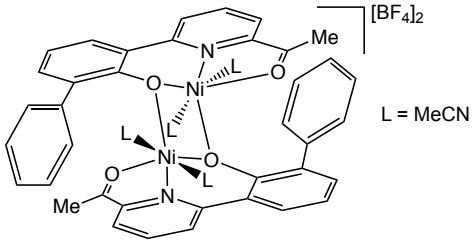

A similar procedure to that outlined for **4.1** was followed using nickel(II) tetrafluoroborate hexahydrate (70.64 mg, 0.208 mmol), Ketone-Ph (50 mg, 0.173 mmol) and dry acetonitrile (5 mL). Crystallisation of the resulting solid from a mixture of acetonitrile and diethylether gave **4.11** as cube-like dark brown crystals (70.85 mg, 56%). ^{19}F{^{1}H} NMR (CD$_3$CN, 375 MHz): δ -150.91 (s, ^{11}BF$_4$), -151.67 (s, ^{10}BF$_4$). IR (cm^{-1}): 1724 (C=O), 1656 (C=N$_{imine}$), 1602 (C=N$_{Py}$), 1219 (C-O), 1049 (B-F). HRMS (FAB): calculated for C$_{46}$H$_{40}$N$_6$Ni$_2$O$_4$ [M-2BF$_4$]$^+$ 858.7300 found 858.7312. Anal. Calc for (C$_{46}$H$_{40}$BF$_4$N$_6$Ni$_2$O$_4$):C 62.51, H 5.37, N 6.63, Found C 62.58, H 5.22, N 6.54%.

6.4.13 Synthesis of [(**L2**)Ni(Py)(MeCN)$_2$][BF$_4$] (**4.12**)

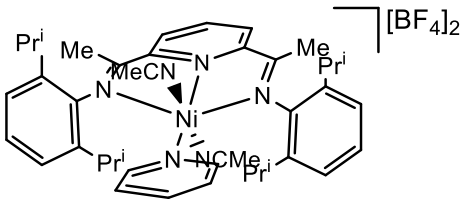

Two small oven dried Schlenk flasks equipped with magnetic stir bars were evacuated and backfilled with nitrogen. In one of the flasks, nickel(II) tetrafluoroborate hexahydrate (42.46 mg, 0.125 mmol, 1.2 eq), dry acetonitrile (5 mL) and three drops of pyridine were added. The solution was stirred for half hour, forming a pale violet/purple solution containing [Ni(Py)$_4$(NCMe)$_2$][BF$_4$]$_2$. The solution of this nickel intermediate was then added dropwise by cannular to the second flask containing **L2** (50 mg, 0.104 mmol) in dichloromethane (5 mL) forming a dark brown solution. After stirring and heating to reflux for 16 h, the reaction mixture was allowed to cool to room temperature. All volatiles were removed under reduced pressure and the residue dried for a further 0.5 h. The residue was then dissolved in dry acetonitrile (1 mL) (heating if necessary) and layered with diethyl ether (8 mL) and left to stand at room temperature. After several days of standing dark brown cube-like crystals of **4.12** were formed (59.10 mg, 65%). ^{19}F{^{1}H} NMR (CD$_3$CN, 375 MHz): δ -151.72 (s, ^{11}BF$_4$), -151.48 (s, ^{10}BF$_4$). IR (cm^{-1}): 1567 (C=N$_{imine}$), 1521 (C=N$_{py}$), 1534 (C=N$_{Py}$), 1033 (B-F). HRMS (FAB): calculated for $C_{42}H_{54}N_6NiB_2F_8$ [M-2BF$_4$-Py-2MeCN]$^+$ 539.6930, found 539.6921. Anal. Calc for ($C_{42}H_{54}N_6NiB_2F_8$): C 57.65, H 6.18, N 9.61, Found C 57.48, H 6.26, N 9.42%.

6.4.14 Synthesis of [(H**L4**)Ni(η^1-OHBF$_3$)(MeCN)][BF$_4$] (**4.13d**)

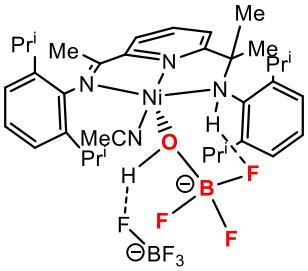

Two small oven dried Schlenk flasks equipped with magnetic stir bars were evacuated and backfilled with nitrogen. In one of the flasks, nickel(II) tetrafluoroborate hexahydrate (41 mg, 0.121 mmol, 1.2 eq), dry acetonitrile (5 mL) and three drops of

pyridine were added. The solution was stirred for half hour, forming an orange/pink solution containing $[Ni(Py)_4(NCMe)_2][BF_4]_2$. The solution of this nickel intermediate was then added dropwise by cannular to the second flask containing H**L4** (50 mg, 0.101 mmol) in acetonitrile (5 mL) forming a dark red solution. After stirring and heating to reflux for 16 h, the reaction mixture was allowed to cool to room temperature. The contents of the flask was transferred to another Schlenk vessel by cannular filtration and concentrated (to *ca.* 2 mL of solvent) under reduced pressure. This solution was then layered with diethyl ether (10 mL) and left to stand at room temperature. After several days of standing dark green cube-like crystals of **4.13d** were formed (0.036 g, 37%). $^{19}F\{^1H\}$ NMR (CD_3CN, 375 MHz): δ -150.89 (s, $^{11}BF_4$), -150.65 (s, $^{10}BF_4$). IR (cm^{-1}): 1570 ($C{=}N_{imine}$), 1501 ($C{=}N_{Py}$), 3308 (N-H), 1041 (B-F). HRMS (FAB): calculated for $C_{34}H_{47}N_3Ni$ $[M\text{-}OHBF_3\text{-}BF_4\text{-}MeCN]^+$, $C_{36}H_{50}N_4Ni$ $[M\text{-}OHBF_3\text{-}BF_4]^+$ 555.3100, 596.3400 found 556.3132, 595.3410. μ_{eff} = 3.11 BM.

6.4.15 Synthesis of $[(H\mathbf{L4})Ni(MeCN)][BF_4]_2$ (**4.14d**)

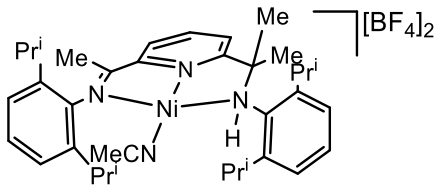

A similar procedure to that outlined for **4.1** was followed using nickel(II) tetrafluoroborate hydrate (23 mg, 0.097 mmol, 1.2 eq), H**L4** (40 mg, 0.080 mmol), and dry acetonitrile (5 mL). Crystallisation of the resulting solid from a mixture of acetonitrile and diethylether gave **4.14d** as yellow cube-like crystals (27 mg, 44%). ^1H NMR (CD_3CN, 400 MHz): δ 8.91 (d, 1H, $^3J_{HH}$ = 8.1 Hz, Py-H_m), 8.67 (d, 1H. $^3J_{HH}$ = 8.0 Hz, Py-H_m), 8.43 (t, 1H, $^3J_{HH}$ = 8.0 Hz, Py-H_p), 7.06 (m, 3H, Ar-H), 6.47 (t, 3H, $^3J_{HH}$ = 8.0 Hz Ar-H), 3.40 (sept, 2H, $^3J_{HH}$ = 6.5 Hz, C*H*Me_2), 3.50 (sept, 2H, $^3J_{HH}$ = 6.5 Hz, C*H*Me_2), 1.19 (d, 6H, $^3J_{HH}$ = 6.7 Hz, CH*Me*$_2$), 1.12 (d, 12H, $^3J_{HH}$ = 7.0 Hz, CH*Me*$_2$), 1.07 (d, 6H, $^3J_{HH}$ = 7.1 Hz, CH*Me*$_2$). $^{19}F\{^1H\}$ NMR (CD_3CN, 375 MHz): δ -151.02 (s, $^{11}BF_4$), -150.79 (s, $^{10}BF_4$). IR (cm^{-1}): 1573.01 ($C{=}N_{imine}$), 3307 (N-H), 1020 (B-F). HRMS (FAB): calculated for $C_{34}H_{47}N_3Ni$ $[M\text{-}BF_4\text{-}MeCN]^+$ 555.6930, $C_{36}H_{50}N_4Ni$ $[M\text{-}BF_4]^+$ 596.6930; found 555.6901, 596.6939. Anal. Calc. for ($C_{36}H_{50}B_2F_8N_4Ni{\cdot}H_2O$): C 54.80, H 6.59, N 7.10. Found C 54.81, H 6.38, N 7.13%.

6.4.16 Synthesis of (**L1**$_{Ph}$)NiOAc (**4.3b**)

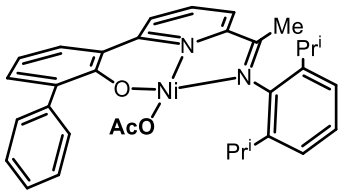

A small oven-dried Schlenk flask equipped with a magnetic stir bar was evacuated and backfilled with nitrogen. The flask was charged with (**L1**$_{Ph}$)NiCl (**4.1b**) (20 mg, 0.0369 mmol), AgOAc (6.0 mg, 0.037 mmol) and dry THF (5 mL). After stirring at room temperature for 16 h, the solution was transferred to a second Schlenk flask using cannular filtration. The solution was concentrated (to *ca.* 1-2 mL) under reduced pressure and layered with diethylether (7 mL). On standing for several days, red cube-like crystals of **4.3b** were formed (4.79 mg, 23%). ^{1}H NMR (400 MHz, CD_2Cl_2, 298 K): δ 8.40 (d, 1H, $^3J_{HH}$ = 8.0 Hz, Py-H$_m$), 8.09 (t, 1H, $^3J_{HH}$ = 8.0 Hz, Py-H$_p$), 7.80 (d, 1H, $^3J_{HH}$ = 8.0 Hz, Py-H$_m$), 7.64 (m, 3H, Ar-H), 7.20 (m, 7H, Ar-H), 6.77 (t, 1H, $^3J_{HH}$ = 8.0 Hz, Ar-H), 3.48 (sept, 2H, $^3J_{HH}$ = 6.8 Hz, C*H*Me$_2$), 1.92 (s, 3H, N=C*Me*), 1.65 (s, 3H, CH_3CO_2), 1.50 (d, 6H, $^3J_{HH}$ = 7.1 Hz, CH*Me*$_2$), 1.07 (d, 6H, $^3J_{HH}$ = 7.0 Hz, CH*Me*$_2$). IR (cm^{-1}): 1590.01 (C=N$_{imine}$), 1210 (C-O), 1029 (B-F). HRMS (FAB): calculated for $C_{33}H_{34}N_2O_3Ni$ $[M+H]^+$ 565.6930, $C_{31}H_{31}N_2ONi$ $[M\text{-}OAc]^+$ 505.6930, $C_{33}H_{34}N_3ONi$ $[M\text{-}OAc+MeCN]^+$ 546.6930; found 565.6951, 505.6932, 546.6926.

6.4.17 Attempted reaction of (**L1**$_{Ph}$)NiCl (**4.1b**) with AgF in THF

An oven dried small Schlenk flask equipped with stirred bar was evacuated and backfilled with nitrogen. The flask was then loaded with (**L1**$_{Ph}$)NiCl (10 mg, 0.019 mmol) and left under reduced pressure for 30 min. The flask was then back-filled with nitrogen and AgF (11.7 mg, 0.092 mmol, 5.0 eq) and THF (5 mL) introduced. Aluminium-foil was used to surround the Schlenk flask to ensure the reaction proceeded in a photophobic environment. After stirring at room temperature for 3 h, the solution was filtered through celite in the air and washed with THF. The solvent was removed under reduced pressure affording a dark orange solid. ^{19}F{^{1}H} NMR (CD_3CN, 375 MHz): δ -138 (*c.f.* AgF at δ -164).

6.5 Experimental procedure for Chapter 5

6.5.1 Synthesis of (**L1**$_{Ph}$)Fe(Py)Cl (**5.1**)

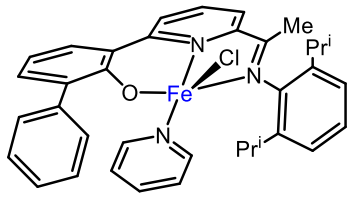

A small Schlenk flask equipped with magnetic stirrer bar was charged with $FeCl_2Py_4$ (112 mg, 0.253 mmol, 1.1 eq) in a glove box under an atmosphere of nitrogen. The flask was removed from the glove box and dry THF (5 mL) added giving a sparingly soluble yellow solution. To another small Schlenk flask, equipped with magnetic stirrer bar, was added NaH (44 mg, 1.84 mmol, 8 eq) and H**L1**$_{Ph}$ (103 mg, 0.230 mmol) along with dry THF (18 mL). The mixture was stirred and heated at 60 ^oC for 16 hours affording intermediate Na**L1**$_{Ph}$ as a bright yellow solution. On cooling to room temperature, the solution of Na**L1**$_{Ph}$ was transferred by cannular to the Schlenk flask containing $FeCl_2Py_4$ resulting in an instant colour change to a dark green solution. After stirring at room temperature overnight, the volume of solution was reduced to 5 mL under reduced pressure. Petroleum ether (20 mL) was added affording a yellow precipitate. All volatiles were then removed under reduced pressure and the resulting pale yellow solid dried overnight. Crystallisation from a concentrated THF solution gave **5.1** as red plate-like crystals (32.79 mg, 21%). IR (cm^{-1}): 2970 (CH_3), 1576 ($C{=}N_{imine}$), 1501 ($C{=}N_{Py}$), 1100 (C-O). μ_{eff} = 4.8 BM.

6.5.2 Synthesis of [(**L2**)Fe(NCMe)$_2$L][BF$_4$]$_2$ (L = H_2O or MeCN) (**5.2**)

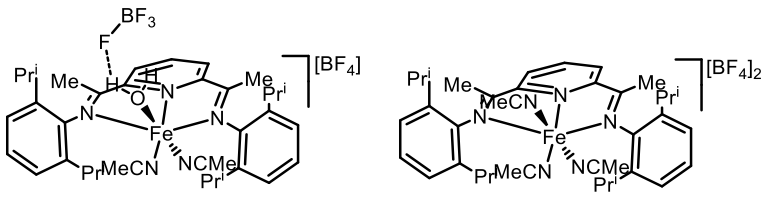

Two small oven dried Schlenk flasks equipped with magnetic stir bars were evacuated and backfilled with nitrogen. In one of the flasks, iron(II) tetrafluoroborate hexahydrate (32 mg, 0.094 mmol, 1.5 eq) was added and the contents dried for 2 h under reduced pressure. The flask was backfilled with nitrogen and dry acetonitrile (5 mL) and two

drops of pyridine added. The solution was stirred for half hour forming a transparent solution containing $[Fe(py)_4(NCMe)_2][BF_4]_2$. The solution of this iron intermediate was then added dropwise by cannular to the second flask containing **L2** (30 mg, 0.0624 mmol) in dichloromethane (5 mL) forming a red solution. After stirring for 30 min at room temperature, all volatiles were removed under reduced pressure by using Schlenk line. The residue was dissolved in acetonitrile (*ca*. 1.5 mL) and layered with diethyl ether (10 mL) and left to stand at -39 ^{o}C. After several days, red needle-like crystals was formed (44 mg, 87 %). $^{19}F\{^{1}H\}$ NMR (CD_3CN, 375 MHz): δ -150.66 (s, 4F). IR (cm^{-1}): 1619 ($C{=}N_{imine}$), 2960 (CH_3), 1017 (B-F). Anal Calc. for ($C_{76}H_{104}N_{11}OFe_2B_4F_{16}{\cdot}4H_2O$): C 53.09, H 6.52, N 8.97. Found: 53.11, H 6.49, N 8.82 %.

6.5.3 Synthesis of [(H**L4**)Fe(NCMe)(η^1-$OHBF_3$)][BF_4] (**5.3**)

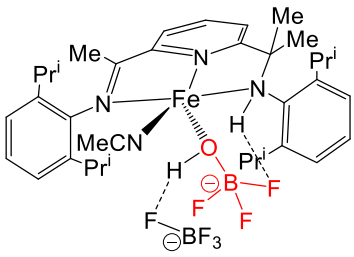

Two small oven dried Schlenk flasks equipped with magnetic stir bars were evacuated and backfilled with nitrogen. In one of the flasks, iron(II) tetrafluoroborate hexahydrate (31 mg, 0.0905 mmol, 1.5 eq) was added and the contents dried for 2 h under reduced pressure. The flask was backfilled with nitrogen and dry acetonitrile (5 mL) and two drops of pyridine added. The solution was stirred for half hour, forming a transparent containing $[Fe(py)_4(NCMe)_2][BF_4]_2$. The solution of this iron intermediate was then added dropwise by cannular to the second flask containing H**L4** (30 mg, 0.0604 mmol) in dichloromethane (5 mL) forming a red solution. After stirring for 30 min at room temperature, all volatiles were removed under reduced pressure. The residue was dissolved in acetonitrile (*ca*. 1.5 mL) and layered with diethyl ether (10 mL) and left to stand at -39 ^{o}C. After several days, a microcrystalline powder was formed (20.83 mg, 16%). $^{19}F\{^{1}H\}$ NMR (CD_3CN, 375 MHz): δ -150.69 (s, 4F). IR (cm^{-1}): 1565 ($C{=}N_{Py}$), 1627 ($C{=}N_{imine}$), 2960 (CH_3), 3309 (N-H), 1029(B-F), 1045 (B-F).

6.5.4 Polymerisation studies

General considerations for polymerisation test. All manipulations involving air and moisture sensitive compounds were carried out under a nitrogen atmosphere by using standard Schlenk techniques. Toluene was heating to reflux over sodium and distilled under nitrogen prior to use. MAO (1.46 M solution in toluene) and MMAO (1.93 M in n-heptane) were purchased from Akzo Nobel Corp. High purity ethylene was purchased from Beijing Yanshan Petrochemical Co. and used as received. Molecular weights and molecular weight distributions of the polyethylene were determined with an Agilent PL-GPC 220 GPC/SEC system at 150 ^{o}C with 1,2,4-trichlorobenzene as solvent. The columns used were three 300 × 7.5 mm PLgel 10 μm MIXED-B LS columns connected in series. The testing was undertaken at 150 ^{o}C with flow rate of 1.0 ml min^{-1} with 1,2,4-trichlorobenzene (TCB) as eluent. The samples were dissolved at a concentration of 0.5 to 2.5 mg ml^{-1}, depending on the molecular weight.[8] The data were collected every second and processed using Cirrus GPC Software and Multi Detector Software with a Polystyrene standard (Calibration KitS-M-10 from PL Company). The melting temperature of the polyethylene were measured from the fourth scanning run on a Perkin Elmer TA-Q2000 differential scanning calorimeter under a nitrogen atmosphere. A sample of about 5.0 mg was heated to 140 ^{o}C at a rate of 20 ^{o}C min^{-1}, kept for 2 min at 140 ^{o}C to remove the thermal history and then cooled to -40 ^{o}C at a rate of 20 ^{o}C min^{-1}. ^{13}C NMR spectra of the polyethylenes were recorded with a Bruker DMX 300 MHz instrument at 135 ^{o}C in 1,1,2,2-tetrachloroethane-d_2 with TMS as internal standard.

Ethylene polymerisation at P_{C2H4} = 5 or 10 atm. The autoclave was evacuated and backfilled with ethylene three times. When the required temperature was reached, the precatalysts (either **5.1**, **5.2** or **L2**$FeCl_2$) (2.0 μmol) were dissolved in toluene (30 mL) in a Schlenk tube and injected into the autoclave containing ethylene (~1 atm) followed by the addition of more toluene (30 mL). The required amount of co-catalyst (MAO and MMAO) and additional toluene were added successively by syringe taking the total volume of toluene to 100 mL. The autoclave was immediately pressurised with 5 or10 atm ethylene and the stirring commenced. After the required reaction time, the reactor was cooled with a water bath and the excess ethylene pressure vented. Following quenching of the reaction with 10% hydrochloric acid in ethanol, the polymer was

collected and washed with ethanol and dried under reduced pressure at 50 ^{o}C and weighed.

Ethylene polymerisation at P_{C2H4} = 1 atm. The polymerisations at 1 atm ethylene pressure were carried out in a Schlenk tube. Under an ethylene atmosphere (1 atm), the iron precatalyst (2.0 μmol) was added followed by toluene (30 mL) and then the required amount of co-catalyst (MAO, MMAO) introduced by syringe. The solution was then stirred at 40 ^{o}C under an ethylene atmosphere (1 atm). After 30 min, the solution was quenched with 10% hydrochloride acid in ethanol. The polymer was washed with ethanol, dried under reduced pressure at 40 ^{o}C and then weighed.

6.6 Crystallographic Studies

Data for all crystallographically characterised samples were collected on a Bruker APEX 2000 CCD diffractometer. The data were corrected for Lorentz and polarisation effects and empirical absorption corrections applied. Structure solution by direct methods and structure refinement based on full-matrix least-squares on F^2 employed SHELXTL version 6.10.[16] Hydrogen atoms were included in calculated positions (C-H = 0.96 – 1.00 Å) riding on the bonded atom with isotropic displacement parameters set to 1.5 U_{eq}(C) for methyl H atoms and 1.2 U_{eq}(C) for all other H atoms. All non-H atoms were refined with anisotropic displacement parameters. Details of data collection, refinement and crystal data for each structure obtained in this thesis are listed in the Appendices.

References

1. J. E. Parks, B. E. Wager and R.H. Holm, *J. Organoment. Chem.,* 1973, **56**, 53-66.
2. T. Robert, Z. Abiri, J. Wassenaar, A. J. Sandee, S. Romanski, J. M. Neudrfl and J. N. Reek, *Organometallics*, 2010, **29**, 478-483.
3. L. A. Wright, E. G. Hope, G. A. Solan, W. B. Cross and K. Singh, *Organometallics,* 2016, **35**, 1183-1191.
4. A. Singh, First year PhD report, University of Leicester, 2013.
5. W. Alkarekshi, A. P. Armitage, O. Boyron, C. J. Davies, M. Govere, A. Gregory, K. Singh and G. A. Solan, *Organometallics,* 2013, **32**, 249-359.
6. a) G. J. P. Britovsek, M. Bruce, V. C. Gibson, B. S. Kimberley, P. J. Maddox, S. Mastroianni, S. J. McTavish, C. Redshaw, G. A. Solan, S. Strömberg, A. J. P. White and D. J. Williams, *J. Am. Chem. Soc*., 1999, **121**, 8728-8740; b) G. J. P. Britovsek, V. C. Gibson, B. S. Kimberley, P. J. Maddox, S. J. McTavish, G. A. Solan, A. J. P. White and D. J. Williams, *Chem. Commun.,* 1998, 849-850.
7. R.-Q. Fan, D.-S. Zhu, H. Ding, Y. Mu, Q. Su and H. Xia, *Synthesis Metals*, 2005, **149**, 135-141.
8. R.-Q. Fan, D.-S. Zhu, Y. Mu, G.-h. Li, Q. Su, J.-G. Ni and S.-H, Feng, *Chem. Res. Chin. Univ.,* 2005, **21**, 496-500.
9. F. Huang, W. Zhang, E. Yue, T. Liang, X. Hu and W.-H. Sun*, Dalton Trans*., 2016, **45**, 657-666.
10. M. A. Guichelaar, J. A. M. van Hest and J. Reedijk, *Inorg. Nucl. Chem. Lett.,* 1974, **10**, 999-1004.
11. D. F. Evans and D. A. Jakubovic. *J. Chem. Soc., Dalton Trans.,* 1988, 2927-2933.
12. W. A. Gobeze, V. A. Milway, N. F. Chilton, B. Moubaraki, K. S. Murry and S. Brooker*, Eur. J. Inorg. Chem*., 2013, 4485-4498.
13. L.-C. Liang, W.-Y. Lee and C.-C. Yin, *Organometallics,* 2004, **23**, 3538-3547.
14. P. V. Petunin, D. E. Votkina, M. E. Trusova, T. V. Rybalova, E. V. Amosov, M. N. Uvarov, P. S. Postnikov, M. S. Kazantsev and E. A. Mostovich, *New J. Chem*., 2019, **43**, 15293-153011.
15. T. Kylmälä, A. Valkonen, K. Rissanen, Y.-J. Xu and R. Franzén, *Tetrahedron Letters,* 2008, **49**, 6679-6682.
16. a) J. Huang, E. D. Stevens, S. P. Nolan and J. L. Peterson, *J. Am. Chem. Soc*., 1999, **121**, 2674-2678. b) M. Scholl, T. M. Trnka, J. P. Morgan and R. H. Grubbs, *Tet,*

Lett., 1999, **40**, 2247-2250. c) M. Scholl, S. Ding, C. W. Lee and R. H. Grubbs, *Org. Lett.*, 1999, **6**, 953-956.

Appendix

Crystal data and structure refinements

Table 1: Crystal Data and structure refinement for H**L1**$_{H}$

Identification code	16126	
Empirical formula	C31 H32 N2 O	
Formula weight	448.59	
Temperature	150(2) K	
Wavelength	0.71073 Å	
Crystal system	Orthorhombic	
Space group	Pna2(1)	
Unit cell dimensions	a = 22.282(5) Å	α= 90°.
	b = 13.317(3) Å	β= 90°.
	c = 8.414(2) Å	γ = 90°.
Volume	2496.5(10) Å^3	
Z	4	
Density (calculated)	1.193 Mg/m^3	
Absorption coefficient	0.072 mm^{-1}	
F(000)	960	
Crystal size	0.22 x 0.15 x 0.13 mm^3	
Theta range for data collection	1.78 to 25.00°.	
Index ranges	-26<=h<=26, -15<=k<=15, -10<=l<=10	
Reflections collected	17375	
Independent reflections	2360 [R(int) = 0.0935]	
Completeness to theta = 25.00°	100.0 %	
Absorption correction	Empirical	
Max. and min. transmission	0.981 and 0.613	
Refinement method	Full-matrix least-squares on F^2	
Data / restraints / parameters	2360 / 1 / 312	
Goodness-of-fit on F^2	0.990	
Final R indices [I>2sigma(I)]	R1 = 0.0536, wR2 = 0.1063	
R indices (all data)	R1 = 0.0742, wR2 = 0.1129	
Absolute structure parameter	?	
Largest diff. peak and hole	0.224 and -0.142 e.Å^{-3}	

Table 2: Crystal Data and structure refinement for H**L1**$_{tBu}$

Identification code	18102	
Empirical formula	C29 H36 N2 O	
Formula weight	428.60	
Temperature	150(2) K	
Wavelength	0.71073 Å	
Crystal system	Triclinic	
Space group	P-1	
Unit cell dimensions	a = 9.421(3) Å	a= 112.566(5)°.
	b = 11.789(3) Å	b= 105.223(6)°.
	c = 13.082(4) Å	g = 97.573(5)°.
Volume	1249.7(6) Å^3	
Z	2	
Density (calculated)	1.139 Mg/m^3	
Absorption coefficient	0.068 mm^{-1}	
F(000)	464	
Crystal size	0.42 x 0.22 x 0.12 mm^3	
Theta range for data collection	1.79 to 25.00°.	
Index ranges	-11<=h<=11, -14<=k<=14, -15<=l<=15	
Reflections collected	9095	
Independent reflections	4367 [R(int) = 0.1025]	
Completeness to theta = 25.00°	99.2 %	
Absorption correction	Empirical	
Max. and min. transmission	0.981 and 0.270	
Refinement method	Full-matrix least-squares on F^2	
Data / restraints / parameters	4367 / 0 / 297	
Goodness-of-fit on F^2	0.855	
Final R indices [I>2sigma(I)]	R1 = 0.0734, wR2 = 0.1317	
R indices (all data)	R1 = 0.1614, wR2 = 0.1565	
Largest diff. peak and hole	0.223 and -0.242 e.Å^{-3}	

Table 3: Crystal Data and structure refinement for H**L1**$_{Ph}$

Identification code	18100	
Empirical formula	C31 H32 N2 O	
Formula weight	448.59	
Temperature	150(2) K	
Wavelength	0.71073 Å	
Crystal system	Monoclinic	
Space group	P2(1)/n	
Unit cell dimensions	a = 13.4877(13) Å	α= 90°.
	b = 13.9166(13) Å	β= 112.827(2)°.
	c = 14.1349(13) Å	γ = 90°.
Volume	2445.4(4) Å^3	
Z	4	
Density (calculated)	1.218 Mg/m^3	
Absorption coefficient	0.073 mm^{-1}	
F(000)	960	
Crystal size	0.24 x 0.11 x 0.08 mm^3	
Theta range for data collection	1.77 to 26.00°.	
Index ranges	-16<=h<=16, -17<=k<=17, -17<=l<=17	
Reflections collected	18957	
Independent reflections	4811 [R(int) = 0.1423]	
Completeness to theta = 26.00°	100.0 %	
Absorption correction	Empirical	
Max. and min. transmission	0.962 and 0.355	
Refinement method	Full-matrix least-squares on F^2	
Data / restraints / parameters	4811 / 0 / 313	
Goodness-of-fit on F^2	0.849	
Final R indices [I>2sigma(I)]	R1 = 0.0697, wR2 = 0.1273	
R indices (all data)	R1 = 0.1478, wR2 = 0.1511	
Largest diff. peak and hole	0.522 and -0.231 e.Å^{-3}	

Table A1: Crystal Data and structure refinement for ($H\mathbf{L1_H}$)$ZnCl_2$ (**2.1a**)

Identification code	18090	
Empirical formula	C25 H28 Cl2 N2 O Zn	
Formula weight	508.76	
Temperature	150(2) K	
Wavelength	0.71073 Å	
Crystal system	Triclinic	
Space group	P-1	
Unit cell dimensions	a = 9.219(4) Å	α= 102.583(7)°.
	b = 10.134(4) Å	β= 99.949(7)°.
	c = 14.285(6) Å	γ = 105.931(7)°.
Volume	1213.5(8) $Å^3$	
Z	2	
Density (calculated)	1.392 Mg/m^3	
Absorption coefficient	1.251 mm^{-1}	
F(000)	528	
Crystal size	0.47 x 0.27 x 0.22 mm^3	
Theta range for data collection	1.51 to 26.00°.	
Index ranges	-11<=h<=11, -12<=k<=12, -17<=l<=17	
Reflections collected	9524	
Independent reflections	4728 [R(int) = 0.0925]	
Completeness to theta = 26.00°	98.7 %	
Absorption correction	Empirical	
Max. and min. transmission	0.859 and 0.599	
Refinement method	Full-matrix least-squares on F^2	
Data / restraints / parameters	4728 / 0 / 285	
Goodness-of-fit on F^2	1.029	
Final R indices [I>2sigma(I)]	R1 = 0.0841, wR2 = 0.1957	
R indices (all data)	R1 = 0.1212, wR2 = 0.2095	
Largest diff. peak and hole	0.887 and -0.714 $e.Å^{-3}$	

Table A2: Crystal Data and structure refinement for (H**L1**$_{ph}$)$ZnCl_2$ (**2.1b**)

Identification code	15079	
Empirical formula	C31 H32 Cl2 N2 O Zn	
Formula weight	584.86	
Temperature	150(2) K	
Wavelength	0.71073 Å	
Crystal system	Tetragonal	
Space group	I-4	
Unit cell dimensions	a = 25.589(3) Å	α= 90°.
	b = 25.589(3) Å	β= 90°.
	c = 8.7148(14) Å	γ = 90°.
Volume	5706.6(13) $Å^3$	
Z	8	
Density (calculated)	1.361 Mg/m^3	
Absorption coefficient	1.074 mm^{-1}	
F(000)	2432	
Crystal size	0.19 x 0.08 x 0.06 mm^3	
Theta range for data collection	1.59 to 25.96°.	
Index ranges	-31<=h<=30, -31<=k<=31, -10<=l<=10	
Reflections collected	22579	
Independent reflections	5603 [R(int) = 0.0961]	
Completeness to theta = 25.96°	100.0 %	
Absorption correction	Empirical	
Max. and min. transmission	0.862 and 0.729	
Refinement method	Full-matrix least-squares on F^2	
Data / restraints / parameters	5603 / 0 / 340	
Goodness-of-fit on F^2	0.861	
Final R indices [I>2sigma(I)]	R1 = 0.0455, wR2 = 0.0714	
R indices (all data)	R1 = 0.0598, wR2 = 0.0752	
Absolute structure parameter	0.013(12)	
Largest diff. peak and hole	0.389 and -0.347 $e.Å^{-3}$	

Table A3: Crystal Data and structure refinement for $(\mathbf{L1}_{tBu})_2Zn_2Cl_2$ (**2.1c**)

Identification code	18086	
Empirical formula	C58 H71 Cl2 N4 O2.50 Zn2	
Formula weight	1065.83	
Temperature	150(2) K	
Wavelength	0.71073 Å	
Crystal system	Monoclinic	
Space group	C2/c	
Unit cell dimensions	a = 12.299(4) Å	α= 90°.
	b = 15.823(4) Å	β= 90.626(6)°.
	c = 27.283(7) Å	γ = 90°.
Volume	5309(2) $Å^3$	
Z	4	
Density (calculated)	1.333 Mg/m^3	
Absorption coefficient	1.051 mm^{-1}	
F(000)	2244	
Crystal size	0.43 x 0.31 x 0.27 mm^3	
Theta range for data collection	1.49 to 26.00°.	
Index ranges	-15<=h<=15, -19<=k<=19, -33<=l<=33	
Reflections collected	20044	
Independent reflections	5224 [R(int) = 0.0467]	
Completeness to theta = 26.00°	100.0 %	
Absorption correction	Empirical	
Max. and min. transmission	0.850 and 0.619	
Refinement method	Full-matrix least-squares on F^2	
Data / restraints / parameters	5224 / 0 / 315	
Goodness-of-fit on F^2	1.072	
Final R indices [I>2sigma(I)]	R1 = 0.0347, wR2 = 0.0822	
R indices (all data)	R1 = 0.0416, wR2 = 0.0846	
Largest diff. peak and hole	0.438 and -0.307 $e.Å^{-3}$	

Table A4: Crystal Data and structure refinement for ($\mathbf{L1}_{Phmes}$)$_2$Zn (**2.4**)

Identification code	15091	
Empirical formula	C56 H50 N4 O2 Zn	
Formula weight	876.37	
Temperature	150(2) K	
Wavelength	0.71073 Å	
Crystal system	Monoclinic	
Space group	C2/c	
Unit cell dimensions	a = 28.765(7) Å	α= 90°.
	b = 10.664(2) Å	β= 124.269(7)°.
	c = 17.380(5) Å	γ = 90°.
Volume	4405.8(19) Å^3	
Z	4	
Density (calculated)	1.321 Mg/m^3	
Absorption coefficient	0.606 mm^{-1}	
F(000)	1840	
Crystal size	0.19 x 0.16 x 0.09 mm^3	
Theta range for data collection	1.71 to 27.00°.	
Index ranges	-36<=h<=36, -13<=k<=13, -22<=l<=21	
Reflections collected	18096	
Independent reflections	4804 [R(int) = 0.0642]	
Completeness to theta = 27.00°	99.7 %	
Absorption correction	Empirical	
Max. and min. transmission	0.862 and 0.719	
Refinement method	Full-matrix least-squares on F^2	
Data / restraints / parameters	4804 / 0 / 289	
Goodness-of-fit on F^2	0.968	
Final R indices [I>2sigma(I)]	R1 = 0.0464, wR2 = 0.1071	
R indices (all data)	R1 = 0.0643, wR2 = 0.1130	
Largest diff. peak and hole	1.059 and -0.284 e.Å^{-3}	

Table A5: Crystal Data and structure refinement for $[(\mathbf{L1}_H)_2Zn_2(MeCN)(Py)][BF_4]_2$ (**2.5a**)

Identification code	18091	
Empirical formula	C57 H62 B2 F8 N6 O2 Zn2	
Formula weight	1167.49	
Temperature	150(2) K	
Wavelength	0.71073 Å	
Crystal system	Monoclinic	
Space group	P2(1)	
Unit cell dimensions	a = 10.958(2) Å	α= 90°.
	b = 20.184(4) Å	β= 112.895(3)°.
	c = 13.767(3) Å	γ = 90°.
Volume	2805.1(9) $Å^3$	
Z	2	
Density (calculated)	1.382 Mg/m^3	
Absorption coefficient	0.928 mm^{-1}	
F(000)	1208	
Crystal size	0.45 x 0.19 x 0.16 mm^3	
Theta range for data collection	1.61 to 26.00°.	
Index ranges	-13<=h<=13, -24<=k<=24, -16<=l<=16	
Reflections collected	22078	
Independent reflections	10818 [R(int) = 0.0805]	
Completeness to theta = 26.00°	99.9 %	
Absorption correction	Empirical	
Max. and min. transmission	0.850 and 0.629	
Refinement method	Full-matrix least-squares on F^2	
Data / restraints / parameters	10818 / 64 / 723	
Goodness-of-fit on F^2	0.938	
Final R indices [I>2sigma(I)]	R1 = 0.0624, wR2 = 0.1222	
R indices (all data)	R1 = 0.0889, wR2 = 0.1331	
Absolute structure parameter	0.041(14)	
Largest diff. peak and hole	0.740 and -0.560 $e.Å^{-3}$	

Table A6: Crystal Data and structure refinement for $[(\mathbf{L1}_H)_2Zn_2(MeCN)_2(\mu\text{-}BF_4)][BF_4]$ (**2.5a'**)

Identification code	18104	
Empirical formula	C60 H75 B2 F8 N6 O3.50 Zn2	
Formula weight	1240.62	
Temperature	150(2) K	
Wavelength	0.71073 Å	
Crystal system	Monoclinic	
Space group	P2/C	
Unit cell dimensions	a = 16.357(4) Å	α= 90°.
	b = 9.162(2) Å	β= 120.965(12)°.
	c = 23.221(4) Å	γ = 90°.
Volume	2984.0(11) $Å^3$	
Z	2	
Density (calculated)	1.381 Mg/m^3	
Absorption coefficient	0.879 mm^{-1}	
F(000)	1294	
Crystal size	0.30 x 0.22 x 0.14 mm^3	
Theta range for data collection	1.45 to 25.00°.	
Index ranges	-19<=h<=19, -10<=k<=10, -27<=l<=27	
Reflections collected	20951	
Independent reflections	5258 [R(int) = 0.0980]	
Completeness to theta = 25.00°	99.9 %	
Absorption correction	Empirical	
Max. and min. transmission	0.849 and 0.525	
Refinement method	Full-matrix least-squares on F^2	
Data / restraints / parameters	5258 / 355 / 364	
Goodness-of-fit on F^2	0.964	
Final R indices [I>2sigma(I)]	R1 = 0.0721, wR2 = 0.1958	
R indices (all data)	R1 = 0.1114, wR2 = 0.2130	
Largest diff. peak and hole	0.696 and -0.833 $e.Å^{-3}$	

Table A7: Crystal Data and structure refinement for [{**L1**$_{Ph}$(BF_3)}Zn(MeCN)(Py)][BF_4] (**2.6b**)

Identification code	18083	
Empirical formula	C38 H39 B2 F7 N4 O Zn	
Formula weight	787.72	
Temperature	150(2) K	
Wavelength	0.71073 Å	
Crystal system	Tetragonal	
Space group	P4(3)	
Unit cell dimensions	a = 15.154(2) Å	α= 90°.
	b = 15.154(2) Å	β= 90°.
	c = 15.875(4) Å	γ = 90°.
Volume	3645.4(12) $Å^3$	
Z	4	
Density (calculated)	1.435 Mg/m^3	
Absorption coefficient	0.747 mm^{-1}	
F(000)	1624	
Crystal size	0.48 x 0.22 x 0.19 mm^3	
Theta range for data collection	1.86 to 26.99°.	
Index ranges	-18<=h<=19, -19<=k<=19, -20<=l<=20	
Reflections collected	30893	
Independent reflections	7936 [R(int) = 0.0927]	
Completeness to theta = 26.99°	100.0 %	
Absorption correction	Empirical	
Max. and min. transmission	0.850 and 0.604	
Refinement method	Full-matrix least-squares on F^2	
Data / restraints / parameters	7936 / 1 / 484	
Goodness-of-fit on F^2	0.900	
Final R indices [I>2sigma(I)]	R1 = 0.0519, wR2 = 0.0879	
R indices (all data)	R1 = 0.0811, wR2 = 0.0967	
Absolute structure parameter	0.022(11)	
Largest diff. peak and hole	0.379 and -0.307 $e.Å^{-3}$	

Table A8: Crystal Data and structure refinement for [{$\mathbf{L1_{tBu}}(BF_3)$}Zn$(MeCN)_2$][BF_4] (**2.7c**)

Identification code	18110	
Empirical formula	C33 H41 B2 F7 N4 O Zn	
Formula weight	729.69	
Temperature	150(2) K	
Wavelength	0.71073 Å	
Crystal system	Triclinic	
Space group	P-1	
Unit cell dimensions	a = 8.664(3) Å	α= 90.200(7)°.
	b = 11.530(4) Å	β= 93.079(8)°.
	c = 17.863(6) Å	γ = 93.247(7)°.
Volume	1779.1(11) $Å^3$	
Z	2	
Density (calculated)	1.362 Mg/m^3	
Absorption coefficient	0.759 mm^{-1}	
F(000)	756	
Crystal size	0.35 x 0.18 x 0.11 mm^3	
Theta range for data collection	1.77 to 26.00°.	
Index ranges	-10<=h<=10, -14<=k<=14, -22<=l<=22	
Reflections collected	13969	
Independent reflections	6881 [R(int) = 0.1003]	
Completeness to theta = 26.00°	98.6 %	
Absorption correction	Empirical	
Max. and min. transmission	0.850 and 0.546	
Refinement method	Full-matrix least-squares on F^2	
Data / restraints / parameters	6881 / 0 / 443	
Goodness-of-fit on F^2	0.878	
Final R indices [I>2sigma(I)]	R1 = 0.0743, wR2 = 0.1247	
R indices (all data)	R1 = 0.1505, wR2 = 0.1472	
Largest diff. peak and hole	0.624 and -0.412 e.$Å^{-3}$	

Table A9: Crystal Data and structure refinement for [(**L2**)Zn(MeCN)(Py)(BF_4)][BF_4] (**2.8**)

Identification code	18075	
Empirical formula	C42 H54.40 B2 F8 N6 O0.20 Zn	
Formula weight	885.51	
Temperature	150(2) K	
Wavelength	0.71073 Å	
Crystal system	Monoclinic	
Space group	P2(1)/c	
Unit cell dimensions	a = 9.979(3) Å	α= 90°.
	b = 20.695(5) Å	β= 97.299(5)°.
	c = 22.011(6) Å	γ = 90°.
Volume	4509(2) $Å^3$	
Z	4	
Density (calculated)	1.304 Mg/m^3	
Absorption coefficient	0.614 mm^{-1}	
F(000)	1848	
Crystal size	0.35 x 0.33 x 0.18 mm^3	
Theta range for data collection	1.36 to 26.00°.	
Index ranges	-12<=h<=12, -25<=k<=25, -27<=l<=27	
Reflections collected	34639	
Independent reflections	8847 [R(int) = 0.0695]	
Completeness to theta = 26.00°	99.8 %	
Absorption correction	Empirical	
Max. and min. transmission	0.850 and 0.643	
Refinement method	Full-matrix least-squares on F^2	
Data / restraints / parameters	8847 / 0 / 553	
Goodness-of-fit on F^2	1.005	
Final R indices [I>2sigma(I)]	R1 = 0.0509, wR2 = 0.1052	
R indices (all data)	R1 = 0.0770, wR2 = 0.1129	
Largest diff. peak and hole	0.554 and -0.362 e.$Å^{-3}$	

Table A10: Crystal Data and structure refinement for [(H**L4**)Zn(MeCN){BF_3(OH)}][BF_4] (**2.9**)

Identification code	18092	
Empirical formula	C42 H63 B2 F8 N5 O Zn	
Formula weight	892.96	
Temperature	150(2) K	
Wavelength	0.71073 Å	
Crystal system	Triclinic	
Space group	P-1	
Unit cell dimensions	a = 10.260(3) Å	α= 90.195(5)°.
	b = 12.976(4) Å	β= 105.752(5)°.
	c = 18.045(5) Å	γ = 91.006(5)°.
Volume	2311.7(12) $Å^3$	
Z	2	
Density (calculated)	1.283 Mg/m^3	
Absorption coefficient	0.600 mm^{-1}	
F(000)	940	
Crystal size	0.46 x 0.42 x 0.36 mm^3	
Theta range for data collection	1.57 to 26.00°.	
Index ranges	-12<=h<=12, -16<=k<=16, -22<=l<=22	
Reflections collected	17843	
Independent reflections	8945 [R(int) = 0.0409]	
Completeness to theta = 26.00°	98.4 %	
Absorption correction	Empirical	
Max. and min. transmission	0.859 and 0.652	
Refinement method	Full-matrix least-squares on F^2	
Data / restraints / parameters	8945 / 2 / 547	
Goodness-of-fit on F^2	1.037	
Final R indices [I>2sigma(I)]	R1 = 0.0629, wR2 = 0.1679	
R indices (all data)	R1 = 0.0766, wR2 = 0.1756	
Largest diff. peak and hole	1.398 and -0.582 e.$Å^{-3}$	

Table A11: Crystal Data and structure refinement for (H**L1**$_R$)$CoCl_2$ (**3.1a**)

Identification code	16110	
Empirical formula	C25 H28 Cl2 Co N2 O	
Formula weight	502.32	
Temperature	150(2) K	
Wavelength	0.71073 Å	
Crystal system	Monoclinic	
Space group	P2(1)/n	
Unit cell dimensions	a = 10.083(4) Å	α= 90°.
	b = 15.723(6) Å	β= 102.501(8)°.
	c = 15.370(6) Å	γ = 90°.
Volume	2379.0(16) $Å^3$	
Z	4	
Density (calculated)	1.402 Mg/m^3	
Absorption coefficient	0.966 mm^{-1}	
F(000)	1044	
Crystal size	0.22 x 0.14 x 0.06 mm^3	
Theta range for data collection	1.88 to 26.00°.	
Index ranges	-12<=h<=12, -19<=k<=19, -18<=l<=18	
Reflections collected	18390	
Independent reflections	4669 [R(int) = 0.1337]	
Completeness to theta = 26.00°	99.9 %	
Absorption correction	Empirical	
Max. and min. transmission	0.862 and 0.648	
Refinement method	Full-matrix least-squares on F^2	
Data / restraints / parameters	4669 / 0 / 285	
Goodness-of-fit on F^2	0.769	
Final R indices [I>2sigma(I)]	R1 = 0.0496, wR2 = 0.0753	
R indices (all data)	R1 = 0.1043, wR2 = 0.0849	
Largest diff. peak and hole	0.423 and -0.429 $e.Å^{-3}$	

Table A12: Crystal Data and structure refinement for $(\mathbf{L1_H})_2Co_2Cl_2$ (**3.2a**)

Identification code	16157	
Empirical formula	C57 H62 B2 Co2 F8 N6 O2	
Formula weight	1154.61	
Temperature	150(2) K	
Wavelength	0.71073 Å	
Crystal system	Monoclinic	
Space group	P2(1)	
Unit cell dimensions	a = 10.920(3) Å	α= 90°.
	b = 20.101(6) Å	β= 112.281(6)°.
	c = 13.834(4) Å	γ = 90°.
Volume	2809.9(14) $Å^3$	
Z	2	
Density (calculated)	1.365 Mg/m^3	
Absorption coefficient	0.664 mm^{-1}	
F(000)	1196	
Crystal size	0.19 x 0.13 x 0.10 mm^3	
Theta range for data collection	1.59 to 26.00°.	
Index ranges	-13<=h<=13, -24<=k<=24, -17<=l<=17	
Reflections collected	22284	
Independent reflections	10704 [R(int) = 0.2345]	
Completeness to theta = 26.00°	99.9 %	
Absorption correction	Empirical	
Max. and min. transmission	0.862 and 0.304	
Refinement method	Full-matrix least-squares on F^2	
Data / restraints / parameters	10704 / 722 / 724	
Goodness-of-fit on F^2	0.702	
Final R indices [I>2sigma(I)]	R1 = 0.0804, wR2 = 0.1076	
R indices (all data)	R1 = 0.2473, wR2 = 0.1443	
Absolute structure parameter	0.13(3)	
Largest diff. peak and hole	0.486 and -0.527 $e.Å^{-3}$	

Table A13: Crystal Data and structure refinement for $(\mathbf{L1_{tBu}})_2Co_2Cl_2$ (**3.2c**)

Identification code	16113	
Empirical formula	C116 H142 Cl4 Co4 N8 O5	
Formula weight	2105.90	
Temperature	150(2) K	
Wavelength	0.71073 Å	
Crystal system	Monoclinic	
Space group	C2/c	
Unit cell dimensions	a = 12.362(10) Å	α= 90°.
	b = 15.738(10) Å	β= 90.816(19)°.
	c = 27.37(2) Å	γ = 90°.
Volume	5325(7) $Å^3$	
Z	2	
Density (calculated)	1.313 Mg/m^3	
Absorption coefficient	0.770 mm^{-1}	
F(000)	2220	
Crystal size	0.24 x 0.21 x 0.18 mm^3	
Theta range for data collection	1.49 to 26.00°.	
Index ranges	-15<=h<=15, -19<=k<=19, -33<=l<=33	
Reflections collected	20422	
Independent reflections	5237 [R(int) = 0.0701]	
Completeness to theta = 26.00°	100.0 %	
Absorption correction	Empirical	
Max. and min. transmission	0.862 and 0.567	
Refinement method	Full-matrix least-squares on F^2	
Data / restraints / parameters	5237 / 1 / 320	
Goodness-of-fit on F^2	0.945	
Final R indices [I>2sigma(I)]	R1 = 0.0415, wR2 = 0.0848	
R indices (all data)	R1 = 0.0578, wR2 = 0.0889	
Largest diff. peak and hole	0.494 and -0.359 $e.Å^{-3}$	

Table A14: Crystal Data and structure refinement for $(H_2\mathbf{L3}_H)_2CoCl_2$ (**3.3**)

Identification code	17139	
Empirical formula	C54 H67 Cl2 Co N5 O2	
Formula weight	947.96	
Temperature	150(2) K	
Wavelength	0.71073 Å	
Crystal system	Triclinic	
Space group	P-1	
Unit cell dimensions	a = 10.518(3) Å	α= 74.040(5)°.
	b = 15.301(4) Å	β= 74.514(5)°.
	c = 16.849(5) Å	γ = 83.106(5)°.
Volume	2509.2(12) $Å^3$	
Z	2	
Density (calculated)	1.255 Mg/m^3	
Absorption coefficient	0.494 mm^{-1}	
F(000)	1006	
Crystal size	0.46 x 0.26 x 0.22 mm^3	
Theta range for data collection	1.64 to 26.00°.	
Index ranges	-12<=h<=12, -18<=k<=18, -20<=l<=20	
Reflections collected	19515	
Independent reflections	9706 [R(int) = 0.0391]	
Completeness to theta = 26.00°	98.5 %	
Absorption correction	Empirical	
Max. and min. transmission	0.862 and 0.669	
Refinement method	Full-matrix least-squares on F^2	
Data / restraints / parameters	9706 / 0 / 562	
Goodness-of-fit on F^2	0.974	
Final R indices [I>2sigma(I)]	R1 = 0.0480, wR2 = 0.1127	
R indices (all data)	R1 = 0.0656, wR2 = 0.1192	
Largest diff. peak and hole	0.696 and -0.583 $e.Å^{-3}$	

Table A15: Crystal Data and structure refinement for (H**L4**)$CoCl_2$ (**3.4**)

Identification code	16160	
Empirical formula	C38 H53 Cl2 Co N5	
Formula weight	709.68	
Temperature	150(2) K	
Wavelength	0.71073 Å	
Crystal system	Monoclinic	
Space group	P2(1)/c	
Unit cell dimensions	a = 14.270(3) Å	α= 90°.
	b = 15.135(3) Å	β= 108.767(4)°.
	c = 18.842(4) Å	γ = 90°.
Volume	3852.8(14) $Å^3$	
Z	4	
Density (calculated)	1.223 Mg/m^3	
Absorption coefficient	0.616 mm^{-1}	
F(000)	1508	
Crystal size	0.37 x 0.16 x 0.10 mm^3	
Theta range for data collection	1.51 to 27.00°.	
Index ranges	-18<=h<=18, -18<=k<=19, -24<=l<=23	
Reflections collected	31733	
Independent reflections	8396 [R(int) = 0.0716]	
Completeness to theta = 27.00°	99.8 %	
Absorption correction	Empirical	
Max. and min. transmission	0.862 and 0.618	
Refinement method	Full-matrix least-squares on F^2	
Data / restraints / parameters	8396 / 0 / 437	
Goodness-of-fit on F^2	0.910	
Final R indices [I>2sigma(I)]	R1 = 0.0422, wR2 = 0.0796	
R indices (all data)	R1 = 0.0652, wR2 = 0.0847	
Largest diff. peak and hole	0.372 and -0.446 $e.Å^{-3}$	

Table A16: Crystal Data and structure refinement for $[(\mathbf{L1_H})_2Co_2(MeCN)(Py)][BF_4]_2$ (**3.5a**)

Identification code	16157	
Empirical formula	C57 H62 B2 Co2 F8 N6 O2	
Formula weight	1154.61	
Temperature	150(2) K	
Wavelength	0.71073 Å	
Crystal system	Monoclinic	
Space group	P2(1)	
Unit cell dimensions	a = 10.920(3) Å	α= 90°.
	b = 20.101(6) Å	β= 112.281(6)°.
	c = 13.834(4) Å	γ = 90°.
Volume	2809.9(14) $Å^3$	
Z	2	
Density (calculated)	1.365 Mg/m^3	
Absorption coefficient	0.664 mm^{-1}	
F(000)	1196	
Crystal size	0.19 x 0.13 x 0.10 mm^3	
Theta range for data collection	1.59 to 26.00°.	
Index ranges	-13<=h<=13, -24<=k<=24, -17<=l<=17	
Reflections collected	22284	
Independent reflections	10704 [R(int) = 0.2345]	
Completeness to theta = 26.00°	99.9 %	
Absorption correction	Empirical	
Max. and min. transmission	0.862 and 0.304	
Refinement method	Full-matrix least-squares on F^2	
Data / restraints / parameters	10704 / 722 / 724	
Goodness-of-fit on F^2	0.702	
Final R indices [I>2sigma(I)]	R1 = 0.0804, wR2 = 0.1076	
R indices (all data)	R1 = 0.2473, wR2 = 0.1443	
Absolute structure parameter	0.13(3)	
Largest diff. peak and hole	0.486 and -0.527 $e.Å^{-3}$	

Table A17: Crystal Data and structure refinement for $[(\mathbf{L1}_{\mathbf{tBu}})_2Co_2(MeCN)_2][BF_4]_2$ (**3.6c**)

Identification code	17052	
Empirical formula	C124 H154 B4 Co4 F16 N12 O5	
Formula weight	2475.55	
Temperature	150(2) K	
Wavelength	0.71073 Å	
Crystal system	Orthorhombic	
Space group	C222(1)	
Unit cell dimensions	a = 9.611(6) Å	α= 90°.
	b = 27.941(17) Å	β= 90°.
	c = 23.634(15) Å	γ = 90°.
Volume	6347(7) $Å^3$	
Z	2	
Density (calculated)	1.295 Mg/m^3	
Absorption coefficient	0.593 mm^{-1}	
F(000)	2588	
Crystal size	0.42 x 0.15 x 0.10 mm^3	
Theta range for data collection	1.46 to 26.00°.	
Index ranges	-11<=h<=11, -34<=k<=33, -29<=l<=28	
Reflections collected	23867	
Independent reflections	6236 [R(int) = 0.1965]	
Completeness to theta = 26.00°	100.0 %	
Absorption correction	Empirical	
Max. and min. transmission	0.850 and 0.263	
Refinement method	Full-matrix least-squares on F^2	
Data / restraints / parameters	6236 / 406 / 407	
Goodness-of-fit on F^2	0.908	
Final R indices [I>2sigma(I)]	R1 = 0.0908, wR2 = 0.2071	
R indices (all data)	R1 = 0.1749, wR2 = 0.2414	
Absolute structure parameter	0.07(4)	
Largest diff. peak and hole	0.686 and -0.734 $e.Å^{-3}$	

Table A18: Crystal Data and structure refinement for $[(H\mathbf{L1}_{Ph})Co(NCMe)_3][BF_4]_2$ (**3.7b**)

Identification code	19016	
Empirical formula	C42 H46 B2 Co F8 N6 O	
Formula weight	883.40	
Temperature	150(2) K	
Wavelength	0.71073 Å	
Crystal system	Rhombohedral	
Space group	R-3	
Unit cell dimensions	a = 25.747(11) Å	α= 117.391(6)°.
	b = 25.747(11) Å	β= 117.391(6)°.
	c = 25.747(11) Å	γ = 117.391(6)°.
Volume	7043(5) $Å^3$	
Z	6	
Density (calculated)	1.250 Mg/m^3	
Absorption coefficient	0.434 mm^{-1}	
F(000)	2742	
Crystal size	0.48 x 0.30 x 0.24 mm^3	
Theta range for data collection	0.93 to 25.99°.	
Index ranges	-31<=h<=31, -31<=k<=31, -31<=l<=31	
Reflections collected	55066	
Independent reflections	9235 [R(int) = 0.3231]	
Completeness to theta = 25.99°	100.0 %	
Absorption correction	Empirical	
Max. and min. transmission	0.831 and 0.262	
Refinement method	Full-matrix least-squares on F^2	
Data / restraints / parameters	9235 / 507 / 549	
Goodness-of-fit on F^2	1.349	
Final R indices [I>2sigma(I)]	R1 = 0.2099, wR2 = 0.4632	
R indices (all data)	R1 = 0.3210, wR2 = 0.5041	
Extinction coefficient	0.070(7)	
Largest diff. peak and hole	1.668 and -0.801 $e.Å^{-3}$	

Table A19: Crystal Data and structure refinement for $[(O,N,O)_2Co_2(MeCN)_4][BF_4]_2$ (**3.8**)

Identification code	18117	
Empirical formula	C54 H52 B2 Co2 F8 N10 O4	
Formula weight	1196.54	
Temperature	150(2) K	
Wavelength	0.71073 Å	
Crystal system	Triclinic	
Space group	P-1	
Unit cell dimensions	a = 10.4029(14) Å	α= 91.490(3)°.
	b = 11.3178(16) Å	β= 91.291(3)°.
	c = 24.035(3) Å	γ = 108.134(3)°.
Volume	2686.9(6) $Å^3$	
Z	2	
Density (calculated)	1.479 Mg/m^3	
Absorption coefficient	0.702 mm^{-1}	
F(000)	1228	
Crystal size	0.24 x 0.12 x 0.10 mm^3	
Theta range for data collection	1.70 to 26.00°.	
Index ranges	-12<=h<=12, -13<=k<=13, -29<=l<=29	
Reflections collected	21261	
Independent reflections	10443 [R(int) = 0.1214]	
Completeness to theta = 26.00°	99.0 %	
Absorption correction	Empirical	
Max. and min. transmission	0.850 and 0.564	
Refinement method	Full-matrix least-squares on F^2	
Data / restraints / parameters	10443 / 25 / 647	
Goodness-of-fit on F^2	0.740	
Final R indices [I>2sigma(I)]	R1 = 0.0690, wR2 = 0.1303	
R indices (all data)	R1 = 0.1537, wR2 = 0.1532	
Largest diff. peak and hole	0.544 and -0.511 $e.Å^{-3}$	

Table A20: Crystal Data and structure refinement for [(**L2**)Co(NCMe)$_2$(Py)][BF$_4$]$_2$ (**3.9**)

Identification code	16150	
Empirical formula	C42 H54 B2 Co F8 N6	
Formula weight	875.46	
Temperature	150(2) K	
Wavelength	0.71073 Å	
Crystal system	Orthorhombic	
Space group	Pbca	
Unit cell dimensions	a = 19.973(7) Å	α= 90°.
	b = 19.527(7) Å	β= 90°.
	c = 22.941(8) Å	γ = 90°.
Volume	8947(5) Å^3	
Z	8	
Density (calculated)	1.300 Mg/m^3	
Absorption coefficient	0.453 mm^{-1}	
F(000)	3656	
Crystal size	0.41 x 0.08 x 0.04 mm^3	
Theta range for data collection	1.71 to 26.00°.	
Index ranges	-24<=h<=24, -23<=k<=24, -28<=l<=28	
Reflections collected	67530	
Independent reflections	8803 [R(int) = 0.3220]	
Completeness to theta = 26.00°	100.0 %	
Absorption correction	Empirical	
Max. and min. transmission	0.862 and 0.675	
Refinement method	Full-matrix least-squares on F^2	
Data / restraints / parameters	8803 / 0 / 544	
Goodness-of-fit on F^2	0.777	
Final R indices [I>2sigma(I)]	R1 = 0.0688, wR2 = 0.0789	
R indices (all data)	R1 = 0.2149, wR2 = 0.1035	
Largest diff. peak and hole	0.358 and -0.314 e.Å^{-3}	

Table A21: Crystal Data and structure refinement for [(H**L4**)Co(NCMe)$_2$(HOBF$_3$)][BF$_4$] (**3.10**)

Identification code	17049	
Empirical formula	C42 H64 B2 Co F7 N5 O2	
Formula weight	884.53	
Temperature	150(2) K	
Wavelength	0.71073 Å	
Crystal system	Triclinic	
Space group	P-1	
Unit cell dimensions	a = 10.237(3) Å	α= 90.461(7)°.
	b = 12.945(4) Å	β= 105.705(6)°.
	c = 18.015(6) Å	γ = 91.095(7)°.
Volume	2297.6(12) Å^3	
Z	2	
Density (calculated)	1.279 Mg/m^3	
Absorption coefficient	0.441 mm^{-1}	
F(000)	934	
Crystal size	0.32 x 0.27 x 0.15 mm^3	
Theta range for data collection	1.17 to 25.99°.	
Index ranges	-12<=h<=12, -15<=k<=15, -22<=l<=22	
Reflections collected	18081	
Independent reflections	8926 [R(int) = 0.0918]	
Completeness to theta = 25.99°	98.7 %	
Absorption correction	Empirical	
Max. and min. transmission	0.862 and 0.409	
Refinement method	Full-matrix least-squares on F^2	
Data / restraints / parameters	8926 / 2 / 547	
Goodness-of-fit on F^2	1.064	
Final R indices [I>2sigma(I)]	R1 = 0.0909, wR2 = 0.2339	
R indices (all data)	R1 = 0.1315, wR2 = 0.2546	
Largest diff. peak and hole	1.456 and -0.547 e.Å^{-3}	

Table A22: Crystal Data and structure refinement for (H**L1**$_{\mathbf{H}}$)$NiCl_2$ (**4.1a**)

Identification code	18122	
Empirical formula	C25 H28 Cl2 N2 Ni O	
Formula weight	502.10	
Temperature	150(2) K	
Wavelength	0.71073 Å	
Crystal system	Monoclinic	
Space group	P2(1)/n	
Unit cell dimensions	a = 9.934(3) Å	α= 90°.
	b = 15.591(4) Å	β= 102.755(5)°.
	c = 15.548(4) Å	γ = 90°.
Volume	2348.7(10) $Å^3$	
Z	4	
Density (calculated)	1.420 Mg/m^3	
Absorption coefficient	1.073 mm^{-1}	
F(000)	1048	
Crystal size	0.33 x 0.25 x 0.22 mm^3	
Theta range for data collection	1.87 to 26.00°.	
Index ranges	-12<=h<=12, -18<=k<=19, -19<=l<=19	
Reflections collected	18148	
Independent reflections	4610 [R(int) = 0.1180]	
Completeness to theta = 26.00°	99.9 %	
Absorption correction	Empirical	
Max. and min. transmission	0.850 and 0.579	
Refinement method	Full-matrix least-squares on F^2	
Data / restraints / parameters	4610 / 0 / 285	
Goodness-of-fit on F^2	0.948	
Final R indices [I>2sigma(I)]	R1 = 0.0579, wR2 = 0.1065	
R indices (all data)	R1 = 0.0966, wR2 = 0.1183	
Largest diff. peak and hole	0.953 and -0.558 $e.Å^{-3}$	

Table A23: Crystal Data and structure refinement for (**L1$_{Ph}$**)NiCl (**4.1b**)

Identification code	17121	
Empirical formula	C126 H127 Cl4 N9 Ni4 O4	
Formula weight	2208.01	
Temperature	150(2) K	
Wavelength	0.71073 Å	
Crystal system	Tetragonal	
Space group	P4/n	
Unit cell dimensions	a = 23.801(5) Å	α= 90°.
	b = 23.801(5) Å	β= 90°.
	c = 9.626(3) Å	γ = 90°.
Volume	5453(2) Å^3	
Z	2	
Density (calculated)	1.345 Mg/m^3	
Absorption coefficient	0.837 mm^{-1}	
F(000)	2316	
Crystal size	0.22 x 0.15 x 0.11 mm^3	
Theta range for data collection	1.71 to 26.00°.	
Index ranges	-29<=h<=29, -29<=k<=29, -11<=l<=11	
Reflections collected	41493	
Independent reflections	5366 [R(int) = 0.1851]	
Completeness to theta = 26.00°	100.0 %	
Absorption correction	Empirical	
Max. and min. transmission	0.862 and 0.554	
Refinement method	Full-matrix least-squares on F^2	
Data / restraints / parameters	5366 / 0 / 339	
Goodness-of-fit on F^2	0.974	
Final R indices [I>2sigma(I)]	R1 = 0.0765, wR2 = 0.1459	
R indices (all data)	R1 = 0.1458, wR2 = 0.1687	
Largest diff. peak and hole	0.429 and -0.690 e.Å^{-3}	

Table A24: Crystal Data and structure refinement for ($\mathbf{L1_{tBu}}$)$_2$Ni$_2$Cl$_2$ (**4.2c**)

Identification code	17114	
Empirical formula	C58 H70 Cl2 N4 Ni2 O2	
Formula weight	1043.50	
Temperature	150(2) K	
Wavelength	0.71073 Å	
Crystal system	Orthorhombic	
Space group	P2(1)2(1)2(1)	
Unit cell dimensions	a = 11.973(2) Å	α= 90°.
	b = 15.351(3) Å	β= 90°.
	c = 29.414(5) Å	γ = 90°.
Volume	5406.5(16) Å^3	
Z	4	
Density (calculated)	1.282 Mg/m^3	
Absorption coefficient	0.840 mm^{-1}	
F(000)	2208	
Crystal size	0.27 x 0.20 x 0.05 mm^3	
Theta range for data collection	1.38 to 26.00°.	
Index ranges	-14<=h<=14, -18<=k<=18, -36<=l<=36	
Reflections collected	42718	
Independent reflections	10615 [R(int) = 0.1423]	
Completeness to theta = 26.00°	100.0 %	
Absorption correction	Empirical	
Max. and min. transmission	0.849 and 0.675	
Refinement method	Full-matrix least-squares on F^2	
Data / restraints / parameters	10615 / 58 / 647	
Goodness-of-fit on F^2	0.864	
Final R indices [I>2sigma(I)]	R1 = 0.0579, wR2 = 0.0896	
R indices (all data)	R1 = 0.1014, wR2 = 0.1015	
Absolute structure parameter	0.020(15)	
Largest diff. peak and hole	0.994 and -0.800 e.Å^{-3}	

Table A25: Crystal Data and structure refinement for (H**L4**)$NiCl_2$ (**4.4**)

Identification code	17119	
Empirical formula	C34 H47 Cl2 N3 Ni	
Formula weight	627.36	
Temperature	150(2) K	
Wavelength	0.71073 Å	
Crystal system	Monoclinic	
Space group	P2(1)/c	
Unit cell dimensions	a = 10.5256(17) Å	α= 90°.
	b = 15.024(3) Å	β= 98.156(3)°.
	c = 20.997(4) Å	γ = 90°.
Volume	3286.9(9) $Å^3$	
Z	4	
Density (calculated)	1.268 Mg/m^3	
Absorption coefficient	0.779 mm^{-1}	
F(000)	1336	
Crystal size	0.36 x 0.18 x 0.12 mm^3	
Theta range for data collection	1.67 to 26.00°.	
Index ranges	-12<=h<=12, -18<=k<=18, -25<=l<=25	
Reflections collected	25290	
Independent reflections	6438 [R(int) = 0.0979]	
Completeness to theta = 26.00°	100.0 %	
Absorption correction	Empirical	
Max. and min. transmission	0.862 and 0.710	
Refinement method	Full-matrix least-squares on F^2	
Data / restraints / parameters	6438 / 0 / 372	
Goodness-of-fit on F^2	0.895	
Final R indices [I>2sigma(I)]	R1 = 0.0502, wR2 = 0.0806	
R indices (all data)	R1 = 0.0916, wR2 = 0.0903	
Largest diff. peak and hole	0.446 and -0.405 e.$Å^{-3}$	

Table A26: Crystal Data and structure refinement for [{$\mathbf{L1_H}$}NiPy][BF_4] (**4.5a**)

Identification code	18093	
Empirical formula	C30 H32 B F4 N3 Ni O	
Formula weight	596.11	
Temperature	150(2) K	
Wavelength	0.71073 Å	
Crystal system	Triclinic	
Space group	P-1	
Unit cell dimensions	a = 11.029(7) Å	α= 86.086(13)°.
	b = 11.575(7) Å	β= 68.572(12)°.
	c = 11.727(7) Å	γ = 75.630(11)°.
Volume	1349.6(14) $Å^3$	
Z	2	
Density (calculated)	1.467 Mg/m^3	
Absorption coefficient	0.776 mm^{-1}	
F(000)	620	
Crystal size	0.24 x 0.19 x 0.14 mm^3	
Theta range for data collection	1.82 to 26.00°.	
Index ranges	-13<=h<=13, -14<=k<=13, -14<=l<=14	
Reflections collected	10641	
Independent reflections	5242 [R(int) = 0.1255]	
Completeness to theta = 26.00°	98.9 %	
Absorption correction	Empirical	
Max. and min. transmission	0.850 and 0.493	
Refinement method	Full-matrix least-squares on F^2	
Data / restraints / parameters	5242 / 0 / 366	
Goodness-of-fit on F^2	0.932	
Final R indices [I>2sigma(I)]	R1 = 0.0811, wR2 = 0.1696	
R indices (all data)	R1 = 0.1369, wR2 = 0.1913	
Largest diff. peak and hole	1.050 and -0.889 e.$Å^{-3}$	

Table A27: Crystal Data and structure refinement for [{$\mathbf{L1_H}$}Ni(3,5-lutidine)][BF_4]$_2$ (**4.6a**)

Identification code	18115	
Empirical formula	C32 H36 B F4 N3 Ni O	
Formula weight	624.16	
Temperature	150(2) K	
Wavelength	0.71073 Å	
Crystal system	Monoclinic	
Space group	P2(1)/c	
Unit cell dimensions	a = 9.027(3) Å	α= 90°.
	b = 19.649(6) Å	β= 102.506(7)°.
	c = 17.205(6) Å	γ = 90°.
Volume	2979.0(17) Å^3	
Z	4	
Density (calculated)	1.392 Mg/m^3	
Absorption coefficient	0.707 mm^{-1}	
F(000)	1304	
Crystal size	0.17 x 0.16 x 0.09 mm^3	
Theta range for data collection	1.59 to 26.00°.	
Index ranges	-11<=h<=11, -24<=k<=24, -21<=l<=21	
Reflections collected	23208	
Independent reflections	5847 [R(int) = 0.1311]	
Completeness to theta = 26.00°	100.0 %	
Absorption correction	Empirical	
Max. and min. transmission	0.862 and 0.632	
Refinement method	Full-matrix least-squares on F^2	
Data / restraints / parameters	5847 / 2 / 413	
Goodness-of-fit on F^2	0.832	
Final R indices [I>2sigma(I)]	R1 = 0.0587, wR2 = 0.0957	
R indices (all data)	R1 = 0.1054, wR2 = 0.1079	
Largest diff. peak and hole	0.686 and -0.600 e.Å^{-3}	

Table A28: Crystal Data and structure refinement for [{**L1$_{Ph}$**}NiPy][BF_4] (**4.7b**)

Identification code	17132	
Empirical formula	C74 H75 B2 F8 N7 Ni2 O2	
Formula weight	1385.45	
Temperature	150(2) K	
Wavelength	0.71073 Å	
Crystal system	Monoclinic	
Space group	Cc	
Unit cell dimensions	a = 11.195(4) Å	α= 90°.
	b = 30.673(10) Å	β= 101.195(7)°.
	c = 20.028(7) Å	γ = 90°.
Volume	6746(4) $Å^3$	
Z	4	
Density (calculated)	1.364 Mg/m^3	
Absorption coefficient	0.632 mm^{-1}	
F(000)	2888	
Crystal size	0.45 x 0.16 x 0.10 mm^3	
Theta range for data collection	1.33 to 26.00°.	
Index ranges	-13<=h<=13, -37<=k<=37, -24<=l<=24	
Reflections collected	26264	
Independent reflections	12921 [R(int) = 0.0880]	
Completeness to theta = 26.00°	100.0 %	
Absorption correction	Empirical	
Max. and min. transmission	0.850 and 0.600	
Refinement method	Full-matrix least-squares on F^2	
Data / restraints / parameters	12921 / 20 / 876	
Goodness-of-fit on F^2	0.901	
Final R indices [I>2sigma(I)]	R1 = 0.0599, wR2 = 0.0841	
R indices (all data)	R1 = 0.0953, wR2 = 0.0941	
Absolute structure parameter	0.060(12)	
Largest diff. peak and hole	0.640 and -0.535 $e.Å^{-3}$	

Table A29: Crystal Data and structure refinement for [{$\mathbf{L1_{Ph}}$}Ni(3,5-lutidine)][BF_4] (**4.8b**)

Identification code	18039	
Empirical formula	C78 H83 B2 F8 N7 Ni2 O2	
Formula weight	1441.55	
Temperature	150(2) K	
Wavelength	0.71073 Å	
Crystal system	Triclinic	
Space group	P-1	
Unit cell dimensions	a = 10.878(3) Å	α= 73.573(6)°.
	b = 11.140(3) Å	β= 88.397(6)°.
	c = 15.390(4) Å	γ = 78.511(5)°.
Volume	1752.1(8) $Å^3$	
Z	1	
Density (calculated)	1.366 Mg/m^3	
Absorption coefficient	0.612 mm^{-1}	
F(000)	754	
Crystal size	0.39 x 0.20 x 0.03 mm^3	
Theta range for data collection	1.91 to 26.00°.	
Index ranges	-13<=h<=13, -13<=k<=13, -18<=l<=18	
Reflections collected	13834	
Independent reflections	6810 [R(int) = 0.1105]	
Completeness to theta = 26.00°	99.0 %	
Absorption correction	Empirical	
Max. and min. transmission	0.858 and 0.447	
Refinement method	Full-matrix least-squares on F^2	
Data / restraints / parameters	6810 / 62 / 513	
Goodness-of-fit on F^2	0.863	
Final R indices [I>2sigma(I)]	R1 = 0.0786, wR2 = 0.1503	
R indices (all data)	R1 = 0.1525, wR2 = 0.1763	
Largest diff. peak and hole	0.683 and -0.547 $e.Å^{-3}$	

Table A30: Crystal Data and structure refinement for [{$\mathbf{L1_{tBu}}$}$_2$Ni$_2$(μ-F$_2$BF$_2$)(MeCN)$_2$][BF$_4$]$_2$ (**4.10c**)

Identification code	18058	
Empirical formula	C62 H80 B2 F8 N6 Ni2 O4	
Formula weight	1264.36	
Temperature	150(2) K	
Wavelength	0.71073 Å	
Crystal system	Orthorhombic	
Space group	C222(1)	
Unit cell dimensions	a = 9.859(6) Å	α= 90°.
	b = 27.781(17) Å	β= 90°.
	c = 23.688(14) Å	γ = 90°.
Volume	6488(7) Å^3	
Z	4	
Density (calculated)	1.294 Mg/m^3	
Absorption coefficient	0.652 mm^{-1}	
F(000)	2656	
Crystal size	0.35 x 0.17 x 0.07 mm^3	
Theta range for data collection	1.47 to 26.00°.	
Index ranges	-12<=h<=12, -34<=k<=34, -29<=l<=28	
Reflections collected	25401	
Independent reflections	6373 [R(int) = 0.1465]	
Completeness to theta = 26.00°	100.0 %	
Absorption correction	Empirical	
Max. and min. transmission	0.843 and 0.568	
Refinement method	Full-matrix least-squares on F^2	
Data / restraints / parameters	6373 / 34 / 386	
Goodness-of-fit on F^2	0.904	
Final R indices [I>2sigma(I)]	R1 = 0.0636, wR2 = 0.1238	
R indices (all data)	R1 = 0.1077, wR2 = 0.1390	
Absolute structure parameter	0.46(2)	
Largest diff. peak and hole	0.634 and -0.672 e.Å^{-3}	

Table A31: Crystal Data and structure refinement for $[(O,N,O)_2Ni_2(MeCN)_4][BF_4]_2$ **(4.11).**

Identification code	19021	
Empirical formula	C46 H40 B2 Ni2 F8 N6 O4	
Formula weight	1155.04	
Temperature	150(2) K	
Wavelength	0.71073 Å	
Crystal system	Triclinic	
Space group	P-1	
Unit cell dimensions	a = 10.4139(3) Å	α= 91.663(5)°.
	b = 11.2568(3) Å	β= 91.250(5)°.
	c = 24.008(3) Å	γ = 108.134(3)°.
Volume	2677.6(6) $Å^3$	
Z	2	
Density (calculated)	1.280 Mg/m^3	
Absorption coefficient	0.784 mm^{-1}	
F(000)	1056	
Crystal size	0.11 x 0.19 x 0.46 mm^3	
Theta range for data collection	1.70 to 26.00°.	
Index ranges	-12<=h<=12, -13<=k<=13, -29<=l<=29	
Reflections collected	21261	
Independent reflections	10443 [R(int) = 0.1214]	
Completeness to theta = 26.00°	99.0 %	
Absorption correction	Empirical	
Max. and min. transmission	0.850 and 0.564	
Refinement method	Full-matrix least-squares on F^2	
Data / restraints / parameters	10443 / 25 / 647	
Goodness-of-fit on F^2	0.740	
Final R indices [I>2sigma(I)]	R1 = 0.0690, wR2 = 0.1303	
R indices (all data)	R1 = 0.1537, wR2 = 0.1532	
Largest diff. peak and hole	0.544 and -0.511 $e.Å^{-3}$	

Table A32: Crystal Data and structure refinement for [(**L2**)Ni(py)(MeCN)$_2$][BF$_4$]$_2$ (**4.12**)

Identification code	18054	
Empirical formula	C42 H54 B2 F8 N6 Ni	
Formula weight	875.24	
Temperature	150(2) K	
Wavelength	0.71073 Å	
Crystal system	Orthorhombic	
Space group	Pbca	
Unit cell dimensions	a = 19.954(7) Å	α= 90°.
	b = 19.422(7) Å	β= 90°.
	c = 22.865(7) Å	γ = 90°.
Volume	8861(5) Å^3	
Z	8	
Density (calculated)	1.312 Mg/m^3	
Absorption coefficient	0.508 mm^{-1}	
F(000)	3664	
Crystal size	0.48 x 0.22 x 0.05 mm^3	
Theta range for data collection	1.71 to 26.00°.	
Index ranges	-24<=h<=24, -23<=k<=23, -27<=l<=28	
Reflections collected	66899	
Independent reflections	8705 [R(int) = 0.2233]	
Completeness to theta = 26.00°	100.0 %	
Absorption correction	Empirical	
Max. and min. transmission	0.843 and 0.545	
Refinement method	Full-matrix least-squares on F^2	
Data / restraints / parameters	8705 / 0 / 544	
Goodness-of-fit on F^2	0.892	
Final R indices [I>2sigma(I)]	R1 = 0.0655, wR2 = 0.1069	
R indices (all data)	R1 = 0.1536, wR2 = 0.1288	
Largest diff. peak and hole	0.541 and -0.343 e.Å^{-3}	

Table A33: Crystal Data and structure refinement for [(H**L4**)Ni(η-$OHBF_3$)(MeCN)][BF_4] (**4.13d**)

Identification code	18006	
Empirical formula	C42 H64 B2 F7 N5 Ni O2	
Formula weight	884.31	
Temperature	150(2) K	
Wavelength	0.71073 Å	
Crystal system	Triclinic	
Space group	P-1	
Unit cell dimensions	a = 10.224(2) Å	α= 90.805(6)°.
	b = 12.913(3) Å	β= 105.653(5)°.
	c = 17.977(4) Å	γ = 90.948(5)°.
Volume	2284.7(9) $Å^3$	
Z	2	
Density (calculated)	1.285 Mg/m^3	
Absorption coefficient	0.493 mm^{-1}	
F(000)	936	
Crystal size	0.27 x 0.12 x 0.09 mm^3	
Theta range for data collection	1.58 to 26.00°.	
Index ranges	-12<=h<=12, -15<=k<=15, -22<=l<=22	
Reflections collected	18006	
Independent reflections	8870 [R(int) = 0.1334]	
Completeness to theta = 26.00°	98.7 %	
Absorption correction	Empirical	
Max. and min. transmission	0.862 and 0.576	
Refinement method	Full-matrix least-squares on F^2	
Data / restraints / parameters	8870 / 2 / 547	
Goodness-of-fit on F^2	0.845	
Final R indices [I>2sigma(I)]	R1 = 0.0812, wR2 = 0.1367	
R indices (all data)	R1 = 0.1768, wR2 = 0.1642	
Largest diff. peak and hole	1.284 and -0.684 e.$Å^{-3}$	

Table A34: Crystal Data and structure refinement for [(H**L4**)Ni(MeCN)][BF_4]$_2$ (**4.14d**)

Identification code	19019	
Empirical formula	C36 H49 B2 F7 N4 Ni	
Formula weight	807.18	
Temperature	150(2) K	
Wavelength	0.71073 Å	
Crystal system	monoclinic	
Space group	P-1	
Unit cell dimensions	a = 19.955(2) Å	α= 90.805(6)°.
	b = 18.243(3) Å	β= 96.321(5)°.
	c = 22.762(4) Å	γ = 90.948(5)°.
Volume	8236(3) Å^3	
Z	8	
Density (calculated)	1.242Mg/m^3	
Absorption coefficient	0.540 mm^{-1}	
F(000)	3224	
Crystal size	0.10 x 0.23 x 0.30 mm^3	
Theta range for data collection	1.58 to 26.00°.	
Index ranges	-24<=h<=24, -22<=k<=22, -28<=l<=28	
Reflections collected	19019	
Independent reflections	8870 [R(int) = 0.1334]	
Completeness to theta = 26.00°	98.7 %	
Absorption correction	Empirical	
Max. and min. transmission	0.862 and 0.576	
Refinement method	Full-matrix least-squares on F^2	
Data / restraints / parameters	8870 / 2 / 547	
Goodness-of-fit on F^2	0.845	
Final R indices [I>2sigma(I)]	R1 = 0.0812, wR2 = 0.1367	
R indices (all data)	R1 = 0.1768, wR2 = 0.1642	
Largest diff. peak and hole	1.284 and -0.684 e.Å^{-3}	

Table A35: Crystal Data and structure refinement for (**L1**$_{Ph}$)Fe(Py)Cl (**5.1**)

Identification code	14041	
Empirical formula	C144 H142.84 Cl5.16 Fe4 N12 O4	
Formula weight	2511.86	
Temperature	150(2) K	
Wavelength	0.71073 Å	
Crystal system	Triclinic	
Space group	P-1	
Unit cell dimensions	a = 14.499(3) Å	α= 90.296(5)°.
	b = 14.685(3) Å	β= 115.332(4)°.
	c = 16.409(3) Å	γ = 96.799(5)°.
Volume	3129.3(11) Å^3	
Z	1	
Density (calculated)	1.333 Mg/m^3	
Absorption coefficient	0.625 mm^{-1}	
F(000)	1315	
Crystal size	0.29 x 0.17 x 0.14 mm^3	
Theta range for data collection	1.57 to 26.00°.	
Index ranges	-17<=h<=17, -18<=k<=18, -19<=l<=20	
Reflections collected	24684	
Independent reflections	12141 [R(int) = 0.1623]	
Completeness to theta = 26.00°	98.8 %	
Absorption correction	Empirical	
Max. and min. transmission	0.862 and 0.432	
Refinement method	Full-matrix least-squares on F^2	
Data / restraints / parameters	12141 / 0 / 785	
Goodness-of-fit on F^2	0.764	
Final R indices [I>2sigma(I)]	R1 = 0.0785, wR2 = 0.1362	
R indices (all data)	R1 = 0.2252, wR2 = 0.1780	
Largest diff. peak and hole	0.501 and -0.743 e.Å^{-3}	

Table A36: Crystal Data and structure refinement for [(**L2**)Fe(NCMe)$_2$L][BF$_4$]$_2$ (**5.2**)

Identification code	18060	
Empirical formula	C94 H130 B4 F16 Fe2 N20 O	
Formula weight	2015.12	
Temperature	150(2) K	
Wavelength	0.71073 Å	
Crystal system	Monoclinic	
Space group	P2(1)/m	
Unit cell dimensions	a = 10.933(3) Å	α= 90°.
	b = 23.512(6) Å	β= 90.000(5)°.
	c = 21.086(5) Å	γ = 90°.
Volume	5420(2) Å^3	
Z	2	
Density (calculated)	1.235 Mg/m^3	
Absorption coefficient	0.347 mm^{-1}	
F(000)	2116	
Crystal size	0.29 x 0.28 x 0.20 mm^3	
Theta range for data collection	0.97 to 26.00°.	
Index ranges	-13<=h<=13, -28<=k<=29, -26<=l<=25	
Reflections collected	42648	
Independent reflections	10916 [R(int) = 0.1276]	
Completeness to theta = 26.00°	100.0 %	
Absorption correction	Empirical	
Max. and min. transmission	0.825 and 0.586	
Refinement method	Full-matrix least-squares on F^2	
Data / restraints / parameters	10916 / 635 / 719	
Goodness-of-fit on F^2	1.050	
Final R indices [I>2sigma(I)]	R1 = 0.1247, wR2 = 0.3368	
R indices (all data)	R1 = 0.1863, wR2 = 0.3653	
Largest diff. peak and hole	1.388 and -0.723 e.Å^{-3}	